Collana Materiali e documenti 00

Pre-print version of ANCRiSST 2019 Procedia:
14th International Workshop on Advanced Smart Materials and Smart Structures Technology

The final version is available online at
https://www.editricesapienza.it/sites/default/files/5935_Atti_Convegno_ANCRISST_LR.pdf

ANCRiSST 2019 Procedia

14th International Workshop on Advanced Smart Materials and Smart Structures Technology

a cura di

Vincenzo Gattulli, Oreste Bursi, Daniele Zonta

SAPIENZA
UNIVERSITÀ EDITRICE
2019

Copyright © 2019

Sapienza Università Editrice
Piazzale Aldo Moro 5 – 00185 Roma

www.editricesapienza.it
editrice.sapienza@uniroma1.it

Iscrizione Registro Operatori Comunicazione n. 11420

ISBN 978-88-xxxx-xxx-x

Pubblicato a luglio 2019

Quest'opera è distribuita
con licenza Creative Commons 3.0
diffusa in modalità *open access*.

In copertina: Colosseum Monitoring - Annamaria Pau

Preface

ANCRiSST 2019 is the Fourteenth International Workshop on Advanced Smart Materials and Smart Structures Technology. ANCRiSST2019 is organised by the Asian-Pacific Network of Centers for Research in Smart Structures Technology (ANCRiSST), European Association for Structural Dynamics (EASD) and Sapienza University of Rome, at the Faculty of Civil and Industrial Engineering from July 18th to 21st, 2019.

To have reached its Fourteenth edition of the workshop it is a testimony to the great success of the prestigious ANCRiSST executive board members. who have driven the organization of the meeting over the years in *Hawaii, USA* 2004, *Kyungju, Korea* 2005, *Lake Tahoe, NV, USA* 2006, *Tokyo, Japan* 2008, *Boston, MA, USA* 2009, *Champaign, IL, USA* 2010, *Dalian, China* 2011, *Bangalore, India* 2012, *Ulsan, Korea* 2013, *Taipei, Taiwan* 2014, *Champaign, IL, USA* 2015, *Cambridge, UK* 2016, *Tokyo, Japan* 2017.

The workshop aims to assess the current progress of smart materials and structures technology and to develop synergies among researchers. Emerging frontiers in automated inspection, sensing and control for civil infrastructure are introduced in the discussions. In particular, the workshop is the occasion for the dissemination of the initial results of the activities of the EU funded project – DESDEMONA - DEtection of Steel DEfects by Enhanced MONitoring and Automated procedure for self inspection and maintenance.

Participants are involved in several scientific and cultural activities including three keynote lectures by prominent leaders in the field, a discussion session to deliberate on future activities, and parallel sessions for more than 60 papers on various topics. The workshop is held along with 2019 Asia-Pacific-Euro Summer School on Smart Structures Technology (APESS) at Sapienza University of Rome. A technical visit co-organized by APESS is also scheduled on July 25 to L'Aquila, where the 2009 earthquake provoked serious damage. We appreciate your active participation in these activities.

Extended abstracts accepted for ANCRiSST 2019 are published by Sapienza Press in hard-copy and made available open access. Special thanks are due to Sapienza Press Staff for their assistance in publishing this book.

Before concluding, we would like to acknowledge the support of ANCRiSST – Asian-Pacific Network of Centers for Research in Smart Structure Technology, IASCM – International Association on Structural Control and Monitoring, EASD – European Association for Structural Dynamics and AIMETA – Associazione Italiana Meccanica Teorica e Applicata.

Special thanks to the Faculty of Civil and Industrial Engineering and Dean, Antonio D'Andrea, and the Department of Structural and Geotechnical Engineering and its Chair, Achille Paolone.

We are indebted to all the members of the Scientific Committee for their valuable support. We are grateful to the distinguished Colleagues who accepted to give Plenary Lectures, ensuring the high standard of the Conference.
Last a sincere thanks to all those colleagues, technical staff, PhD and post-graduate students who have
contributed to the organization of ANCRiSST, along with the support of our Sponsors.

Editors
Vincenzo Gattulli, Chair
Oreste Bursi, Chair
Daniele Zonta, Chair

ANCRiSST 2019 Procedia

14th International Workshop on Advanced Smart Materials and Smart Structures Technology

18 – 21 July 2019

Rome, Italy

http://www.desdemonaproject.eu/ancrisst2019/

ANCRiSST 2019 COMMITTEES

ANCRISST EXECUTIVE BOARD

Chia Ming Chang, National Taiwan University, Taiwan

Yozo Fujino, Yokohama National University, Japan

Hyung-Jo Jung, Korea Advanced Institute of Science and Technology, South Korea

Hui Li, Harbin Institute of Technology, China

Tomonori Nagayama, University of Tokyo, Japan

Yi Qing Ni, The Hong Kong Polytechnic University, China

Hoon Sohn, Korea Advanced Institute of Science and Technology, South Korea

Billie F. Spencer, University of Illinois, USA

Chung-Bang Yun, University of Zhejiang, China

IASCM EXECUTIVE BOARD

James L. Beck, California Institute of Technology, USA

Raimondo Betti, Columbia University, USA

Fabio Casciati, University of Pavia, Italy

Yozo Fujino, University of Yokohama, Japan

Kuo-Chun Chang, National Taiwan University, Taiwan

Srinivasan Gopalkrishnan, Indian Institute of Science, India

Akira Iragashi, Kyoto University, Japan

Ho-Kyung Kim, Seoul National University, South Korea

Michael Krommer, Vienna University of Technology, Austria

Hui Li, Harbin Institute of Technology, China

Jerome P. Lynch, University of Michigan, USA

Sami Masri, University of Southern California, USA

Akira Nishitani, Waseda University, Japan

Jose Rodellar, Polytechnic University of Catalonia, Spain

Bijan Samali, Western Sydney University, Australia

Andrew Smyth, Columbia University, USA

Toru Watanabe, Nihon University, Japan

You-Lin Xu, The Hong Kong Polytechnic University, China

Daniele Zonta, University of Strathclyde, Glasgow, UK

SCIENTIFIC COMMITTEE

Dionisio Bernal, Northeastern University, USA

Eleni Chatzi, ETH Zurich, Switzerland

Zhang Chunwei, Qingdao University of Technology, China

Álvaro Cunha, University of Porto, Portugal

Dina D'Ayala, University College of London, UK

Shirley Dyke, Purdue University, USA

Yozo Fujino, Yokohama National University, Japan

Carmelo Gentile, Polytechnic University of Milan, Italy

Branko Glisic, Princeton University, USA

Salvador Ivorra, University of Alicante, Spain

Marco Lepidi, University of Genoa, Italy

Hong-Nan Li, Dalian University of Technology, China

Hui Li, Harbin Institute of Technology, China

Kenneth Loh, University of California, San Diego, USA

Yaozhi Luo, Zhejiang University, China

Jerome P. Lynch, University of Michigan, USA

Sami Masri, University of Southern California, USA

Satish Nagarajaiah, Rice University, USA

Tomonori Nagayama, University of Tokyo, Japan

Yi Qing Ni, Hong Kong Polytechnic University, Hong Kong

Mayuko Nishio, University of Tsukuba, Japan

Wieslaw Ostachowicz, Polish Academy of Sciences, Poland

Marcus Perry, University of Strathclyde, Glasgow, UK

Matteo Pozzi, Carnegie Mellon University, USA

Jose Rodellar, Polytechnic University of Catalonia, Spain

Walter Salvatore, University of Pisa, Italy

Kenichi Soga, University of California, Berkeley, USA

Hoon Sohn, Korea Advanced Institute of Science and Technology, South Korea

Billie F. Spencer, University Illinois, USA

Quek Ser Tong, National University of Singapore, Singapore

Limin Sun, Tongji University, China

Yang Wang, Georgia Institute of Technology, USA

Chung-Bang Yun, University of Zhejiang, China

ORGANIZING COMMITTEE

Vincenzo Gattulli, Sapienza University of Rome, Italy, Chair

Oreste Bursi, University of Trento, Italy, Chair

Daniele Zonta, University of Strathclyde, Glasgow, UK, Chair

Achille Paolone, Sapienza University of Rome, Italy

Francesco Romeo, Sapienza University of Rome, Italy

Davide Bernardini, Sapienza University of Rome, Italy

Jacopo Ciambella, Sapienza University of Rome, Italy

Annamaria Pau, Sapienza University of Rome, Italy

Mary Joan Crowley, Sapienza University of Rome, Italy

Elisabetta Meluzzi, Comitato Cometa, Italy

ORGANIZING ASSOCIATION

ANCRiSST - Asian-Pacific Network of Centers for Research in Smart Structure Technology

IASCM - International Association on Structural Control and Monitoring

EASD - European Association for Structural Dynamics

AIMETA - Associazione Italiana Meccanica Teorica e Applicata.

ORGANIZING INSTITUTION

Sapienza University of Rome, Faculty of Civil and Industrial Engineering

Department of Structural and Geotechnical Engineering

PARTNERSHIP

Ordine degli Ingegneri della Provincia di Roma

Municipio Roma 1 Centro

SPONSOR

Desdemona Project

Diamonds srl

MTS Systems srl

PCB Piezotronics

CSPFea

MIDAS

SESSIONS

Smart Materials for Sensing and Actuation

Session Chairs: Hyung-Jo Jung, Marco Lepidi, Kenneth Loh

Response Prediction and Evaluation

Session Chairs: Salvador Ivorra, Hui Li, Akira Nishitani, Francesco Potenza

Measurements and Health Monitoring

Session Chairs: Eleni Chatzi, Jacopo Ciambella, Jean Dumolin, Luca Martinelli, Carlos Moutinho, Yi-Qing Ni, Annamaria Pau, Yang Wang

Structural Control

Session Chairs: Andrea Arena, Oreste Bursi, Fernando Gomez, Hyung-Jo Jung

Damage Detection

Session Chairs: Egidio Lofrano, Francesco Potenza, Yong Xia, Chung-Bang Yun

Mechatronics and Automated Inspection

Session Chairs: Fernando Castillo, Fernando Moreu, Mayuko Nishio, Erika Ottaviano

TABLE OF CONTENTS

Smart Materials for Sensing and Actuation

Measurements and Health Monitoring

Response Prediction and Evaluation

Damage Detection

Structural Control

Mechatronics and Automated Inspections

Smart Materials for Sensing and Actuation

Graphene sensing mesh for distributed strain field monitoring

S. Gupta[1], G. Vella[2], W.-H. Chiang[3], K. J. Loh[1,2,*]

[1] *Department of Structural Engineering, University of California, San Diego, CA, U.S.A.*
**E-mail: kenloh@ucsd.edu*

[2] *Material Science and Engineering Program, University of California, San Diego, CA, U.S.A.*

[3] *Department of Chemical Engineering, National Taiwan University of Science & Technology, Taiwan.*

ABSTRACT

A patterned nanocomposite "sensing mesh" was designed, and electrical impedance tomography (EIT) was employed for distributed strain field monitoring. Previous works showed that EIT, when coupled with piezoresistive nanocomposite thin films, could be used for distributed strain sensing and damage mapping. However, only distributed strain magnitudes could be determined but not their directionalities. In order to address this limitation, a net- or mesh-like, graphene-based, nanocomposite sensing mesh that featured high aspect ratio "struts" was designed so that the entire sensing mesh behaved like an interconnected network of strain gages. The sensing mesh was fabricated by depositing graphene dispersions onto a patterned polymer substrate. The sensing mesh was then affixed onto a test coupon and subjected to uniaxial tensile loading. EIT measurements were recorded at different strain states, and the induced strains in each strut were determined from the EIT-estimated conductivity changes. Good agreement between the experimental results and finite element simulations was also observed, which served to validate the graphene-based nanocomposite sensing mesh for distributed strain field monitoring.

KEYWORDS: *Electrical impedance tomography, graphene, nanocomposite, patterned, strain field, thin film*

INTRODUCTION

Damage in civil, mechanical, and aerospace structures can occur due to long-term deterioration, extreme loading, fatigue, aging of materials, and their exposure to aggressive environments. Structural health monitoring (SHM) aims to detect the presence of damage, their locations, and severity so as to assess residual structural performance and to facilitate decision making (*i.e.*, if damage was present) [1]. Among the various structural parameters that can be measured and be used for SHM, stress and strain remain to be the most critical, especially since the failure of materials is often defined by its stress limits. However, since stress is an engineered quantity and cannot

be directly measured, it can be calculated from actual measured strains. One of the most widely used strain transducer is the foil-based strain gage. Despite their accuracy and high resolution, the strain gage can only measure strain at its instrumented location (*i.e.*, it is a point sensor). Distributed strain monitoring would require a dense array of gages installed on the structure.

More recently, distributed strain sensing and damage detection was achieved by coupling piezoresistive thin films with an electrical impedance tomography (EIT) measurement technique and algorithm [2]. While strain distributions could be characterized, this approach was unable to extract strain directionalities from the reconstructed EIT conductivity maps. The sensing mesh concept introduced this study aims to address this limitation. Here, a graphene-based thin film of high strain sensitivity was designed and deposited onto a patterned substrate to form the sensing mesh. Each strut of the sensing mesh was designed to be of high aspect ratio so as to form an interconnected network of distributed uniaxial linear strain sensors. EIT was implemented to reconstruct the conductivity changes of the struts in the mesh. The estimated conductivity changes were then used to calculate the induced strains in each strut. This paper begins with a brief overview of EIT, followed by the experimental details and corresponding distributed strain monitoring results.

EIT Background

EIT is a soft-field imaging technique that reconstructs the conductivity distribution of a conductive body using its boundary electrical measurements [3]. A direct current (DC) is injected through a pair of boundary electrodes, and the resulting voltage differences between all other remaining electrode pairs are measured. This excitation-measurement pattern is repeated for all possible combinations of adjacent boundary electrodes, and the recorded voltage set is used to solve an inverse problem to estimate its spatial conductivity distribution. More details regarding EIT are described by Vella *et al.* [4].

Experimental Details

Fabrication of the sensing mesh began by dispersing graphene nanosheets (GNS) in poly(vinyl alcohol) (PVA) solution [4]. A laser cutter (Orion Motor Tech) was used for patterning and forming the polyethylene terephthalate (PET) substrates to form a grid-like pattern. The GNS-PVA solution was spray-coated onto PET grids to form the sensing mesh (Figure 1a). Conductive threads (Adafruit) were used as electrodes and were attached to the sensing mesh using colloidal silver paste (Ted Pella). Then, the sensing mesh was affixed onto a 100 × 30 mm^2 PET strip using quick-curing superglue (Figure 1b). After the glue fully cured, the PET strip with the sensing mesh was mounted in a Test Resources 150R load frame, at which point, an initial baseline EIT dataset was

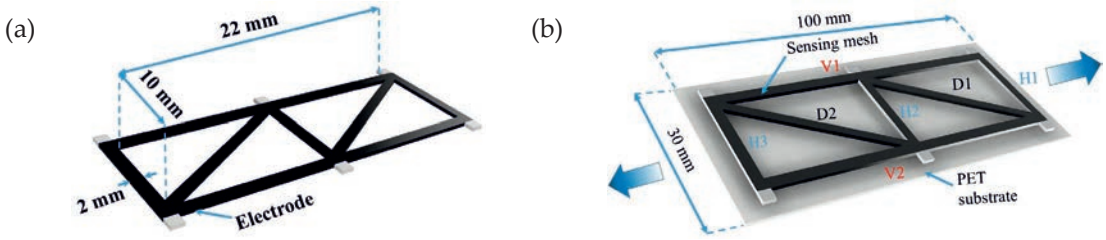

Figure 1: (a) The dimensions of the sensing mesh specimen are shown. (b) The sensing mesh was affixed onto a PET strip and subjected uniaxial loading. H, V, and D indicate the horizontal, vertical, and diagonal struts, respectively.

recorded (corresponding to 0 με). The load frame then applied monotonic uniaxial tensile strain to 6,000 με at a fixed strain rate of 1,000 με/min. The load frame was manually paused every 1,000 με for EIT interrogations.

Results and Discussions

Following EIT reconstruction of all sensing mesh data, Figure 2 shows the average change in conductivity of each sensing mesh strut for three consecutive strain states. Figure 2 shows that both the vertical (*i.e.*, V1 and V2) and diagonal struts (*i.e.*, D1 and D2) decreased in conductivity with increasingly applied tension, while conductivity increased for the horizontal struts (*i.e.*, H1 and H2). These results make sense, since the vertical and diagonal struts were subjected to tension, while the horizontal struts were compressed due to Poisson's effect [4]. The induced strain in each strut was calculated using known values of the GNS-based thin film's nominal conductivity at 0 με (*i.e.*, 0.1846 S/m) and its gage factor (*i.e.*, ~ 8.25) [4].

A linear-elastic, plane-stress, finite element (FE) model of the test coupon was created in ABAQUS to investigate the accuracy of the EIT results. The strains in each strut in their axial directions were estimated by dividing the observed change in their axial lengths with their undeformed lengths and then comparing them with the EIT results (Figure 3). Figure 3 shows good agreement between the EIT- and FE-estimated strains, with only a difference of ~ 5% . This mismatch could be a result of imperfect strain transfer from the test coupon to the sensing mesh and/or misalignment and slippage of the test coupon from the load frame's grips, among others. Nevertheless, these results validated distributed strain magnitude and directionality sensing on a structural surface.

Conclusions

In this study, a GNS-PVA thin film sensing mesh was coupled with EIT for distributed strain field monitoring. The test results showed that EIT was able to identify if any of the

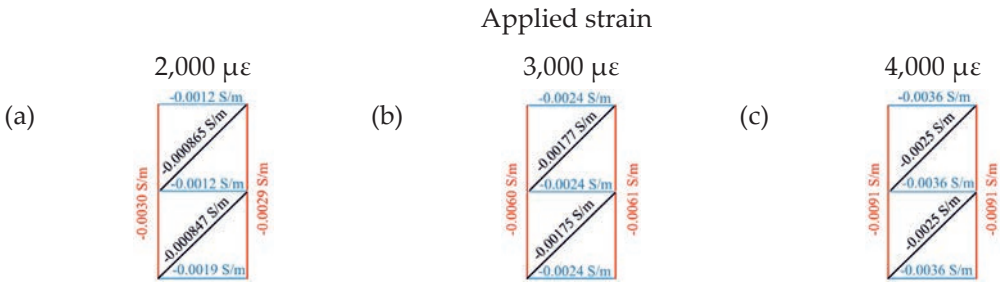

Figure 2: The estimated average conductivity change of all the struts with respect to its undeformed state when the specimen was strained to (a) 2,000 με, (b) 3,000 με, and (c) 4,000 με are shown.

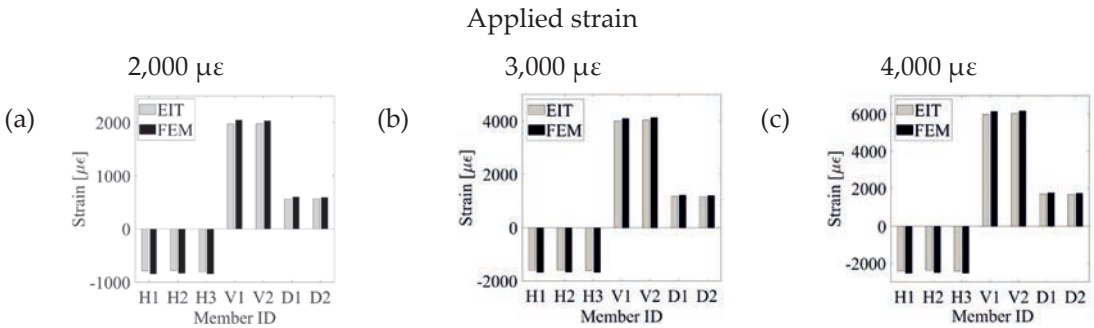

Figure 3: The EIT-estimated strain for the different struts when the specimen was strained to (a) 2,000 με, (b) 3,000 με, and (c) 4,000 με are compared with the FE analysis results.

struts in the sensing mesh was subjected to tension or compression, as well as the corresponding magnitude and directionality of strain. The EIT-estimated strains were compared with FE analysis for verification, and good agreement was observed. Future work will consider more complex sensing mesh designs and different load patterns.

REFERENCES

[1] Farrar, C. R., and Worden, K. (2007) An Introduction to Structural Health Monitoring, *Philos Trans A Math Phys Eng Sci*, **365**:1851, 303-315.

[2] Hou, T. C., Loh, K. J., and Lynch, J. P. (2007) Spatial Conductivity Mapping of Carbon Nanotube Composite Thin Films by Electrical Impedance Tomography for Sensing Applications, *Nanotechnology*, **18**:31, 315501.

[3] Gupta, S., Gonzalez, J. G., and Loh, K. J. (2016) Self-Sensing Concrete Enabled by Nano-Engineered Cement-Aggregate Interfaces, *Struct Health Monit*, **16**:3, 309-323.

[4] Vella, G., Gupta, S., Loh, K. J., and Netchaev, A. (2019) Large-Area Distributed Strain Monitoring using Patterned Nanocomposite Sensing Meshes, presented at the SPIE – 26th Annual Symposium on Smart Structures and Materials & Nondestructive Evaluation and Health Monitoring, Denver, CO.

Active Metamaterial Skins for Actuation and Gripping

Y. Park[1], G. Vella[1], K.J. Loh[1,2]

[1] *Materials Science and Engineering Program, University of California-San Diego, La Jolla, CA, USA.*
E-mail: y4park@ucsd.edu, gvella@ucsd.edu

[2] *Department of Structure Engineering, University of California-San Diego, La Jolla, CA, USA.*
E-mail: kenloh@ucsd.edu

ABSTRACT

Instability-induced morphable structures fall within the large spectrum of mechanical metamaterials and give materials unconventional properties by harvesting their extrinsic instabilities. This study introduces a 3D-printed mechanical metamaterial, or "Active Skin", that enables on-demand, reversible, surface morphing through buckling-induced feature deployment. The unit geometry of the proposed metamaterial is a star-shaped, re-entrant structure, first introduced as a topologically optimized design exhibiting auxetic behavior (i.e., negative Poisson's ratio). It was noticed that the behavior of the auxetic, star-shaped geometry varied as the geometry's thickness was progressively decreased. As uniaxial strains were applied to the thin, elastic, star-shaped pattern, the mechanical instabilities induced out-of-plane (i.e., 2D to 3D) deformations in the form of pop-up of surface features. The introduction of weak points, or notches, at key locations throughout the structure enabled directional control and the possibility of harvesting the instability-induced surface feature deployments for different applications. This reversible, on-demand, surface morphing mechanism was validated as active surfaces for gripping. The Active Skin is unique in that the grippers were actuated by applying tension rather than compression.

KEYWORDS: *3D printing, actuation, gripper, instability, mechanical metamaterial, patterning*

INTRODUCTION

Many biological organisms possess the unique capability of exhibiting reversible skin morphing for various purposes, including camouflage, locomotion, signaling, and hunting [1]. Mankind has sought to replicate these unique attributes by developing bio-inspired materials with properties that mimic or even potentially outperform their natural counterparts [2-4] However, creating structures that could achieve active (and reversible) camouflage remains challenging.

Mechanical metamaterials, which possess well-ordered and sometimes periodic structures, are a new class of materials that exhibit unconventional response to mechanical forces, where they can deform, rotate, buckle, fold, and snap. In particular, mechanical metamaterials have exploited shape morphing, as well as instabilities and nonlinear responses, to achieve and demonstrate various functionalities [5].

ACTIVE SKINS RESULTS AND DISCUSSION

In this study, a star geometry, which was first introduced as a topologically optimized design that exhibits auxetic behavior, was leveraged for designing Active Metamaterial Skins for actuation (Fig. 1). When strained in uniaxial tension, the petal and sepal tips would buckle out-of-plane but in random directions, especially considering the thinness of the star pattern and their susceptibility to slight nonuniform load perturbations and material inhomogeneities. Therefore, to control buckling directions, notches were introduced at precise locations in the unit cell (i.e., red-shaded region in Fig. 1(a)). Moreover, to maintain symmetry and to facilitate out-of-plane deformations, additional notches were introduced adjacent to the petal tips (i.e., blue-shaded region in Fig. 1(a)).

Unit cell star geometries were 3D-printed, and uniaxial tension were applied. In the deformed state, each of the four petal and sepal tips would buckle locally in its programmed direction and induce out-of-plane deformations (Fig. 1) (i.e., solid blue and red curved arrows in Fig. 1(b), respectively). An additional important benefit of introducing notches in the Active Skin's surface was demonstrated by analyzing its mechanical behavior. Fig. 2 plots the stress-strain responses of Active Skin unit cells of

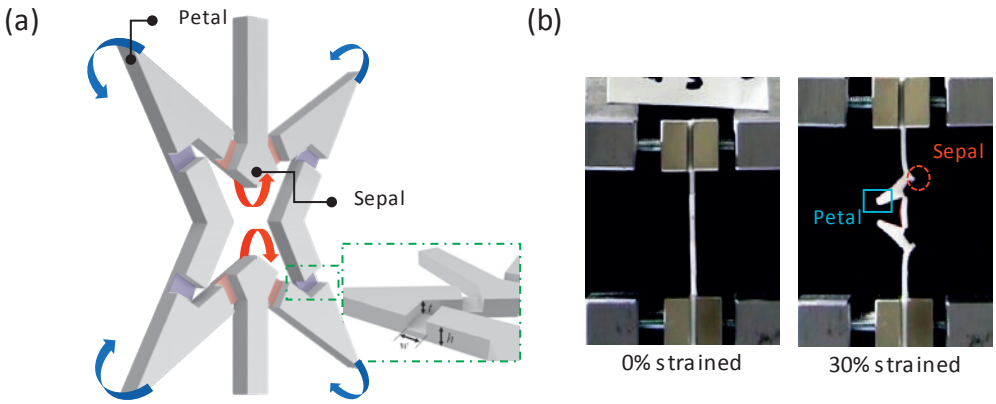

Figure 1: (a) A rendering of the notched Active Skin is shown, with notch dimensions of thickness *t*, depth *h*, and width *w*. The arrows indicate the out-of-plane buckling directions of the petal and sepal tips. (b) (left) An Active Skin was mounted in a load frame. (right) When strained, the petal and sepal tips were deployed accordingly.

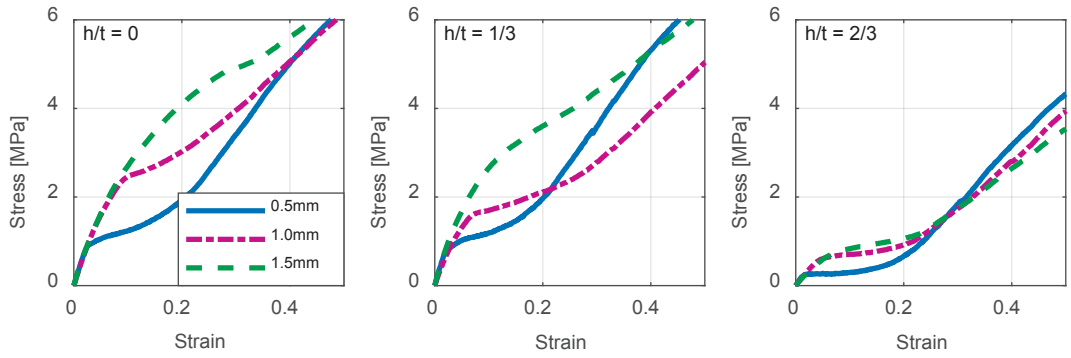

Figure 2: The stress-strain response of (a) unnotched ($h/t = 0$) and notched ((b) $h/t = 1/3$ and (c) $h/t = 2/3$) Active Skin unit cells were characterized. Specimens of different substrate thickness (where $t = 0.5$, 1.0, and 1.5 mm) were tested, and the results are overlaid.

different normalized notch depths (i.e., h/t ratios). The results showed that deeper notches or larger h/t ratios effectively reduced the magnitude of stress and strain required to trigger buckling-induced out-of-plane deformations. This advantage is especially obvious when comparing the response of the notched Active Skins to the unnotched results shown in Fig. 2(a). Overall, the Active Skins were shown to be fully reservisble, where they can return to its initial flat state when tension is released.

Based on these results, the unique properties of Active Skins could be leveraged for applications related to soft robotics, as an example. Here, two different gripper designs based on Active Skins were fabricated. First, two Active Skin unit cells were symmetrically placed on opposite faces of an accordion pneumatic actuator as shown in Fig. 3(a). It should be clarified that the top accordion actuator in Fig. 3(a) was for controlling lifting of the soft gripper. Unlike conventional soft robotic grippers, which require compressive forces to be applied to grip an object in between its fingers, inflating the accordion structure induced tension in the Active Skins to grip (and lift) a gummy bear. The second design was based on 3D-printing a 5×5 array of interconnected, notched, unit cell, star geometries. It can be seen from Fig. 3(b) that straining the 5×5 array deployed the grippers in its programmed direction, and the array was validated for simultaneously gripping numerous fur balls placed on the surface. Overall, these two Active Skin structures successfully validated that these structures can be used as soft grippers.

CONCLUSIONS

In conclusion, Active Metamaterial Skins that exhibit on-demand surface morphing and can undergo dramatic shape changes for various purposes when actuated by applied in-plane tensile strains were demonstrated. The role of instability-induced

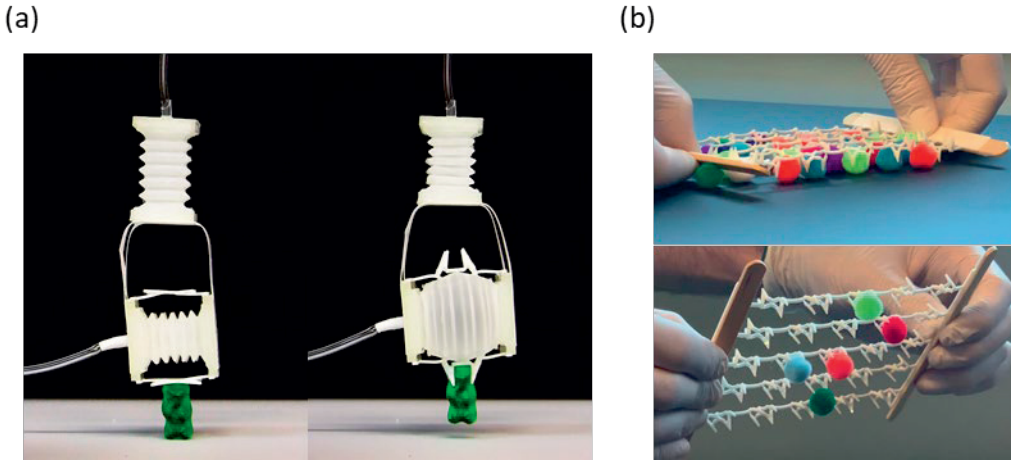

Figure 3: (a) Two Active Skin unit cells were combined with accordion pneumatic actuators to demonstrate gripping of a gummy bear. (b) A 5×5 array of notched stars was 3D-printed and validated for large-area gripping of fur balls.

surface features (i.e., purposefully introduced notches) was studied by characterizing the mechanical response of unit cell star geometries when subjected to uniaxial tensile loading. The stress-strain responses not only showed that the notches reduced the magnitude of stress and strain required for deploying these out-of-plane features but also enabled the petal and sepal tips to deploy in controlled directions. In short, this simple but innovative approach demonstrated that these architected materials could be used for different applications, such as for gripping or for surface morphing.

REFERENCES

[1] A. Rafsanjani, Y. R. Zhang, B. Y. Liu, S. M. Rubinstein,K. Bertoldi (2018) Kirigami Skins Make a Simple Soft Actuator Crawl. *Science Robotics* **3**.

[2] G. Mayoral, J. Jimenez (2011) Drag Reduction by Riblets. *Philosophical Transactions of the Royal Society A: Mathematica* **369**: 1412-1427.

[3] A. Bauhofer, S. Krodel, J. Rys, O. R. Bilal, A. Constantinescu,C. Daraio (2017) Harnessing Photochemical Shrinkage in Direct Laser Writing for Shape Morphing of Polymer Sheets. *Advanced Materials* **29**.

[4] S. Das, N. Cadirov, S. Chary, Y. Kaufman, J. Hogan, K. L. Turner,J. N. Israelachvili (2015) Stick-Slip Friction of Gecko-Mimetic Flaps on Smooth and Rough Surfaces. *Journal of The Royal Society Interface* **12**.

[5] K. Bertoldi, V. Vitelli, J. Christensen, M. V. Hecke (2017) Flexible Mechanical Metamaterials. *Nature Reviews Materials* **2**.

Development of automated cable tension monitoring system using smart sensors

Seunghoo Jeong[1], Hyunjun Kim[2], Junhwa Lee[3], Sung-Han Sim[4]

[1] *School of Urban and Environmental Engineering, Ulsan National Institute of Science and Technology (UNIST), Republic of Korea.*
E-mail: shjeong@unist.ac.kr

[2] *School of Urban and Environmental Engineering, Ulsan National Institute of Science and Technology (UNIST), Republic of Korea.*
E-mail: lee.junhwa@unist.ac.kr

[3] *School of Urban and Environmental Engineering, Ulsan National Institute of Science and Technology (UNIST), Republic of Korea.*
E-mail: guswns3@unist.ac.kr

[4] *School of Urban and Environmental Engineering, Ulsan National Institute of Science and Technology (UNIST), Republic of Korea.*
E-mail: ssim@unist.ac.kr

ABSTRACT

As a demand for long-span bridges is increasing worldwide, effective maintenance has become a critical issue to keep the structural safety and prolong bridge lifetime. Given that a stay-cable is the principal load carrying component in cable-stayed bridges, monitoring the tension forces in the stay-cables provides important information regarding the status of the bridge structures. Indeed, various methodologies have been proposed to measure cable tension forces, including magneto-elastic effect-based sensor technique, direct measurement using load cells, and indirect tension estimation based on cable vibration. Particularly, the vibration-based tension estimation has been widely applied to systems for tension monitoring, which is known as a cost-effective approach. However, full automation considering varying cable tension has not been reported in the literature. Accordingly, this study aims to develop an automated cable tension monitoring system using smart sensors that is possible to measure varying tension forces without prior knowledge of the cable system. A fully automated peak-picking algorithm tailored to the cable vibration is developed using the convolution neural network to apply the vibration-based tension estimation method to automated cable tension monitoring. The developed system features embedded processing on smart sensors, including data acquisition, power spectral density calculation, automated peak-picking, and tension estimation. A series of laboratory

tests are conducted on a cable to validate the performance of the proposed automated monitoring system.

KEYWORDS: *Automated cable monitoring, embedded processing, smart sensors, peak-picking*

INTRODUCTION

This study aims to develop the automated cable tension monitoring system using smart sensors, possible to measure the tension under the varying tension conditions. A peak-picking algorithm tailored to cable vibration is proposed using a Faster R-CNN, one of region-based CNN methods, to apply the vibration-based tension estimation method to automated cable tension monitoring. The developed system features embedded processing on smart sensors, including data acquisition, power spectral density analysis, automated peak-picking, and tension estimation for varying tension forces. A series of laboratory tests are conducted on a cable to verify the operation of proposed automated monitoring system under the variety of tension forces. The experimental results validate the proposed system for automated cable tension monitoring with different tension conditions.

VIBRATION-BASED METHOD FOR CABLE TENSION MONITORING

This study selects the vibration-based method proposed by [1] to implement cable tension estimation in the cable tension monitoring system. As a one of commonly used vibration-based method, this method can estimate the cable tension force, T by using an explicit relationship with natural frequencies, f_n and corresponding mode number, n of the cable. If both ends of the cable are assumed pin-connected (Figure 1), a cable tension T can be written as a linear regression form in terms of $(fn/n)^2$ and n^2 as shown in Eq. (1) where cable length L, bending stiffness EI, weight density per length w, and the gravitational constant g .

$$T = \frac{4wL^2}{g}\left(\frac{f_n}{n}\right)^2 - \frac{EI\pi^2}{L^2}n^2 \tag{1}$$

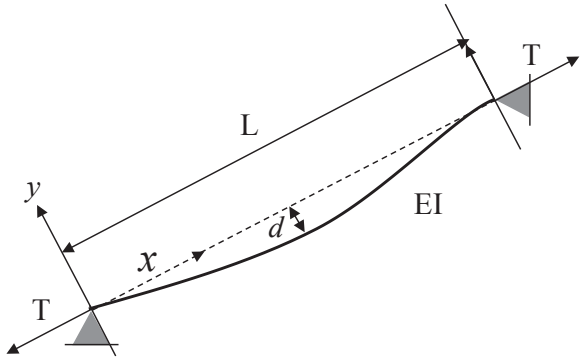

Figure 1: Inclined cable with tension force T

DESIGN OF AUTOMATED PEAK DETECTOR

For training the automated peak detector tailored to the stay-cable, a numerical model of the stay-cable with four mode numbers was used to obtain training images that are power spectral density of a cable response under the white noise. Under the white noise input, this study generates cable responses in terms of acceleration with cable properties indicated in Table 1. A total of 5,000 cable responses are obtained by varying cable tension forces from 1,000 N to 5,999 N with 40 Hz sampling rate for 500 seconds, and these data are transformed into frequency domain representation by analyzing power spectral density with 2048 fft. Each frequency representation data is converted to image format for generating images. As modal information of each training image is known, and each image contains four peaks, this study can generate a total of 20,000 peaks for training data. Note that this study generates boxes containing each peak with 30 pixels of width and 70 pixels of height. A total of 20,000 peaks obtained from cable responses is used to train the automated peak detector.

Tab. 1. Cable properties used to generate training data

Mass per unit length (m)	Damping per unit length (c)	Cable length (L)	Number of modes (n)	Cable tension (T)
2.906 kg/m	0.005 kg/s/m	6.95 m	4	1,000 – 5,999 N

DESIGN OF CABLE TENSION MONITORING SYSTEM

This study selects a Raspberry Pi 3 B+ model, which is a state-of-the-art Raspberry platform with low-cost, as the main body of a hardware of the automated cable tension monitoring system (Figure 2). This single-board computer features vibration sensing, power spectral density analysis, automated peak-picking, and cable tension estimation. This study selects a Raspbian, which is an official operating system for all Raspberry Pi model and installs this through the micro SD card. This study implemented an automated peak-picking algorithm and vibration-based tension estimation method in the Raspbian operating system. Cable vibration is measured by tri-axial MEMS-based analog accelerometer, named ADXL 335 which is small, low-cost, and low-power consumption (Figure 2). Also, this study uses an ADS1115 16-bit analog-to-digital converter (ADC) to convert the analog type of acceleration into digitalized data for transmitting the digitalized sensing data to the Raspberry Pi 3 B+ (Figure 2).

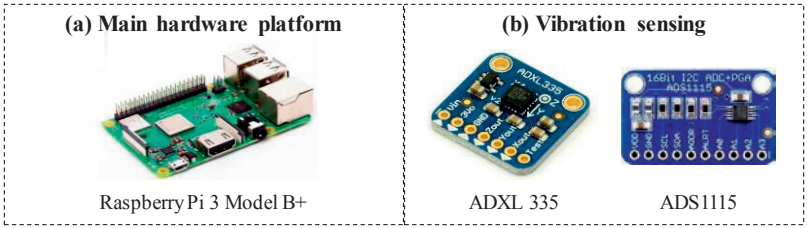

Figure 2: Hardware components of the automated cable monitoring system

RESULT

A series of experiments were conducted to validate the performance of the developed automated cable tension monitoring system under the varying tension conditions. First, the system started to acquire a cable response during 30 seconds with 100 Hz sampling rate under the impulse excitation, and an exponential window was applied to measured data to prevent spectral leakage (Figure 3(a)). The system analyzed a power spectral density using the measured response to convert time-history data to frequency domain representation (Figure 3(b)). The developed automated peak detector was applied to the image of frequency domain representation, and peaks were identified with bounding boxes (Figure 3(c)). After the post-processing for peak selection, this study examined the actual peaks with natural frequencies and corresponding mode numbers (Figure 3(d)). Based on the embedded vibration-based tension estimation method, the system calculated the cable tension force from the identified modal properties of the (Figure 3(e)). This study validated the performance of the developed automated cable tension monitoring system.

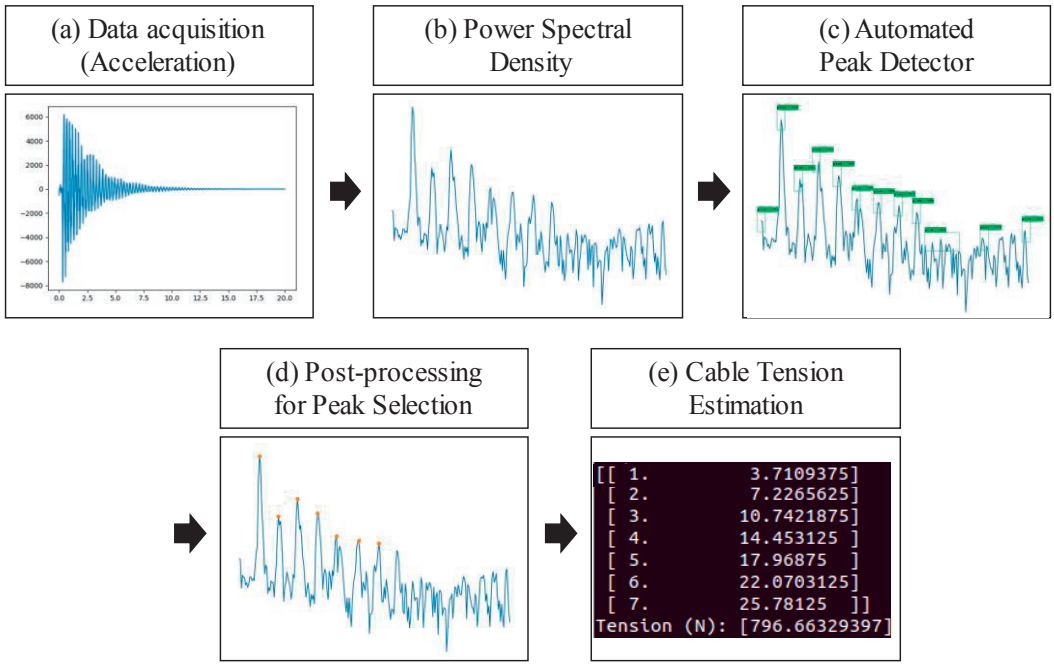

Figure 3: Results of Automated Cable Tension Monitoring

REFERENCES

[1] Shimada T. (1994) Estimating method of cable tension from natural frequency of high mode. *Doboku Gakkai Ronbunshu* 1995(501): 163-171.

VOLTAMMETRIC SENSOR FOR CHLORIDE DETECTION, OXYGEN AVAILABILITY AND HUMIDITY

A. Martínez Ibernón[1*], J.R .Lliso Ferrando[1], I.Gasch[1] , J.M.Gandia-Romero[1], J.Soto[1]

[1] *Instituto Interuniversitario de Investigación de Reconocimiento Molecular y Desarrollo Tecnológico (IDM). Universitat Politècnica de València, Camino de Vera s/n, 46022 Valencia, España. [*]E-mail: anmarib@arqt.upv.es*

ABSTRACT

The chlorides content, the oxygen availability and the amount of humidity in the cementitious matrix of the reinforced concrete structures are critical factors in the development of active steel corrosion processes. This phenomenon seriously jeopardized the structural safety of the buildings.

Therefore, the quantification of the above-mentioned factors is a key point to the buildings proper conservation. The early detection and quantification of them, allow taking preventive measures, avoiding critical deterioration states, reducing the reparation cost and minimizing the probability of structural failure.

The voltammetric sensors are capable to quantify these variables. In these sensors, is applied a non-steady voltage signal, achieving a current response associated with electrochemical phenomena in which chlorides, oxygen and humidity are involved. In addition, the electric current response depends on the type of sensor used. Thus with a different kind of sensors and by means of statistical multivariate analysis of the signal, we can isolate the different processes and identify each one with the phenomenon that governs them, furthermore quantify the mentioned parameters.

In this research, the use of silver electrodes is presented to the development of voltammetric sensors for the chlorides detection and the evaluation of oxygen and humidity availability in the concrete matrix.

In order to this, several samples of different W/C concrete ratios with silver embedded sensors were prepared. These samples were studied under different humidity conditions by means a climatic chamber. On the other hand, the samples were immersed in different concentration sodium chloride dissolution.

KEYWORDS: *Voltammetric sensors, concrete durability, chlorides penetration, oxygen availability*

INTRODUCTION

The chloride penetration and the oxygen availability and moisture content in the reinforcement concrete structures, are critical factors in the corrosion of the reinforced bars [1, 2]. Therefore, the use of monitoring systems capable to monitor the evolution of this parameters in the concrete matrix will be very effective in the development of forecasting models, these allow us to take a preventive action avoiding the damaging of the reinforced bars [1,2].

The main objective of this research was the initial study of the voltammetric silver sensor efficiency for the detection of the chlorides presences, oxygen availability and moisture content in hardened concrete.

With this purpose, two different experiences were carried out. Experience 1: The concrete samples are conditioned over different moisture conditions. Thus, different oxygen and humidity availability conditions are achieved in the concrete matrices. Experience 2: The concrete samples are submerged in dissolutions with different sodium chloride concentration. In this way, the quantity of chloride into the concrete matrices was changing with the time.

MATERIALS AND METHODS

Concrete samples of 4x4x16 cm were made; in each one were embedded two voltammetric silver sensors (Figure 1 and Figure 2).

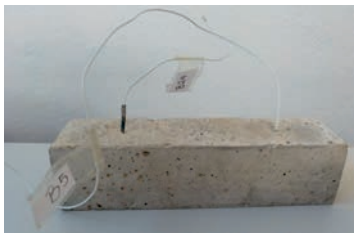

Figure 1: Concrete sample

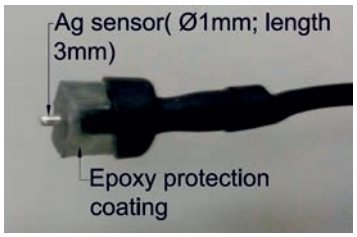

Figure 2: Voltammetric silver sensor

In order to study the response of the sensors in different types of concretes, three different concrete batches were used: w/c=0.6, w/c=0.5 y w/c=0.4.

For each concrete three mixes were made, preparing two samples for each mix. The total number of samples were 18. Nine of these samples were used in the Experience 1 and the other nine in the Experience 2.

The scenarios studied in the experiences are depicted in the **Table 1**.

In the Experience 1, the different conditions were achieved by means of a climatic chamber. Whereas, in the Experience 2 the samples were sequentially submerged in the different dissolutions.

The technique applied to obtain the variables of interest was the cyclic voltammetry [1].

Table 1: Scenarios defined in the study

	STUDIED VARIABLES	CONDITIONS
EXPERIENCE1	*Oxygen and humidity availability*	*C1: T=20°C, HR=60%* *C2: T=20°C, HR=50%* *C3: T=20°C, HR=75%* *C4: T=20°C, HR=100%* *C5: submerged* *C6: T=40°C, HR≅10%*
EXPERIENCE 2	*Cl^- presence detection*	*Water without NaCl* *Dissolution [NaCl]=0.1m* *Dissolution [NaCl]=0.25m* *Dissolution [NaCl]=0.5m*

The results were analysed and processed obtaining two parameters:

- O_2-Value: Oxygen availability identifier. It allows us to identify variations in the available oxygen and humidity into of the concrete.
- Cl^--Value: Chlorides presence identifier. It allows us to identify the presence of chlorides into of the concrete.

RESULTS AND DISCUSSION

In the Figure **3** and Figure 4 we can see the average results for the O_2-Value and Cl^--Value for each batch.

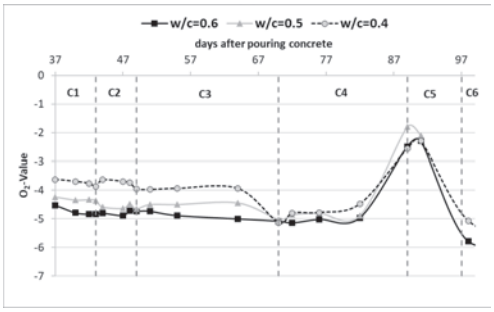

Figure 3: O_2-Value evolution over time. Average values for each batch.

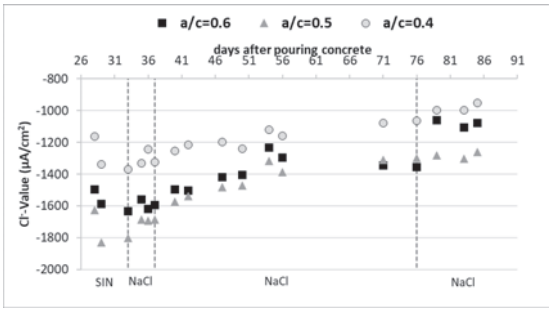

Figure 4: Cl--Value evolution over time. Average values for each batch.

Figure **3** shows how O_2-Value is different for each type of concrete for the periods C1 to C4 and C6. The higher value in absolute terms is for the less compact concrete (w/c=0.6) and the lower absolute value is for the most compactness concrete (w/c=0.4). In the high porosity concretes, there is more O_2 availability, because the high porosity makes easier the diffusion of O_2 through the concrete matrix. However, when the samples are

submerged the O_2-Value tends to be the same in all of the concretes, achieving a minimum in absolute terms. In these conditions, the available oxygen is limited by the maximum solubility of this gas in the water according to the conditions inside the matrix. Therefore, this parameter allows us to detect variations in the humidity and O_2 availability.

On the other hand, the results showed in **Figure 4**, prove as by means of the parameter Cl^--Value we can detect the presence of the chlorides in the concrete matrices and also the variation of their quantity. The higher variations of this parameter occur in the w/c=0.6 concrete. In that concrete the chlorides penetrate easier and the quantity of free chlorides is higher than in the other ones. Our sensor detects the presence of the free chlorides, which cause the localized passive layer destruction of the Steel.

CONCLUSIONS

By means of the voltammetric silver sensors, we can monitor the oxygen and moisture availability into of the hardened concrete matrix. This can allow us to define forecasting models for the prevention of active corrosion of the reinforcement bars. Moreover, it can support the detection of cracks in the concrete, due to in the cracking zone the penetration of humidity and oxygen will be occurred in a massive way, producing a sharp change in the O_2-Value.

Regarding to the chlorides detection, the developed sensor has a high potential, due to it is very sensitive even at low salt concentrations. Besides, it detects changes in the quantity of free chlorides into the concrete.

ACKNOWLEDGEMENTS

The authors would like to express their gratitude to the Spanish Ministry of Science and Innovation for the pre-doctoral scholarship granted to Ana Martínez Ibernón (FPU 13/00723). In addition, to the Universitat Politècnica de València for the pre-doctoral scholarship granted to Josep Ramon Lliso Ferrando (FPI-UPV-2018). To the Universitat Politècnica de València for the financial support in the project "Ayudas a Primeros Proyectos de Investigación (PAID-06-18)".

Also, Rafael Calabuig, Jesus Martínez and Manolo Calabuig, Laboratory technicians of the Escuela Técnica Superior de Ingeniería de Edificación of Universitat Politècnica de València, for their invaluable cooperation.

REFERENCES

[1] Ramón Zamora, J.E. (2018). Sistema de Sensores Embebidos para Monitorizar la Corrosión en Estructuras de Hormigón Armado. Fundamentos, Metodología y Aplicaciones (Tesis Doctoral). Universitat Politècnica de València, España.

[2] Correia, M. J. et al. (2006) 'Sensor for oxygen evaluation in concrete', Cement and Concrete Composites, 28(3), pp. 226–232. doi: 10.1016/j.cemconcomp.2006.01.006.

SENSOR NETWORK FOR STRUCTURAL DURABILITY CONTROL

Lliso Ferrando, Josep Ramon[1], Martínez Ibernón, Ana[1], Ramón Zamora, José Enrique[1], Bataller Prats, Román[1], Valcuende Payá, Manuel[2].

[1]*Instituto Interuniversitario de Investigación de Reconocimiento Molecular y Desarrollo Tecnológico (IDM), Universitat de València, Universitat Politècnica de València, Spain*

[2]*Departamento de Construcciones Arquitectónicas, Universitat Politècnica de València*

ABSTRACT

In recent years, one of the main issues in the structural health monitoring is to detect and control the durability loss precursors by means of non-invasive techniques. The answer to this necessity is the use of embedded multisensor systems, because they allow to real-time monitor the structure condition.

In this studio, "The Integrated Network Sensors for Smart Corrosion monitoring (INESSCOM)" is presented as an autonomous system capable to real-time monitor the steel corrosion processes in reinforced concrete structures. This system has been installed in a prototype structure where different corrosion levels have been induced in order to test the effectiveness of the sensor network. In this paper, the monitoring results collected for a period of over one year are presented.

KEYWORDS: *sensor network, corrosion, monitoring, structural durability.*

INTRODUCTION

Reinforced concrete is a widely used construction material, but there is a big concern about the damage these structures can suffer during its lifespan. Corrosion of embedded steel due to the environment where structures are located is the most critical concern [1]. These deterioration problems occur inside the piece and they can be observed outside externally once the damage is already advanced. Reparation costs are very high and most countries in the world spend a great part of the GDP in periodic repairs of reinforced concrete structures [2]. One alternative can be the periodic analysis and observation using destructive methods, but this procedure will also imply high costs and sometimes the impossibility to check zones as buried or submerged ones. Accordingly, since decades there is an increasing interest about using embedded sensors which can allow a real-time assessment of the structures in a non-destructive way. This enables to detect beforehand the aggressive agents presence and/or the corrosion processes can affect the structure durability [3].

In this paper, "The Integrated Network Sensors for Smart Corrosion monitoring (INESSCOM)" is presented. It is an autonomous system capable to monitor in real-time the corrosion processes of reinforced concrete structures [4].

EXPERIMENTAL

RCS Prototype

The structure has been designed and manufactured by the Department of Architectural Constructions of the *Universitat Politècnica de València* (UPV) and it is located at the *Escuela Técnica Superior de Ingeniería de Edificación* (ETSIE). As seen in the scheme of Figure 1, the structure is composed of a slab supported by a wall and three square-section pillars. The reinforcements were rebars of Ø 12 mm with a minimum concrete cover of 20 mm.

The water-cement ratio (w/c) of the concrete was 0.65 in all the cases. The upper part of the wall and the pillar number 3 were chloride contaminated (adding 35 g/L of NaCl to the mixing water) to accelerate the corrosion of the reinforcements (Figure 1).

INESSCOM configuration

INESSCOM is a measurement system conceived to be permanently installed in the structure and monitor all its elements simultaneously. For a complete assessment, sensors have been embedded in all the supporting elements and in the slab. As a result, 18 control points (CPs) are monitored, whose location can be seen in Figure 1.

In each CP, two embedded sensors were implemented in order to ensure the reproducibility of the measurement (Figure 2a). The working electrode was made of mild steel bar. The reference electrode was a metal / metal oxide (MMO) type in solid state. The auxiliary electrode was a stainless steel rebar of 12 mm in diameter. The corrosion rate of embedded steel is evaluated from the corrosion current density (i_{CORR}), which is determined by an approximation of the Tafel intersection technique when a sequence of potentiostatic pulses of different amplitudes are applied to the sensors [4]. In addition, a K type thermocouple was installed to monitor the temperature.

INESSCOM houses all the electronic components in an accessible central module (Figure 2b). It consists of a number of miniaturized potentiostats (as many as CP) which register the response of sensors twice a day. These electronic devices are controlled by a minicomputer that analyzes all the information and stores the real-time monitoring results in a remote server. In this case, INESSCOM is power supplied via a photovoltaic system (Figure 2c).

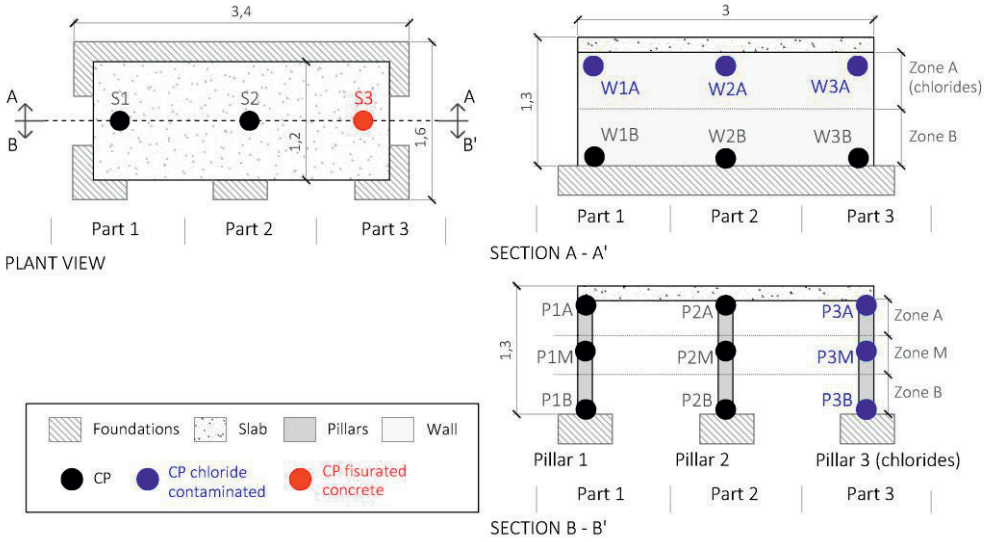

Figure 1: Scheme of the structure monitored with INESSCOM.

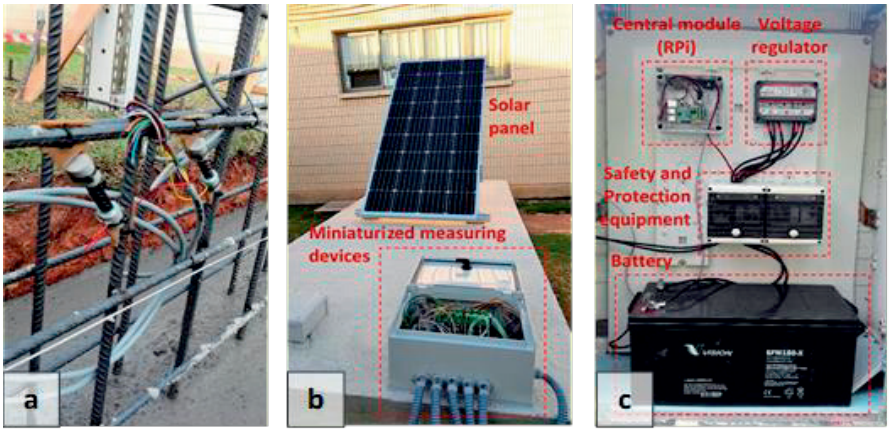

Figure 2: Main components of the INESSCOM system.

RESULTS

After more than one year operating, the INESSCOM system has been able to monitor the corrosion level of different areas of the structure. In figure 3b density corrosion (i_{CORR}) in different pillars is compared. Pillar P3A shows higher i_{CORR} since it is chloride contaminated. As a result, the passive layer of the P3A reinforcements could has been destroyed and then active corrosion processes have been enhanced. On the other hand, in figure 3a several control points of the slab are analysed. In this case, S3 zone shows higher i_{CORR} values due to a number of cracks appeared in this zone which could enhance CO_2 diffusion to the reinforcements destroying its passive layer too. In all cases, it is possible to see i_{CORR} variations are directly related with temperature fluctuations (Figure 3).

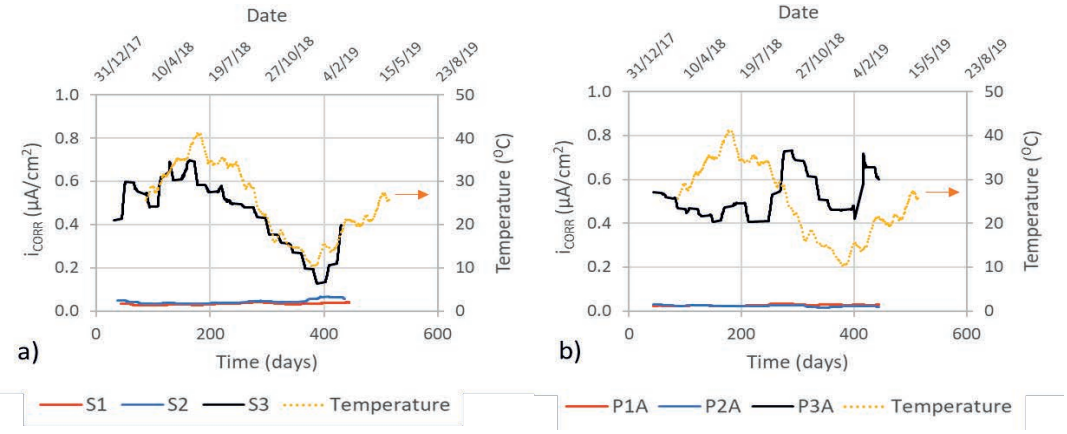

Figure 3: Corrosion current density (i_{CORR}) and temperature monitoring: slab (a) and pillars (b).

CONCLUSIONS

The INESSCOM system has been successfully installed to monitor a real structure automatically and simultaneously. In this case, 18 control points have been installed, some of them in buried zones, which are inaccessible once the prototype has been built.

The system is able to monitor, analyse and save all data automatically despite the high number of control points. In addition, the INESSCOM prototype has detected the initiation of corrosion processes in chloride contaminated areas or in cracked zones.

AKNOWLEDGEMENTS

The authors would like to express their gratitude to the Universitat Politècnica de València for the pre-doctoral scholarship granted to Josep Ramon Lliso Ferrando (FPI-UPV-2018), and to the Spanish Ministry of Science and Innovation for the pre-doctoral scholarship granted to Ana Martínez Ibernón (FPU 13/00723). To José Enrique Ramón Zamora, author of the Thesis [4], and to Karen Díaz, author of the FDT used to build the prototype presented in this paper.

REFERENCES

[1] S. G. Dong, C. J. Lin, R. G. Hu, L. Q. Li, and R. G. Du, "Effective monitoring of corrosion in reinforcing steel in concrete constructions by a multifunctional sensor," *Electrochim. Acta*, vol. 56, no. 4, pp. 1881–1888, 2011.

[2] T. H. Ha *et al.*, "Role of sensors in corrosion monitoring and durability assessment in concrete structures: The state of the art," *Sensors Mater.*, vol. 16, no. 3, pp. 133–158, 2004.

[3] J. E. Ramón, J. M. Gandía-Romero, M. Valcuende, and R. Bataller, "Integrated sensor network for monitoring steel corrosion in concrete structures," *Vitr. - Int. J. Archit. Technol. Sustain.*, vol. 1, no. 1, p. 65, 2016.

[4] J. E. Ramon Zamora, "Sistema de Sensores Embebidos para Monitorizar la Corrosión en Estructuras de Hormigón Armado . Fundamentos , Metodología y Aplicaciones," 2018.

Smart Kinesiology Tape for Human Physiological Monitoring

Yun-An Lin[1], Andrew Pedtke[2], Kenneth J. Loh[1]

[1] *Department of Structural Engineering, University of California-San Diego, La Jolla, CA, USA.*

[2] *LIM Innovations, San Francisco, CA, USA.*

ABSTRACT

Wearable sensors for human motion and physiological monitoring has attracted substantial attention in recent years, especially for applications such as sports performance, virtual/augmented reality, gesture recognition, and healthcare. Most commercial wearable sensor platforms today are based on physical electronic devices such as watches, bracelets, and necklaces, which require individuals make a conscious effort to incorporate such technologies in their daily life. In contrast, wearable sensors in the form of patches or thin films can be worn and be forgotten. Therefore, the objective of this study is to integrate sensing functionalities with kinesiology tape (K-Tape), which, on its own, is already widely used in athletics and rehabilitation. This is achieved by directly spray-coating and depositing graphene-based thin film strain sensors onto K-Tape. Upon fabricating smart K-Tape specimens, their strain sensing properties were characterized. Then, the sensor was adhered onto a subject's arm for validating its ability to capture and quantify repetitive motions. The results confirmed their stable and repeatable strain sensing performance, and this study is the first step towards designing multifunctional low-profile sensors for human motion monitoring.

KEYWORDS: *Human motion monitoring, graphene nanosheets, strain sensing, wearable*

INTRODUCTION

"Internet-of-Things" have revolutionized how individuals perceive and interact with the world on almost all facets of life. With rising global health issues as well as greater desires for improving personal wellness and health, wearable sensors have drawn immense interests due to their ability to monitor an individual continuously. For instance, many wearable sensors employ conventional accelerometers and gyroscopes, which are packaged in the form of a watch, bracelet, or necklace, as means to monitor human motion [1]. Although many commercial devices are available and are popular, these wearables require individuals make a conscious effort to incorporate such technologies in their daily life. These wearables are often too bulky, which remains to be

the major limitation for acceptance and use by certain population groups such as athletes, the military, and the elderly. Therefore, there is a need to develop lightweight, flexible, and low-profile sensors that can be mounted on an individual's skin and be forgotten by the user while continuously recording human performance-related parameters of interest. Such wearable sensors could find broad uses cases ranging from human performance assessment to personal activity monitoring to gesture recognition to rehabilitation to general health and well-being assessment.

One approach to effectively monitor human physical activity and motion is to directly measure strains on the skin. However, conventional strain gages are not suitable for this due to their rigid nature. Instead, piezoresistive nanocomposite thin films whose electrical resistance changes when strained are promising for designing low-profile, conformable, wearable sensors. For example, such strain sensors have been fabrciated using dry-spun carbon nanotube fibers embedded in Ecoflex, which is a highly flexible elastomer [2]. Wang *et al.* [3] directly printed graphene ink onto commercial medical tape to realize a wearable strain sensor. It was shown that the highly flexible printed graphene sensor could be used for monitoring physical motion, eye blinks, and pulse.

In this study, a graphene-based wearable strain sensor was designed using commercial kinesiology tape (K-Tape) as the sensor substrate. K-Tape is a highly elastic cotton tape used in sports medicine and rehabilitation, where the tape and acrylic adhesive backing are designed to pull the skin surface in a way that could either facilitate or inhibit musculoskeletal motions. This study began by spray-coating graphene nanosheet (GNS) dispersions onto masked K-Tape strips. Then, their strain sensing properties were characterized through electromechanical tests conducted using a load frame. Last, the sensor was adhered onto a subject's arm and validated for capturing repeated muscular contraction and extension motions.

SMART K TAPE FABRICATION

The smart K-Tape sensors were fabricated by integrating a sprayable GNS-based thin film with commercially available K-Tape. The GNS used here was synthesized using water-assisted liquid-phase exfoliation [4], and the ink and film formulation followed previous work by Vella *et al*. [5]. To start, poly(vinyl alcohol) (PVA) was slowly added to boiling deionized water and stirred at 300 rpm to make a 5 *wt*.% solution. Upon cooling of the solution to room temperature, a 0.1 *wt*.% GNS-PVA mixture was prepared and then dispersed by subjecting it to 1 h of high-energy probe-sonication (150 W, 22 kHz). Then, the GNS-PVA solution was sprayed using a Paasche airbrush operated at 30 psi and onto masked commercial K-Tape to form rectangular thin films on the substrate. Conductive threads were sewn at opposite ends of the GNS-PVA sensing element to form the electrodes. In addition, colloidal silver paste was also applied over the conductive threads and film to reduce contact impedance (Figure 1a).

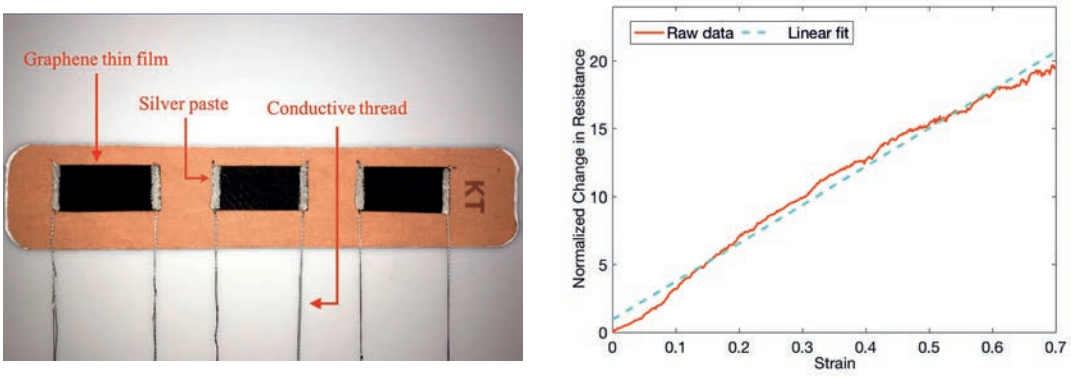

(a) (b)

Figure 1: (a) A smart K-Tape with three discrete GNS-PVA strain sensing elements is shown. (b) The normalized change in resistance of a representative smart K-Tape sensor subjected to uniaxial tensile strains is plotted with respect to the applied strains to show its near-linear performance.

STRAIN SENSING CHARACTERIZATION

The strain sensing properties of smart K-Tape sensors were characterized by subjecting them to monotonic uniaxial tensile loading (using a Test Resources 100R load frame) while simultaneously recording their electrical resistance. Each specimen was loaded to a maximum strain of 72.5% at a constant displacement-controlled rate of 5%/min. Electrical resistance was measured using a Keysight 34465A digital multimeter recording data at a sampling rate of 2 Hz. Figure 1b shows that, with increasing applied tensile strains, the electrical resistance increased as well. From Figure 1b, the strain sensitivity or gage factor was calculated to be ~ 28.

HUMAN MOTION MONITORING

The next set of tests aimed to validate the smart K-Tape sensors for characterizing human motions. Smart K-tape specimens were adhered onto the upper arm of a subject, and the subject curled and uncurled her arm for numerous cycles, which resulted in the bicep muscles to contract and expand during this test (Figure 2a). Figure 2b shows that the smart K-Tape resistance decreased when the arm was curled (i.e., when the bicep muscles contracted), and the opposite was true when the arm was uncurled and relaxed. This result was expected, since contraction of the bicep muscles would induce local compression of the skin in that area, even though that section of the upper arm physically becomes thicker. It can also be observed from Figure 2b that the smart K-Tape specimen demonstrated relatively stable and repeatable behavior.

CONCLUSIONS

In this study, a low-cost, low-profile, and high-performance wearable strain sensor was developed by depositing GNS-PVA thin films directly onto commercial K-Tape. The

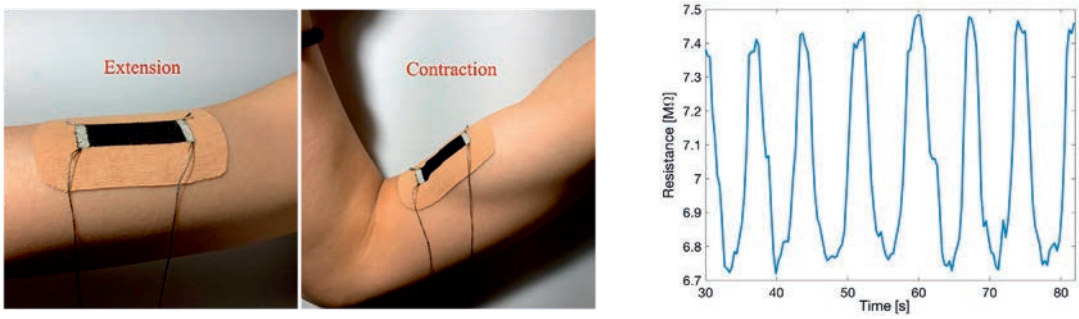

(a) (b)

Figure 2: (a) A smart K-Tape was adhered to a subject's upper arm for testing. (b) Human motion monitoring was validated, where the smart K-Tape sensor's resistance time history showed repeatable changes as the subject curled and relaxed her arm.

electromechanical properties of the smart K-Tape specimens were characterized, and it was found that its resistance increased in tandem with increasingly applied tensile strains. Its average gage factor was calculated to be ~ 28. The last set of tests validated the use of smart K-Tape for human motion monitoring. Smart K-Tape was adhered on a subject's arm, and the sensor's performance was characterized as the subject performed repetitive motions (i.e., curling and contracting/relaxing the bicep muscles). The results showed that the sensor was able to capture the subject's arm motions, and the sensing response was fairly stable and repeatable. In the near future, the smart K-Tape specimens will be attached onto different parts of the body for characterizing its ability to quantify different types of human motions and activity.

REFERENCES

[1] Cooper, G., Sheret, I., McMillian, L., Siliverdis, K., Sha, N., Hodgins, D., Kenney, L. and Howard, D., (2009) "Inertial sensor-based knee flexion/extension angle estimation." *Journal of biomechanics* 42(16): 2678-2685.

[2] Ryu, S., Lee, P., Chou, J.B., Xu, R., Zhao, R., Hart, A.J. and Kim, S.G., (2015) "Extremely elastic wearable carbon nanotube fiber strain sensor for monitoring of human motion." *ACS nano* 9(6): 5929-5936.

[3] Wang, L., Loh, K.J., Chiang, W.H. and Manna, K., (2018) "Micro-patterned graphene-based sensing skins for human physiological monitoring." *Nanotechnology* 29(10): 105503.

[4] Manna, K., Wang, L., Loh, K.J. and Chiang, W.H., (2019). "Printed Strain Sensors Using Graphene Nanosheets Prepared by Water-Assisted Liquid Phase Exfoliation." *Advanced Materials Interfaces*: 1900034.

[5] Vella, G., Gupta, S., Loh, K.J. and Netchaev, A., (2019) "Large area distributed strain monitoring using patterned nanocomposite sensing meshes." *Proceedings of SPIE – Smart Structures/NDE* 10970: 109702E.

Multi-objective optimization of actuator and sensor location of diagrid structures subjected to earthquake loading

Alejandro Palacio-Betancur[1] , Mariantonieta Gutiérrez Soto[1]*

[1] *University of Kentucky, 161 Raymond Blg., Lexington, KY 40506*

∗Corresponding author Email address: mariant.gutierrezsoto@uky.edu

ABSTRACT

Major signature structures such as the 30 St. Mary Axe in London and the Hearst Tower in New York use the diagrid structural system. The diagrid structural system has a unique geometric configuration that has structural efficiency and aesthetic potential. However, the seismic performance and vibration control of buildings designed with diagrid structural system have not been studied in depth. In this paper, a multi-objective soft-computing optimization algorithm is investigated to obtain the number and location of actuators and sensors to mitigate vibration of diagrid structures subjected to earthquake loading. A modified patented neural dynamic model of Adeli and Park is investigated to minimize the dynamic response of the building, number and placement of actuators and sensor layout. The results of the proposed methodology uses Linear Quadratic Gaussian control algorithm and floor acceleration feedback of control vibration of buildings with diagrid structural system of different diagrid angle configuration.

KEYWORDS: *Diagrid, multi-objective, optimization, neural dynamic, optimal control*

INTRODUCTION

The desire for one-of-a-kind signature structures that are comprised of high-rise and irregular buildings has increase the design and construction of the *diagrid* structural systems in recent years [1]. The traditional combination of vertical columns and horizontal beams in building structures are replaced by diagonal members with rigidly connected beams, namely the diagrid structural system. This configuration is an efficient structural system that produces, in its majority, axial loads and the shear-lag effect is lower than other structural systems [2], allowing more lightweight structures. Several efforts have been made to optimize the total weight of the structure based on the angle of the members, the aspect ratio and the shape of the building [2], [3].

Natural disasters continue to pose a great threat to critical infrastructure and are becoming more frequent, intense and costly. Earthquakes are especially unpredictable and studies on seismic performance of diagrid building structures aim to understand the failure mechanism and ductility properties [4], [5]. One of the disadvantages of this system is the lower stiffness in stories inside a module, hence, investigating advance mitigation strategies to preserve functionality and serviceability is critical. Smart

structures have technology installed to dampen the vibration caused by environmental loads. To the authors knowledge, structural control of buildings design with diagrid structural systems has not been studied in depth. This research studies optimal actuator placement for vibration control of diagrid high-rise building structures. Cha et al. [6] use genetic algorithm to obtain the layout of control devices in a structure; other optimal placement studies are found in [7]. The patented neural dynamic model (ND) for design optimization algorithm of structural buildings was introduced by Adeli and Park and also for solving problems in design of reinforced concrete flat slabs in irregular buildings [8] and vibration control of high-rise building structures subjected to seismic loading [9]. This research novelty is two-fold as it uses a modified ND to determine: a) number and placement of control devices and 2) optimal vibration control of diagrid building structures subjected to seismic loadings. The proposed method is used to find the optimal actuator layout to mitigate vibration of three building structures with different diagrid angle configurations subjected to seismic loading.

STRUCTURAL CONTROL MODEL

This study considers three steel diagrid structures with 24 stories and a story height of 3.6 m. The diagonal angles are 50˚ 67˚ and 74˚, and a floor plan as shown in Figure 1. This configuration has been used in previous studies of weight optimization and seismic performance of diagrid structures [3], [4], [5].

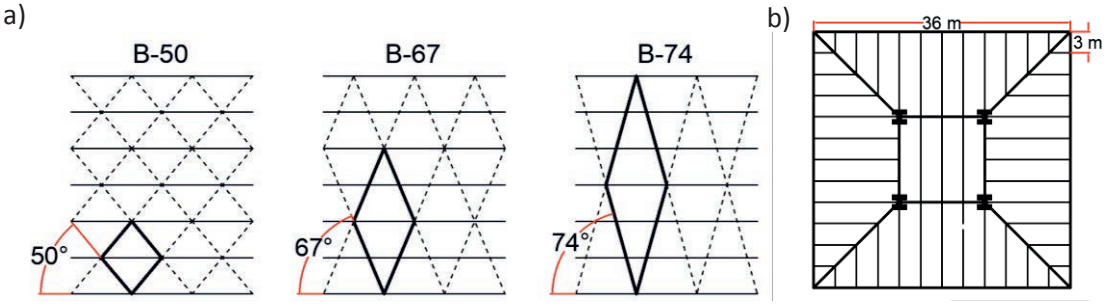

Figure 1: Buildings geometry (a) Diagrid patterns (b) Floor plan

The models of the buildings are composed of standard W steel sections and their preliminary design led to fundamental periods of 2.74, 1.93 and 1.78 s for 50˚ 67˚ and 74˚, respectively. The state space model considers feedback force for a determined vector of actuator location. This study implements the linear quadratic Gaussian (LQG) algorithm with weighted matrices $Q = [I]_{24x24}$ and $R = R_{lqg}10^{-12}[I]_{24x24}$, where R_{lqg} is a positive value adjusted to generate actuator forces lower than 200 kN, in order to compare future results with large-scale MR dampers with this capacity.

OPTIMIZATION ALGORITHM

The optimization is carried out using neural dynamics model of Adeli and Park, which is based on the integration of neural dynamics concept, Lyapunov stability theorem, a penalty function method, and the KarushKuhn-Tucker (KKT) conditions. A modified version of ND is implemented in this research to solve the multi-objective optimization of control of diagrid structure. The objective of the minimization problem is the reduction of interstory drifts and total number of actuators. The design variables (**X**) are the actuator locations and R_{lqg}. The total cost function of the nonlinear constrained multi-objective optimization problem takes the following form:

$$F_{tot}(\mathbf{X}) = \sum_{i=1}^{N} \lambda_i \rho_i F_1^i(\mathbf{X}) + \lambda_2 \rho_2 F_2(\mathbf{X}) \qquad (1)$$

Where N is the number of stories, $F_1^i(X) = \max(|d_i(t)|)$ is the maximum interstory drift, $F_2(X)$ is the number of actuators in the buildings, λ_m are relative importance factors and ρ_m are leveling factors for each objective function to ensure that each term has no undue dominance. The solution that minimizes the total cost function is subjected to 50 inequality constraints to ensure an actuator force lower than the maximum stablished and a maximum of 5 actuators in each story.

RESULTS OF OPTIMIZATION

The buildings were subjected to El Centro earthquake and the variation in performance normalized with respect to each uncontrolled structure is shown in Figure 2. The implemented approach shows an improvement in displacement for each proposed diagrid structure and the equilibrium point yields a total of 35, 29 and 26 actuators for 50˚ 67˚ and 74˚, respectively. The algorithm has a tendency of placing more actuators at the top 12 stories. The lowest improvement is on the 74˚ diagrid and the best on the 50˚ diagrid.

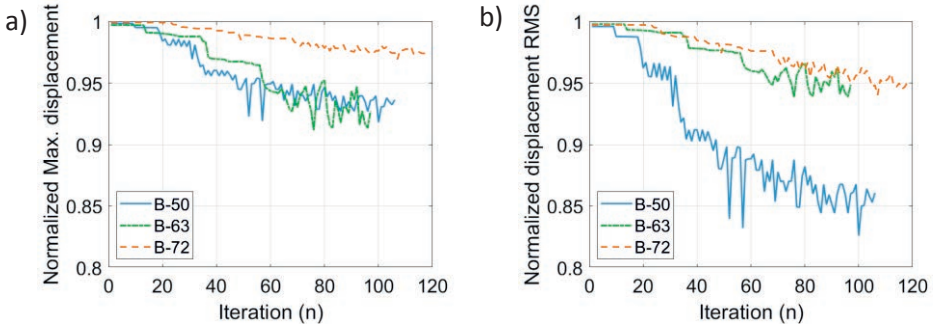

Figure 2: Results (a) Normalized max. displacement (b) Normalized displacement RMS

CONCLUSIONS

In this paper the multi-objective optimization of controlled diagrid structures is presented using a modified version of the neural dynamic model of Adeli and Park. It is the first time that ND is implemented to obtain optimal layouts of actuators inside a structure. The relative importance and leveling factors of the problem play an important role in the stability of the algorithm, they dictate the rate of change of the design variables and this problem was very sensitive to the LQG controller parameter. The variation in the total cost function is not smooth compared to other optimization problems with ND due to the sudden changes of actuator layouts. Lower values of interstory drift can be obtained if the relative importance of the actuators is reduced Future research must be done integrating the sensors as design variables in the ND optimization algorithm, implementing different controllers and subjecting the buildings to more historical and artificial accelerograms.

REFERENCES

[1] Liu, C., Li, Q., Lu, Z., & Wu, H. (2018). A review of the diagrid structural system for tall buildings. *The Structural Design of Tall and Special Buildings*, *27*(4), e1445.

[2] Shi, Q., & Zhang, F. (2019). Simplified calculation of shear lag effect for high-rise diagrid tube structures. *Journal of Building Engineering*, *22*, 486-495.

[3] Moon, K. S., Connor, J. J., & Fernandez, J. E. (2007). Diagrid structural systems for tall buildings: characteristics and methodology for preliminary design. *The Structural Design of Tall and Special Buildings*, *16*(2), 205-230.

[4] Kim, J., & Lee, Y. H. (2012). Seismic performance evaluation of diagrid system buildings. *The Structural design of tall and special buildings*, *21*(10), 736-749.

[5] Asadi, E., & Adeli, H. (2018). Seismic performance factors for low-to mid-rise steel diagrid structural systems. *The Structural Design of Tall and Special Buildings*, *27*(15), e1505.

[6] Cha, Y. J., Kim, Y., Raich, A. M., & Agrawal, A. K. (2013). Multi-objective optimization for actuator and sensor layouts of actively controlled 3D buildings. *Journal of Vibration and Control*, *19*(6), 942-960.

[7] Gutiérrez Soto, M., & Adeli, H. (2013). Placement of control devices for passive, semi-active, and active vibration control of structures. *Scientia Iranica*, *20*(6), 1567-1578.

[8] Aldwaik, M., & Adeli, H. (2016). Cost optimization of reinforced concrete flat slabs of arbitrary configuration in irregular highrise building structures. *Structural and Multidisciplinary Optimization*, *54*(1), 151-164.

[9] Gutiérrez Soto M., & Adeli, H. (2017). Many-objective control optimization of high-rise building structures using replicator dynamics and neural dynamics model. *Structural and Multidisciplinary Optimization*, *56*(6), 1521-1537.

Measurements and Health Monitoring

Inspection of Wire Breaks in Stay Cables or Post-tension Tendons

S. Joye[1], Q. Common[2], L. Laguerre[3]

[1] *Director of SHM Activities, SIXENSE, France.*
E-mail: stephane.joye@sixense-group.com

[2] *Design Office Manager and Projects Manager for SHM Activities, SIXENSE, France.*
E-mail: quentin.common@sixense-group.com

[3] *Groupe Géophysique et Evaluation Non Destructive, Laurent LAGUERRE, IFSTTAR, France.*

ABSTRACT

The following paper present the technology of acoustic detection of wire break of stay cables or pre-stressing cables. Tension wires elements in civil infrastructures are submitted to fatigue and corrosion that increase the risk of failure despites all technics operated to reduce the two phenomena. The USCAN® technology has been developed and patented by IFSTTAR and SIXENSE. It is a non-destructive ultrasonic method that allows to better know the state of the external post-tensioning cable or stay cable in order to anticipate their maintenance, plan their replacement and then avoid unexpected failure that generates a loss of serviceability of the infrastructure.

KEYWORDS: *Post-tensioning, stay cables, steel wires, acoustics, ultrasonic, corrosion.*

INTRODUCTION

Tensioned wire elements like pre-stressing and stay cables are key elements in civil structures. However, tensioned wire can be vulnerable corrosion or hydrogen embrittlement. To reduce the probability of these phenomenon's, sophisticated protection systems are used. To confirm that the design strength of the tendon is available through time, extensive inspection and maintenance regimes are required.

POST TENSIONNING CABLES

External post-tensioning cable are used in France and worldwide since the 90's. This technology has allowed for the construction of more and more complex structures increasing their main span between two piles. Stay cable, anchored at the top of the pylon and down to the deck, acts as an alternative support for the deck. On the other hand, the efficiency of the cable bears in the strength and the shape of the cable which runs along the bottom of the box girder and then rise up at their two extremities to be

anchored at the higher level of the box girder. This shape compensates the traction strength at the bottom fiber of the deck generated by the flexion of the span. Each cable is made from multi strand technology (generally 19 strands type T15,7) guided in a HDPE duct. The load is transferred from the cable to the structure by anchoring the strand individually in the two anchorages at the extremity of the cable. Anchoring is made by friction with steel wedges. Corrosion protection of the steel strands is made by injection of the general HDPE duct with cement grout. The grout also ensures the homogeneity of the cable and avoid local friction between two strands. However, the injection of the grout inside the general duct is a complex operation due to the length of the cable, the "U" shape of the cable and operability of the mixed grout. This can eventually result in local lack of concrete where the steel strands are exposed to air and later corrosion. This is particularly true at the extremities of the cable, near the anchorages where the cables are rising up. This void behind the anchorages create a strong risk of corrosion leading ultimately to failure of the wires.

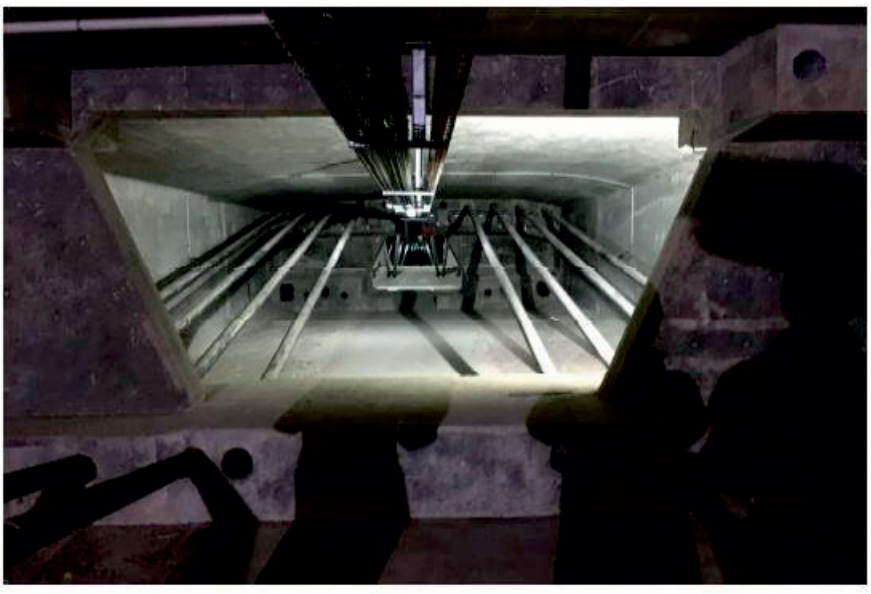

TECHNOLOGY

UScan® is a patented non-destructive testing service that applies to detect flaws in these steel wires and strands. The system is applicable to T15,7 strands (7x5mm wires) with wedge anchoring. These strands have been widely used for decades as pre-stressing active reinforcements or as stay cables. The USCAN® technology allow to detect probability of broken wires in the several decimeters behind the anchorage, where there is a risk of void in the cement grout, generating corrosion and ultimately failure. The technique is based on the fact that once an ultrasonic wave is sent from the tip of a steel wire, a reflected signal is generated once it encounters a crack/break along the wire. These reflected signals will be recorded by the system and analyzed by a qualified engineer. The wave is generated by an ultrasonic transducer held in contact of the prepared wireend. The echo in return allows the identification of the damaged wire, and the approximate location of the discontinuity in length. The detection is possible from several decimeters to a few meters, which is usually the non-accessible zone of the anchorage, where the corrosion and crack probability is the highest because of possible water presence, reduced strand protection or higher tensile stress.

APPLICATION

This technology has been applied in signatures bridges in France such as Normandy bridge since 2012 and mores recently in Ile-de-Ré Viaduct in 2018 and 2019.

CONCLUSIONS

The technic is applicable in both stay cables and post tensioning cable. It has been experience in stays cables for several years and recently applied to post-tension cables. Its ability has been demonstrated by visual confirmation of the general acoustic detection on a cable cut out from a box girder bridge in France. Considering the increasing events of external post-tensioning cable failures in the world, this technic allows to better know the state of the cables, anticipating unexpected failure and increase the safety of our infrastructure.

REFERENCES

[1] SIXENSE Data sheet : USCAN Ultra sonic detection of broken wires in strand.

Real Time Detection of Wire Failure in Stay Cables or Post-tension Tendons

S. Joye[1], Q. Common[2]

[1] *Director of SHM Activities, SIXENSE, France.*
E-mail: stephane.joye@sixense-group.com

[2] *Design Office Manager and Projects Manager for SHM Activities, SIXENSE, France.*
E-mail: quentin.common@sixense-group.com

ABSTRACT

The following paper present the technology of real time acoustic detection of wire failure on stay cables or pre-stressing cables. Tension wires elements in civil infrastructures are submitted to fatigue and corrosion that increase the risk of failure despites all technics operated to reduce the two phenomena. The EVERSENSE® Acoustic technology has been developed by SIXENSE. It is a proprietary Structural Health Monitoring technology that allows to listen and register the occurring wire failure of tensioned wires in Civil Infrastructure. It allows to better know the evolution of the state of a cable in order to anticipate their maintenance, plan their replacement and then avoid unexpected failure that generates a loss of serviceability of the infrastructure.

KEYWORDS: *Post-tensioning, stay cables, steel wires, acoustics, failure, SHM, sensors.*

INTRODUCTION

Tensioned wire elements like pre-stressing and stay cables are key elements in civil structures. However, tensioned wire can be vulnerable to fatigue, corrosion or hydrogen embrittlement. To reduce the probability of these phenomenon's, sophisticated protection systems are used. To confirm that the design strength of the tendon is available through time, specific monitoring and maintenance regimes are required.

POST TENSIONNING CABLES

Post-tensioning and Stay Cables are wildly used in France and worldwide since the 90's. Those technologies have allowed for the construction of more and more complex structures increasing their main span between two piles or pylon. Stay cable, anchored at the top of the pylon and down to the deck, acts as an alternative support for the deck. On the other hand, the efficiency of post-tensioning cables bears in the strength and the shape of the cables that run along the bottom of the girder and then rise up at their two extremities to be anchored at the higher level of the girder.

This shape compensates the traction strength at the bottom fiber of the girder generated by the flexion of the span. Both Stay Cables and post-tensioning cable are made of multi strand technology, guided in a duct. The load is transferred from the cable to the structure by anchoring the strands individually in the two anchorages at the extremities of the cable. Anchoring is made by friction with steel wedges. Despite smart design for all type of cables, local bending, lack of corrosion protection and fatigue loading leads to failure of wires though time.

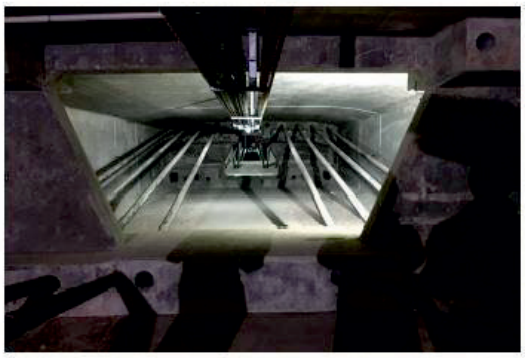

TECHNOLOGY

Sixense developed EverSense® Acoustics, a unique technology capable of detecting wire ruptures in all type cable structures: stay cable and suspension bridges, internal and external prestressed concrete structures. The system has demonstrated its capabilities to detect a single wire failures in structures, even in a noisy traffic environment.

The technology consists of an array of acoustic sensors which is distributed along the Joye, Real Time Detection of Wire Failure structure, detecting and recording the acoustic

signal. In case of a potential rupture, real time computation of the waves filters the false alarms and provides valuable information about the event: location, origin, energy, frequency, etc. The raw data for each event is kept for further analyses, including pre-trigger. Those custom filters allow the system to be very reliable, even in noisy or construction environments.

Analysis of the data: the events of interest are stored and automatically sent to Sixense' processing center for a detailed analysis by an expert engineer. A sophisticated EverSense® custom software module located in our data processing center gives a detailed analysis of each acoustic event and determinates:

- Date and time the event

- Precise localization of the event on the structure

- Origin of the event (ambient noise, wire break, expansion joint, etc.)

Each structure has its own 'acoustic response' and ambient noises. Thanks to numerous years of experience and references, our analysts are able to identify numerous different types of acoustic events, which usually occur on structures: joint expansion, construction activities, steel/concrete interface slippages, rainfalls, cable vibrations due to traffic, concrete cracks, etc.

APPLICATION

This technology has been applied in many structures worldwide (bridges stadium, nuclear, dam…) for 20 years.

CONCLUSIONS

The technic is applicable in all type of structures with tensioned wire (internal or external pre-stressing, stay cables). It has been experience in many structures with success. It can be installed independently or be integrated to a general Structural Health Monitoring architecture. It allows to follow and witness the state of a tensioned element by listening to its ageing in real time. Considering the increasing events of external post-tensioning cable failures in the world, this technic allows to better know the state of the cables, anticipating unexpected failure and increase the safety of our infrastructure.

REFERENCES

[1] SIXENSE Data sheet : SIXENSE EVERSENSE ® ACOUSTICS TECHNOLOGY: REAL TIME DETECTION OF WIRE FAILURE IN STAY CABLES OR POST-TENSION TENDONS

Experimental Model Updating of a Full-Scale Concrete Frame Structure

X. Liu[1], X. Dong[2], Y. Wang[3], R. L. Muhanna[4], F. Fedele[5]

[1,2,3,4,5] *School of Civil and Environmental Engr., Georgia Institute of Technology, Atlanta GA, USA.*

[3] *School of Electrical and Computer Engr., Georgia Institute of Technology, Atlanta GA, USA.*

[1] *E-mail: sissy.liu@gatech.edu;* [2] *E-mail: xinjundong@gatech.edu;* [3] *E-mail: yang.wang@ce.gatech.edu*

[4] *E-mail: rafi.muhanna@gatech.edu;* [5] *E-mail: fedele@gatech.edu*

ABSTRACT

In structural analysis, it is common practice to construct a finite element (FE) model of an as-built structure using nominal material properties and idealized boundary conditions. However, behaviors of the FE model generally differ from the as-built structure in the field. To minimize the differences, selected parameters of the FE model can be updated using experimental measurements from the as-built structure. This paper investigates the FE model updating of a full-scale concrete frame structure with over a thousand degrees-of-freedom. Given experimental measurements obtained during a shaker test, frequency-domain modal properties of the concrete structure are identified. A non-convex optimization problem is then formulated to update parameter values of the FE model by minimizing the difference between the experimentally identified modal properties and those generated from the FE model. The selected optimization variables include concrete elastic moduli of the columns, beams and slabs. Upon model updating, the modal properties of the FE model can match better with the experimentally identified modal properties.

KEYWORDS: *model updating, modal analysis, full-scale concrete frame*

INTRODUCTION

To a certain degree, as-built civil structure always behaves differently from its corresponding finite element (FE) model. The reason can be attributed to both model idealizations and nominal values of material properties. This paper investigates a frequency domain approach to update the material parameter values of an FE model by minimizing the difference between the experimentally identified modal properties and those of the FE model. The test structure is a full-scale concrete frame excited by a hydraulic shaker. Acceleration measurements of the structure are used to extract modal properties based on the Numerical Algorithms for Subspace State Space System Identification (N4SID). Given the experimentally identified modal properties, the

material parameters of the FE model are updated by solving a non-convex optimization problem through multiple starting points.

TEST STRUCTURE

A full-scale reinforced concrete frame is used as the test structure in this study. The story height of the reinforced concrete frame is 3.66 meters, the column spacing is 5.49 meters and the width of the two elevated slabs is 2.74 meters (Figure 1). When constructing the frame, concrete pouring was conducted in five stages, indicated by five different colors shown in Figure 1. During testing, the frame was excited in the in-plane longitudinal direction by a hydraulic linear inertia shaker mounted at the center of the second elevated slab. With a scaled El Centro record, the inertia force of the moving mass on the shaker excited the structure dynamically. Structural responses under shaker excitation were measured using accelerometers (Kinemetrics EpiSensor ES-T and ES-U) instrumented at the middle and quarter locations of columns and longitudinal beams of the frame (see Figure 1 and [1]).

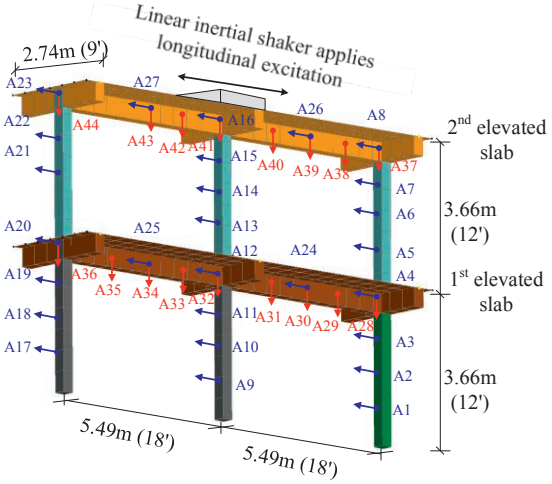

Figure 1. Accelerometer instrumentation of a full-scale test frame

MODAL ANALYSIS AND FE MODEL UPDATING

A total of 27 in-plane longitudinal and 17 vertical acceleration channels are used to perform modal analysis and FE model updating. Using the experimental measurements when the maximum displacement of the shaker mass is scaled to 25.4 mm (1 inch), modal properties of the concrete frame are obtained using N4SID (Figure 2). The first two modes mainly consist of in-plane longitudinal movement of columns. On the contrary, higher modes are mainly characterized by vertical movement of beams.

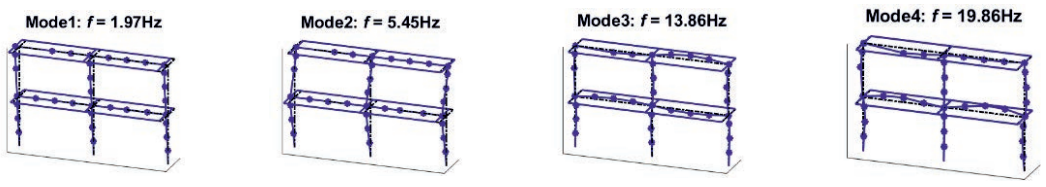

Figure 2. Experimentally identified modes under shaker excitation

An FE model of the concrete frame is built using SAP2000. The initial FE model utilizes nominal material properties of the concrete, obtained from cylinder tests for five concrete pours. To update the model, the five concrete moduli of the FE model (corresponding to

the five pours) are selected for updating. The structural stiffness matrix is thus parameterized on the five concrete moduli as $\mathbf{K}(\boldsymbol{\alpha}) = \mathbf{K}_0 + \sum_{i=1}^{n_\alpha} \alpha_i \mathbf{K}_i$. Here $\boldsymbol{\alpha} \in \mathbb{R}^{n_\alpha}$ is a vector representing the relative changes of elastic moduli from nominal values and treated as the updating variables ($n_\alpha = 5$); $\mathbf{K}_0$ is the initial stiffness matrix before model updating and using nominal concrete moduli; and $\mathbf{K}_i$ is a constant stiffness matrix contributed by structural members from one pour and corresponding to one α_i.

An optimization problem is formulated as follows to minimize the modal property differences between the FE model and experiments. Similarities in mode shapes between the FE model and experimental results are quantified using modal assurance criterion (MAC). For the i-th mode, the criterion is defined as $\mathrm{MAC}_i = \left(\left(\boldsymbol{\psi}_i^{\mathrm{EXP,m}}\right)^{\mathrm{T}} \boldsymbol{\psi}_i^{\mathrm{FE,m}}\right)^2 \Big/ \left(\left\|\boldsymbol{\psi}_i^{\mathrm{EXP,m}}\right\|_2^2 \left\|\boldsymbol{\psi}_i^{\mathrm{FE,m}}\right\|_2^2\right)$, where $\boldsymbol{\psi}_i^{\mathrm{EXP,m}}$ denotes the experimentally identified mode shape vector and $\boldsymbol{\psi}_i^{\mathrm{FE,m}}$ denotes the simulated mode shape vector at measured DOFs (from the FE model).

$$\underset{\boldsymbol{\alpha}}{\text{minimize}} \quad \sum_{i=1}^{n_{\mathrm{modes}}} \left\{ \left(\frac{\lambda_i^{\mathrm{EXP}} - \lambda_i(\boldsymbol{\alpha})}{\lambda_i^{\mathrm{EXP}}} \cdot w_{\lambda_i} \right)^2 + \left(\frac{1 - \sqrt{\mathrm{MAC}_i}}{\sqrt{\mathrm{MAC}_i}} \cdot w_{\mathrm{MAC}_i} \right)^2 \right\} \tag{1a}$$

$$\text{subject to} \quad \boldsymbol{L}_{\boldsymbol{\alpha}} \leq \boldsymbol{\alpha} \leq \boldsymbol{U}_{\boldsymbol{\alpha}} \tag{1b}$$

Here $\boldsymbol{L}_\alpha$ and $\boldsymbol{U}_\alpha$ denote the lower and upper bounds of the updating variable $\boldsymbol{\alpha}$; n_{modes} denotes the number of modes used for updating; λ_i denotes the i-th eigenvalue of FE model obtained by solving the generalized eigenvalue problem between the stiffness matrix $\mathbf{K}(\boldsymbol{\alpha})$ and mass matrix $\mathbf{M}$; λ_i^{EXP} denotes the experimentally identified i-th eigenvalue; w_{λ_i} and w_{MAC_i} denote the weights of the eigenvalues and MAC values of the i-th mode, respectively. Note here the objective function is an oracle formulation of updating variable $\boldsymbol{\alpha}$, which results in a nonconvex optimization problem. An open-source MATLAB package for structural model updating (SMU) is used to solve the optimization problem with the trust-region-reflective algorithm [2]. The upper and lower bounds of $\boldsymbol{\alpha}$ are set as 0.3 and -0.3. In this example, the weights are set the same to all four modes as $w_{\lambda_i} = 1, 1, 1, 1$, for $i = 1, \ldots, 4$. The weights for MAC values are set as $w_{\mathrm{MAC}_i} = w_{\lambda_i}$. Starting from 100 randomized points of $\boldsymbol{\alpha} \in [\boldsymbol{L}_{\boldsymbol{\alpha}}, \boldsymbol{U}_{\boldsymbol{\alpha}}]$, optimization searches are performed. Figure 3(a) plots the objective function values of the 100 runs, among which the 96th run (marked as a star) finishes as the smallest. Correspondingly, Figure 3(b) shows the optimal/updated values of $\boldsymbol{\alpha}$ from the 96th run.

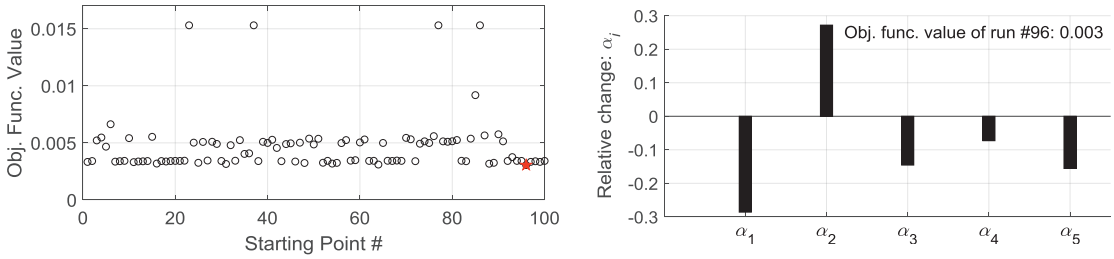

(a) Objective function values of 100 starting points (b) Updated parameters α_i from the 96th run

Figure 3. FE model updating results from 100 starting points

Finally, for both the initial model and the updated model, Table 1 summarizes the relative errors in resonance frequencies, defined as $e \triangleq \left(f_i^{\mathrm{FE}} - f_i^{\mathrm{EXP}}\right)/f_i^{\mathrm{EXP}}$, and the MAC values. Overall, a much better match in resonance frequencies of the 2nd to 4th modes is obtained, with a relatively small sacrifice in MAC values and a slight increase in the relative errors of the first mode.

Table 1. Comparison of modal properties before and after FE model updating

Mode	f_i^{EXP} (Hz)	$f_i^{\mathrm{FE,init}}$ (Hz)	e^{init}	$\mathrm{MAC}^{\mathrm{init}}$	$f_i^{\mathrm{FE,updt}}$ (Hz)	e^{updt}	$\mathrm{MAC}^{\mathrm{updt}}$
1st	1.972	1.964	-0.40%	0.999	1.952	-1.02%	0.997
2nd	5.453	5.631	3.27%	0.990	5.499	0.84%	0.990
3rd	13.861	14.957	7.91%	0.959	14.025	1.18%	0.936
4th	19.864	20.612	3.76%	0.974	19.670	-0.98%	0.969

CONCLUSIONS

In this study, material properties of a full-scale concrete frame model are updated using experimental measurements during a shaker test. A non-convex optimization problem is formulated to minimize the differences between the experimentally identified modal properties of the as-built frame and those of the initial FE model. The resonance frequencies of the updated FE model match better with the experimental modal analysis results than the initial model.

REFERENCES

[1] Dong, X., Liu, X., Wright, T., Wang, Y. and DesRoches, R. (2016) Validation of wireless sensing technology densely instrumented on a full-scale concrete frame structure. *Proceedings of International Conference on Smart Infrastructure and Construction (ICSIC)*, Cambridge, United Kingdom.

[2] Wang, Y., Dong, X., Li, D. and Otsuki, Y. SMU: MATLAB Package for Structural Model Updating, version 1.1. (2019). https://github.com/ywang-structures/Structural-Model-Updating.

Bayesian forecasting approach for structure response prediction and load effect separation of a revolving auditorium

Z. Ma, C.B. Yun, and Y.Z. Luo

College of Civil Engineering and Architecture, Zhejiang University, China.
E-mail: mazhi1224@163.com, ycb@zju.edu.cn, luoyz@zju.edu.cn

ABSTRACT

A Bayesian dynamic linear model (BDLM) is presented for a data-driven analysis for response prediction and load effect separation of a revolving auditorium structure. Analyses are carried out based on the long-term monitoring data for static strains on several key members of the structure. In this study three improvements are introduced to the ordinary regression BDLM, which are a classificatory regression term to address the temporary audience load effect, improved inference for the variance of observation noise to be updated continuously, and component discount factors for effective load effect separation. The performance of the present BDLM has been successfully verified based on the simulated data and the real data obtained from the structural health monitoring system installed on the revolving structure.

KEYWORDS: *Bayesian dynamic linear model; data-driven method; response prediction; load effect separation; revolving structure;*

INTRODUCTION

The main objective of this study is to develop a data-driven method for the prediction of stress response and the separation of various load effects for the revolving auditorium structure shown in Figure 1. This structure is a steel truss structure for outdoor musical performances. It can revolve on a track system to provide 360-degree panoramic views of the stage show and background natural landscapes. An extensive structural health monitoring (SHM) system, primarily consisting of 55 wireless channels of wireless strain sensors, was installed after the completion of construction in 2015 to assure the safety of the audience as well as the integrity of the structure [1]. This revolving structure is subjected to various uncertainties in the loading, particularly the audience load and the wheel-rail contact conditions during and after the rotating operations. Hence it is difficult to create a reliable FE model for the structure condition assessments while in service.

A Bayesian dynamic linear model (BDLM) [2] is employed in which the predictions for the responses and the state variables representing various load effects can be updated based on the new monitoring data at each time step. There have been a large volume of research works on the BDLM for various applications in the SHM field [2-4]. However, the BDLM variants used in the above studies are not suitable for the structures subjected to a large-scale temporary load (such as the audience load in this study) and various uncertainties related to environmental and operational conditions. Hence, three improvements are introduced to the general BDLM in this study.

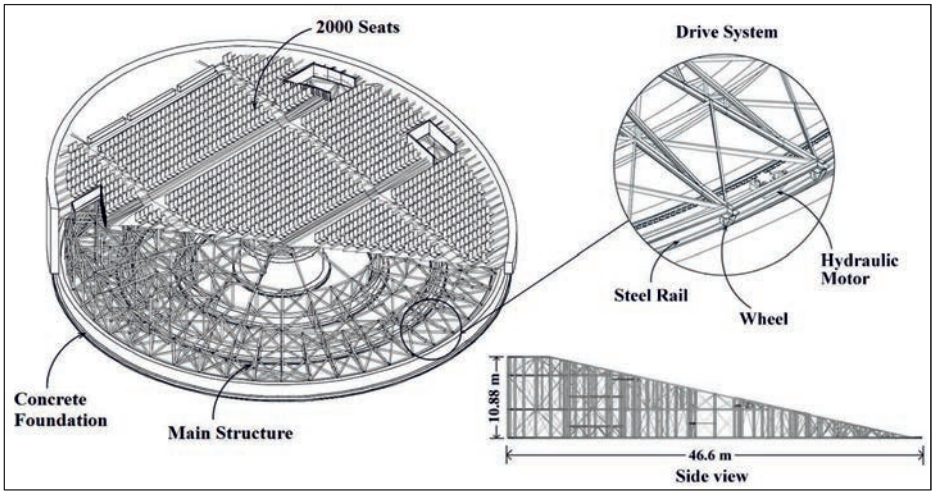

Figure 1 Revolving auditorium structure and its wheel-rail system

METHODOLOGY

Three improvements are introduced to the BDLM for the revolving auditorium in this study. First, a classificatory regression BDLM is employed to address the unknown temporary audience load effect. A classificatory regression BDLM is defined as follows:

Observation equation: $y_t = \alpha_t + \gamma_t x_t + \lambda_t z_t + v_t, \quad v_t \sim N[O, V_t]$ (1)

System equation: $\boldsymbol{\theta}_t = \boldsymbol{\theta}_{t-1} + \boldsymbol{\omega}_t, \quad \boldsymbol{\omega}_t \sim N[\boldsymbol{O}, \boldsymbol{W}_t]$ (2)

where y_t is the observed structure response at time t; $\boldsymbol{\theta}_t' = \langle \alpha_t, \gamma_t, \lambda_t \rangle$, α_t denotes the basic structural response due to the self-weight and dead loads; x_t is a measurable regression variable related to a time-varying load such as temperature; and γ_t is a regression parameter for x_t; z_t is the classificatory regression variable, $z_t = 1$ when structure is under the temporary load, $z_t = 0$ when there is no temporary load; λ_t is the temporary load effect. The posterior probability distributions for the state parameters at t and the distribution for the predicted structural response at the next time step t+1 can be obtained by Bayesian inference.

Second, the variance of observation noise (V_t) is treated as a random variable and updated along with other random variables using the Bayesian inference at each time step. It follows the inverse gamma distribution $IG[n_t/2, d_t/2]$ with the shape and scale parameters $n_t/2$ and $d_t/2$.

Finally, component discount factors are introduced to the covariance matrix of the system noise to address the different uncertainties in each state parameter, so that the load separation result can be improved.

RESULTS AND DISCUSSIONS

Verification of the present BDLM is successfully carried out using the simulation data and the real monitoring data obtained from the long-term online SHM system on the structure. To investigate the effectiveness of the model improvements, 4 different BDLMs are considered. CRICM represents the BDLM with all three improvements. CRIM denotes the BDLM with first and second improvements. CRM represents the BDLM with first improvement. RM stands for the basic BDLM with no improvement.

Figure 2 shows example cases of the predicted stress responses and the 95% confidence intervals for a column member C25 by different BDLMs. It can be found that the CRICM and CRIM gives the smallest predicted errors and confidence interval compared with the other BDLMs. The results of the load effect separation for C25 are shown in Figure 3. The mean values by CRICM are found to be consistently close to the true value, while the other results are very erroneous.

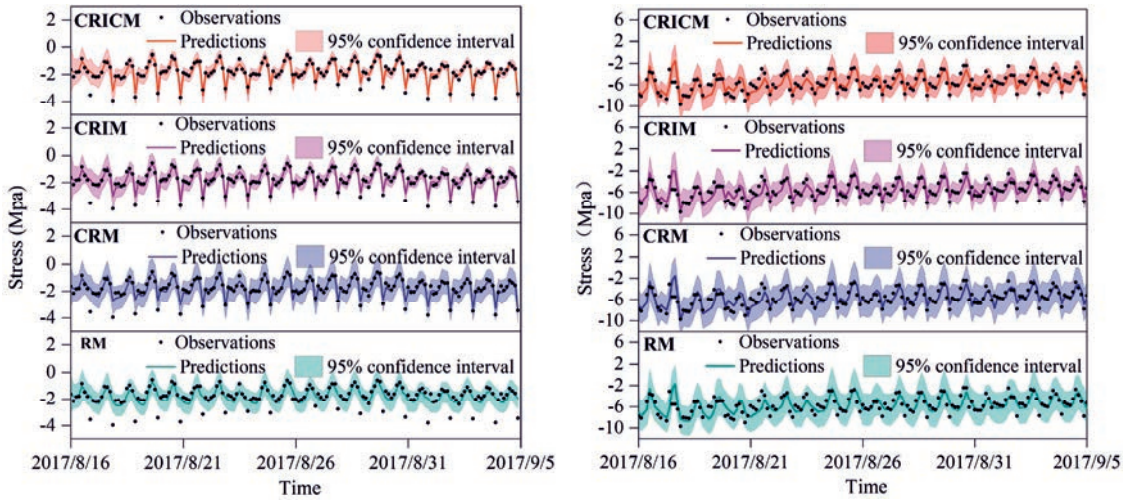

(a) Simulation study (b) Real monitoring application

Figure 2 Stress response predictions for Column C25 by four BDLMs

CONCLUSIONS

The main conclusions of this study are summarized as follows:

- The classificatory regression component brings significant improvements not only in the load effect separation for the temporary audience but also in the total stress response prediction. The results of the simulation study show that the RMSE levels of the prediction become less than 6% of the range of the observations by including the classificatory term.

- The results of confidence interval indicate that the improved inference for the variance of the observation noise results in a large improvement in the probability distribution of the prediction, which is essential for the outlier identification and reliability assessment of structures. The standard deviations of the prediction become less than 7% of the range of the observations by including the improved inference.
- The component discount factors result in significant improvements in the accuracy of the load effect separation.

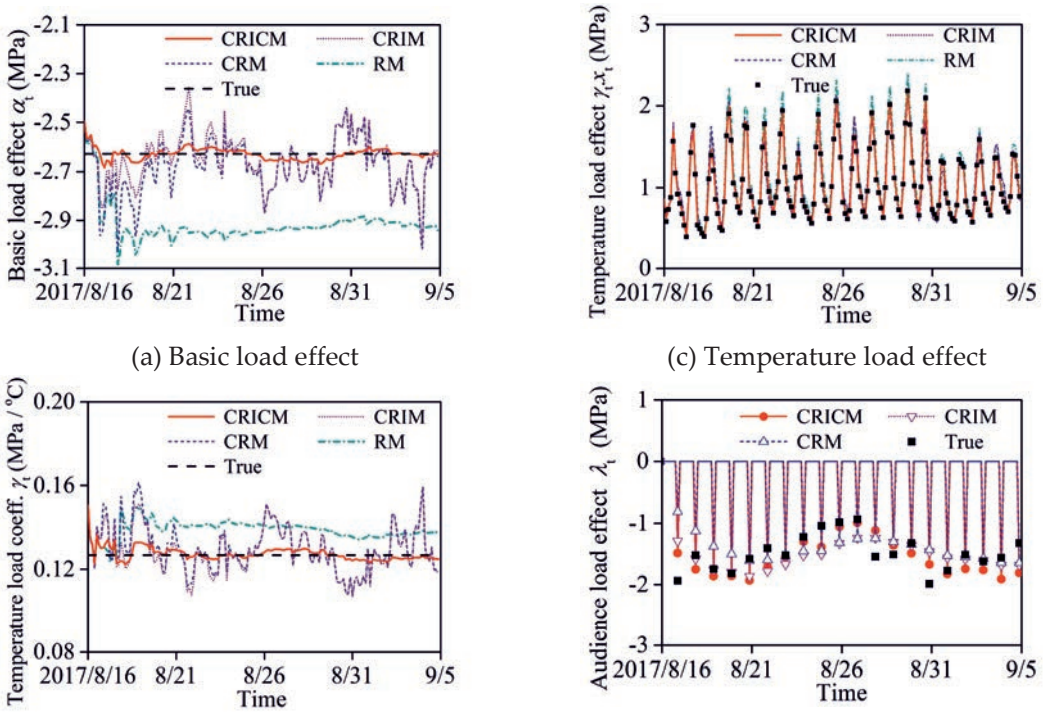

(a) Basic load effect

(c) Temperature load effect

(c) Temperature load coefficient

(d) Audience load effect

Figure 3 Load effect separation results for C25 (based on simulation data)

REFERENCES

[1] Luo, Y.Z., Yang, P.C., Shen, Y.B., Yu, F., Zhong, Z.N. and Hong, J. (2014), "Development of a dynamic sensing system for civil revolving structures and its field tests in a large revolving auditorium", Smart Structures and System, 13(6), 993-1014.

[2] West, M. and Harrison, J. (1997), Bayesian Forecasting and Dynamic Models. Springer, New York, USA.

[3] Goulet, J.A., Koo, K. (2018), "Empirical validation of Bayesian dynamic linear models in the context of structural health monitoring", Journal of Bridge Engineering, 23(2), 05017017

[4] Zhang, L.H., Wang, Y.W., Ni, Y.Q. and Lai, S.K. (2018), "Online condition assessment of high-speed trains based on Bayesian forecasting approach and time series analysis", Smart Structures and Systems, 21(5), 705-713.

Rail-strain-based identification of freight train loads

A. Pau[1], F. Vestroni[1]

[1] *Department of Structural and Geotechnical Engineering, Sapienza University of Rome, Italy.*

E-mail:{annamaria.pau,vestroni}@uniroma1.it

ABSTRACT

Increased standards of safety in railway transport require control of train loads on behalf of railway administration, in view of programmed maintenance and monitoring of wear and fatigue of rails. This paper presents a procedure that applies interpretative mechanical models to the modelling of time-histories of rail strains, in view of the identification of travelling loads. On comparing the model output to experimental time-histories, we verify their ability to describe satisfactorily the real response. Then, given a time-history of rail strains, the travelling load is identified minimizing an objective function which measures the match between the experimental time-histories and the model response in terms of curvatures. The inverse problem is solved in two steps. First, the stiffness of the foundation is identified using a known load. Then, the unknown loads are determined by a least square procedure. An application to experimental data recorded on the foot of a rail is also presented. The identified train load is finally compared to the train loads as declared by the carrier, providing satisfactory results, with mean errors around 7%.

KEYWORDS: *load identification, rail monitoring, rail strains.*

INTRODUCTION

The development of methods for the identification of travelling loads is gaining more and more interest in the industrial environment for the increased standards of safety required in the railway transport. Awareness of the loads actually travelling on railway lines enables to timely schedule maintenance and wear, as well as to check unbalanced loads which can affect vehicle safety. A one-dimensional Euler-Bernoulli beam with constant geometric and mechanical properties, resting on a linear elastic soil with viscous damping, and subjected to a Dirac delta load travelling at constant speed was used in past research to describe the response of rocket test tracks (Kenney, 1954) and train tracks (Lei, 2011). This model has proved its ability to describe the real experimental response. More complex models involving 2D descriptions of the elastic foundation were also pro-

posed (Shamalta and Metrikhine, 2002). Identification of the load involves the evaluation of the Dirac delta amplitude, which requires the solution of an inverse problem. An overview of the different approaches presented in the literature for the solution of load identification problems can be found in Ouyang (2011). It is worth citing the approach proposed by Trujillo and Busby (1997), based on dynamic programming, where not only the forcing term which provides the best match is sought, but also that which has a certain degree of smoothness according to Tikhonov's regularization. An application of dynamic programming to train load identification is presented by Zhu et al. (2013). Among other possible approaches, Ronasi et al. (2011) calculate the minimum of an objective function measuring the distance between experimental and analytical data. In the framework of an algebraic solution, Meli and Pugi (2014) made hypotheses to simplify the load time-histories and adopted a multibody model for the railway vehicle. In this paper, we present a procedure for the identification of travelling loads based on the measurement of the rail longitudinal strains at the foot of the rail.

DIRECT PROBLEM

The rail is represented as a plane beam with constant geometrical and mechanical properties resting on a linearly elastic foundation with viscous damping, and subjected to a Dirac delta load moving at constant speed v. On setting E the Young's modulus of the cross section, I its moment of inertia, w the transverse displacement, and P the amplitude of the Dirac delta, the solution takes the form

$$w(z,t) = \begin{cases} \frac{P}{EI}\left(\frac{e^{(z-vt)k_3}}{(k_3-k_4)(k_3-k_1)(k_3-k_2)} + \frac{e^{(z-vt)k_2}}{(k_2-k_4)(k_2-k_1)(k_2-k_3)}\right) & z \leq 0 \\ \frac{-P\left(\frac{e^{(z-vt)}k_4}{(k_4-k_3)(k_4-k_2)} + \frac{e^{(z-vt)k_1}}{(k_1-k_3)(k_1-k_2)}\right)}{EI(k_4-k_1)} & z > 0. \end{cases} \tag{1}$$

with k_1, k_2, k_3 and k_4 the wavenumbers. Figure 1 a shows the analytical time-history of the strains due to a series of ten Dirac loads with P=78400 N, which is approximately the load insisting on one wheel of an unalden ETR324, obtained using Equation 1 for a travelling speed of 28 km/h. Figure 1 b reports, for comparison, the experimental time-history of an ETR324, travelling at around 30 km/h. The pattern of the time-history obtained satisfactorily agrees with the time-history observed experimentally.

INVERSE PROBLEM AND EXPERIMENTAL RESULTS

The inverse problem consists in the identification of the amplitude of the train loads. The solution is obtained through minimization of the difference between the measured time-history of the strain $\boldsymbol{\epsilon}_e$ at the foot of the rail and the same quantity $\boldsymbol{\epsilon}_a$ a provided by the model. The analytical time-histories $\boldsymbol{\epsilon}_a$ a are modelled as a linear superposition of n

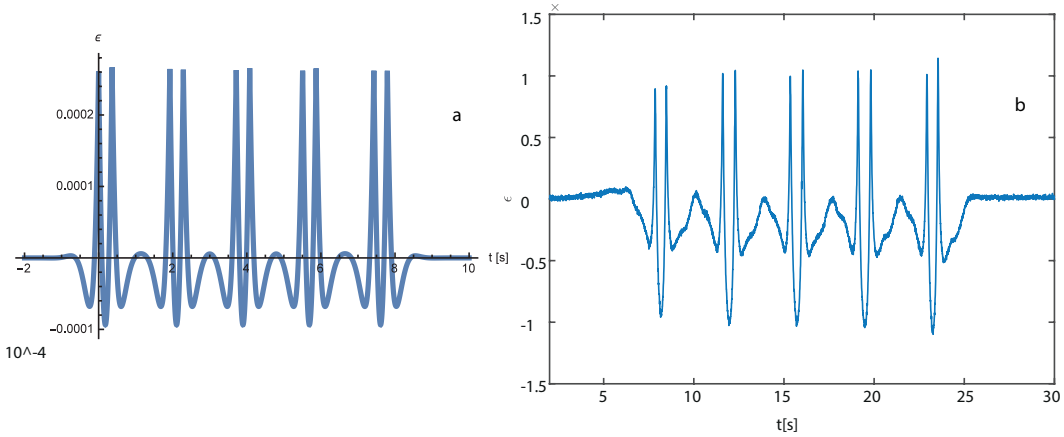

Figure 1: Analytical (a) and experimental (b) strain time-histories of an ETR324.

strains due to a unit load $\boldsymbol{\epsilon}_a^1$, expressed in N^{-1}, with coefficients P_i which are the object of identification. Since experimental time-histories are actually discrete, we will refer to them as m-length column vectors $\boldsymbol{\epsilon}_a$, whose component ϵ_j is the quantity measured at the j-th time step. The same can be done for the analytical time-histories, whose linear superposition can be written as:

$$\boldsymbol{\epsilon}_a(P_i) = \sum_{i=1}^{n} \boldsymbol{\epsilon}_a^1 P_i = \mathbf{E}_a^1 \mathbf{P} \tag{2}$$

where the vector $\mathbf{P}$ collects the unknown load amplitudes and $\mathbf{E}_a^1$ is a matrix collecting n $\boldsymbol{\epsilon}_a^1$ column vectors with m rows. The time at which the maximum of the load occurs is not considered a parameter to be identified, as it can easily be determined from the time-history. Among the system parameters which can influence the result of the load identification, the soil stiffness k_v is one of the most important. The load identification procedure is hence performed as a two-steps procedure. The first step consists in the identification of k_v: using a known load, an objective function which measure the difference between numerical and experimental data is minimized. The second step is the actual load identification. The difference between analytical and experimental data is minimized in a least-square sense, so that the vector of unknown loads is obtained as:

$$\mathbf{P} = (\boldsymbol{\epsilon}_a^{1T} \boldsymbol{\epsilon}_a^1)^{-1} \boldsymbol{\epsilon}_a^{1T} \boldsymbol{\epsilon}_e \tag{3}$$

Time-histories of strains were measured experimentally using fiber Bragg grating strain gauges, with a sampling frequency of 1000 Hz. Six sensors were installed at the foot of both rails near a station, where trains run at a speed of around 30 km/h. Freight trains only were analyzed, for some of which the loads were also declared by the carrier. Table 1 reports a sample of the results obtained for one train.

carriage #	l_d[tons]	l_i	% error	carriage #	l_d[tons]	l_i	% error
Locomotor	89	90	-1.12	14	69	69	0.00
2	31	30	3.23	15	70	71	-1.43
3	36	29	19.44	16	64	67	-4.69
4	37	35	5.41	17	63	67	-6.35
5	72	61	15.28	18	67	70	-4.48

Table 1: Sample of comparison of loads declared by the carrier (l_d) and identified (l_i) for a freight train

CONCLUSIONS

We presented an approach for the identification of travelling loads of freight trains based on the minimization of the difference between the experimental time-history of strains at the base of the rail and their analytical counterpart. The model describing the response is a one-dimensional Euler-Bernoulli beam resting on an elastic soil, whose stiffness is one of the unknowns of the problem. The load is modelled as a Dirac delta load travelling at constant speed, whose amplitude is unknown. The procedure of identification is performed in two steps, first identifying the soil stiffness, then the amplitude of travelling loads. The results obtained are compared with the loads of a train of known weights, providing satisfactory results, with mean errors of about 7%.

References

[1] Kenney J.T. (1954) Steady-state vibration of beam on elastic foundation for moving load, J Appl Mech, 76, 359-364.

[2] Lei X. (2017) Analytic method for dynamic analysis of the track structure, in High Speed Railway Track Dynamics, 37- 56, Springer.

[3] Trujillo D.M., Busby H.R. (1997) Practical Inverse Analysis in Engineering, CRC press.

[4] Ouyang H. (2011) Moving-load dynamic problems: A tutorial (with a brief overview), Mech Syst Signal Pr, 25, 20392060.

[5] Ronasi H., Johansson H., Larsson F. (2100) A numerical framework for load identification and regularization with application to rolling disc problem, Comput Struct, 89, 38-47.

[6] Zhu T., Xiao S., Yang G., Wang M. (2013)Estimation of wheel/wail contact forces based on an inverse technique, 13th International Conference on Fracture June 1621, 2013, Beijing, China

[7] Meli E., Pugi L. (2014) Preliminary development, simulation and validation of a weigh in motion system for railway vehicles, Meccanica, 48, 25412565.

Influence of directionality of bi-directional ground motions on seismic response of bridge bearings

X. He[1], A. Igarashi[2]

[1] *Department of Urban Management, Kyoto University, Japan.*
E-mail: he.xinhao.25u@st.kyoto-u.ac.jp

[2] *Disaster Prevention Research Institute, Kyoto University, Japan.*
E-mail: igarashi.akira.7m@kyoto-u.ac.jp

ABSTRACT

This study focuses on the directionality effect of bi-directional ground motions on the seismic response of bridge bearings of two types, namely the high damping rubber (HDR) bearing and the functionally discrete bearing (FDB) in their bi-directional application. Artificially generated spectrum compatible bi-directional ground motions are used as the input to specify the directionality effect in terms of the degree of the elliptic property. With a special interest in the seismic displacement response, the numerical results indicate a notable difference between the two seismic bearings to the directionality effect, even though they have almost the same level of response as in the unidirectional condition. A method of assessing the directionality effect is proposed based on a simple stochastic approximation.

KEYWORDS: *High damping rubber bearings, functionally discrete bearings, bi-directional ground motion, directionality effect, seismic performance assessment.*

INTRODUCTION

In the present practice of seismic design based on the Japanese Specifications for Highway Bridges, unidirectional seismic loads are applied in various concerned directions of bridge systems for seismic performance assessment. This concept is based on the idea that the maximum rotated elastic spectral [1] (or bi-axial spectrum) which measures the maximum value of the response spectra for the axes of input in various directions rotated on the horizontal plane is considered as an appropriate representative of bi-directional seismic demand.

On the other hand, since the response of a single-degree-of-freedom (SDOF) oscillator to the rotated ground motion can be expressed as a function of the rotation angle and time, the directionality effect of bi-directional ground motion is defined as the ratio of the minimum value to the maximum value of this function for a given period of oscillator. The fact that structural behavior can be significantly affected by the

directionality effect of bi-directional loading has been reported by a previous study [2]. It is of great importance to investigate whether the unidirectional design of bridge systems with seismic bearings satisfies the requirement of the seismic demand under bi-directional input with various degrees of directionality effect.

The spectrum compatible bi-directional accelerograms with the specified elliptical component of polarization proposed in Ref. [3] is proposed to be an appropriate solution for this purpose, since the bi-axial spectrum of the generated bi-directional input consisting of the standard and complementary ground motions is almost the same as that of the unidirectional input of the standard ground motion. In the present study, the directionality effect of the bi-directional ground motion is investigated in two types of seismic bridge bearings in their bi-directional application: the high damping rubber (HDR) bearings and the functionally discrete bearings (FDB). A method for assessment of the directionality effect is proposed based on a simple stochastic approximation.

BI-DIRECTIONAL INPUT AND MODELLING

For a given target spectrum and a spectrum-compatible unidirectional input a_x, the bi-directional accelerograms that match the target spectrum with a specified degree of directionality effect can be synthesized by the following equation proposed in Ref. [3]:

$$\begin{Bmatrix} a'_x(t) \\ a'_y(t) \end{Bmatrix} = \begin{bmatrix} \cos\theta & -\sin\theta \\ \sin\theta & \cos\theta \end{bmatrix} \begin{bmatrix} \cos\theta & \sin\theta \\ -\alpha\sin\theta & \alpha\cos\theta \end{bmatrix} \begin{Bmatrix} a_x(t) \\ a_y(t) \end{Bmatrix} \quad (1)$$

where $a_y(t) = H[a_x(t)]$ is the complementary orthogonal component corresponding to $a_x(t)$, by applying Hilbert transform. The constant α represents the elliptical component, which implies the degree of directionality effect ranging from zero to unity, and θ is the major direction angle. When α is equal to unity, it is a non-directivity case with uniform contribution over all directions, while a smaller value indicates a greater fluctuation of intensity among various direction. The standard design ground motions in the Japanese Specifications for Highway Bridges, are used as original components considering different ground condition and intensities: II-I-1, II-II-2, II-III-3, II-I-1, II-II-2, II-II-3, II-III-3.

The dynamic response of a straight girders bridge supported by single columns with the HDR or FDB in their bi-directional application is investigated. The system is simplified as a lumped mass type with two translational DOFs in the horizontal plane in a single span. The assumed weight of the superstructure is 900 tons.

The FDB system consists of the pure friction bearings and linear elastomeric bearings set in parallel. The linear spring representing the behavior of elastomeric bearings are independently applied in the longitudinal and transverse directions. The Coulomb model with a circular interaction surface is used to represent the bi-directional coupled effect of the friction force in the pure friction bearings. The magnitude of the friction

force is proportional to the friction coefficient and the self-weight of the girder. Two cases of linear spring stiffness with natural periods of 1.0 and 2.0 sec are assumed. The friction coefficient is 0.15.

The modified Park-Wen model [4] to represent the bi-directional behavior of HDR is used. The effect of bi-directional shear strain components at high strain levels involving increased hysteretic energy dissipation is included with the use of the modified Park-Wen model. The planar dimensions of each layer of sample rubber are 160mm×160mm, with a total thickness of 10mm in 4 layers. The size scale factor is selected as 3.38, and five bearings are set in parallel in this study.

NUMRICAL RESULTS AND ASSESSMENT

The relationship between the maximum absolute response of the bearings and the level of elliptical component compared with the maximum response in the unidirectional input case is shown in Figure 1. It is observed that the effect of the elliptical component value on the maximum response is different depending on the bearing type. Despite some variation due to the ground motion characteristics, the maximum response of HDR tends to decrease with a higher elliptical component, while the opposite tendency is shown for FDB. As indicated in the hysteresis loops of the two seismic bearings in Figure 1, the energy dissipation of these devices subjected to bi-directional displacement loading are considerably affected by the directionality effect. The different tendencies of the maximum response can be reasonably explained by this mechanism.

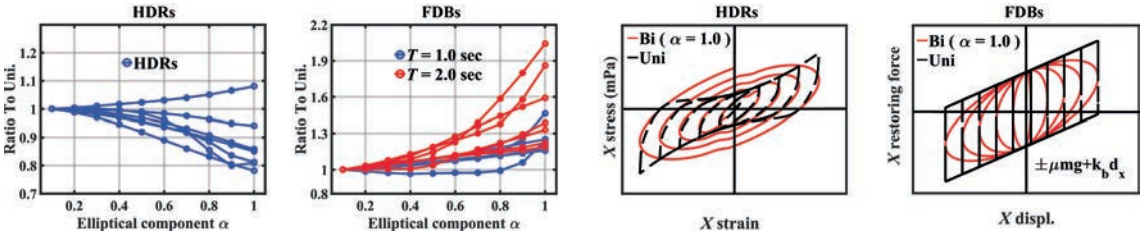

Figure 1: Directionality effect of bi-directional loadings on maximum response and the hysteresis loops

In order to estimate the statistical variance of the response under bi-directional loading to that under unidirectional loading, application of a simple stochastic dynamic approximation with white-noise excitation to a SDOF system is investigated. The equivalent stiffness and damping ratio are evaluated by applying bi-directional displacement loading with various amplitudes and specified elliptical component on the original bi-directional model. The ratio of statistical variance of the response under bi-directional loading to that under unidirectional loading is obtained in Figure 2. It is noted that the results for FDB are almost similar for two natural period cases.

The ratio of the statistical mean of the maximum response for the bi-directional case to that of the unidirectional case are shown in Figure 3. A good agreement with Figure 2 can be seen.

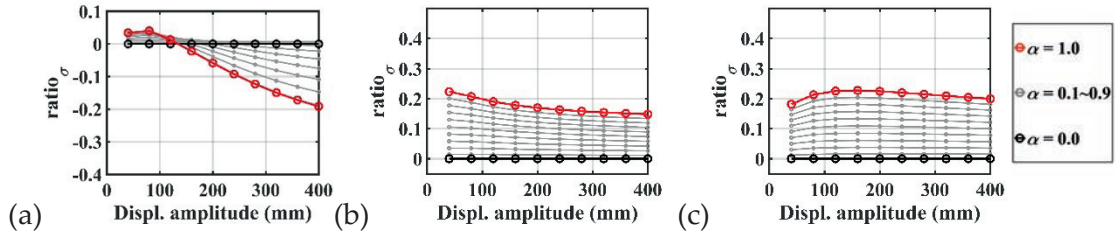

Figure 2: Response variance ratio with various elliptical components (a) HDRs, (b) FDB, $T = 1.0$ sec, and (c) FDB, $T = 2.0$ sec

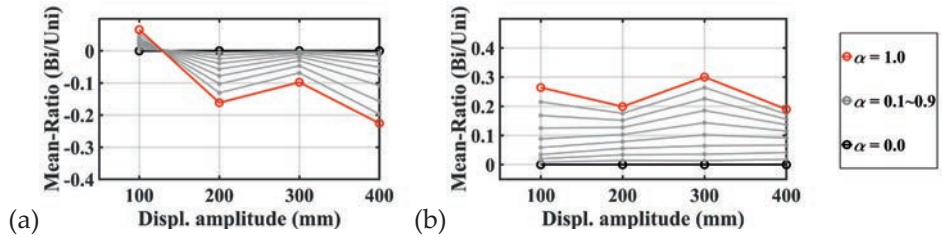

Figure 3: Response mean ratio of maximum response with various elliptical components (a) HDRs, (b) FDBs

CONCLUSIONS

The influence of the directionality effect of spectrum compatible bi-directional input on the maximum response of bi-directional seismic bearings of two types is investigated. The maximum response of HDR tends to decrease with a higher elliptical component, while the opposite tendency is shown for FDB. It is observed that the equivalent stiffness and damping ratio of restoring force in the two bearings undergo significant change under the bi-directional loading with specified directionality effect due to the bearing's path-dependence feature. A method of assessing the directionality effect is proposed based on a simple stochastic approximation.

REFERENCES

[1] Grant, D. N. (2010). Response spectral matching of two horizontal ground-motion components. *Journal of Structural Engineering*, 137(3), 289-297.

[2] Liu, Y., & Igarashi, A. (2017). Characterization of radial and circumferential mechanical energy components in bi-directional nonlinear seismic response of steel bridge piers. *Procedia engineering*, 199, 3009-3014.

[3] Igarashi, A., & Gigyu, S. (2015). Synthesis of spectrum-compatible bi-directional seismic accelerograms with target elliptical component of polarization. *Earthquake Resistant Engineering Structures X*, *WIT Transactions on The Built Environment*, 152, 63-72.

[4] Dang, J., Igarashi, A., & Murakoshi, Y. (2016). Development of Hysteretic Model for High-Damping Rubber Bearings Under Bi-Directional and Large Strain Domain Loading. *Journal of Japan Society of Civil Engineers, Ser. A1 (Structural Engineering & Earthquake Engineering (SE/EE))*, 72, 250-262. (in Japanese)

Monitoring-Driven Seismic Assessment of Existing Masonry Buildings

P. Martakis[1*], Y. Reuland[2*], V. Dertimanis[1], E. Chatzi[1], P. Lestuzzi[2]

[1] *Institute of Structural Engineering and Monitoring, ETH, Zurich, Switzerland.*
**E-mail: martakis@ibk.baug.ethz.ch*

[2] *Applied Computing and Mechanics Laboratory (IMAC), EPFL, Lausanne, Switzerland*
**E-mail: yves.reuland@epfl.ch*

ABSTRACT

Earthquake is the natural hazard with the largest loss potential even for places of moderate seismicity. Central Europe has not experienced strong ground motions in the past century, in contrast to the Mediterranean countries, where earthquake triggered massive seismic retrofit campaigns and the adaption of strict regulations for the seismic design. A large part of the existing building stock in central European countries is not designed to fulfill the current seismic standards, while most of them have already exceeded the design life span. Unfortunately, the seismic assessment of existing buildings is undermined by the perception that low probability translates to low risk, which is misleading due to the high consequences of rare earthquake events.

Given the inherent uncertainties of masonry as a composite material and the corresponding difficulty to capture reliably the nonlinear response of such structures, data-driven health monitoring provides an efficient way to reduce the epistemic uncertainty, to validate the modeling assumptions, and to identify the structural health of existing buildings. This work comprises an effort to summarize those SHM methodologies, featuring an advanced technological readiness level, for the seismic assessment of existing masonry buildings. An outline of the structural categorization of the existing masonry building stock with a focus on central Europe is also pursued. Finally, a state-of the-art SHM concept is designed for a typical masonry building in central Europe and discussed from the practitioner's point of view.

KEYWORDS: *SHM, Seismic assessment, Ambient vibration, Masonry buildings*

INTRODUCTION

The rapid development in sensor technology allows engineers to gather huge amounts of data by measuring the response of real structures. This information, though potentially informative for designers and researchers, is not easy to manage and requires firm knowledge in a wide spectrum of different disciplines to be interpret. System identification methods, nonlinear structural dynamics and data analysis should be

implemented to make use of the available information. While such practices are often considered as costly for the assessment of common building structures, they inevitably resurface as unexploited potential after catastrophic events. Scope of this work is to apply advanced monitoring methodologies in order to increase the reliability of the seismic assessment of existing buildings.

EXPERIMENTAL MODAL ANALYSIS AS A TOOL FOR THE SEISMIC ASSESSMENT OF EXISTING BUILDINGS

The seismic assessment of existing structures consists a major challenge for practicing engineers due to lack of available structural information. The non-standardized materials, the usually incomplete documentation, the effect of ageing and the unclear boundary conditions inflate the uncertainty of engineering judgement. Particularly in places of moderate seismicity the lack of recent events prevents a realistic assessment of the seismic performance, while enhancing the misleading perception that low seismic hazard translates to low seismic risk. Several researcher have shown that experimental modal analysis (EMA) provides an elegant and cost-effective way to reduce these uncertainties by measuring the global dynamic response of the examined structure under ambient excitation ([1], [2]). Although EMA is based on small levels of excitation, the derived structural properties are invaluable for the reduction of the uncertainties in the equivalent elastic range and for the interpretation of the response in the nonlinear range [3]. Snoj et al [4] highlight through a parametric study the importance of the identified elastic properties of existing structures for the reliable assessment of the nonlinear response. The variation of the elastic properties due to the excitation amplitude were thoroughly examined by [5], [6]. The experimental findings confirmed that for response amplitudes ranging between 10^{-5} g and 10^{-2} g, the identified elastic properties do not show significant variability. Consequently, ambient vibration tests are sufficient to identify the structural behavior in the equivalent elastic domain.

APPLICATION ON A CASE STUDY

In order to illustrate the benefits of ambient vibration measurements for the seismic assessment of existing buildings, a typical case study of a masonry building constructed at the end of 19th century is presented. The available structural information comprises an incomplete set of drawings, most of them referring to the numerous retrofit works. Based on the available data and extensive visual inspections, the geometry of the building was retrieved with adequate confidence (Figure 1). The properties of the masonry material, however, cannot be justified a priori and thus they induce a significant uncertainty in the analysis. The current guidelines provide a span for the elastic properties of unknown masonry material ranging between ± 70 % of the mean value. A parametric analysis on the seismic performance of the structure has exposed

high sensitivity of the performance point to changes of the elastic properties. Considering the large variability of the suggested values, a reduction in the uncertainties is essential for a reliable assessment of the seismic performance. Plenty of destructive and non-destructive methods have been developed so far for the estimation of elastic and capacity properties of masonry. Yet, it should be noted that these methods are rather costly and highly depended on the local conditions of the tested area. On the contrary, ambient vibration measurements offer an insight into the global response of the structure at a significantly lower cost.

A monitoring concept tailored to the specific structure is designed to identify the natural frequencies and the governing modal shapes (Figure 1). Since the contact conditions between the studied and the adjacent building are unknown, a further goal of the monitoring concept is to verify the usual hypothesis that the two buildings are separated through a gap and can be analyzed independently. Since the structural integrity and the vulnerability of the masonry walls against local (out of plane) failure mechanisms are strongly depended on the floor stiffness, the monitoring concept was conceived to provide information regarding the in plane stiffness of the wooden girder floors. Finally, yet importantly, sensors have been placed in the basement as well as outside the building in order to capture the effect of the foundation impedance.

A typical response of the system in time-frequency domain is presented in Figure **2** (right). SHM algorithms allow for the extraction of the modal properties that can be implemented for the calibration of the uncertain material properties and the validation of the assumptions regarding the floor stiffness and the boundary conditions. Overall, the presented monitoring concept offers an efficient and cost-effective solution to enhance the reliability of the seismic assessment of existing buildings.

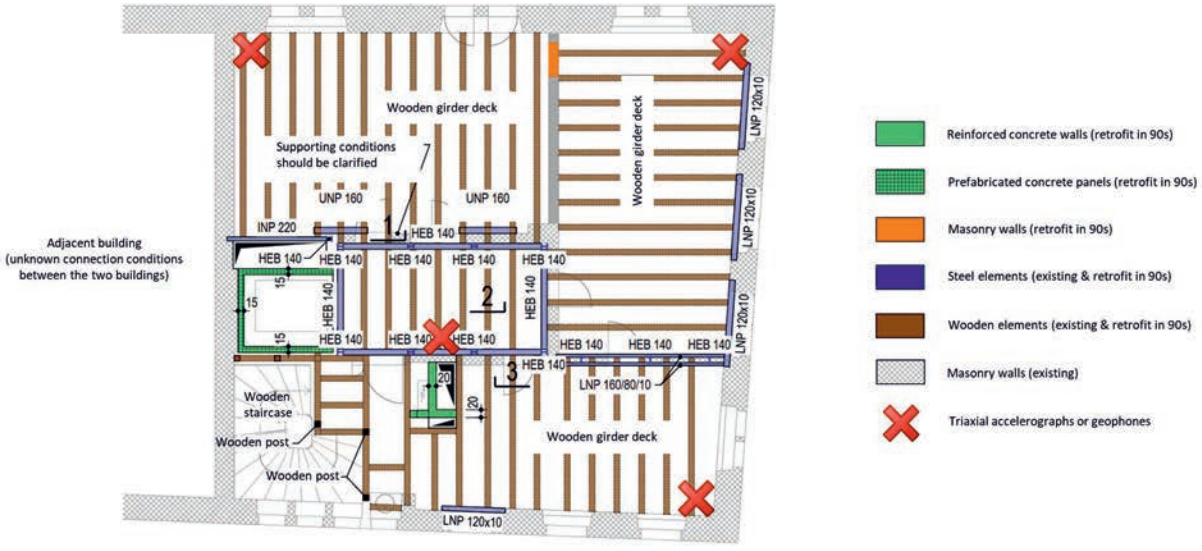

Figure 1: Structural information and sensor positions for a typical floor.

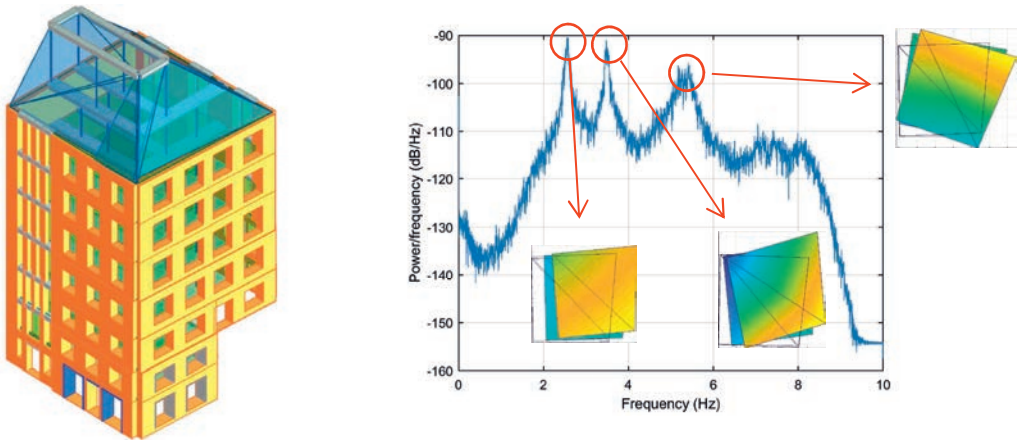

Figure 2: *Left:* 3D view of the numerical model, *Right:* Typical response in Frequency domain with schematic representation of the identified characteristic modes.

CONCLUSIONS

A significant part of the existing building stock in places of low-to-moderate seismicity is not designed to fulfill the current seismic standards, while most of the existing buildings have already exceeded the design life span. The seismic assessment of such structures is challenging due to the lack of structural data and the large uncertainties pertaining to material properties and boundary conditions. Ambient vibration measurements in conjunction with the implementation of SHM methodologies provide an efficient and cost effective solution to reduce these uncertainties and enhance the reliability of the seismic assessment of existing structures.

REFERENCES

[1] K. Kusunoki, D. Hinata, Y. Hattori, and A. Tasai, "A new method for evaluating the real-time residual seismic capacity of existing structures using accelerometers: Structures with multiple degrees of freedom," *Japan Archit. Rev.*, vol. 1, no. 1, pp. 77–86, 2018.

[2] C. Michel, A. Karbassi, and P. Lestuzzi, "Evaluation of the seismic retrofitting of an unreinforced masonry building using numerical modeling and ambient vibration measurements," *Eng. Struct.*, vol. 158, no. December 2017, pp. 124–135, 2018.

[3] M. D. Trifunac, "Comparisons between ambient and forced vibration experiments," *Earthq. Eng. Struct. Dyn.*, vol. 1, no. 1972, pp. 133–150, 1972.

[4] J. Snoj, M. Österreicher, and M. Dolšek, "The importance of ambient and forced vibration measurements for the results of seismic performance assessment of buildings obtained by using a simplified non-linear procedure: Case study of an old masonry building," *Bull. Earthq. Eng.*, vol. 11, no. 6, pp. 2105–2132, 2013.

[5] S. Hans, C. Boutin, E. Ibraim, and P. Roussillon, "In situ experiments and seismic analysis of existing buildings. Part I: Experimental investigations," *Earthq. Eng. Struct. Dyn.*, vol. 34, no. 12, pp. 1513–1529, 2005.

[6] C. Michel, B. Zapico, P. Lestuzzi, F. J. Molina, and F. Weber, "Quantification of fundamental frequency drop for unreinforced masonry buildings from dynamic tests," *Earthq. Eng. Struct. Dyn.*, vol. 40, no. 11, pp. 1283–1296, Sep. 2011.

A Spectral Peak-Picking Method for On-board Operational Modal Analysis of Multi-type Vibration-based SHM

F. Zonzini, M. M. Malatesta, D. Bogomolov, N. Testoni, L. De Marchi, A. Marzani

Advanced Research Center on Electronic Systems "Ercole De Castro" (ARCES), University of Bologna, Italy.

E-mail: federica.zonzini@unibo.it (F.Z.), michelange.malatest2@unibo.it (M.M.M.), denis.bogomolov2@unibo.it (D.B.), nicola.testoni@unibo.it (N.T.), l.demarchi@unibo.it (LDM), alessandro.marzani@unibo.it (AM)

ABSTRACT

This paper outlines a versatile and effective method for operational modal analysis of vibrating structures. Considering the quasi-sinusoidal dynamic regime of civil infrastructures, the technique extrapolates modal parameters exploiting a Spectral Peak-Picking (SPP) algorithm. The proposed approach has three main advantages: i) it is not based on a priori modal information; ii) it is applicable for inspecting both translational and rotational signatures of vibrating structures, iii) it inherently supports the design of parallel and automated modal analysis systems. The technique was successfully applied to translational and rotational mode shapes experimentally extracted from a pinned-pinned steel beam. The implemented SPP is highly coherent with respect to theoretical predictions and substantially equivalent to traditional eigen-based techniques, which are very onerous and must be computed in a centralized manner. As such, the proposed method is favorable for distributed, large scale, and heterogeneous monitoring solutions, where minimizing communication bandwidth and power consumption is a primary requirement.

KEYWORDS: *multi-type sensor node, rotational displacement mode shapes, spectral peak-picking algorithm, translation displacement mode shapes.*

INTRODUCTION

In the wide field of vibration-based Structural Health Monitoring (SHM), inclinometers have been scarcely adopted to measure structural vibrations due to the poor low-frequency sensitivity of gyroscopes, which makes them unsuitable for civil applications, where the frequency range of interest is quite low. Consequently, they are less often adopted for modal analysis purposes, too. This work introduces an effective method to infer modal information from tilt signals, gathered from gyroscopes, based on a combined exploitation of spectral analyzers and Peak-Picking (PP) algorithm. A similar technique, devised in Ref. [1] for an automated modal parameters estimation by means of a Wireless Sensor Network (WSN) of accelerometers, has proved to be effective in

signal compressing, time-saving and accuracy of inspection. The novelty of the approach here proposed consists in feeding the algorithm either with acceleration and tilt angles, to extract translational displacement mode shapes (TDMS) and rotational displacement mode shapes (RDMS), respectively.

SPECTRAL PEAK-PICKING METHOD FOR OPERATIONAL MODAL ANALYSIS

Eigen-based approaches, Frequency Domain Decomposition (FDD) [2] being among them, are usually applied to extract modal coordinates. To account for the demanding computational costs involved in these procedures, in this work a "sensor-near-electronic" paradigm is adopted, tackling real-time functionalities and early damage detection. Considering a quasi-sinusoidal dynamic regime, typical for civil structures, this strategy exploits the spatial dependency of energy embedded within vibration signals. Therefore, the parallel estimation of sensor-driven spectra followed by PP algorithms replaces the SVD of acquired data performed in a centralized manner. The proposed processing scheme is addressed to as Spectral Peak Peaking (SPP). Basing on the desired number of m output modal components, a handshake method discerns among real and spurious peaks. First, the Fast Fourier Transform (FFT) of the data recorded by each of the n sensing units is obtained. Then the m most energetic acceleration and angular spectral peaks and their correspondent modal frequencies are extracted by means of PP techniques. These modal values are then forwarded to a majority voter: its output is the most probable set of modal frequencies the structure is really experiencing. Designed as a 2-step voter, it acts separately on acceleration and tilt peaks, comparing the n tuples of m values extracted by each sensing unit. A candidate frequency is selected if at least $n/2 + 1$ sensors identify it. The resulting peak sets are then combined to notify back to every node a common set of spectral bands inside which the PP algorithm must be instructed to find local maxima and their associated spectral coordinates. The outcome of this process forms the final m-tuple of n modal values to designate the m global mode shapes. Since spectral maxima are positive quantities, the proposed algorithm only provides the magnitude of inspected curves, disregarding any phase information. This also helps to avoid the real mode shapes variability in terms of sign across the nodal values. Our approach, not requiring an *a priori* knowledge about the physical quantities of the signals, is better suited to reconstruct mode shapes in complex, heterogeneous frameworks.

EXPERIMENTAL RESULTS

A simply supported steel beam was instrumented with a network of seven sensor nodes, equipped with DSP functionalities to on-line extract accelerations and tilt values [3-4]. The nodes were designed to best exploit the peculiarity of acceleration and tilt signals to capture the same vibrational signature in two different directions: while spectral

contents are similar, the modal relation occurring in the spatial domain makes RDMS the derivative of TDMS. Following this observation, devices were installed exactly in correspondence of nodal and antinodal points of the first three modal components, strictly symmetric with respect to the mid-span, as sketched in Fig. 1.a.

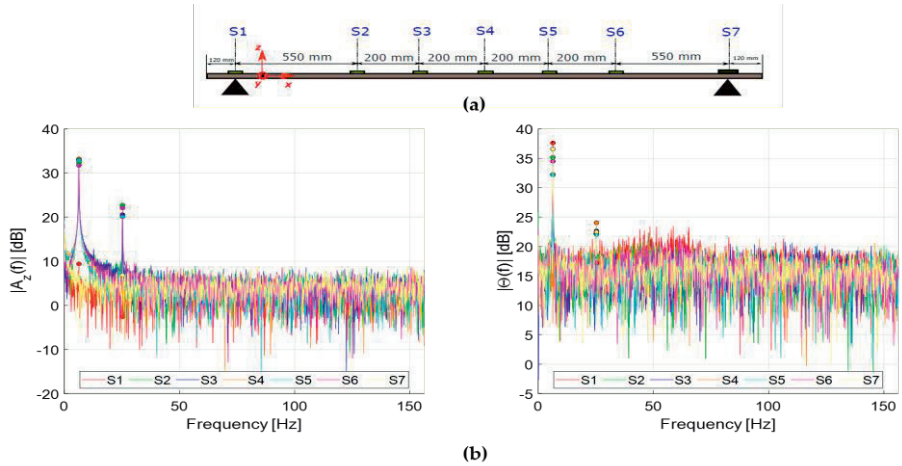

Fig. 1 (a) Schematic view of the instrumented beam and (b) spectral trends of acceleration (left) and tilt signals (right) computed by means of FFT with identified peaks correspondent to the first and second mode of vibration.

Therefore, 4 was chosen as the majority threshold in the frequency selection procedure. The dynamic behavior of the beam was induced by means of hammer strikes at the mid-point between sensors S_5 and S_6, allowing the first odd modal component to be excited. Predictions about the expected dynamic response of the structure were made using a Finite Element discretization of the beam based on its physical and geometrical properties (discussed in [4]). Sets of $\boldsymbol{N_s}$=2500 samples were collected at a sampling rate $\boldsymbol{f_s}$=312.5 Hz. This configuration allows to inspect up to the first two modes, theoretically estimated at $\boldsymbol{f_1}$= 6.332 Hz and $\boldsymbol{f_2}$= 25.33 Hz according to a length of $\boldsymbol{L = 1900\,mm}$. Voted vibration frequencies were experimentally estimated to be $\widehat{\boldsymbol{f_1}}$=6.394 Hz and $\widehat{\boldsymbol{f_2}}$=25.31 Hz, resulting in a worst-case error of $\boldsymbol{0.062\,Hz}$, inferior to the frequency resolution $\boldsymbol{\Delta_f = f_s/N_s = 0.125\,Hz}$, which confirms the high spectral consistency of acquired data. Spectral magnitudes $\boldsymbol{|A_z(f)|}$ and $\boldsymbol{|\Theta(f)|}$, respectively referred to acceleration and tilt values, are depicted in Fig. 1.b.

Spectral envelopes computed on acceleration-driven signals appear sharply defined, with high Signal-to-Noise Ratio (SNR), and precisely concentrated around single spectral bands. The influence of noise on rotational spectra reduces estimation accuracy, especially in the proximity of the second modal component. In Fig. 2, reconstructed TDMs and RDMs are superimposed to the outputs of the classical FDD method, whereas point-wise Modal Assurance Criterion (MAC) percentages between numerical and experimental shapes are reported in legend.

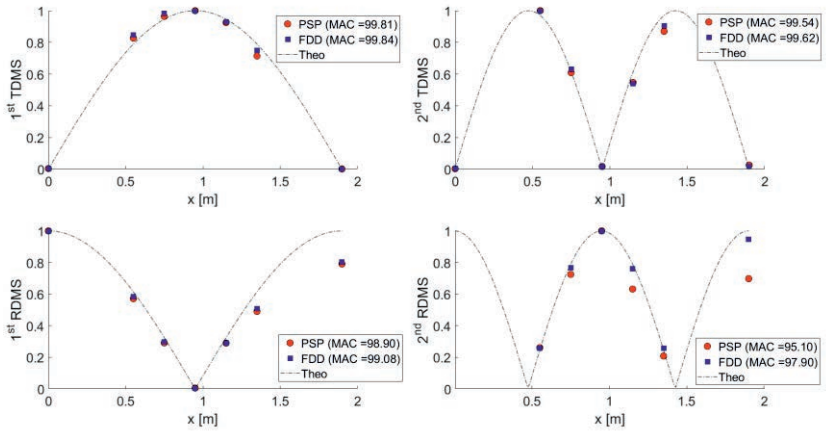

Fig. 2 First two translational and rotational envelopes reconstructed by means of SPP method compared to traditional FDD results.

While considering the most energetic vibrational component MAC, percentages above 98.9% both for translational and rotational shapes show an almost perfect fitting for both SPP and FDD. The minor deviation characterizing RDMs is attributable to the lower SNR ratio, which reduces the differences in spectral peaks amplitude. The performance of the parallel SPP is practically equivalent to the strictly centralized FDD, the difference among them being always less than 3%.

CONCLUSION

Going through the capability of a multi-type sensor network to locally gather real-time accelerations and onboard processed tilt angles, a spectral-based technique was successfully applied to experimentally inspect the translational and rotational properties of vibrating structures, hereby to increase the accuracy of modal inspection. The processing is suited to be straightforwardly implemented on-sensor, thus striving to realize a parallel monitoring platform based on a hierarchical orchestration of actors involved.

REFERENCES

[1] Zimmerman et al. (2008). Automated modal parameter estimation by parallel processing within wireless monitoring systems. *Journal of Infrastructure Systems*, *14*(1), 102-113.

[2] Brincker et al. (2001). Modal identification of output-only systems using frequency domain decomposition. *Smart materials and structures*, *10*(3), 441.

[3] Testoni et al. (2019). A Tilt Sensor Node Embedding a Data-Fusion Algorithm for Vibration-Based SHM. *Electronics*, *8*(1), 45.

[4] Testoni et al. (2018). A Sensor Network with Embedded Data Processing and Data-to-Cloud Capabilities for Vibration-Based Real-Time SHM. *Journal of Sensors*, *2018*.

Vibration data processing to assess the rigidity of diaphragms in existing building

Daniele Sivori, Marco Lepidi, Serena Cattari

Department of Civil, Chemical and Environmental Engineering (DICCA), University of Genova, Italy
E-mail: daniele.sivori@dicca.unige.it, marco.lepidi@unige.it, serena.cattari@unige.it

ABSTRACT

Ambient vibration tests are important tools for the calibration of structural models targeted at damage detection, health monitoring, seismic retrofitting, vibration control. The conceptual process of synthesizing mechanical models unavoidably involves a priori simplifications. Their a posteriori validation is a mandatory step to check the actual reliability of theoretical results. The in-plane rigidity of diaphragms is a common assumption in the seismic assessment of existing buildings, allowing simplified and cost-saving structural analyses. In this regard, the paper proposes a vibration-based procedure to assess the validity of the rigid diaphragm hypothesis. The procedure, requiring at least two bi-axial sensors, exploits a perturbative approach to distinguish and separately estimate the time histories of in-plane rotations and shear deformations of each diaphragm. A frequency domain representation allows the assessment of these variables for the identifiable modes. The effects of measurement noise, errors in sensor position and signal desynchronization are discussed through numerical simulations. The procedure is experimentally validated on a laboratory frame and applied to full-scale vibration measurements of a building. The outcomes highlight how higher modes tend to violate the rigid-body assumption.

KEYWORDS: *ambient vibration tests, operational modal analysis, power spectral density, deformable diaphragms, existing buildings*

INTRODUCTION

Ambient vibration tests (AVTs) offer a valuable support in the updating of mechanical models in several fields of engineering. In structural engineering, in particular, AVTs provide a straightforward experimental technique to determine the dynamic response and assess the seismic behavior of existing buildings. When dealing with building stocks, the employment of simplified models is essential to reduce the computational costs [1]. To this purpose, low-dimensional shear-type models, based on the in-plane rigid diaphragm assumption, are usually employed. Nonetheless, this assumption can be violated in the presence of damages, poor design and/or manufacturing, deformable

structural components (timber floors or masonry vaults). Based on these motivations, the paper aims at defining operational procedures, working in the frequency domain, to validate the in-plane rigidity of diaphragms by means of vibration measurements. The procedure is checked against unfavorable operational conditions and therefore successfully applied to a laboratory scaled steel frame and to a real scale building.

DATA-DRIVEN IDENTIFICATION OF DIAPHRAGM DEFORMABILITY

The ambient vibration data acquired on a floor diaphragm – measured by two or more bi-axial sensors – can be employed to estimate its two-dimensional displacement field

$$\boldsymbol{v}_j = \boldsymbol{v}_0 + \boldsymbol{H}\,\boldsymbol{\Delta x}_j \tag{1}$$

where $\boldsymbol{v}_j = (u_j, v_j)$ is the displacement measured by the *j-th* sensor in the position $\boldsymbol{x}_j = (x_j, y_j)$, depending - through the coefficient matrix $\boldsymbol{H}$ - on the relative position $\boldsymbol{\Delta x}_j = \boldsymbol{x}_j - \boldsymbol{x}_0$ with respect to a reference sensor measuring the displacement $\boldsymbol{v}_0$ in the position $\boldsymbol{x}_0$. An inverse problem can be stated to determine the four independent components H_{hk} (with $h, k = 1,2$) or, equivalently, the physical quantities

$$\Omega = \tfrac{1}{2}(H_{21} - H_{12}), \qquad \Gamma = H_{21} + H_{12}, \qquad E_{xx} = H_{11}, \qquad E_{yy} = H_{22} \tag{2}$$

where the diaphragm *rigid rotation* Ω, *shear strains* Γ and *normal strains* E_{xx}, E_{yy} can be regarded as the analogous to the components of the (infinitesimal) rotational tensor $\boldsymbol{\Omega}$ and strain tensor $\boldsymbol{E}$ in solid mechanics

$$\boldsymbol{\Omega} = \frac{1}{2}(\boldsymbol{G} - \boldsymbol{G}^T) = \begin{pmatrix} 0 & -\Omega \\ \Omega & 0 \end{pmatrix}, \qquad \boldsymbol{E} = \frac{1}{2}(\boldsymbol{G} + \boldsymbol{G}^T) = \begin{pmatrix} E_{xx} & \frac{1}{2}\Gamma \\ \frac{1}{2}\Gamma & E_{yy} \end{pmatrix} \tag{3}$$

Introducing the unknown vector $\boldsymbol{y} = (\Omega, \Gamma, E_{xx}, E_{yy})$, if vibration data from a number $N \geq 2$ of bi-axial sensors are available, the general identification problem reads

$$\mathbf{A}\boldsymbol{y} = \boldsymbol{b}, \qquad \boldsymbol{A} = \begin{pmatrix} \boldsymbol{A}_1 \\ \vdots \\ \boldsymbol{A}_j \\ \vdots \\ \boldsymbol{A}_{N-1} \end{pmatrix} \quad \boldsymbol{b} = \begin{pmatrix} \boldsymbol{b}_1 \\ \vdots \\ \boldsymbol{b}_j \\ \vdots \\ \boldsymbol{b}_{N-1} \end{pmatrix} \tag{4}$$

where the matrices $\boldsymbol{A}_j, \boldsymbol{b}_j$ are related to the identification problem $\boldsymbol{A}_j\boldsymbol{y} = \boldsymbol{b}_j$ of the *j-th* sensor. Assuming that sensors are *well placed* (matrix $\boldsymbol{A}$ full row ranked) and recalling that $n = 4$ is the number of unknowns, in the case of minimum sensor availability ($N = 2$) the linear system (4) is underdetermined ($rank(\mathbf{A}|\boldsymbol{b}) < n$). However, a suitable solution [2] can be obtained through a perturbation approach, assuming the ordering

$$\Omega = \varepsilon\Omega' + \varepsilon^2\Omega'', \quad \Gamma = \varepsilon^2\Gamma'', \quad E_{xx} = \varepsilon^3 E_{xx}''', \quad E_{yy} = \varepsilon^3 E_{yy}''' \qquad \varepsilon \ll 1 \tag{5}$$

which states that the shear strain Γ and the normal strains E_{xx}, E_{yy} are respectively small ($O(\varepsilon^2)$) and extremely small ($O(\varepsilon^3)$) with respect to the rigid rotations Ω ($O(\varepsilon)$).

Solving the perturbation problem at each order, reconstructing the general solution and then reabsorbing the auxiliary parameter ε leads to

$$\Omega = \frac{1}{2}\left(\frac{\Delta \mathrm{v}}{\Delta x} + \frac{\Delta u}{\Delta y}\right), \qquad \Gamma = \frac{\Delta \mathrm{u}}{\Delta y} + \frac{\Delta v}{\Delta x}, \qquad E_{xx} = 0, \qquad E_{yy} = 0 \tag{6}$$

where it should be remarked that other orderings of the variables – based on different engineering considerations – would result in different analytical solutions.

NUMERICAL SIMULATIONS AND LABORATORY MEASUREMENTS

Numerical simulations have been run to apply the procedure to pseudo-experimental vibration data. The dynamic response of the finite element model simulating a scaled two-storey frame under white-noise base input has been used as benchmark. A pair of ideal (noise-free and synchronized) bi-axial accelerometers ($N = 2$) have been assumed to apply the perturbation solution (6). The Power Spectral Density (PSD) show that the shear strains Γ are ideally negligible and frequency-independent, while the rigid rotation Ω peaks at the frequencies of the torsional modes (Figure 1a). Errors in the sensor position cause the rising up of Γ-peaks at the same frequencies of Ω-peaks, with error-dependent magnitude (Figure 1b). Measurement noise determines an uplift of the Γ noise floor without affecting its spectral content (Figure 1c). Lastly, the desynchronization causes disturbing unphysical Γ-peaks at several resonance frequencies, approaching the magnitude of the actual rigid rotation (Figure 1d).

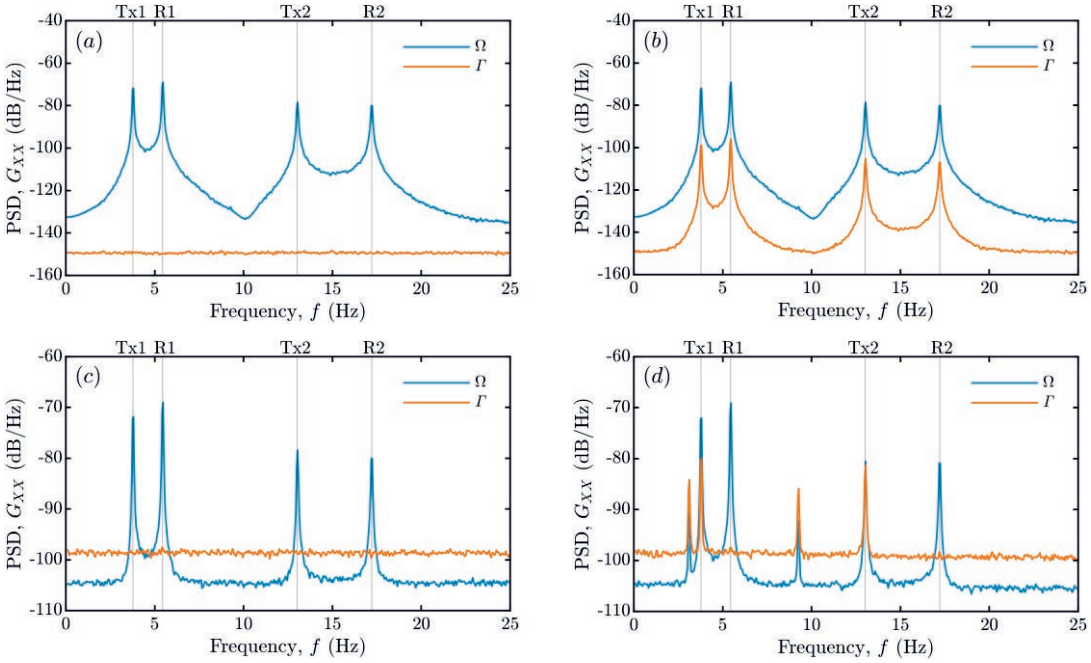

Figure 1: Pseudo-experimental PSD of the rigid rotation Ω and of the shear strain Γ: (a) error-free condition and effects of (b) position errors, (c) measurement noise, (d) desynchronization.

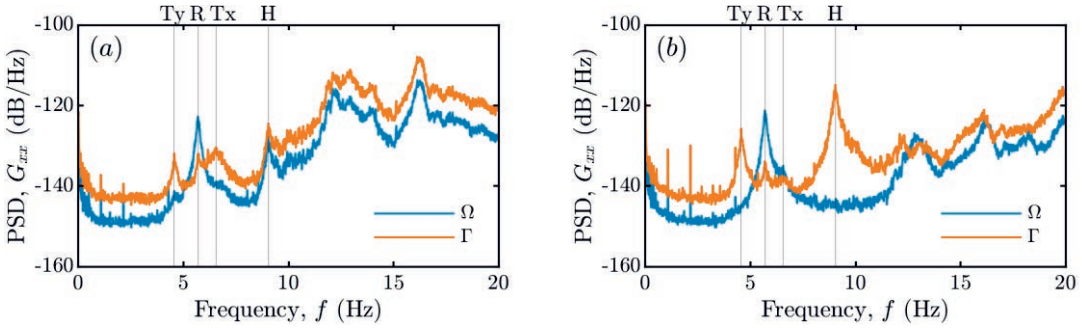

Figure 2: PSD of the rigid rotation Ω and of the shear strain Γ from the ambient response of the Pizzoli town hall using (a) two sensors and (b) three sensors placed at the second floor.

FULL-SCALE MEASUREMENTS

Ambient vibration measurements have been carried out on the Pizzoli (AQ) town hall, a monitored two-story masonry building [3]. The PSD of the rigid rotation Ω and the shear strain Γ have been estimated trough the perturbation solution based on two sensors ($N = 2$) and through the exact solution based on three sensors ($N = 3$). A good agreement is found in the frequency band of the lowest three modes, supporting the reliability of the approximated solution (Figure 2). The spectra highlight a leading Ω-peak at the frequency of the torsional mode (labeled "R") two orders of magnitude higher than the Γ-PSD value, pointing out a quasi-rigid diaphragm behavior. On the other hand, the shear strain Γ tends to overcome the rigid rotation Ω in the high frequency band. The non-rigid behavior of the fourth mode (labeled "H") is evidenced by a significant Γ-peak. The higher magnitude of Γ estimated from the exact solution reflects the not-negligible floor deformation in the proximity of the third sensor.

CONCLUSIONS

A mathematically consistent procedure, solving an inverse linear kinematic problem based on ambient vibration data, has been proposed to operationally validate the in-plane rigidity assumption in structural shear-type models of multi-storey buildings. The procedure is successfully verified through numerical simulations and experiments.

REFERENCES

[1] Spina, D., Acunzo, G., Fiorini, N., Mori, F., Dolce, M. (2019). A probabilistic simplified seismic model of masonry buildings based on ambient vibrations. *Bull Earthq Eng*, 17(2), 985-1007.

[2] Sivori D., Lepidi M., Cattari S. (2019). Ambient vibration tools to validate the rigid diaphragm assumption in the seismic assessment of buildings. *Earthq Eng Struct Dyn*. Under review.

[3] Cattari S., Degli Abbati S., Ottonelli D., Marano C. et al. Discussion on data recorded by the Italian structural seismic monitoring network on three masonry structures hit by the 2016-2017 central Italy earthquake. *Proc. of 7th COMPDYN*, Crete, Greece, 24-26 June, 2019.

Measuring Total Transverse Displacement of Railroad Bridges Using Lasers and Vision-Based Structural Health Monitoring (SHM) on Unmanned Aerial Systems (UAS)

X. Yuan[1], R. Nasimi[2], F. Moreu[3]

[1] *Department of Civil, Construction & Environmental Engineering, University of New Mexico, USA.*
E-mail: xyuan@unm.edu

[2] *Department of Civil, Construction & Environmental Engineering, University of New Mexico, USA.*
E-mail: rhnasimi@unm.edu

[3] *Department of Civil, Construction & Environmental Engineering, University of New Mexico, USA.*
E-mail: rhnasimi@unm.edu

ABSTRACT

Accurate and dependable measurement of bridge displacement is important to obtain bridge's condition under loads, and safety of operations. This paper summarizes the development of a new Structural Health Monitoring (SHM) system that enables measuring reference-free real-time total transverse displacement of railroad bridges using Unmanned Aerial Systems (UAS). Researchers selected a wide range of low-cost lasers for efficient measurement of transverse displacements and tested them first in a shake table and later using an UAS. Researchers validated their estimation in a laboratory environment. The accuracy of the results using the laser and the cost of the investment were compared to help selecting an efficient implementation for the railroad bridge industry, with recommendations for different operations, budgets, and resolution needs. The implementation of this experiment has been designed in collaboration with the Transportation Technology Center, Inc. (TTCI) of the Association of American Railroads (AAR). The research team visited TTCI and collected information about railroad bridges needs and train crossing information. The field implementation will be tested on Fall 2019 under train traffic crossing railroad bridges.

KEYWORDS: *Railroad Bridge, Unmanned Aerial System (UAS), Bridge Displacement, Laser, Real-time Monitoring*

INTRODUCTION

Reference-free displacements are of great interest for structural health monitoring (SHM) that can be applied towards the maintenance of railroad bridges (F. Moreu, 2016; Yoon, H,2018). It will be low-cost, high safety and effectively than traditional methods such as

manual inspection (Judi E. See, 2017). This paper summarizes the development of a new vision-based SHM system that enables measuring reference-free real-time total transverse displacement of railroad bridges using UAS. The method of using UAS to measure the displacement of bridge is validated in structure lab by lasers, cameras and dynamic 3D cloud data acquisition. Displacements of the railway bridge is collected by low-cost sensors on UAS with a laser attached on it. The results are compared to LVDT displacement for validation.

HARDWARE DEVELOPMENTS

For higher displacement accuracy, the team tested three different lasers from the manufacturer Keyence. Researchers tested the accuracy of the three lasers vs. the accuracy of the LVDT. The goal was to select the best laser to test using the UAS that satisfies railroad accuracy standards. Figure 1 shows the layout of the experiment. The three lasers work with 8.6 Volts power, which is beneficial to make the drone payload lighter.

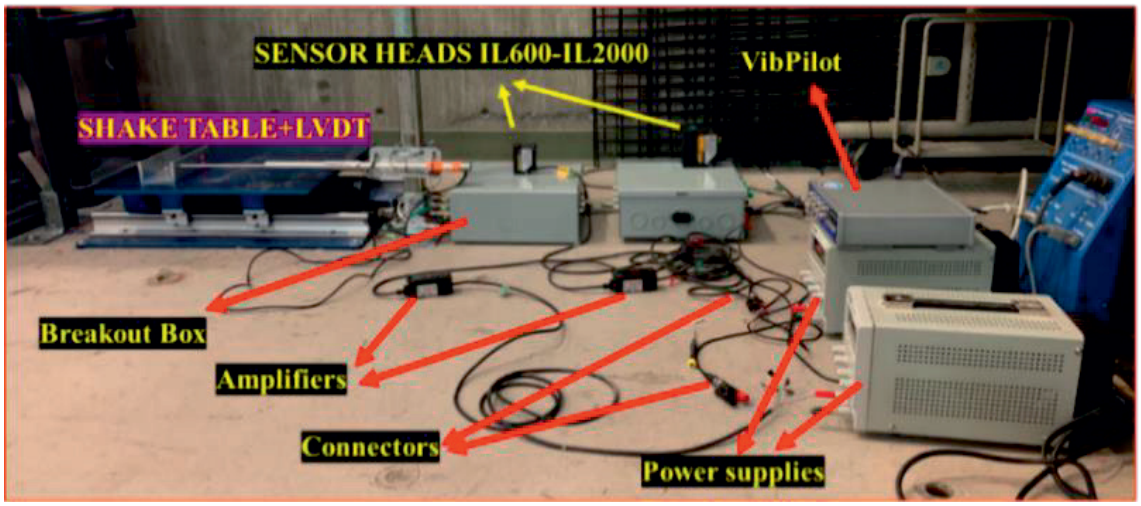

Figure 1: Lasers-shake table experiment layout.

For validation purposes, the research team compared the lasers' and LVDT's measurement to sinusoidal and various bridge train crossing events collected previously in the field. Figure 2 shows the result of the three different laser experiments measuring a railroad bridge crossing event simulated using the shake table. Considering accuracy and range aspects, the research team selected the IL-600 which accuracy is comparable to that of the LVDT.

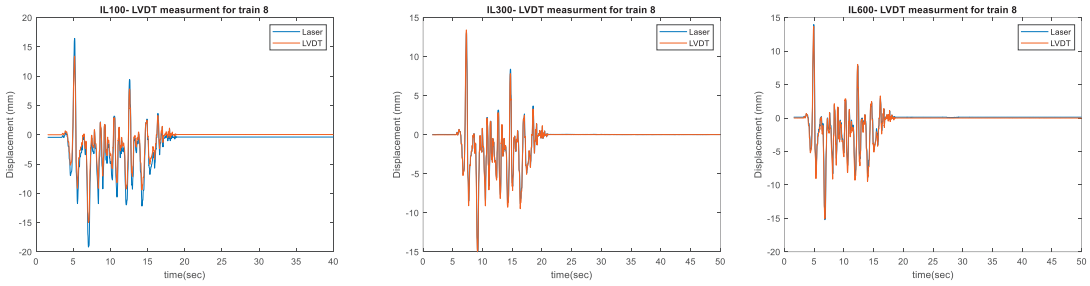

Figure 2: Lasers' and LVDT's measured displacement to train bridge crossing event: (a) results of laser Keyence IL-100; (b) results of laser Keyence IL-300; (c) results of laser Keyence IL-600.

ALGORITHM EXPERIMENTS "SHAKE TABLE"

For a preliminary test of the algorithm, an iPhone was attached to the shake table and a sinusoidal signal with the amplitude of 20 mm was imposed, after that target was filmed. By use of the algorithm, calculated displacement is plotted and compared with an LVDT measurements as shown in Figure 6. The results show that that the algorithm can estimate dynamic displacements within a 15% error. Further development of the algorithm will be conducted using the UAS.

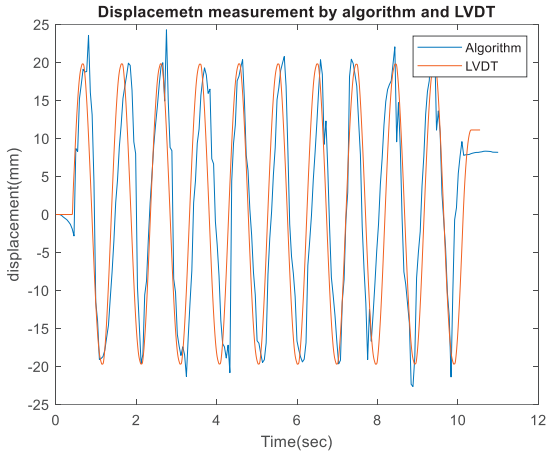

Figure 3: Displacement recorded by LVDT and calculated by algorithm.

PRELIMINARY LABORATORY 3D HOVERING DATA ACQUISITION

The next stage of this experiment is testing the positioning of the drone with the camera in comparison with the Vicon data to enable researchers to obtain total displacement of the moving bridge under trains with an UAS, laser, and camera (Figure 4). This data is used to validate the camera displacement algorithm and to inform of the hovering of the drone carrying the laser in the field in subsequent phases of the research.

FUTURE WORK

The future stages of this research will combine the laser technology, the displacement from the camera and validate it against the LVDT displacement collected in the laboratory.

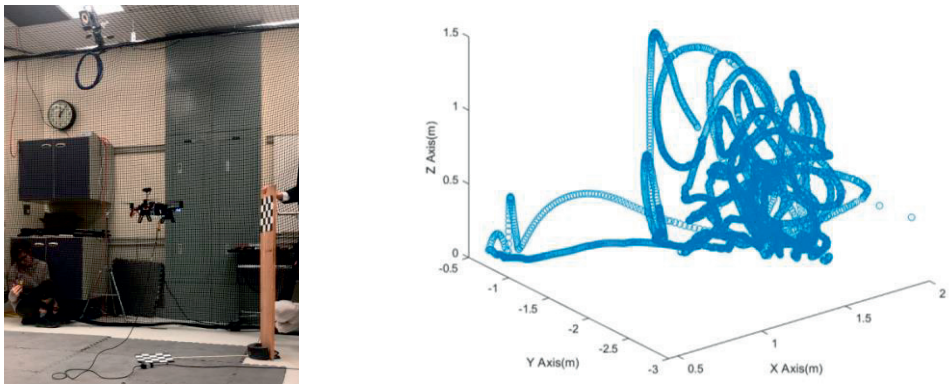

Figure 4: UAS laser/camera experiment; (a) new system in laboratory; (b) movement captured by the VICON cameras.

CONCLUSIONS

The results of the algorithm comparing LVDT's measured displacement with phone displacement will enable the total displacement estimation of the transverse movement of the bridge while the UAS is flying near to it. Future applications include testing at the Transportation Technology Center Inc. (TTCI) of the Association of American Railroads (AAR) and the CN railway.

REFERENCES

[1] F. Moreu, R. E. Kim2and B. F. Spencer Jr.3, 2016. Railroad bridge monitoring using wireless smart sensors. Structural Control and Health Monitoring, 24(2), 10.1002/stc.1863.

[2] Judi E. See, Colin G. Drury, Ann Speed, Allison Williams Negar Khalandi, 2017. The Role of Visual Inspection in the 21st Century. Proceedings of the Human Factors and Ergonomics Society 2017 Annual Meeting, pp.262-266.

[3] Yoon, H., Shin, J. and Spencer Jr, B.F., 2018. Structural displacement measurement using an unmanned aerial system. Computer-Aided Civil and Infrastructure Engineering, 33(3), pp.183-192.

Nontarget-based Displacement Measurement Using Combined RGB-D Information

Sahyeon Lee[1], Junhwa Lee[2], Jong-Woong Park[3], Sung-Han Sim[4]

[1] *School of Urban and Environmental Engineering, Ulsan National Institute of Science and Technology (UNIST), Republic of Korea.*
E-mail: sh_lee@unist.ac.kr

[2] *School of Urban and Environmental Engineering, Ulsan National Institute of Science and Technology (UNIST), Republic of Korea.*
E-mail: lee.junhwa@unist.ac.kr

[3] *School of Civil and Environmental Engineering, Urban Design and Studies, Chung-Ang University, Republic of Korea.*
E-mail: jongwoong@cau.ac.kr

[4] *School of Urban and Environmental Engineering, Ulsan National Institute of Science and Technology (UNIST), Republic of Korea.*
E-mail: ssim@unist.ac.kr

ABSTRACT

Computer vision-based methods for structural displacement measurement have typically used targets with predefined clear patterns. Although the use of the targets has advantages such as robust pattern tracking and transformation between the images and displacement, the nontarget-based measurement has been desired because of its installation convenience which allows a wider adoption in practice. As RGB images taken from digital cameras are projected two-dimensional information, displacement in the three-dimensional space cannot be fully recovered. This research proposes a nontarget-based method to measure structural displacement using a RGB-D camera that produces three-dimensional (3-D) information of a target object. The proposed method utilizes the RGB-D information, from which 3-D coordinates are extracted and converted to displacement measurement in the physical domain. Experimental validation is conducted in the laboratory environment using a pan-tilt that are designed to provide 6-DOF translational and rotational displacements.

KEYWORDS: *Nontarget, Vision-based method, Displacement Measurement, RGB-D camera, Coordinate Transformation*

INTRODUCTION

As displacement is a useful measurement for structural maintenance purposes, various displacement measurement methods have been developed for SHM of civil infrastructure [1]-[7]. The computer vision-based measurement has been recently drawn great attention as a promising alternative to the traditional contact-type sensors [8]. In particular, the nontarget-based method, which uses the structural features such as edges or textures on the structure instead of targets, is developed for the vision-based displacement measurement in practice [9]. Despite the convenience in the pre-designed target installation, the previous nontarget-based method still requires the calibration process using target to obtain the scale factor for the conversion of the image information to physical displacement. This prevents a wider adoption in the field tests because the camera should always be in the designated position [10]. As such, the development of conversion algorithm that allows the flexibility for camera position is required to improve the applicability to the field measurement.

This study proposes a nontarget-based method to measure structural displacement using a RGB-D camera. Using the combined RGB and real-time depth information, the coordinates are extracted from the images and converted to displacement measurement in the physical domain. The laboratory experiment using pan-tilt, which provides the translational and rotational displacements of structure, is conducted to validate the proposed method.

NONTARGET-BASED DISPLACEMENT MEASUREMENT

To obtain the physical displacement, the image coordinates should be converted to the RGB camera coordinates and subsequently to the world coordinates. The RGB camera coordinates $c(x, y, z)$ can be derived using the following relationship with the RGB image coordinates (u, v) [11]:

$$s\begin{bmatrix} u \\ v \\ 1 \end{bmatrix} = \begin{bmatrix} f_x & 0 & p_x \\ 0 & f_y & p_y \\ 0 & 0 & 1 \end{bmatrix}\begin{bmatrix} x \\ y \\ z \end{bmatrix} \tag{1}$$

where s is the scale factor; (f_x, f_y) and (p_x, p_y) are the focal lengths and principal points of the RGB camera in the x and y directions, respectively. Because the RGB-D camera provides the real-time depth, the RGB camera coordinates in Equation (1) can be directly obtained. The obtained RGB camera coordinates need to be converted to the world coordinates. The world coordinates $w(X, Y, Z)$ has the following rotational and translational relationship with the RGB camera coordinates:

$$w = R(c - T) \tag{2}$$

where R is a rotation matrix, and T is a translation vector. To obtain the relationship between two coordinate systems in Equation (2), the axes of world coordinate system

are defined using the structural features: for example, the horizontal line of structure is specified as *X*-axis while the vertical line is selected for *Y*-axis. The cross product of two axes yields the *Z*-axis in the transverse direction. Once the RGB camera coordinates are converted to the world coordinates, the structural displacement can be finally estimated based on the rotational and translational changes of world coordinates.

EXPERIMENTAL VALIDATION

The experimental validation using pan-tilt is conducted to validate the proposed method. The experimental setup consists of RGB-D camera (i.e., Kinect), DSLR, user-defined target, and pan-tilt. Kinect and DSLR are placed 1.2 m and 0.5 m away from the target, and DSLR is used to provide the reference data for comparison. The user-defined target has two parts, which are the picture of concrete bridge for Kinect and checkerboard for DSLR, is placed on the pan-tilt. The target rotates around Z-axis as the pan-tilt produces rotations. The world coordinate system is defined on the vertical and horizontal lines on the concrete bridge.

The structural displacement is measured by the proposed nontarget-based method and compared with those of DSLR as shown in Figure 1. The comparison result shows a good agreement even though the results from the proposed method presents high noise in displacement measurement due to its depth measurement error. The translations in *X*- and *Y*-axes are produced as the origin of the world coordinate system is moved when the target rotates around the *Z*-axis. The *X*- and *Y*-rotations are negligible while the *Z*-rotation is observed that is consistent with the experimental setup. As such, the proposed nontarget-based method can accurately measure the displacement of structure.

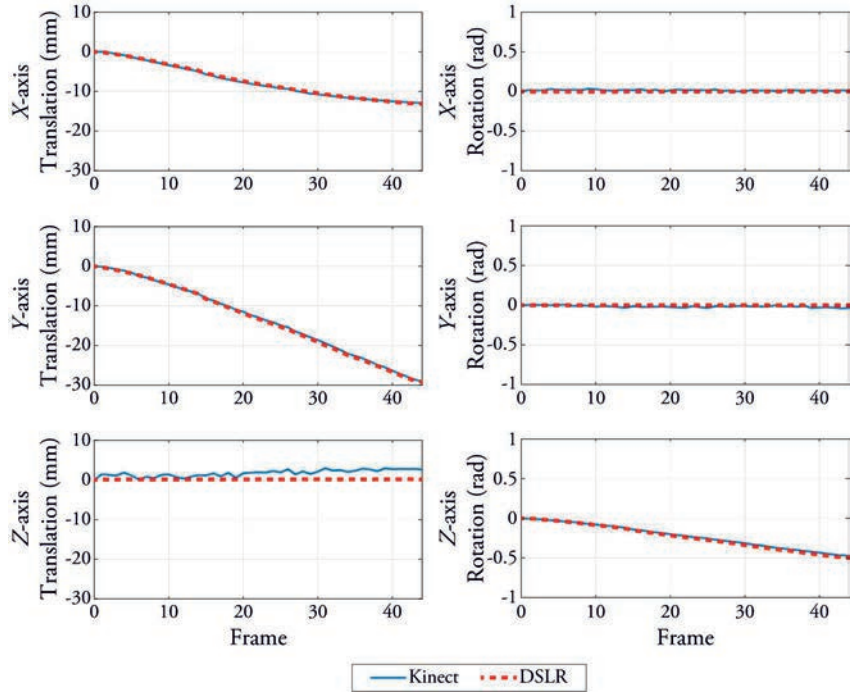

Figure 1: Comparison of the measured displacements for *Z*-axis rotation test

CONCLUSIONS

This paper proposes the nontarget-based displacement measurement method using the RGB-D camera. The combined RGB and real-time depth information that is used to convert the RGB image coordinate system to the world coordinate system. The structural displacement can be estimated based on the transformation and rotation of the world coordinates. The proposed approach was validated in the laboratory tests using the pan-tilt with the measurement plate that rotates in *Z*-direction.

REFERENCES

[1] Nassif, H.H., Gindy, M., and Davis, J. (2005) Comparison of laser Doppler vibrometer with contact sensors for monitoring bridge deflection and vibration. *NDT & E International* **38**(3): 213-218.

[2] Kijewsji-Correa, T.L., Kareem, A., Kochly, M. (2006) Experimental verification and full-scale deployment of global positioning systems to monitor the dynamic response of tall buildings. *Journal of Structural Engineering-ASCE* 2006 **132**: 1242-1253.

[3] Jo, H., Sim, S.-H., Tatkowski, A., Spencer, B.F., and Nelson, M.E. (2013) Feasibility of displacement monitoring using low-cost GPS receivers. *Structural Control and Health Monitoring* **20**(9): 1240-1254.

[4] Lee, H.S., Hong, Y.H., and Park, H.W. (2010) Design of an FIR filter for the displacement reconstruction using measured acceleration in low-frequency dominant structures. *International Journal of Numerical Methods in Engineering* **82**: 403-434.

[5] Shin, S., Lee, S.U., Kim, Y., and Kim, N.S. (2012) Estimation of bridge displacement responses using FBG sensors and theoretical mode shapes. *Structural Engineering Mechanics* **42**: 229-245.

[6] Park, J.W., Jung, H.J., and Sim, S.-H. (2013) Displacement estimation using multimetric data fusion. *IEEE/ASME Transactions on Mechatronics* **18**: 1675-1682.

[7] Cho, S., Yun, C.-B., and Sim, S.-H. (2015) Displacement estimation of bridge structures using data fusion of acceleration and strain measurement incorporating finite element model. *Smart Structures and Systems* **15**(3): 645-663.

[8] Lee, J., Lee, K.C., Cho, S., and Sim, S.H. (2017) Computer Vision-Based Structural Displacement Measurement Robust to Light-Induced Image Degradation for In-Service Bridges. *Sensors* **17**(10): 2317.

[9] Fukuda, Y., Feng, M.Q., Narita, Y., Kaneko, S., and Tanaka, T. (2013) Vision-Based Displacement Sensor for Monitoring Dynamic Response using Robust Object Search Algorithm. *IEEE Sensors Journal* **13**(12): 4725–4732.

[10] Yoon, H., Elanwar, H., Choi, H., Golparvar-Fard, M., and Spencer, B.F. (2016) Target-Free Approach for Vision-Based Structural System Identification using Consumer-Grade Cameras. *Structural Control and Health Monitoring* **23**(12): 1405–1416.

[11] Hartley, R. and Zisserman, A. (2003) Multiple View Geometry in Computer Vision. Cambridge University Press.

Study of an optimal command law combining weather forecast and energy reduction for transport structure surface de-icing by Joule effect

N. Le Touz[1,2], J. Dumoulin[1,2]

[1] *IFSTTAR, COSYS-SII, Allée des Ponts et Chaussées, 44344 Bouguenais, France*

E-mail: ***nicolas.le-touz@ifsttar.fr, jean.dumoulin@ifsttar.fr***

[2] *Inria, I4S Team, Campus Beaulieu, 35042 Rennes, France*

ABSTRACT

In this paper, we study an optimal energetic solution applied to a Joule heating solution for prevention from black-ice occurring at the surface of transport infrastructures. After a presentation of the heating system, several control laws are presented with the objective to prevent ice formation while avoiding excessive energy consumption. The adjoint state method is applied to perform optimal control. To preserve the structure and maintain its lifetime, operational constraints are added. Different adaptations for the control law are proposed and presented. Results obtained by numerical simulations for different operative conditions and with regularly updated weather forecasts are presented and discussed. Finally, conclusion and perspectives are proposed.

KEYWORDS: *Optimal control, adjoint state method, finite element method*

INTRODUCTION

In temperate regions, winter season is favorable to formation of black-ice on transport infrastructures, what impacts on economy and transport safety. Salt pouring is a common solution, but it pollutes aquifer and accelerates corrosion of cars and bridges. Furthermore, for some infrastructures devoted to guided transport systems salt pouring is also not recommended to preserve electrical components. To prevent from black-ice occurring, some solutions have been developed to heat the surface of the infrastructures. For instance, a fluid can flow inside [1]. Another solution consists in putting heating wire with Joule effect inside the structure. This is this solution that is studied in this paper. In particular, a focus is performed on the command strategy, aiming at prevent from icing and minimizing needs in energy. Some adaptations are described to take into account operational constraints. Finally, conclusions and prospects are proposed.

Modelling of Joule effect heating

The studied structure is shown in figure 1. A domain Ω contains four heating wires denoted by S. The aim is to prevent from black-ice occurring on the surface Γ_{target} by activating heating when necessary.

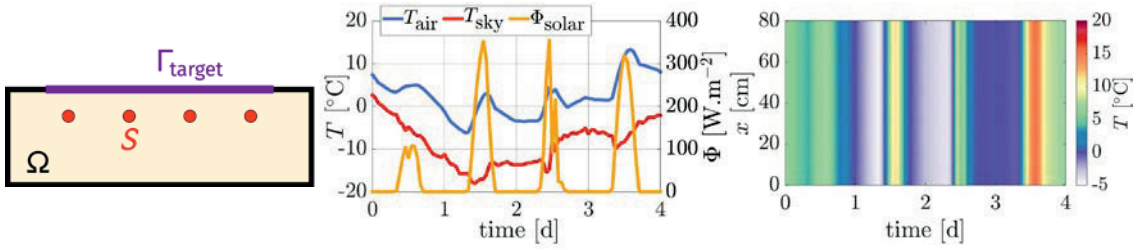

Figure 1: Structure scheme with heating wires (left), example of environmental conditions evolution (middle) and surface temperature evolution (right)

Temperature field in the structure is computed from internal thermal properties, supposed given, and environmental conditions. These one can come from local weather forecast services (here simulated by using weather databases). Heat tranfer equation (equations (1) and (2)), allows to calculate the temperature field evolution with time. The studied structure is supposed to be submitted to environmental solicitations only at its surrounding boundary. Other boundaries are supposed adiabatic. A finite element formulation for spatial solving and a Crank-Nicolson scheme for temporal dimension are used [2].

$$\rho c \frac{\partial T}{\partial t} - \nabla \cdot (k \nabla T) = \begin{cases} q \text{ in } S \\ 0 \text{ elsewhere} \end{cases} \tag{1}$$

$$k \nabla T \cdot \vec{n} = \begin{cases} \Phi_{solar} + h(T_{air} - T) + 4\epsilon\sigma T_{sky}^3 \left(T_{sky} - T\right) \text{ at the surface} \\ 0 \text{ elsewhere} \end{cases} \tag{2}$$

Environmental conditions are considered for Nancy during winter and plotted in figure 1 (middle) from MeteoNorm database. Evolution of surface temperature without heating is plotted in figure 1 (right). This figure shows that the surface temperature can be negative, particularly during the night.

Command law

To prevent from black-ice occurring at the surface, the temperature is maintained higher than a given set point T_{sp} on Γ_{target} with a minimization of energy needs. This optimization problem is written under a weak formulation:

$$\text{find } q = \arg\min_{\tilde{q} \in \mathcal{U}} J(\tilde{q}) \quad \text{with } J(q) = \frac{1}{2} \left\| \left(T_{sp} - T\right)^+ \right\|_{\mathcal{M}}^2 + \frac{\varepsilon}{2} \|q\|_{\mathcal{U}}^2 \tag{3}$$

Where $(\cdot)^+$ is the positive part and $\mathcal{U} = L^2([0, t_a])$ and $\mathcal{M} = L^2(\Gamma_{target} \times [0, t_a])$ refer respectively to spaces of parameters and surface temperature, t_a being time horizon. $\|\cdot\|_{\mathcal{U}}$ and $\|\cdot\|_{\mathcal{M}}$ are norms associated to natural inner products $\langle \cdot, \cdot \rangle_{\mathcal{U}}$ and $\langle \cdot, \cdot \rangle_{\mathcal{M}}$ on $\mathcal{U}$ and $\mathcal{M}$. $\frac{1}{2} \left\| \left(T_{sp} - T\right)^+ \right\|_{\mathcal{M}}^2$ represents the gap between setpoint and temperature on Γ_{target} and $\frac{\varepsilon}{2} \|q\|_{\mathcal{U}}^2$ the energy consumption. ε is chosen such that

the solution allows to respect the constraint $T \geq T_{sp}$ with a fixed tolerance $\Delta T \approx 0.1$°C in the present study. For a surface Γ_{target} of 1 m², a value $\varepsilon \approx 10^{-12}$ is used.
To minimize $\boldsymbol{J}$, gradient of the functional is computed with adjoint state method [3]. Adjoint problem, equation (4) and (5), has the same structure as the direct problem (equations (1) and (2)) and can also be solved with the same techniques.

$$-\rho c \frac{\partial \delta T^*}{\partial t} - \nabla \cdot (k \nabla \delta T) = \begin{cases} -\left(T_{sp} - T\right)^+ \text{ in } \Gamma_{target} \\ 0 \text{ elsewhere} \end{cases} \quad (4)$$

$$k \nabla T \cdot \vec{n} = \begin{cases} -\left(h + 4\epsilon\sigma T_{sky}^3\right)\delta T^* \text{ at the surface} \\ 0 \text{ elsewhere} \end{cases} \quad (5)$$

From adjoint problem solution δT^*, gradient of functional J can be computed with equation (6) and conjugate gradient method is used to minimize J. Optimal heat source q can then be computed from environmental conditions.

$$J'(q)\delta q = \langle \delta q, \int_S \delta T^* d\Omega + \varepsilon q \rangle_{\mathcal{U}} \quad (6)$$

To maintain the lifetime of some electrical power components, a minimal duration for commutation is used. Furthermore, to take into account the limitation of power supply, a maximal value is used for thermal source. Both operation constraints lead to consider a subset of $\mathcal{U}$ for q: this source is constant on time intervals and bounded in $[0, q_{max}]$. A projection of (6) in this subset is performed to get source evolution. For the set point, two approaches can be considered: a constant set point, higher than ice fusion temperature can be used with a margin, for instance +4°C. On another hand, humidity can be taken into account. In fact, black ice cannot occur if the temperature is higher than frozen point. In particular, for a dry air, this frozen point is largely lower than 0°C. It can be computed from humidity value [4].
Power needs Q is computed from integration of q on heating wires as $Q(t) = \int_S q(t)\,\Omega$ and shown in figure 2 for both set points. Surface temperature stays globally higher than the set point if the mean difference $\boldsymbol{e(t)} = \frac{\int_{\Gamma_{target}} \left(T_{sp} - T(t)\right)^+ d\Gamma}{\Gamma_{target}}$ is lower than about 0.1°C during the four days. Figure 3 shows also that source needs to reach about 180 W/m for $T_{sp} = +4$°C and 100 W/m for $T_{sp} = T_f + 4$°C.
More than a decrease of system dimensioning, heat consumption also decreases by taking into account frozen point as set point: consumption goes from 9.60 kWh/m with $T_{sp} = +4$°C ($Q_{max} = 180$ W/m) to 6.16 kWh/m (-36 %) with $T_{sp} = T_f + 4°C$ ($Q_{max} = 100$ W/m).

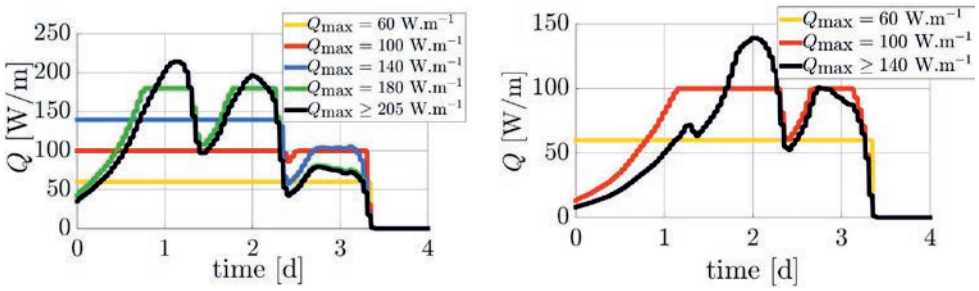

Figure 2: Source consumption for $T_{sp} = +4°C$ (left) and $T_{sp} = T_f + 4°C$ (right)

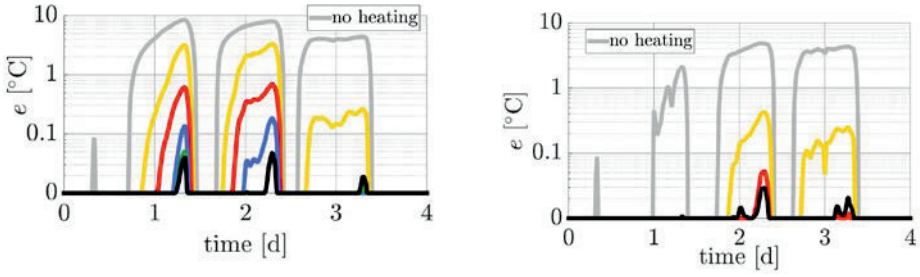

Figure 3: Mean difference between set point and surface temperatures with $T_{sp} = +4°C$ (left) and $T_{sp} = T_f + 4°C$ (right)

CONCLUSIONS

In this paper, a command law has been presented to prevent surface of transport infrastructures from black-ice occurring. By using adjoint state method, optimal heat source has been computed. Results shows an important decrease of energy needs by considering frozen point as a set point. To take into account system operation, adaptations have been added for commutation duration and maximum power supply. To go further, effects of rainfall can be considered and a validation with a mock-up will be realized.

Acknowledgments: French Ministry of "Transition Ecologique et Solidaire" for supporting part of this work under grant agreement DGITM N 17/389

REFERENCES

[1] Le Touz, N., Conception et étude d'infrastructures de transports à énergie positive: de la modélisation thermomécanique à l'optimisation de tels systèmes énergétiques, PhD thesis, 2018

[2] Gartling, D. K. and Reddy, J. N., The finite element method in heat transfer and fluid dynamics, Third edition, CRC Press, 2014

[3] Lions, J.-L., Contrôle optimal de systèmes gouvernés par des équations aux dérivées partielles, Dunod, 1968

[4] Buck, A. L., New equations for computing vapor pressure and enhancement factor, Journal of Applied Meteorology, 20 :1527 :1532, 1981

Measurement of Deflection of Concrete Beam Strengthened with UV-Cured Glass-Fiber Reinforced Polymer Using a Computer Vision Method

B.H. Shan[1], Y. Shen[1], X.S. Su[1], G.J. Xian[2]

[1] *School of civil engineering, Harbin Institute of Technology, China*
E-mail: shanbaohua@hit.edu.cn

[2] *Key Lab of Structures Dynamic Behavior and Control, Ministry of Education, Harbin 150090, China*

[3] *Key Lab of Smart Prevention and Mitigation of Civil Engineering Disasters of the Mining of Industry and Information Technology, Harbin Institute of Technology, Harbin 150090, China*

ABSTRACT

To measure the deflection of concrete beam strengthened with UV-cured glass-fiber reinforced polymer, a stereovision measurement method is proposed in the present paper, and the structural displacements are acquired by establishing the structure coordinate system. To testify the effectiveness of the proposed method, a destructive test of concrete beams strengthened with ultraviolet (UV)-cured glass fiber reinforced polymer (GFRP) is conducted in lab. Results indicate that the load-displacement curves attained by the proposed vision method agree well with that of LVDT, this demonstrate that the proposed vision method is feasible and effective for measuring the deflection of concrete beam in a destructive test.

KEYWORDS: *Structural health monitoring, vision, structure coordinate system, measurement.*

INTRODUCTION

In recent years, the stereovision measurement method based on DIC attracts more and more attention. However, the 3D DIC method usually need to spray speckles or plot grids on structural surface, and the prepare work is complicated. Essentially the DIC method is a kind of area matching algorithm, it's difficult to ensure the uniqueness of any grid or speckle. Therefore, there exist the image mismatch when the DIC method is used to conduct 3D matching in stereovision measurement[1].

To solve the problem of image mismatch, a stereovision displacement measurement method based on structure coordinate system is proposed in the present paper. To testify the effectiveness of the proposed method, a destructive test of concrete beams strengthened with UV-cured GFRP is performed in lab.

Stereovision measurement method based on structure coordinate system

Considering the general case, that is no requirement of two cameras' position. As shown in Figure 1, assume that the left camera coordinate system $o_l - x_l y_l z_l$ coincides with the world coordinate system $o_w - x_w y_w z_w$.

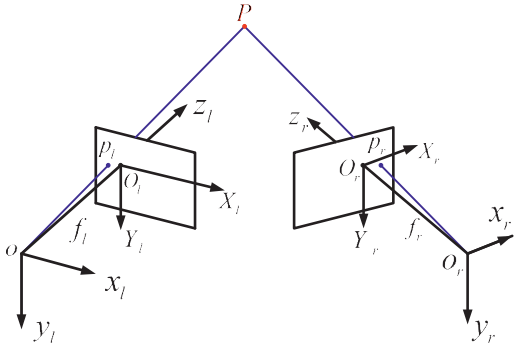

Figure 1: Binocular stereovision model.

The 3D coordinates of a spatial point P in the left camera coordinate system $o_l - x_l y_l z_l$ can be obtained by equations (1)[2].

$$\begin{cases} x_l = z_l X_l / f_l \\ y_l = z_l Y_l / f_l \\ z_l = \dfrac{f_l (f_r t_x - X_r t_z)}{X_r (r_7 X_l + r_8 Y_l + f_l r_9) - f_r (r_1 X_l + r_2 Y_l + f_l r_3)} \end{cases} \tag{1}$$

where f_l and f_r are the scale factors of left and right cameras, respectively.

The 3D coordinates of the spatial point in left camera coordinate system can be calculated provided that rotation matrix $\mathbf{R}_{lr} = \begin{bmatrix} r_1 & r_2 & r_3 \\ r_4 & r_5 & r_6 \\ r_7 & r_8 & r_9 \end{bmatrix}$ and translation matrix $\mathbf{T}_{lr} = \begin{bmatrix} t_x \\ t_y \\ t_z \end{bmatrix}$ can be solved by Zhang's calibration algorithm based on 2D planar pattern[3].

To visually express structural displacement, xoy plane of the structure coordinate system $o - xyz$ is usually established on structural surface as shown in Figure 2.

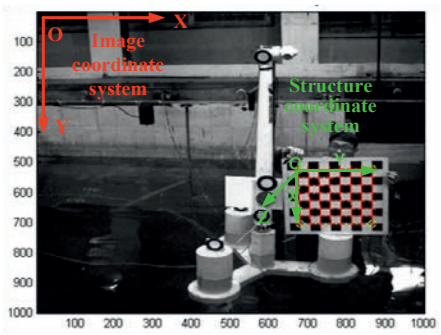

Figure 2: Establishing the structure coordinate system on structural surface

The structure coordinate system does not coincide with the left camera coordinate system. The transformation matrix $[\mathbf{R} \quad \mathbf{T}]$ between structural coordinate system and

the left camera coordinate system must be firstly obtained. The solving process is given in Figure 3.

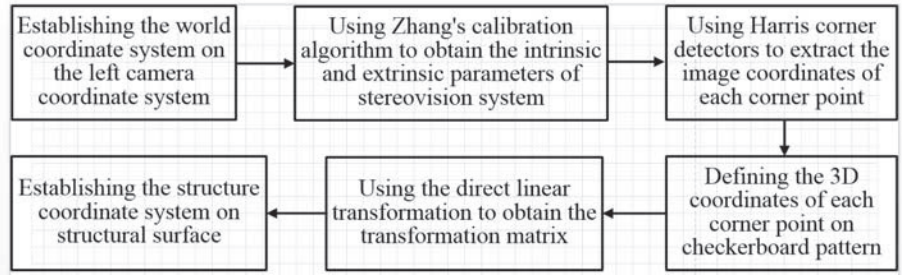

Figure 3: Flowchart of establishment of structure coordinate system by checkerboard pattern.

Therefore, the 3D coordinates of the measured point in the structure coordinate system $o-xyz$ can be given by equation (2), and the out-of-plane and in-plane displacements of structure at each moment can also be acquired from equation (2).

$$\begin{bmatrix} x \\ y \\ z \end{bmatrix} = \mathbf{R}^{-1}\left(\begin{bmatrix} x_l \\ y_l \\ z_l \end{bmatrix} - \mathbf{T}\right) \tag{2}$$

Destructive test of concrete beams strengthened with UV-cured GFRP

As shown in Figure 4, the UV-cured GFRP sheet was pasted on the middle part of bottom side of concrete beam. The size of UV-cured GFRP sheet was $200mm \times 20mm \times 1.3mm$. In test, a linear variable differential transformer (LVDT) was put on the mid-span of concrete beam. A circular target with 15mm diameter was pasted on one side of concrete beam, which was right under the position where the universal testing machine applied the load. The sampling frequency of stereovision system is 1Hz.

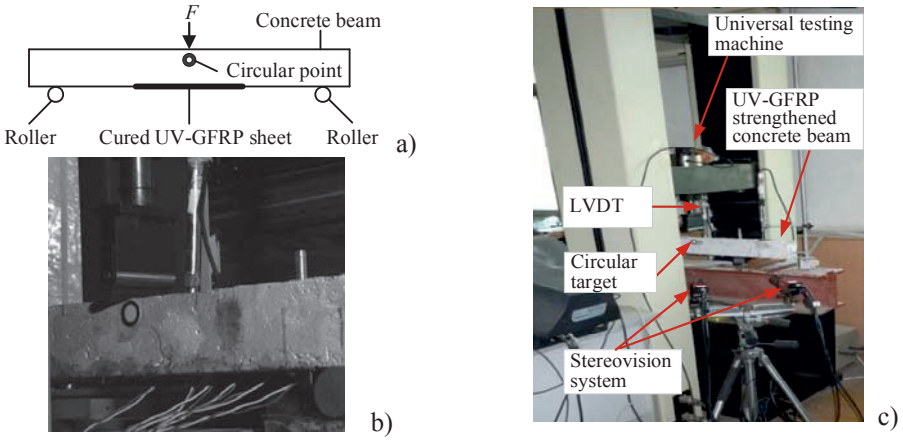

Figure 4: Experimental setup: a) loading schematic; b) local photo; c) experimental photo.

The measurement result of three concrete beams strengthened with UV-cured GFRP are shown in Figure 5. From Figure 5, the load-displacement curves obtained by the proposed stereovision method and LVDT have the same trend and agree well with each other. The reason of slightly different between the two methods is the difference in the measurement positions and the local compression damage of concrete beam.

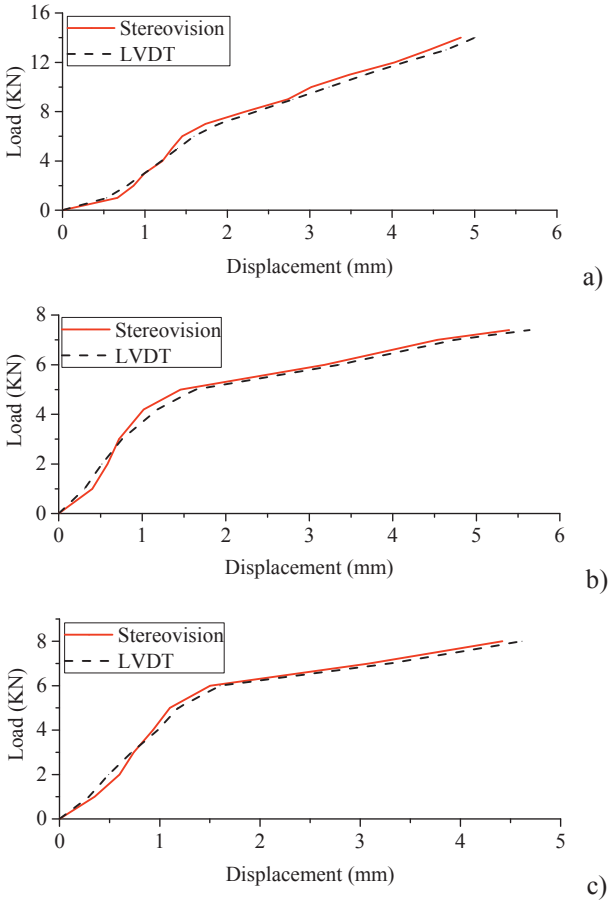

Figure 5: Load-displacement curves of concrete beams strengthen with UV-cured GFRP: a) 1st beam (indoor environment); b) 2nd beam (alkaline solution); c) 3rd beam (alkaline solution).

CONCLUSIONS

Based on the stereovision model, a 3D displacements measurement method based on structure coordinate system is proposed in the present paper, and the absolute displacements of structure can be acquired by establishing the structure coordinate system. Stereovision measurement results are compared with the corresponding results of LVDT, results show that the load-displacement curves obtained by the proposed stereovision method and LVDT agree well with each other, this verifies the effectiveness of the proposed stereovision measurement method.

REFERENCES

[1] Kashfuddoja M., Ramji M. (2013)Whole-field strain analysis and damage assessment of adhesively bonded patch repair of CFRP laminates using 3D-DIC and FEA. *Composites Part B: Engineering* 53: 46-61.

[2] Sun J., Zhang G. J., Wei Z. (2006)Large 3D free surface measurement using a mobile coded light-based strereo vision system, *J. Sensors & Actuators A Physical* 132(2): 460–471.

[3] Zhang Z. Y. (2000) A flexible new technique for camera calibration. IEEE Trans. On Pattern Analysis and Machine Intelligence 22(11): 1330-1334.

New solutions of sensors and instrumentation for dynamic monitoring of Civil Structures: ViBest/FEUP experience

C. Moutinho[1], A. Cunha[1]

[1] *ViBest, Faculty of Engineering (FEUP), University of Porto.*
E-mail: moutinho@fe.up.pt

ABSTRACT

This paper describes the work developed by ViBest research group in the area of new solutions of sensors and instrumentation of Civil Structures aiming its long term dynamic monitoring. It identifies the main challenges in this area, and describes the general characteristics of the developed measurement systems, which have been used for the monitoring of some actual structures.

KEYWORDS: *Continuous Dynamic Monitoring, Operational Modal Analysis, Data Acquisition Systems, New Generation of Measurement Systems.*

INTRODUCTION

The continuous dynamic monitoring of structures is an area that has lately assumed great importance in Civil Engineering. The main reason is related to the subject of Operational Modal Analysis (OMA), which aims to identify the modal parameters of a structure in operating conditions (particularly with regard to natural frequencies, damping ratios and mode shapes) taking into account the measured ambient vibrations at critical points. In these cases, the measurement of vibrations is performed without disturbing the normal functioning of the structures, which may be implemented in buildings, bridges (railway, roadway, highway), dams and offshore structures. Given the importance of this subject, the Laboratory of Vibrations and Structural Monitoring FEUP (ViBest) has carried out consistent work in this area, both in the development of numerical tools for identifying modal parameters and in the continuous measurement of vibrations in actual structures (see **www.fe.up.pt/vibest**). Parallel to this area, ViBest has also developed and implemented vibration measurement techniques that enable to solve specific problems of current systems and to evolve toward a new generation of measurement systems. In this context, this paper intends to divulge the instrumentation solutions that have been used by ViBest in the continuous dynamic monitoring of some structures using this technology.

CONTEXT OF THE RESEARCH

Researchers who work in actual structures with data acquisition systems, often face many challenges and problems. The lack of robustness of some traditional instrumentation solutions is one of these difficulties. The failure of these systems when working for long periods is not the only cause of that lack of robustness. Sometimes there also external causes like power failures and adverse weather conditions, beyond to other causes of diverse origin. Some data acquisitions systems are also too complex, involving too many cables and connections. The high cost of measurement systems is another factor that hinders the widespread use of these systems in common Civil Structures. In this context, the objective of the research in this area is to develop instrumentation that meets the following characteristics: i) wireless and compact size, for easy integration and installation in structures; b) robust, allowing the functioning of the system for long periods with no crashes; c) long autonomy; d) flexible, by allowing a variety of different sensors in several mounting schemes; e) accurate, and; f) cost attractive. The role of these systems is not certainly to substitute the traditional systems. However, there are many applications where these instruments have the same effectiveness as the traditional ones, with additional advantages. In fact, they can simplify the process of installation and operation; they can be custom-made, including the use of 3D printing; maintenance and replacement is facilitated, and; more interesting, their attractive cost may allow the generalization of dynamic monitoring systems in Civil Structures. Nevertheless, the implementation of these new data acquisition systems also raises some challenges. Particularly with regard to the following issues: a) power supply; b) data transmission; c) reduced energy consumption; d) miniaturization of the systems, and; e) reliability.

DEVELOPED INSTRUMENTATION

In the context of what was said in the previous section, during last years the ViBest research group at FEUP, developed some instrumentation for dynamic monitoring of structures. There are basically two kinds of sensors: those that are powered by batteries, and those that are powered by solar energy. The earliest developments were based on portable battery-powered devices. In figure 1a) is shown the system here designated by "Portable 1" which was used for the first measurements in 2014, in particular to measure the "lock-in" effect in Luiz I bridge over Douro River in Porto [1]. This device is a little bigger than the size of a credit card and has an autonomy of 6 hours, being possible to adapt it to metal structures by powerful magnets. In order to improve system autonomy, another compact system, designated by "Portable 2" was used to measure simultaneously vertical and horizontal vibrations at same section (see Figure 1b). This device, a little smaller than the previous one, also comes with magnets. It works with 3 AA batteries allowing the system to work continuously for close to a

month. This model is clearly geared to higher periods of measurements. More recently, these battery-powered devices evolved to a more reduced energy consumption system ("Portable 3"), incorporating a much better tri-axial MEM accelerometer. It uses 3D printing to optimize the shape and space occupied by the device. Figure 2a) represents a very compact model endowed with magnets for fixation to structures, which has an autonomy of 15 days using a battery of 2500 milliamps. The autonomy of these systems may be increased by adding more batteries. For instance, Figure 2b) represents a model with an autonomy of 6 months using 9 batteries of 3400 milliamps of capacity. Aiming long periods of data acquisition for enabling the long-term dynamic monitoring of structures, two solar-powered solutions were developed and implemented. The first one ("Solar 1"), was installed in two structures in 2014 [2]. It comprises a 10-W 40×28-cm solar panel which is used to power the system and to charge 3 × 12-V batteries to maintain the system working during the night and on cloudy days. However, "Solar 1" has some issues that needed to be improved upon: i) external dimensions are relatively high; ii) it is inefficient in terms of power consumption, and: iii) there is no way to check if the system is working properly without being physically accessed. For these reasons, a new version of a solar powered device was developed ("solar 2"). This one is significantly smaller than the previous one (11×14 cm plan view) and the panel has a power of 2W that feeds a 3.3-V system (Figure 3b). In order to monitor the functioning of the acquisition system, this particular model periodically sends a report to an RF serial receiver including the following information: i) device ID; ii) current date and time; iii) current file name; iv) total number of files; v) temperature inside the box, and; vi) battery voltage. This information may be collected locally, for instance, using a smartphone, and allows checking if the system is working properly. Access to the data is only available using a physical connection.

CONCLUSIONS

This paper describes the work developed at ViBest research group located in FEUP, on the topic of a new generation of dynamic monitoring systems applied to Civil Structures. It was pointed out that some traditional systems have some drawbacks, particularly related to the lack of robustness, complexity, and high cost. In the other hand, simpler systems based on microcontrollers may substitute that classical systems in certain applications, offering some advantages like the ease of installation and operation, less maintenance and attractive cost. In this context, this document presents several generations of measurement devices based on battery-powered solutions and solar-powered solutions. In many practical situations, the results obtained with these systems can be comparable to those obtained with traditional systems, which makes possible the widespread use of these systems in the dynamic monitoring of structures.

a)  b) 

Figure 1: Battery-powered devices: a) "Portable 1" ; b) "Portable 2" measurement system

a)  b) 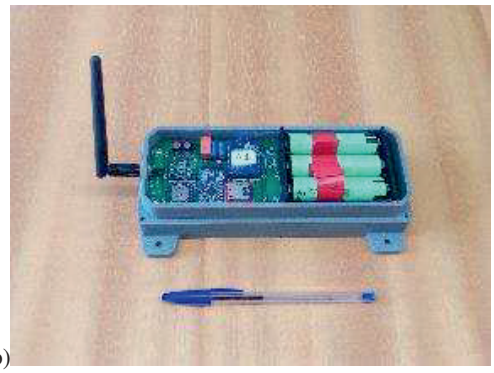

Figure 2: Battery-powered "Portable 3" devices: a) 15 days autonomy ; b) 6 months autonomy

a)  b) 

Figure 3: Solar-powered devices: a) "Solar 1" ; b) "Solar 2"

ACKNOWLEDGEMENT

This research is part of a project that has received funding from the Research Fund for Coal and Steel under grant agreement No 800687.

REFERENCES

[1] Moutinho, C. and Cunha, A. (2019), Continuous dynamic monitoring of large human-induced vibrations at the Luiz I Bridge. Submitted to structural control and health monitoring, (2019).

[2] Moutinho, C., Magalhães, F. and Caetano, E. (2015), Analysis of the vibration levels of a slender footbridge measured by a continuous dynamic monitoring system. Compdyn 2015, Greece.

Uncooled infrared thermal camera for thermal monitoring or Non-Destructive Testing of Civil Engineering structures

J. Dumoulin[1, 2]

[1] *IFSTTAR, COSYS-SII, Allée des Ponts et Chaussées, F-44344, Bouguenais, France.*
E-mail: jean.dumoulin@ifsttar.fr

[2] *Inria, I4S Team, Campus Beaulieu, 35042 Rennes, France.*
E-mail: jean.dumoulin@inria.fr

ABSTRACT

In this paper, we address a review of studies, carried-out at IFSTTAR this last decade, and based on the use of uncooled infrared thermal cameras at ground level. We present different outcomes extracted from Non-Destructive Testing (NDT) laboratory studies and experiments. Analysis of their extension to outdoor application is proposed and discussed. Long term thermal monitoring by uncooled infrared thermal camera is introduced with its natural environment constraints and issues. On-site instrumentation studied is presented and results obtained on some structures are discussed. Finally, conclusion and perspectives are proposed, with a focus on last trends in term of uncooled infrared sensor technological evolution, instrumentation system and ongoing research works associated.

KEYWORDS: *Infrared thermography, Long term thermal monitoring, Thermal model, Transport Infrastructure, Non Destructive Testing*

INTRODUCTION

Being able to perform full field easily non-invasive diagnostics for surveillance and monitoring of transport infrastructures and structures is a major preoccupation of many technical offices. Among all the existing electromagnetic methods [1], using uncooled infrared camera is a promising full field technique both for long term thermal monitoring [2-3] and non-destructive testing [4-7]. In this paper, we first introduce the problematic of long term thermal monitoring by infrared thermography using uncooled infrared camera and discuss on complementary environmental conditions monitoring. Furthermore, we present some laboratory non destructive testing methods based on active infrared thermography and their potential application to real site. Finally, an example of coupling of long term thermal monitoring with data processing mainly used for NDT by active infrared thermography in controlled conditions is presented and discussed. Conclusion and perspectives are proposed.

LONG TERM THERMAL MONITORING BY INFRARED THERMOGRAPHY

Temperature retrieval from infrared measurements in outdoor conditions on built or natural targets is facing, in many real situations, lack of knowledge about the observed

surfaces and surrounding environment. The irradiance received at camera's sensor level is a combination of all the scene contribution as illustrated in Figure 1. Therefore, one needs to gather information about the geometry of the scene, the meteorological conditions, and the radiative properties of the observed surfaces in order to retrieve the temperature from those measurements. Such approach can be achieved by implementing multiple sensors *in-situ*.

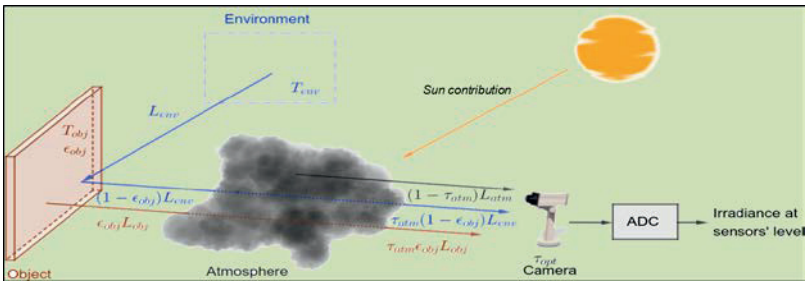

Figure 1: Schematic representation of radiative heat flux composition received by the infrared camera in outdoor conditions.

To extract the direct contribution of the monitored structure $\boldsymbol{L_{obj}^{i,j}}$ (i.e. estimate its apparent temperature with time) from the total radiative heat flux received at sensor camera level $\boldsymbol{L_{total}^{i,j}}$, the simplified radiative transfer equation [8] has to be extended and takes the following expression:

$$L_{total}^{i,j} = \epsilon_{obj}\tau_{atm}\tau_{opt}L_{obj}^{i,j} + (1-\epsilon_{obj})\tau_{atm}\tau_{opt}(L_{env}^{i,j} + L_{sun}^{i,j}) + (1-\tau_{atm})\tau_{opt}L_{atm} + (1-\tau_{opt})L_{opt} \quad (1)$$

In outdoor conditions, environmental quantities can be derived from local weather station's data. The emissivity, the reflection coefficient and the transmission coefficient of the added protective window are computed by injecting a priori knowledge about the monitored objects and the components of the infrared system implemented. Furthermore, in particular when no reference targets can be implemented on real site, a sky temperature correlation [9] combined with inputs from in-situ solar and meteorological measurements can be used to estimate the reflected radiance contribution and atmospheric transmission [10]. In other case, when data are missing, environmental information can be retrieved from meteorological aerodrome report (METAR) data, if available and by taking care of the scene geographical location.

In order to get consistent measurements, a thermal calibration has to be performed in laboratory conditions, prior to the experiment. Then, alteration of measurement performances and accuracy have to be checked during the life cycle of the implemented instrumentation.

Example of results obtained, on a concrete structure, with and without Tsky correction effect is presented in figure 2.

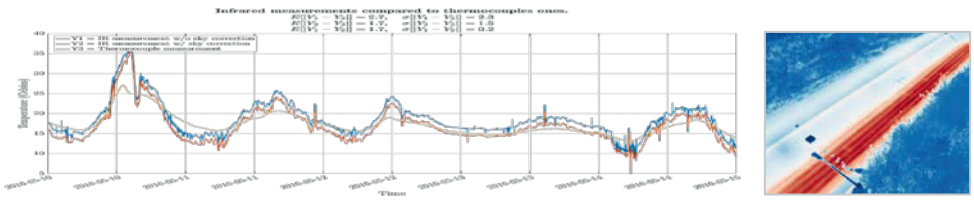

Figure 2: Sky temperature correction using correlation with local measurements

Comparison with surface temperature measurement carried out with local temperature sensor shows a decrease of the standard deviation.

NDT ANALYSIS METHODS APPLIED TO OUTDOOR MEASUREMENTS

A measurement campaign, with an IR thermography system designed for long term thermal monitoring and implemented on a viaduct, was carried out during several days on top of the deck using a signaling arch.

A Fourier analysis was applied to temporal evolution of each pixel of the whole thermal image sequence acquired. The magnitude and phase maps were analyzed to detect constitutive elements in the inner structure of the bridge deck, Figure 3.

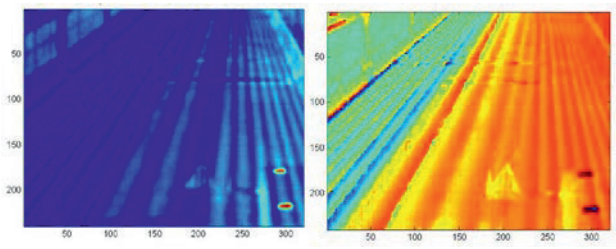

Figure 3: Amplitude and phase maps

The inner structure of the bridge deck could be observed on both images. In particular, post tensioned transversal tendons could be detected in the upper part of the maps around no50 pixel (supposed to be located in the upper part of the concrete deck under the asphalt wearing course). For longitudinal post-tensioned duct complementary analysis should be required. Nevertheless, the phase map seems more affected by the presence of some security signal on the deck during lane closing due to temporary access to the arch for other different measurements realized during this trial.

CONCLUSIONS

Different parameters involved into the long-term monitoring of structures through infrared thermography were introduced. The temperature estimation from IR measurements needs to take into account many parameters or at least be aware of the involved difficulties to consider the estimation uncertainties. Using coupled measurements with those infrared data enables the temperature estimation to be more accurate as presented for real concrete structure in oudoor conditions. An example of transposition from laboratory to real structure of NDT analysis methods to outdoor measurements on real bridge was presented. Analysis of results obtained showed that

inner structure of the bridge deck was retrieved by FFT analysis; in particular, post-tensioned duct was detected and located in the concrete deck. Future works will address conjoint estimation of emissivity and temperature with IR system and study robotized active infrared NDT approaches.

Acknowledgments: Author wish to thank Research Fund for Coal and Steel for funding part of this work under grant agreement No 800687 in the framework of DESDEMONA project.

REFERENCES

[1] Proto, M. et al., "Transport infrastructure surveillance and monitoring by electromagnetic sensing: the istimes project.," Sensors 10 (2010).

[2] J. Dumoulin, A. Crinière, R. Averty ," Detection and thermal characterization of the inner structure of the "Musmeci" bridge deck by infrared thermography monitoring ",Journal of Geophysics and Engineering, Volume 10, Number 2, 17 pages ,November 2013, IOP Science, doi:10.1088/1742-2132/10/6/064003.

[3] J Dumoulin and V Boucher, "Infrared thermography system for transport infrastructures survey with inline local atmospheric parameter measurements and offline model for radiation attenuation evaluations," J. Appl. Remote Sens., 8(1), 084978 (2014). doi:10.1117/1.JRS.8.084978.

[4] X. P. V. Maldague, Theory and Practice of Infrared Technology for Non-Destructive Testing, John Wiley & sons Inc., Hoboken, NJ (2001).

[5] Maierhofer CH, Arndt R, Röllig M, Rieck C, Walther A, Scheel H, Hillemeier B. Application of impulse-thermography for non-destructive assessment of concrete structures. Journal of Cement & Concrete Composite. 2006;28:393–401.

[6] Valluzzi MR, Grinzato E, Pellegrino C, Modena C. IR thermography for interface analysis of FRP laminates externally bonded to RC beams. Materials and Structures. 2009;42:25–34. doi:10.1617/s11527-008-9364-z.

[7] A. Crinière, J. Dumoulin, C. Ibarra-Castanedo and X. Maldague ," Inverse model for defect characterization of externally glued CFRP on reinforced concrete structures: Comparative study of square pulsed and pulsed thermography ", Quantitative InfraRed Thermography Journal, Taylor & Francis Editor, vol 11, pp 84-114, 2014. DOI: 10.1080/17686733.2014.897512.Icer D.F., Adams J.A. (1977) Mathematical Elements for Computer Simulation. McGraw Hill, NY.

[8] G. Gaussorgues, S. Chomet, Infrared Thermography, en, Springer Science & Business Media, Dec. 1993

[9] L. Adelard, F. Pignolet-Tardan, T. Mara, P. Lauret, F. Garde, and H. Boyer, "Sky Temperature Modelisation and Applications in Building Simulation," Renew. Energy, vol. 15, pp. 418–430, Sep. 1998

[10] Shettle, E. P. and Fenn, R. W., "Models for the aerosols of the lower atmosphere and the effects of humidity variations on their optical properties," tech. rep. (Sept. 1979).

Structural Health Monitoring Using a Generative Model

Y.Q. Ni*, Y. Gong & Y.H. Wei

Department of Civil and Environmental Engineering, The Hong Kong Polytechnic University, Hung Hom, Kowloon, Hong Kong.

Corresponding author: Prof. Y.Q. Ni (E-mail: Yiqing.ni@polyu.edu.hk)

ABSTRACT

Variational auto-encoder (VAE) is a generative model in terms of latent variables, which is amenable to extracting intrinsic feature and handling uncertainty inherent in data. Recent years have witnessed the huge successful progress of generative models in many domains, including image generation, text generation and other fascinating applications. In this study, the VAE for structural health monitoring using only dynamic response data that contains uncertainty of different sources is explored based on a reconstruction-based theory. The monitoring data collected under healthy condition is used to train a model in the auto-encoding framework, and the structural health index based on reconstruction probability is operated as a core indicator for identifying possible structural damage when a new set of data from an unknown status of the structure is available. A case study on the detection of high-speed train wheel defects using the online monitoring data of dynamic strain on the rail track collected during the passage of the train is provided to illustrate the applicability of the proposed method.

KEYWORDS: *Structural health monitoring, Generative model, Variational auto-encoder (VAE), Online monitoring system, Wheel defect detection*

INTRODUCTION

Variational auto-encoder (VAE) [1] is a promising generative model. Apart from the original function: "generation", it also could be exploited to achieve anomaly detection. The aim of anomaly detection is to search the objectives with patterns that are different from the expectation. This is consistent with the goal of structural health monitoring (SHM), which is to detect the location and severity of damage in a structure. For now, a mature solution approach on exploiting VAE to detect anomaly is the reconstruction-based theory, which has been employed in the anomaly detection of image [2, 3] and multimodal [4]. The main principle behind it is to train a model in the auto-encoding framework using monitoring data collected under healthy condition. When the data

gathered from the structure with damage is fed into the model, the reconstruction probability would be very low and can be operated as a core indicator for identifying possible structural damage.

In this study, a framework based on variational auto-encoder (VAE) is built to detect the wheel defects in high-speed trains in real time. During the long-term service period, the wheels of high-speed trains would encounter a variety of inevitable defects and further affect the safety of the train's operation, passenger comfort and the service life of railway components. This study focuses on the detection of wheel flat spot, which is a common local defect. The reconstruction probability of each set of strain data is treated as the structural health index (SHI). If contiguous data's SHIs are lower than the threshold, then the corresponding location can be perceived with the existence of wheel flat spot. The online monitoring data of dynamic strain on the rail track collected using an FBG-based wheel impact load detector (WILD) during the passage of the train is used to illustrate the applicability of the proposed method. A comparison between the detected and offline inspection results verifies that the proposed framework is competent to detect the wheel flat spot effectively.

MODEL FORMULATION

The philosophy behind a generative model is to learn the distribution inside the data. The proposed framework for SHM and the basic structure of VAE are shown in Figure 1. Basic VAE model is comprised of two parts: one is variational inference network (Encoder) and the other one is the generation model (Decoder). The model is trained by maximizing the evidence lower bound (ELBO):

$$\text{ELBO}(q) = -\text{KL}\left[q_\phi(z|x)||p_\theta(z)\right] + \mathbb{E}_{q_\phi(z|x)}\left[\log\left(p_\theta(x|z)\right)\right] \quad (1)$$

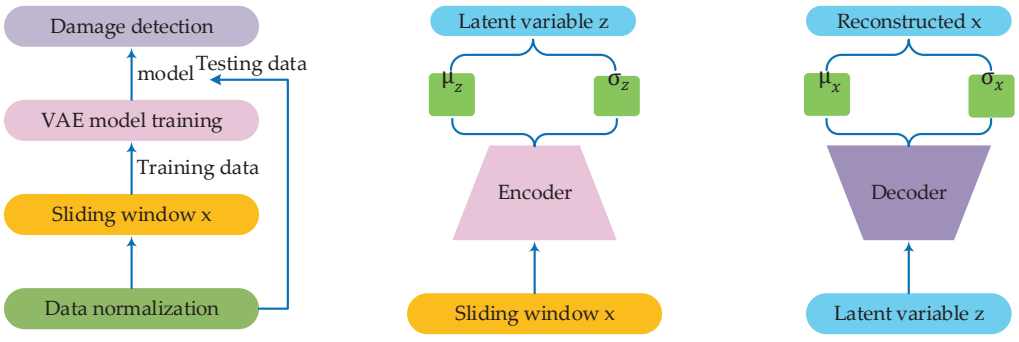

Figure 1: Proposed framework for damage detection: (a) structure of framework, (b) variational net $q_\phi(z|x)$, and (c) generative net $p_\theta(x|z)$

The first term on the right-hand side of Eq. (1) is the KL divergence between the approximate posterior and the prior of latent space, which acts as the regularization term. The second term is explained as the reconstruction probability [2]. It can be understood in terms of reconstruction of x through maximizing the log likelihood $\mathbf{log}(\mathbf{p}_{\boldsymbol{\theta}}(\boldsymbol{x}|\boldsymbol{z}))$ with sampling from $\mathbf{q}_{\boldsymbol{\phi}}(\boldsymbol{z}|\mathbf{x})$.

EXPERIMENTAL RESULTS

The online monitoring data of strain on the rail track collected using an FBG-based WILD during the passage of a train is used to illustrate the applicability of the proposed method. The monitoring data from wheelset No. 6 under the running speed of 50 (kph) is used for illustration. Figure 2(a) gives the structural health index for each data set gathered from one FBG sensor. First, the structural health index (SHI) for the majority of normal strain data falls inside the range of [0, 2.5]. Meanwhile the threshold of SHI is set to be -10. If there are more than 3 data point's SHI lower than -10, it can be determined as the occurrence of wheel flat. Figure 2(b) illustrates the variation of SHI versus train's speed. Both mean value of positive SHI and best SHI would decrease with the increase of train's velocity due to the amplified influence of wheel flat spot on strain response.

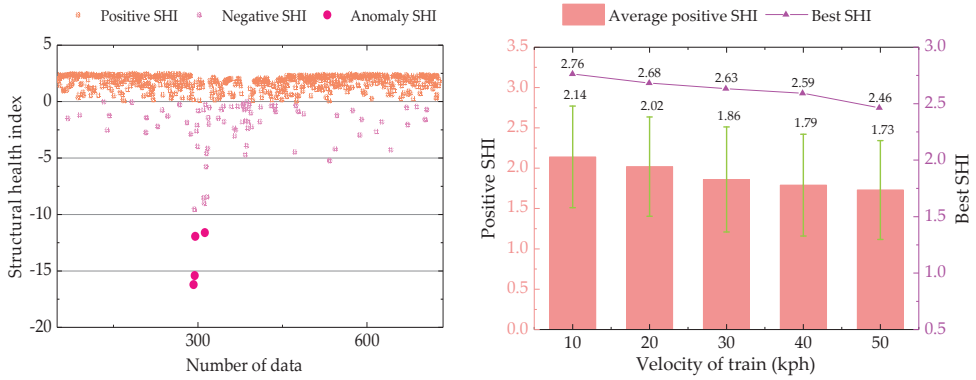

Figure 2: Testing results: (a) SHI of each data set, and (b) variation of SHI with train's speed

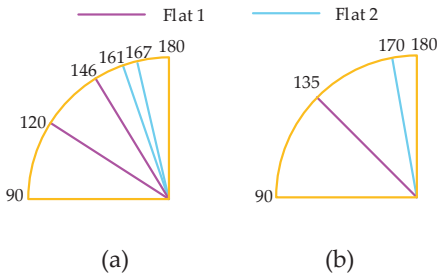

Figure 3: Wheel flat detection result for right wheel of wheelset No.6 (Unit: degree, one quarter of wheel): (a) detected location of flat spot, (b) offline inspection result (centre radian of flat)

The detected location of wheel flat around circumference for wheelset No.6 is shown in Figure 3(a). The offline inspection location of flat 1 (135°) falls within the detected range [120°, 146°] and the radian of flat 2 (170°) is also very close to the detected range [161°, 167°]. Besides, the detected angle between the two flats is 31°. This is close to the offline inspection result: 35°.

CONCLUSIONS

This study presents a VAE-based framework for high-speed train's wheel flat detection. The VAE is a probabilistic model which assumes that the latent variables satisfy the Gaussian distribution and are sampled from the mean vector and standard deviation vector, thus making them more stochastic and suitable for accommodating uncertainty in the real-world monitoring data. The reconstruction probability of the monitored dynamic strain data is derived to formulate the structural health index (SHI). The effectiveness of the method is verified by using the data gathered from an FBG-based online monitoring system and the results show high accuracy for flat detection.

ACKNOWLEDGMENTS

The work described in this paper is supported by a grant from the Research Grants Council of the Hong Kong Special Administrative Region, China (Project No. PolyU 152024/17E). The authors would also like to appreciate the funding support by the Ministry of Science and Technology of China and the Innovation and Technology Commission of Hong Kong SAR Government to the Hong Kong Branch of Chinese National Rail Transit Electrification and Automation Engineering Technology Research Center (Grants No. 2018YFE0190100 and K-BBY1).

REFERENCES

[1] Kingma, D. P., & Welling, M. (2013) Auto-encoding variational bayes. *arXiv preprint arXiv:1312.6114*.

[2] An, J., & Cho, S. (2015) Variational autoencoder based anomaly detection using reconstruction probability. *J. Special Lecture on IE*, *2*, 1-18.

[3] Zimmerer, D., Kohl, S. A., Petersen, J., Isensee, F., & Maier-Hein, K. H. (2018). Context-encoding Variational Autoencoder for Unsupervised Anomaly Detection. *arXiv preprint arXiv:1812.05941*.

[4] Park, D., Hoshi, Y., & Kemp, C. C. (2018) A multimodal anomaly detector for robot-assisted feeding using a lstm-based variational autoencoder. *J. IEEE Robotics and Automation Letters*, *3*(3), 1544-1551.

Hand phones, handy sensors: walking-induced vibration testing of slab floors assisted by mobile phone recordings

M. Catena[1], B.A. Dal Lago[2], F. Foti[3], L. Martinelli[4]

[1] *Department of Civil and Environmental Engineering, Politecnico di Milano, Milano, Italy.*
E-mail: marcello.catena@gmail.com

[2] *Department of Civil and Environmental Engineering, Politecnico di Milano, Milano, Italy.*
E-mail: brunoalberto.dallago@polimi.it

[3] *Structural Engineering Division, Faculty of Applied Sciences, University of Liège, Liège, Belgium*
E-mail: f.foti@uliege.be

[4] *Department of Civil and Environmental Engineering, Politecnico di Milano, Milano, Italy.*
E-mail: luca.martinelli@polimi.it

ABSTRACT

Mobile phones are rapidly evolving and are being equipped with sensors of growing accuracy, mainly due to the precision needed for various functions that are not directly related to structural monitoring. The paper describes the results of an experimental activity carried out on a prestressed concrete prefabricated slab of peculiar slenderness through walking-induced vibrations. Data obtained for the input motion, easily recorded with phones positioned at the pedestrian center of gravity, allowed to reproduce the test results within a finite element model. Test results were not reproducible with standard load models for a walking person.

KEYWORDS: *walking vibrations, prestressed floors, smartphones, sensors, monitoring*

INTRODUCTION

Modern buildings have the tendency to adopt longer floor spans than what it was usual a few decades ago. At the same time the mass of the floor and of non-structural elements tends to decrease, due to advances in the building industry and materials and the request of multifunctional space arrangements. This results in an increased importance of vibrations on the serviceability (comfort) of new structures.

Due to the expected response to human walking, floors are categorized as either low-frequency floors (LFFs) or high-frequency (HFFs) ones depending if the frequency of their first vertical mode falls below or above a threshold of approximately 10 Hz.

LFFs are expected to develop a resonant build-up type of response. HFFs are expected not to undergo a resonant response, but rather a transient response to each individual footfall impact. The 10 Hz limit is somewhat conventional, see [1] and [2].

Assessment of vibration serviceability requires appropriate modeling of the vibration source, the vibration transmission path and the vibration receiver.

Mobile phones are rapidly evolving and are being equipped with sensors of growing accuracy, mainly due to tasks not directly related to structural monitoring. The performance of the phone accelerometers is studied in this paper with reference to walking tests conducted on a prestressed concrete prefabricated slab of peculiar slenderness. Data obtained on the input motion, easily recorded with phones, fixed with a belt close to the pedestrian center of gravity, were crucial to enhance numerical simulations of the tests and reconcile them with the experimental measurement. This result was not obvious, since experimental measurements have highlighted as a nominally LFF was actually responding as an HFF one.

THE TESTED STRUCTURE

The general view of the plan of the tested floor structure is depicted in Figure 1. The floor system is made of prestressed voided elements connected to each other at a quarter of the span by 10 cm long butt-welds of embedded steel plates.

The structure was instrumented with 4 accelerometers Wilcoxon Research Model 731A, arranged in different configurations, the results here analyzed pertain to the instrument layout depicted in Figure 3.

The natural frequencies and damping ratios were estimated from experimental results. The natural frequencies of the first four modes of the floor system are f_1 = 8,2958 Hz; f_2 = 10,6946 Hz; f_3 = 14,6926 Hz; f_4 = 19,3903 Hz. The corresponding damping ratios are: z_1 = 1,10%; f_2 = 1,04%; f_3 = 0,90% Hz; f_4 = 0.80%.

Accordingly, the floor can be classified as a LFF, and thus being prone to resonance built up of vibrations. The tests outcome, however, proved differently.

In the following, the results for a person walking along trajectory T1 (from right to left) in Figure 1 will be shown. Figure 2 depicts the readings from the 4 Wilcoxon accelerometers, located at stations “A1”-“A4” as shown in Figure 1.

A first attempt at reproducing the experimental behaviour was carried out with a Finite Element (FE) model applying a traditional continuous forcing function (computed according to [3] for f_{pacing} = 1,625 Hz, person weight G = 0,9 kN, 3 harmonics) applied at mid span. The predicted vertical accelerations are shown in Figure 3, and highlight a HFF trend with way too small accelerations.

By subsequently applying on the FE model as Ground Reaction Force (GRF) the scaled vertical accelerations registered near the CM of the walking individual, similarly to the

approach in [4], the results in Figure 4 were obtained. These are in much better agreement with the experimental measures, both in amplitude and general trend.

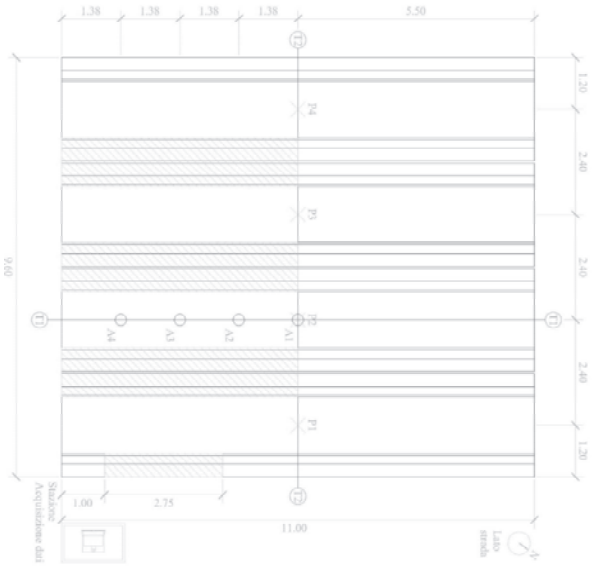

Figure 1: Plan view of the tested floor.

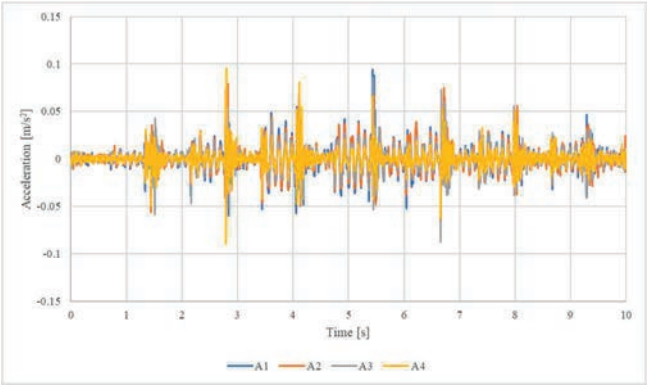

Figure 2: Experimentally measured accelerations (units are m and s) at stations from A1 to A4..

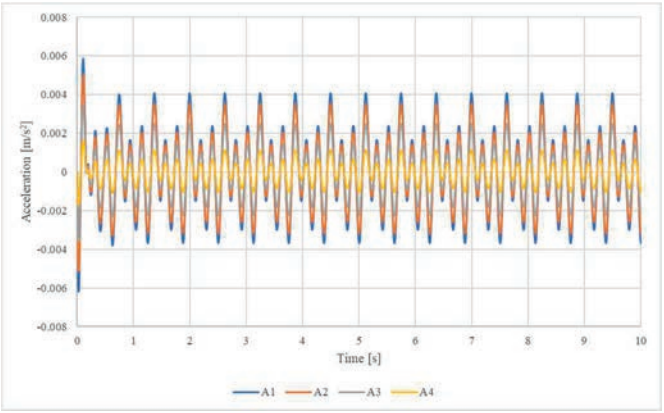

Figure 3: Numerically computed accelerations with standard forcing function.

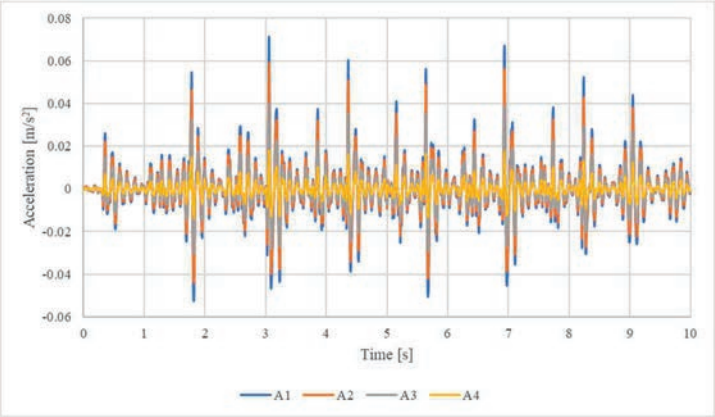

Figure 4: Numerically computed accelerations (measures in meters) with GRF obtained from recorded vertical acceleration near the CM of the walking person.

CONCLUSIONS

In spite accelerometers in smartphone have been introduced for different tasks, their precision is sufficient to serve as monitoring instruments. A GRF derived from data obtained from phone recordings of the vertical acceleration of the CM of the person walking allowed to reproduce the test results within a finite element model. Test results were not reproducible with standard load models for a walking person, based on a Fourier series expansion.

REFERENCES

[1] Muhammad, Z., Reynolds, P., Avci, O., Hussein, M. (2018), Review of Pedestrian Load Models for Vibration Serviceability Assessment of Floor Structures Vibration 2018, 2, 1–24; doi:10.3390/vibration2010001

[2] Mohammed, A.S., Pavic, A., Racic V. (2018), Improved model for human induced vibrations of high-frequency floors, Engineering Structures 168 (2018) 950–966.

[3] Bachmann, Vibration Problems in Structures: Practical Guidelines, Birkhouser 1995.

[4] Van Nimmen, K., Lombaert, G., De Roeck, G., Van den Broeck, P. Simulation of Human-induced Vibrations Based on the Characterized In-field Pedestrian Behavior. J. Vis. Exp. (110), e53668, doi:10.3791/53668 (2016).

Application of Ultrasonic Guided Waves Technology to Inspection of Bolt Group Joints

Yue Zhang, Dongsheng Li

School of Civil Engineering, Dalian University of Technology, Dalian, China.
E-mail: yuezhang@mail.dlut.edu.cn

ABSTRACT

Bolt connection, as an important form of structural connection, which is widely used in the structure and equipment of various industries and is very important to guarantee the safety of overall structure. However, bolt looseness or preload deterioration may threaten the safety of the structure, so it is necessary to monitor the bolt group joints in real time. This article presents a study of assessing the loosening/tightening health state and identifying the loose bolt by using ultrasonic guided wave in a bolt group joint. A bolt-tightening index was proposed for evaluating the looseness of a bolt connection based on correlation coefficient. The tightening/loosening state of the bolt was simulated by changing the bolt torque. With the bolt torque increases, value of the proposed bolt-tightening index increases. The proposed bolt-tightening index trend was very well reproduced by an analytical expression using a function of the torque applied. To verify the effectiveness of the proposed method, a bolt group joint experiment with different damage levels was performed. Experimental results show that the proposed approach is effective to detect and locate bolt looseness and has a good prospect of finding applications in real-time structural monitoring.

KEYWORDS: *Ultrasonic guided wave, Bolt looseness, Correlation coefficients, Structural health monitoring*

INTRODUCTION

The general methods of detecting the preload force of the bolt used in the project are torque wrench method, resistance strain gauge measurement method, detection method based on structural modal information and ultrasonic guided wave method. Ultrasonic guided wave is a kind of stress wave , which can interact with different damages in structures by advantages of their high sensitivity to micro-damage and low energy attenuation through long distance, so it has tremendous potential in structural non-destructive evaluation(NDE)[1-4].In view of the virtues of ultrasonic guided wave, which can be applied to bolt joints damage detection. Lighth et al.[5] identified the

damage characteristics of the bolt and found that the bolt looseness damage has a certain relationship with the wave group velocity by measuring the speed of the reflected waves. Yang and Chang [6,7] proposed the mathematical relationship between the energy attenuation of ultrasonic guided wave propagation and the specific damping of the system according to the Hertzian contact theory and the damping principle. An and Sohn[8] presented a combination of methods using impedance and elastic wave techniques. Contraposing the problems of the Lamb wave method in bolt debonding monitoring of composite joint, Wang et al[9] studied the method based on the time-reversal theory to improve the Signal-to-Noise quality of monitoring signal and the monitoring system stability.

In this study, piezoelectric patches were utilized as transducers to assess the health state of a bolted joint. Various tests were performed by increasing the applied bolt torque to simulate various configurations, i.e. from a full loosened state to a tight configuration. For the ultrasonic method, a tightening/loosening state index based on the correlation coefficient of mathematical statistics was developed. In contrast with the previous studies which used a damage index to estimate bolted status, in this approach, the relationship between correlation damage index and the bolt torque is established. The experimental results show that the proposed tightening/loosening state index is exponentially increasing with bolt torque..

BOLT LOOSENESS DETECTION

The change of torque to bolts was chose as the variable in the paper to learn the influence of the damage degree to the signal. The torque of No.1 bolt changes from 0Nm to 50Nm with the interval torque 5Nm. During experiment, other bolts was set fixed torque of 50Nm, which were applied through the digital torque wrench. Due to the complexity of joint damage of the bolts, the general bolt-tightening index is often difficult to apply. The correlation coefficient was developed as the bolt-tightening index. The DI_{CC} of two waveforms can be expressed as follow:

$$DI_{CC} = \frac{C_{BD}}{\sigma_B \sigma_D} \times 100\% \tag{1}$$

where C_{BD} is the covariance of two waveforms.

Figs. 1(a)-(d) shows the bolt-tightening index DI_{CC} under different bolt torque value from 0 to 50 Nm in six kinds of loosened configurations experiments. The analysis shows that the sensitivity of the DI_{CC} value is related to the angle between the two piezoelectric ceramics and the loosened bolt. The increase of the angle will make the superposition and dispersion phenomenon of waves more serious, and also make the difference between the detection signal and the baseline signal more obvious. The results highlighted that the DI_{CC} index is highly sensitive to the bolt-tightening state,

providing a reliable and promising index able to assess the health state of bolted joints.

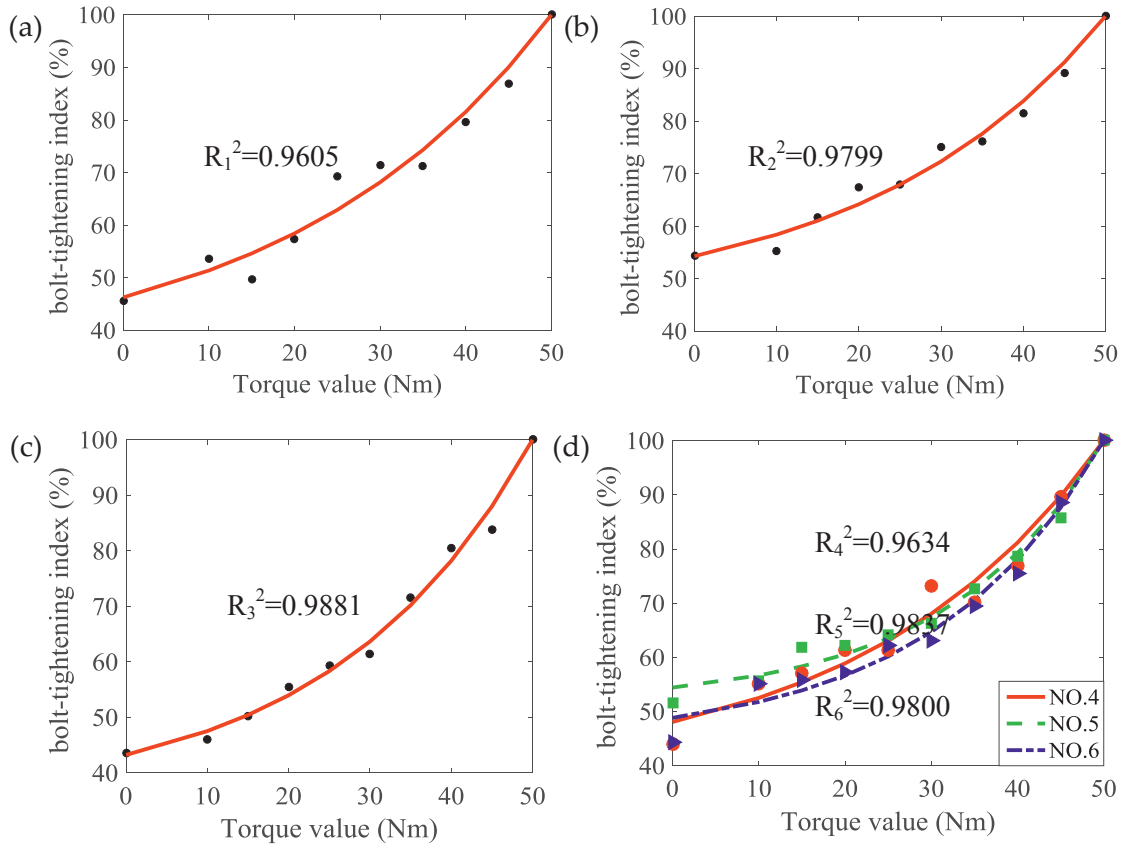

Figure 6: *DIcc* results vs torque, for the six kinds of loosened configurations: (a) No. 1 loosened bolt, (b) No. 2 loosened bolt, (c) No. 3 loosened bolt and (d) No. 4,5 and 6 loosened bolts

Figure 1 shows how the *DIcc* Trend value changes, by increasing the torque applied at the joint. The graphs highlight, in all cases, that the trend is well approximated by a exponential function:

$$DI_{cc} = (1-\xi)e^{a(T-T_{\max})} + \xi \tag{2}$$

This equation is a fitting curve where the parameters in the equation have been extrapolated by a careful study of the experimental results. Where T is the bolt torque, T_{max} the maximum torque bolt，ξ the index value which related to the angle between the loose bolt and the Piezoceramics, α a factor proportional to the slope of the curve. As shown in Figure 6, the accuracy of the exponential function, with respect to the experimental results, is higher than 95%. This means that the correlation coefficient method, based on the calculation of the *DIcc*, provides a reliable and thoroughly sensitive index in detecting the health state of bolted structures.

CONCLUSIONS

In this study, new indices were developed to assess and locate the loosening/tightening health state of a bolted structure by using the ultrasonic method. The correlation coefficient index provided results to be able to assess the health state of a bolted joint with an overall percentage error lower than 5%. It was observed that the index trend as a function of the applied torque was well approximated by a exponential function. This means that the calculation of the bolt-tightening index, provides a reliable and thoroughly sensitive index in detecting the health state of bolted structures. The proposed method of using a small number of active piezoelectric actuator/sensors to quickly and conveniently obtain the health state of the bolt group joint by calculating the correlation index has better engineering applicability. Detection of multiple bolt damage is another issue worthy of investigation. The use of Lamb waves seems more viable than other tools for its exclusive responses to different damage status, so intensive investigation and improvement are matters for further research.

REFERENCES

[1] Aymerich, F., and Meili, S. (2000) Ultrasonic evaluation of matrix damage in impacted composite laminates. COMPOSITES PART B-ENGINEERING, 31(1), 1-6.

[2] Cawley P, A.R.D. (1989) Defect types and non-destructive testing techniques for composites and bonded joints. Metal Science Journal, 5(5), 413-425.

[3] Ibrahim, M.E. (2014) Nondestructive evaluation of thick-section composites and sandwich structures: A review. Composites Part A: Applied Science and Manufacturing, 64, 36-48.

[4] Rose, J.L. (1999) Ultrasonic waves in solid media. Cambridge University Press.

[5] Light, G.M., Ruescher, E.H., Bloom, E.A., Joshi, N.R., Tsai, Y.M., and Liu, S.N. (1993) Application of the cylindrically guided-wave technique for bolt and pump shaft inspections. Nuclear Engineering and Design, 144(3), 465-468.

[6] Yang, J.Y., and Chang, F.K. (2006) Detection of bolt loosening in C-C composite thermal protection panels: I. Diagnostic principle. Smart Materials and Structures, 15(2), 581-590.

[7] Yang, J., and Chang, F.K. (2006) Detection of bolt loosening in C‐C composite thermal protection panels: II. Experimental verification. Smart Materials and Structures, 15(2), 591-599.

[8] An, Y., and Sohn, H. (2012) Integrated impedance and guided wave based damage detection. Mechanical Systems and Signal Processing, 28, 50-62.

[9] Wang, Q., Yuan, S.F., and Qiu, L. (2007) Study on bolt de-bonding monitoring of composite joint based on time-reversal method. Journal of Astronautics, 28(06), 1719-1723.

IoT Based Monitoring and Assessment System for Construction-induced Vibration

Qiuhan MENG[1], Songye ZHU [2]

[1] *Department of Civil and Environmental Engineering, The Hong Kong Polytechnic University, Hong Kong, China.*

E-mail: qiuhan.m.meng@connect.polyu.hk

[2] *Department of Civil and Environmental Engineering, The Hong Kong Polytechnic University, Hong Kong, China.*

E-mail: songye.zhu@polyu.edu.hk

ABSTRACT

On-site vibration impact monitoring and assessment is an effective way to ensure structure safety, equipment functionality and human comfort during construction processes. However, many existing vibration monitoring devices have some deficiencies, including high costs, specialized operation requirements, and complicated management. With the advancement in wireless sensing technology that processes high performance, cost-effectiveness and other merits, integrating vibration monitoring and assessment with Internet of Things (IoT) becomes an alternative choice. The implementation of IoT system paves an effective and reliable way for real-time data transmission and accurate analysis. In addition, it reduces the installation and maintenance costs compared with adoption of wired ad-hoc sensing system. The proposed system consists of an Arduino Mega board, an IoT shield kit, a real time clock module, and a micro-electromechanical (MEMS) accelerometer. In this system, Arduino board collects data and uploads it to the cloud, while the IoT shield kit provides the latest cutting-edge LTE CAT-M and NB-IoT technology. The measurements are stored and analyzed in the cloud, which is available for remote access by any authorized mobile device through Internet.

KEYWORDS: *Internet of Things (IoT), cloud computing, construction-induced vibration monitoring and assessment*

INTRODUCTION

Construction activities, such as piling and excavation, often generate excessive ground-borne vibration that may affect the surroundings. Increasing demand for the expansion and renovation of existing buildings leads to inevitable impact on structural

safety, equipment functionality and human comfort. It is necessary to give a knowledge of vibration levels from mechanized construction activities that may cause environmentally intrusive ground-borne vibration. Ground-borne vibrations are estimated by different indices, including peak particle velocity (PPV), root-mean-square (RMS) velocity and acceleration in 1/3 octave band spectrum. PPV has been found to be correlated with structural damage since particle velocity is proportional to the strain induced during the passage of a wave [1]. RMS velocity in 1/3 octave band spectrum is defined as vibration index with regard of sensitive equipment and facilities, while RMS acceleration in 1/3 octave band spectrum has been used in a baseline standard curve corresponding to perception level of human comfort. Over the past decades, the effects of construction-induced vibration have attracted attention from academic and industry. For example, ISO [2], British Standards [3], Eurocode [4], as well as Hong Kong Government [5], have suggested acceptable vibration limits. On the other side, there is an increasing need to minimize the instructive effects of vibration that induced by construction works. As early as 2014, Hong Kong Hospital Authority stipulated a compulsory guideline that requires all hospital redevelopment projects to consider the negative impact of construction-induced vibrations on ultra-precision medical equipment and facilities. Even though commercial monitoring devices are adopted by local construction industries, limitations such as high costs, specialized operation requirements, inaccurate monitoring results are identified. In addition, it is hard to realize continuous monitoring and remote data sharing when using such devices.

The Internet of Things (IoT) provides a new solution to this problem. The “things” in the concept of IoT have the capability to sense physical phenomena and trigger actions on physical actuators. With the integration of IoT and cloud computing, the efficiency and performance of the construction-induced vibration impact monitoring and assessment system can be improved.

IoT relies on a wide range of materials, network infrastructure, communication protocols, Internet services, and computing technologies [6]. WSN is considered as one of the key technologies in IoT and it is widely used. For example, one of the most popular low-power WSN protocols is ZigBee, but it has disadvantages in low data rate. Compare with ZigBee, data communication of Wi-Fi can reach up to 54 Mbps and distance up to 100 m. But it consumes more power. Besides standard protocols, other low-power communications protocols, such as NB-IoT and LTE M1, can be connected in mobile environment due to high spectral efficiency, bandwidth, and coverage. They are suitable for long range transmission while maximizing the battery lifetime.

SYSTEM DESIGN

The adopted IoT-based sensor module consists of a high-sensitivity Microelectromechanical system (MEMS) accelerometer, a data acquisition system (DAQ), and IoT shield for remote data transmission.

MEMS sensor advantages in small size, light weight, low power consumption, high reliability, high sensitivity and easy integration. In order to prove the effectiveness and accuracy, three different MEMS accelerometers, namely, MMA8451Q, MPU-6050 and BMI160, were selected and calibrated through shaking table tests. Calibration to the gravitational reference of all MEMS accelerometers were conducted before shaking table tests. One commercial tri-axial piezoelectric accelerometer, PCB356B18, was tested as well for comparison. The data processing was conducted using MATLAB software (MATLAB 2016a). The shaking table tests proved that the MEMS accelerometers can accurately measure harmonic vibration as low as 2 Hz, a lower limit of frequency relevant to vibration impact on structural damage, equipment accuracy, and human feelings.

Arduino is a widely used open-source board that could meet the specific requirements of different applications and provides the possibilities in paring with MEMS sensors. Data collection and transmission are conducted by Arduino Mega 2560, which could be powered by a micro-USB connector or an external power supply (e.g. a battery). The low-power cellular module, named SIM7000C, supports the new LTE CAT-M1 and NB-IoT technologies. It can be used by plugging the shield into an Arduino board, inserting a compatible SIM card, and attaching the dual LTE/GPS antenna. The price of Arduino Mega 2560 and SIM7000C are 40 US dollars and 70 US dollars respectively.

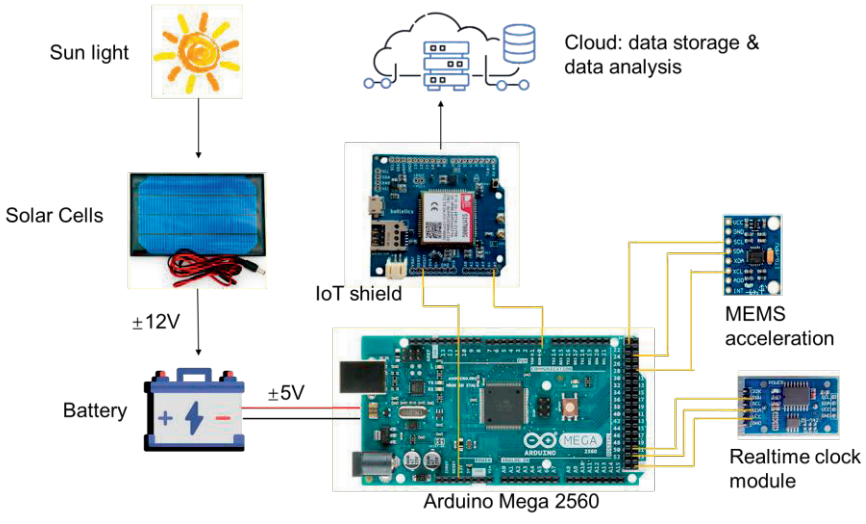

Figure 1: The proposed IoT sensing system

For long-term field monitoring, IoT devices suffer from limited battery volume, and the replacement or recharging the battery is difficult. A solar panel and LiPo battery are equipment in the system. Solar energy is retrieved to recharge LiPo battery which powers the Arduino board. To balance the computation power and service time, the measurement data will be transferred to the cloud and post-processed by the cloud. The cloud system consists of software that realizes data storage and data processing. Real-time data cleansing, analyzing, and vibration impact assessment are conducted via different algorithms. The software also integrates the database of vibration limits for various types of medical equipment that cloud evaluate real-time vibration level through comparison.

CONCLUSIONS

An IoT based monitoring and assessment system for construction-induced vibration is developed. This system combines novel IoT and cloud computing technologies, as well as low-cost MEMS accelerometers and Arduino Mega 2560 board as DAQ. The accuracy of MEMS accelerometers, as well as the capability of Arduino board and SIM7000C IoT shield have been tested. The Cloud allows the measurements to be stored and processed, which reduces the computational time and costs. Considering the electricity in the battery is limited, renewable energy source (e.g. solar energy) is proposed to use as power supply for Arduino board. In the future, this newly developed system should be tested in real construction projects for validation purpose.

REFERENCES

[1] New, B. (1986). Ground vibration caused by civil engineering works (0266-5247). Retrieved from

[2] ISO2631.2. (1989). International Organization for Standardization. *Evaluation of human exposure to whole-body vibration. Part 2: Continuous and shock-induced vibration in buildings (1 to 80Hz)*.

[3] BS5228-2. (2009). British Standards Institution. Part 2 : 2009. *Code of practice for noise and vibration control on construction and open sites – Part 2: Vibration*, BSI(London).

[4] ENV3-5. (1993). Eurocode 3. *Design of Steel Structures Part5- Piling*, ENV 1993-5(European Committee for Standardization), Brussels.

[5] HKSARG. (2017). Code of Practice for Foundations. HKSARG: *Building Department, HongKong*(China).

[6] P. Suresh, J. V. Daniel, V. Parthasarathy, and R. H. Aswathy, "A state of the art review on the Internet of Things (IoT) history, technology and fields of deployment," in *Proc. IEEE Int. Conf. Sci. Eng. Manag. (ICSEMR)*, Chennai, India, 2014, pp. 1–8.

Response Prediction and Evaluation

Structural Reliability Calculation Method Based on Deep Reinforcement Learning

Yuequan Bao[1,2*], Zhengliang Xiang[1,2], Zhiyi Tang[1,2], Hui Li[1,2]

[1] *School of Civil Engineering, Harbin Institute of Technology, Harbin,150090, China.*

[2] *Artificial Intelligence Lab, Harbin Institute of Technology, Harbin, 150090, China.*

[*] *E-mail: baoyuequan@hit.edu.cn*

ABSTRACT

The surrogate model is widely used to reduce the computational cost of the Monte Carlo Simulation (MCS) in structural reliability assessment. The prediction accuracy of surrogate model is heavily determined by model accuracy around the limit state surface. Most sampling method distribute the representative samples in the sampling space, while it will loss the model accuracy around the limit state surface. Deep reinforcement learning is expert in observing state and taking action to achieve a goal. Inspired by this, this paper proposes a new sampling method for structural reliability assessment based on the deep reinforcement learning (DRL). First, the sampling space and the existing samples are transformed into an array which is treated as the state. Second, deep neural network is designed as the agent to observe the sampling space and to select new representative samples, the samples are treated as the actions. Finally, a specific reward function is proposed to guide the deep neural network to select representative samples along the limit state surface. The numerical example demonstrate that the proposed method learns to select representative samples along the limit state surface. The results show that the proposed method can achieve higher accuracy in sample classification and structural reliability assessment than the uniform sampling method.

KEYWORDS: *Structural reliability, Deep reinforcement learning, Surrogate model*

INTRODUCTION

Surrogate model methods are widely developed in recent years, which aim at finding an approximate response function to replace the finite element model in the MCS method, so as to reduce the computational cost [1][3]. However, the accuracy and efficiency of surrogate model method are heavily affected by the selection of training samples. Conventional strategies for select training samples are based on the theory of design of experiments [4]. These methods try to fill the sampling space with the

selected representative samples, and the surrogate model may lose the accuracy around the limit state surface, which is the key area in sample classification.

Deep learning-based artificial intelligence has been developed rapidly in recent years. *AlphaGo Zero* carries out self-learning with a reinforcement learning algorithm; the trained program can select the move with the maximum winning probability in each position[5]. Inspired by this, we propose a sampling method for structural reliability analysis based on a deep reinforcement learning (DRL) algorithm [6][7]. In the proposed method, the sampling space for structural reliability assessment is treated as a hypothetical *Go* board, the candidate samples can be regarded as the chess pieces of *Go*, and the DRL method is employed to train *police* to select representative samples along the limit state surface.

MODEL FORMULATION

To use DRL to select representative samples along the limit state surface, we replace the *state* of the DRL framework with a sampling space, use a deep neural network as the *agent*, and treat the selected samples as *actions* of each training step, shown in Figure 1. The framework and architecture of our DRL-based sampling method are shown in Figure 2.

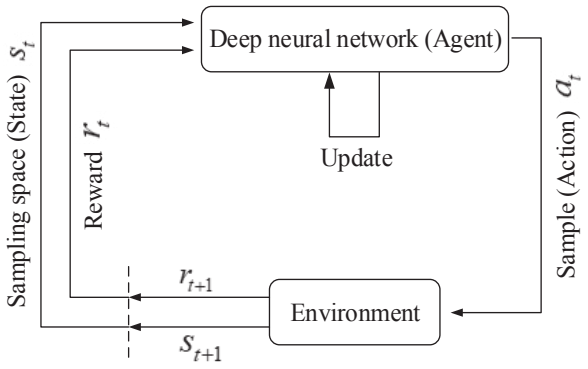

Figure 1: Proposed framework of DRL-based sampling method.

As illustrated in Figure 2, the *State* is an *n*-dimensional array that represents the *n*-dimensional the sampling space and the existing samples. The deep neural network is used as the *agent*, which can observe the *state* and take *action* to the *environment*. The network consists of the *actor* and *critic* networks. The *actions* are the samples selected by the *agent* at each training step. The *reward* is a real value comes from the *environment* after each *action* is taken. Besides, to improve the stationarity and efficiency of training, the parallel agents and multi-threaded asynchronous learning algorithm [6] are applied to train the deep neural network. At each training step, the *agent* can observe the input *state*, and puts out the mean value and the standard deviation of the random an *action*. Then an *action* is randomly generated according to the statistical parameters. The

environment uses the *action* to update the *state* and put out a *reward*. At last the deep neural network update its parameters using the *reward*.

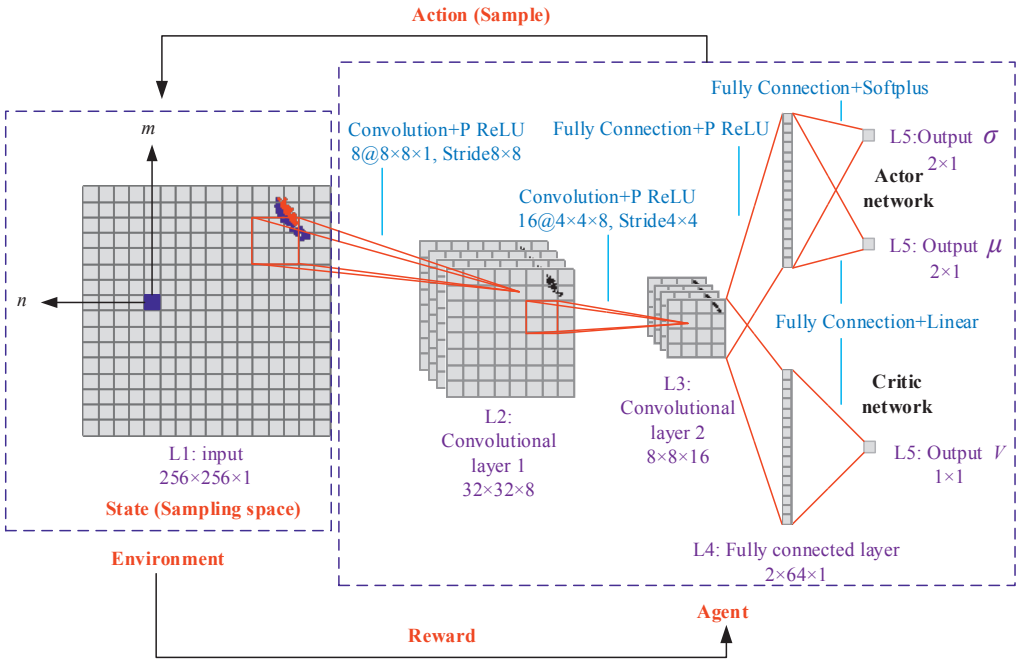

Figure 2: Proposed framework of DRL-based sampling method.

NUMERICAL EXAMPLE

In this example, the highly nonlinear limit state function is considered. It is defined as

$$g(x_1,x_2)=4-\frac{(x_1+x_2)}{\sqrt{2}}+0.1(x_1-x_2)^2+0.5\sin\left(5\left(4-\frac{(x_1+x_2)}{\sqrt{2}}+0.1(x_1-x_2)^2\right)\right) \quad (1)$$

where x_1 and x_2 are independent standard normal random variables, and the probability information is $x_1 : N(0,1)$ and $x_2 : N(0,1)$. First, the DRL method is applied to select training samples. The sampling processes are illustrated in Figure 3.

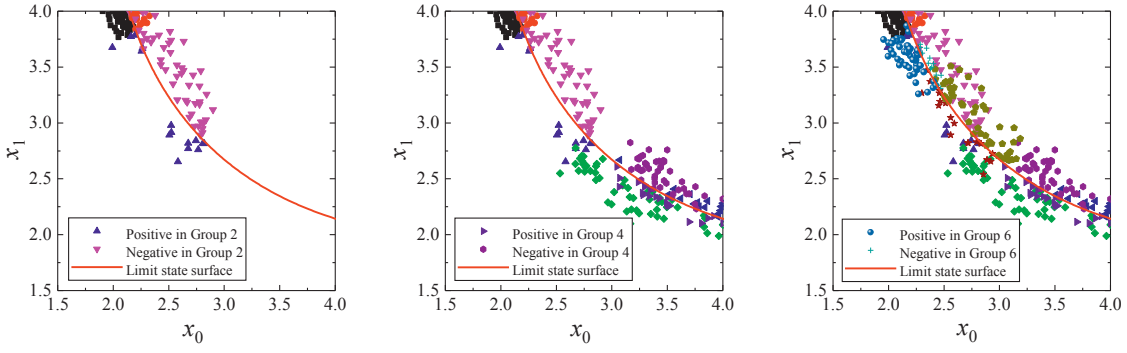

(a) (b) (c)

Figure 3: Sampling process of DRL method.

Two deep neural networks surrogate models are trained with the samples selected by DRL and the same number of samples selected by uniform sampling. Then the two surrogates are used to calculate the reliability of the same sample set, and the results are compared with that of the direct MCS method, as presented in Tab. 1. The results show that the DRL method can obtain higher accuracy in sample misclassification and reliability assessment.

Tab. 1. Result comparison of DRL method and uniform sampling methods.

Methods	*TN*	*FN*	*FP*	*FN+FP*	N_f	P_f (1e-5)	Precision of N_f (%)	Recall of N_f (%)	Error of P_f (%)
MCS					371	1.855			
DRL	371	3	0	3	374	1.870	99.2	100.0	0.8
US	332	18	39	57	350	1.750	94.9	89.5	-5.7

N_f: number of failure samples; *TN*: true negative; *FN*: false negative; *FP:* false positive.

CONCLUSIONS

In this paper, a novel deep reinforcement learning (DRL)-based sampling method for structural reliability assessment is developed. The sampling space and the information of the existing samples are transformed to a n-dimensional array, and it is treated as the state of DRL. New selected samples are treated as the actions of DRL method. Deep neural network is used as the agent, it can observe the state and select new samples. A specific reward function is proposed to guide the deep neural network to select more samples along the limit state surface. Numerical example demonstrates that the proposed DRL-based sampling method can learn to select representative samples along the limit state surface. With the same number of representative samples, the surrogate model of proposed method has higher accuracy around the limit state surface than the uniform sampling method.

REFERENCES

[1] Melchers RE. Structural reliability analysis and prediction. 2nd ed. West Sussex, England: John Wiley & Sons; 1999.

[2] Chojaczyk A A, Teixeira A P, Neves L C, et al. Review and application of Artificial Neural Networks models in reliability analysis of steel structures[J]. Structural Safety, 2015, 52(3):78-89.

[3] Bucher, C. G, Bourgund. A fast and efficient response surface approach for structural reliability problems[J]. Structural Safety, 1990, 7(1):57-66.

[4] Fang K T, Lin D K J, Winker P, et al. Uniform Design: Theory and Application[J]. Technometrics, 2000, 42(3):12.

[5] Silver D, Schrittwieser J, Simonyan K, et al. Mastering the game of Go without human knowledge[J]. Nature, 2017, 550(7676):354-359.

[6] Mnih V, Badia, Adrià Puigdomènech, Mirza M, et al. Asynchronous Methods for Deep Reinforcement Learning[J]. 2016.

[7] Sutton R S, Barto A G. Reinforcement Learning: An Introduction[J]. IEEE Transactions on Neural Networks, 1998, 9(5):1054-1054.

A PROBABILISTIC ANALYSIS OF THE WIND FIELD AT SULAFJORDEN BRIDGE SITE

Dario Fernandez[1], Aksel Fenerci[1], Ole Øiseth[1]

[1] *Department of Structural Engineering, Norwegian University of Science and Technology, Norway.*

E-mail: dario.r.f.castellon@ntnu.no

E-mail: aksel.fenerci@ntnu.no

E-mail: ole.oiseth@ntnu.no

ABSTRACT

The Ferry Free Coastal Highway E39 is an outstanding project directed by the Norwegian Public Roads Administration. It has the aim of connecting the Norwegian western coast with a ferry-free trail. Nevertheless, Norway's western coast is characterized by the presence of numerous fjords. Therefore, the project requires the construction of several long span bridges. Furthermore, the mountainous topography of the track alters flow of the sea winds and directs it towards the fjord channels. This generates a statistically random, wind turbulent condition at the bridge's location. The purpose of this study is to analyze the wind conditions at the 3.8 km Sulafjorden Bridge site and, to settle the basis for the development of a probabilistic model to forecast the extreme aeolian actions in the place. Since 2016, the Sulafjorden is equipped with a network of sensors measuring the in-land environmental conditions. To describe the wind conditions at the bridge site, a probabilistic analysis was developed by fitting probabilistic distributions to the data.

KEYWORDS: *Turbulence intensity, probabilistic modelling, suspension bridge, wind field.*

INTRODUCTION

The Sulafjorden Bridge is a challenging project. It will span over 3.8 km across the fjord which gives it its name. Located near Ålesund, Norway, a few kilometers away from the open sea, this outstanding project will require novel solutions made to its magnitude. Many research projects are running now in Norway to achieve its development.

From 2016, a team leaded by the Norwegian Public Road Administration deployed a network of sensors on the Sulafjorden's site. Their objective is to measure the variation of the wind conditions at the E-39 fjord-crossing sites [1].

In this document, four of the stations were chosen due to their proximity to the Sulafjorden's site. The stations names are Kvitneset, Trælboneset, Kårsteinen and Langenset. Basically, each one is composed by mast structure and equipped with a set

of anemometers at different heights. The anemometers record the wind speed and direction at 10hz. The information is consolidated in a monthly file per station and is available on the web site [2].

The scope of the present study is to give an insight of the wind conditions at the site and provide an initial probabilistic analysis of the wind field. The wind records were analyzed to obtain the variations of the mean wind speed and direction as well as the turbulence intensities. For the development of the probabilistic analysis, it was implemented a procedure like that of the Hardanger Bridge [3]: histogram fitting based on data analysis for the specific site.

WIND CONDITIONS AT SULAFJORDEN SITE

To obtain a description of the variability of the wind it was applied a straight forward procedure. The monthly records were divided into a set of ten-minute intervals. The mean direction in each interval was computed with a circular mean algorithm to avoid the overlapping between 0° and 360°. Then, the wind velocity was decomposed in mean wind speed and three turbulent components: along-wind, cross wind and vertical. The wind rose diagram of the four stations is presented in Figure 1. It is possible to observe that the dominant wind direction is blowing from the fjord channel. Therefore, it is expected that the stronger winds impact the Sulafjorden Bridge transversally. These results match with those reported by Kjeller Vindteknikk [4].

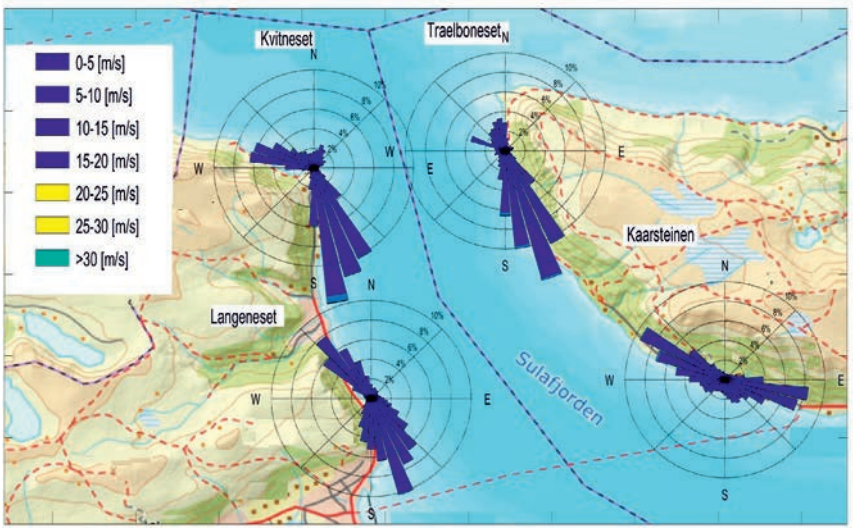

Figure 1: Wind Rose diagram.

From the diagram, it is possible to appreciate that the stations giving the most relevant information of the unfavorable wind conditions at the bridge section are the Kvitenset and the Trælboneset in the directions 175° and 165°, respectively. Therefore, a more detailed analysis will be performed in these dominant regions.

The next step in the analysis is to assess the statistical behavior of the turbulence. In this framework, the turbulence intensities of the three components were computed as:

$$I_U = \frac{\sigma_u}{\bar{V}} \;\; ; \;\; I_V = \frac{\sigma_v}{\bar{V}} \;\; ; \;\; I_W = \frac{\sigma_w}{\bar{V}} \qquad (1)$$

Where $\sigma_u \sigma_v \sigma_w$, represents the standard deviation of along wind, cross wind and vertical, respectively, while $\bar{V}$, stands for the mean wind velocity.

These intensities give a measure of the energy content in the wind field since they depend on the turbulence standard deviation. Further, those records with mean wind speed lower than 3m/s were filtered out, because the chaotic behavior of low speed wind fields produces out of trend values of turbulence intensity.

MEAN WIND SPEED AND TURBULENCE INTENSITIES

With the analysis coming from the data it is possible to build a model of the wind behavior at the Sulafjorden Bridge site. The description proposed in this study, consists in fitting probability distributions to the data histograms of wind direction, mean speed and the three turbulent components.

Figure 1 shows that for each of the 4 stations there are two dominant directions. Therefore, the analysis is divided into sectors with different expected behavior. Moreover, a further division will be added because the sensors on each mast are located at different heights, approx. 25m vertical spacing.

In Figure 2 it is shown a sample set of histograms and distribution fittings for the stations Kvitneset and Trælboneset from the month of January to March 2019. It can be highlighted that the *LogNormal* distribution was used to make the distribution fittings. The parameters of the distribution are reported in Table 1.

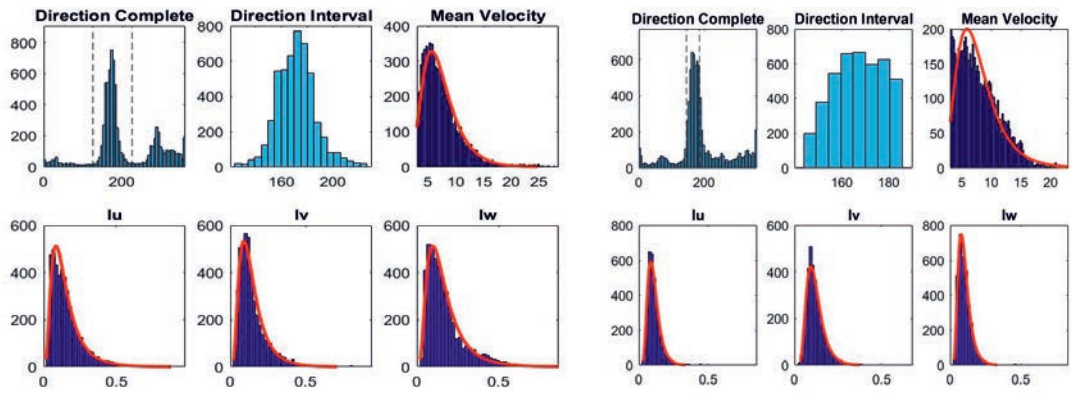

Figure 2: Histograms Jan-Mar.19: a) Kvitneset 175° Height 95m b) Trælboneset 165° Height 76m.

Tab. 1 Parameters of the Distribution

	Kvitneset				Trælboneset			
	Mean	**Iu**	**Iv**	**Iw**	**Mean**	**Iu**	**Iv**	**Iw**
$\mu = E[Ln\ X]$	*1.916*	*-2.058*	*-2.074*	*-1.946*	*1.966*	*-2.290*	*-2.196*	*-2.369*
$\sigma = \sqrt{Var[Ln\ X]}$	*0.431*	*0.643*	*0.577*	*0.627*	*0.447*	*0.399*	*0.404*	*0.423*

From the histograms of direction, it is possible to observe small unevenness in the steps between the histogram-bins in the dominant directions. This effect is more appreciable in Trælboneset than in Kvitneset. This behavior is associated to different meteorological processes, occurring in the similar directions, and driven by the mountainous terrain's topography near the stations.

CONCLUSIONS

The probabilistic modeling of the wind field proposes an appealing idea for bridge design. However, for its implementation at Sulafjorden Bridge site it must be considered that the terrain's topography causes different meteorological processes at close directions. Therefore, it is recommended to apply a separation procedure on the records based on their variation of turbulence intensity as function of mean wind speed.

On the other hand, the wind roses reported dominant wind velocities transversal to the bridge's cross section. In addition, the histogram analysis revealed a difference in the wind behavior depending on the incoming direction and observation height. Further, the authors will investigate an appropriate method to fit probabilistic model to data, such that, it can be suitable for bridge design.

REFERENCES

[1] The Norwegian Public Roads Administration, "Målinger," 22 02 2018. [Online]. Available: https://www.vegvesen.no/Europaveg/e39sulafjorden/malinger. [Accessed 07 05 2019].

[2] Norwegian Meteorological Institute, "MET Norway Thredds service," 26 02 2019. [Online]. Available: http://thredds.met.no/thredds/catalog/obs/mast-svv-e39/catalog.html. [Accessed 07 05 2019].

[3] A. Fenerci and O. Øiseth, "Site-specific data-driven probabilistic wind field modelling for wind-induced response predeiction of cable-supported bridges," Journal of Wind Engineering and Industrial Aerodynamics, vol. 181, pp. 161-179, 2018.

[4] K. Vindteknikk, "Sulafjorden og Vartdalsfjorden, Møre og Romsdal. Rapport nummer: KVT/KH/2018/R0105," Kjeller Vindteknikk for Statens Vegvesen region Midt, 2018.

Research Project toward Enhancement of Resilience for Tokyo Metropolitan Area Preparing for Severe Seismic Event in Tokyo

A. Nishitani[1], K. Kajiwara[2], T. Nagae[3], T. Inoue[2], K. Kusunoki[4], I. Nakamura[2], M. Kurata[5], Y. Kawamata[2], E. Sato[2], K. Hayashi[6], T. Morii[7], R. Okazawa[7], K. Okada[7], M. Shiraishi[7]

[1] *Department of Architecture, Waseda University, Japan,*
E-mail: anix@waseda.jp

[2] *Hyogo Earthquake Engineering Research Center, NIED, Japan.*

[3] *Disaster Mitigation Research Center, Nagoya University, Japan.*

[4] *Earthquake Research Institute, The University of Tokyo, Japan.*

[5] *DPRI, Kyoto University, Japan.*

[6] *Architecture and Civil Engineering, Toyohashi University of Technology, Japan.*

[7] *Institute of Technology, Shimizu Corporation, Japan.*

ABSTRACT

Risk and chaotic situations resulting from a severe seismic event in the Tokyo metropolitan area are one of the major concerns for Japan. The advanced well-preparation toward the enhancing of the Tokyo metropolitan resilience should be urgently demanded. With such a demand, a research project started in April 2017 with the support of MEXT and NIED, scheduling several E-defense shake table experiments during FY2018-2021. The experiments are conducted with building models with structural/nonstructural elements and equipment included, focusing on the collection and effective usage of variety of data. This paper presents the outline of this research project, and then report the experimental results for several wireless sensors.

KEYWORDS: *Health monitoring, Resilience, Tokyo metropolitan area, Severe seismic event*

INTRODUCTION

The Japanese Government is deeply concerned about the risk and chaotic situation induced by a severe seismic event in Tokyo in the not-too-distant future. It is said that the resulting economic loss may reach US$880 trillion. Advanced and effective preparations are strongly demanded toward the enhancement of the Tokyo resilience. With such a purpose, a research project [1] has started with the support of MEXT (Ministry of Education, Culture, Sports, Science and Technology) and NIED (National Research Institute for Earth Science and Disaster Resilience).

For an important facility such as hospital, for instance, it would be of great significance to promptly identify whether that building could continue its business after a severe

quake. Focusing on that target, the project aims to collect a variety of data indicating the margin to building collapse or the loss of building function. Those data are going to be collected through several E-defense shake table tests of different types of buildings scheduled during the fiscal years of 2018 to 2020. (The Japanese fiscal year (FY) starts in April and ends in March in the next year.) This paper presents, in the first place, the outline of this research project, and then reports some test results of wireless accelerometers.

OUTLINE OF RESEARCH PROJECT

This research project has started in April 2017, as one of the three subprograms under a large research framework abbreviated as "Tokyo Resilience Project." [1] The general PI to supervise the entire framework is N. Hirata, University of Tokyo. Three of Sub-A, B, and C are currently going on. Each subprogram is supervised by two co-PIs: one from university and the other from NIED. Sub-A aims at constructing the public-private collaboration system for the data acquisition to enhance the Tokyo resilience. Sub-B aims at realizing the dense data-collection of earthquake records covering the Tokyo metropolitan area. Then, Sub-C is the one which this paper focuses on.

The main purpose of Sub-C is the data collection and synthesis for evaluating the structural/nonstructural element combined performance. The constructing of data acquisition/processing/utilization system is targeted toward the rapid evaluation of building collapse margin and effective judgement of business continuity. To collect the necessary data, E-defense shake table tests with four different types of structures have been scheduled from FY2018 to FY2021.

Sub-C research group consists of five teams. Teams 1, 2, 3 and 4 are, respectively, in charge of the experiments of wooden structure (FY2018), reinforced concrete (RC) structure (FY2019), steel structure (FY2020) and room interior model structure (FY2021). Cooperated with Teams 1-4, Team 5 processes all the shake table test data toward the effective/efficient assessment of damage and business continuity. The leaders are T. Nagae for Team 1; K. Kusunoki for Team 2; M. Kurata for Team 3; E. Sato and K. Hayashi for Team 4; and A. Nishitani for Team 5.

The purposes of the experiments of Teams 1-4 are more mentioned in the following.

Team 1 targets at making a comprehensive loss assessment of the typical wooden residential houses area. Tokyo has a lot of such regions. Two types of real-sized, furnished model houses were already tested at E-defense in January/February 2019. One model was set on the shake table, but the other was built on RC foundation on a constructed soil foundation on the shake table. The latter model would give the information about how the soil foundation would affect the wooden house response to a severe quake. The obtained data are now being processed.

Team 2 aims at enhancing the resiliency of RC headquarters buildings for disaster mitigation/prevention and developing a scheme to evaluate the function continuity level. The target of Team 3 is to construct a holistic assessment scheme of seismic damage for steel-structured medical facility buildings. In the experiments, various medical equipment and instruments are planned to be placed, such as artificial heart lung machine, water service pipe for medical use, etc. The performance of these equipped things is critical to the judgement of hospital business continuity. Team 4 focuses on the performances of various types of rooms on various floor locations of buildings with various numbers of stories. The room model structures with furniture and nonstructural elements are shaken by giving the floor movement data to E-defense shake table. Having cooperation with all Teams, Team 5 takes the role of supervisor for all the experiments.

TESTS OF WIRELESS SENSORS

Prior to the scheduled E-defense experiments, Team 5 conducted experiments of three kinds of wireless sensors: sonas x01 [2], Swing Minder [3] and G-Link-200 [4]. They are planned to be used for the scheduled E-defense experiments. The test was conducted at the shake table of 7 m by 7 m of Shimizu Corporation, with the sensors installed into a four-story structure model exhibiting a perfectly-shear-structure type of behavior. Figure 1 shows the shaking table and four-story model structure.

Firstly, the time synchronization performance has been tested by placing two of the same sensors directly on the table subject to a white-noise excitation. Taking an example of sonas x01, Figure 2 depicts the phase angles (blue dots) of the computed transfer function from one sensor to the other. Compared to the dashed lines indicating the situation for a time lag of ±1 ms, the blue dots show that the time synchronization is less than 1 ms. The other sensors have demonstrated the almost same level of performance.

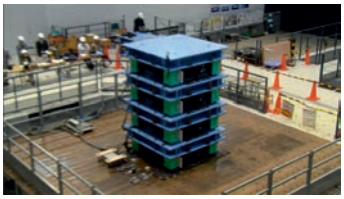

Figure 1: Shake table test experiment for wireless sensor performance.

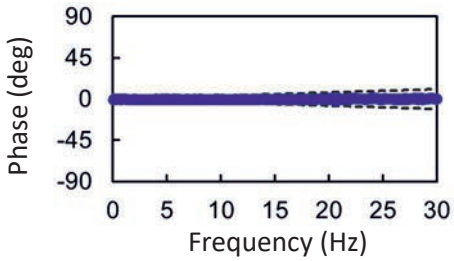

Figure 2: Time synchronization performance.

Many of already practically-employed health monitoring schemes are based on the computation of drift displacements from wired accelerometer data. If wireless sensors could be used in the similar way, structural health monitoring schemes would be easier integrated into building structures. Utilizing the obtained data of wireless sensors, the similar scheme has been tested with the employment of wireless accelerometers. In the case of 3 Hz sinusoidal excitation, the drift angles numerically computed from the wireless accelerometer data are compared with the data directly measured by laser displacement meters (LK-G505A). The sensors of LK-G505A have been installed into all the four stories to make the direct measurement of drift displacements. In Figure 3, the peak values calculated from the data of Swing Minder, for instance, have demonstrated good agreement with the directly measured drift displacement data. The time histories also agree with each other, though they are not shown herein. It can be said that the drift displacements could be computed and utilized even with the usage of wireless sensors.

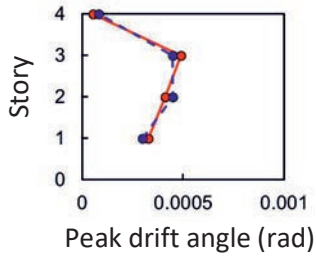

Figure 3: Peak drift angles (Blue: measured results; Red: computed results)

CONCLUSIONS

This paper has presented the research project aiming at the data collection/synthesis for the evaluation of the total building performance toward enhancing the Tokyo metropolitan resilience. Some wireless sensor test results have been also reported. This research is partially supported by Tokyo Metropolitan Resilience Project of National Research Institute for Earth Science and Disaster Resilience (NIED).

REFERENCES

[1] Tokyo Metropolitan Resilience Project, website **https://forr.cc.niigata-u.ac.jp/**

[2] Sonas, website **https://www.sonas.co.jp/**

[3] Sikoku Research Institute Inc., website **https://www.ssken.co.jp/**

[4] LORD MicroStrain, website **https://www.microstrain.com/**

Experimental investigation on the ball drop impact resistance of traditional glass windows

L. Figuli[1], C. Bedon[2], D. Papán[3], Z. Papánová[3]

[1] *University of Žilina, Faculty of Security Engineering, Univerzitná 8215/1, 01026 Žilina, Slovakia. E-mail: lucia.figuli@fbi.uniza.sk*

[2] *University of Trieste, Department of Engineering and Architecture, Piazzale Europa 1, 34127 Trieste, Italy E-mail: chiara.bedon@dia.units.it*

[3]*University of Žilina, Faculty of Civil Engineering, Univerzitná 8215/1, 01026 Žilina, Slovakia E-mail: daniel.papan@fstav.uniza.sk*

ABSTRACT

Given the typical features of glass fenestrations and façade systems, and their common use in buildings with several classes of use, the research on their impact resistance represents a key task for the protection of people. In this regard, the paper focuses on the experimental analysis of the impact performance and resistance of ordinary glass windows. Special care is spent for traditional systems that can be typically found in residential / commercial buildings, namely windows with timber frame as well as windows with plastic (PVC) frame. The dynamic performance of such systems is analysed experimentally, in accordance with the standard ball drop test method, and the collected outcomes are discussed to assess the fundamental dynamic mechanical characteristics of the examined fenestrations.

KEYWORDS: *Glass windows, impact test, impact resistance, wood frame, PVC frame*

INTRODUCTION AND STATE-OF-THE-ART

The actual motivations for the experimental research on the dynamic response of glass systems under ball drop impact are various, and typically reflect the intrinsic vulnerability and fragility of these systems [1]. Most of the studies, however, are focused on glass for automobilistic of electronic applications, and limited efforts can be found for constructions. Tests on laminated glass panels under the hard body impact (pedestrians or driver heads) can be found in [2]. Impact experiments are reported in [3] to estimate the resistance of glass against scratches, drop impact and bumps, for the protection of displays (smartphones, tablets, etc.). Full-scale glass columns under impact are investigated in [4]. In [5, 6], experiments for the burglary resistance and protection of glass "soft targets", as well as preliminary dynamic considerations for glass windows

under shock, are reported.

EXPERIMENTAL INVESTIGATION

The series of dynamic experiments summarized herein was carried out at the laboratory of structural mechanics of the Faculty of Civil Engineering, University of Zilina, Slovakia (May 2019). Given two glass window systems with identical dimensions and glass composition, in particular, special care was spent on the sensitivity of their impact response to the type and features of the supporting frame. Each glass sample was in fact characterized by a total size of 1.21×1.38 m, consisting of a frame (made of timber (and reflecting the use in Czechoslovakia over 1960s) or PVC) and a monolithic glass plate. The nominal thickness of glass was 3 mm for the wooden specimen, and 4mm for the PVC frame. Regarding the size of glass, the dimensions where defined from the total size of window samples and the frames in use. Accordingly, glass surface was 1.20x1.05 m for the wooden frame and 8.10x9.70 m for the PVC window.

Modal analysis

Modal dynamic analyses were carried out at a preliminary stage of the experimental study, so as to assess the fundamental vibration frequency and modal shape of the examined windows. A rectangular grid with 16 Deltatron accelerometers (type 4508 B 002) was installed evenly on the glass surfaces (Figure 1a). Three six channels input modules (Type 3050-B-060) were used. Each accelerometer was cable-connected to an Input Module (with two inactive positions). The measuring interfaces were connected to a PC and test records were processed via the PULSE software. The imposed excitation was realized by tapping the glass plate with various levels of impact softness, at the middle grid points of the glass surface. The measured data were then transformed into ARTeMIS and processed by FDD (Figure 1b).

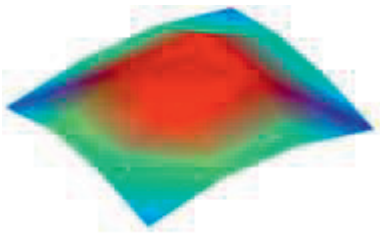

$f_{(1)}^{w} = 13.1\ Hz$

(a) (b)

Figure 1: Modal experiments. (a) Placement of sensors and (b) predicted fundamental mode of vibration.

Dynamic impact experiments

Later on, dynamic impact experiments were performed on the same windows. The reference test setup is shown in Figure 2. It was organized so that each steel ball could impact the window in the middle of glass, while the overall sample was attached to a rigid metal frame and. Different impact bodies (two steel balls with nominal weight of 2.644 kg and 4.571 kg) and drop height (i.e., horizontal distance between the ball and the window) were used. For each drop test, accelerations were measured by means of a set of sensors positioned in the lower part of glass (right side, at a distance of 0.2m from the edge). A high-speed camera (FASTEC TS3100SC4256 Imaging) was also used, to investigate the impact velocity based also on slow motion registrations.

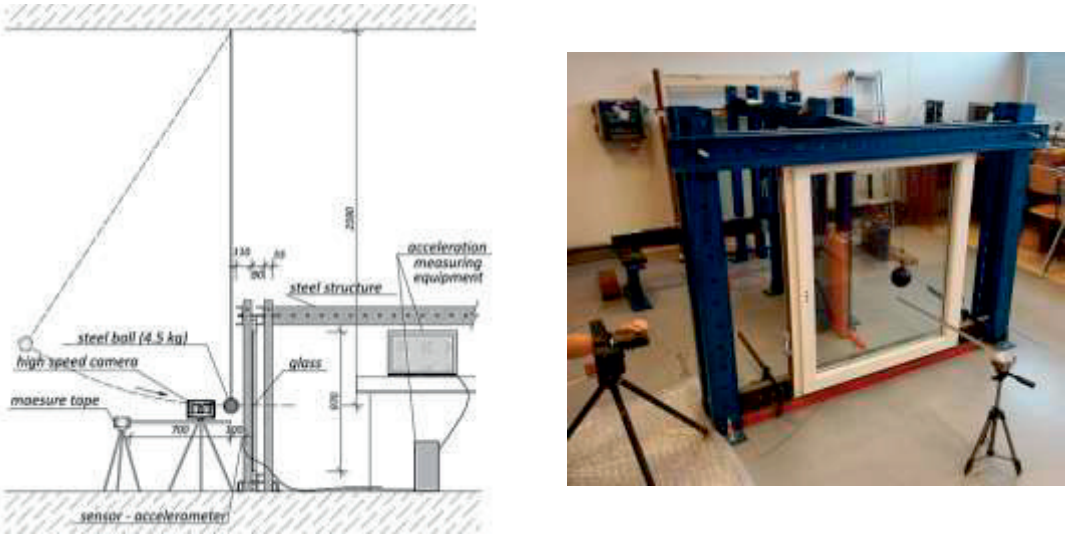

(a) (b)

Figure 2: Impact tests. (a) Reference setup (lateral view) and (b) laboratory test.

Four experiments were carried out on two windows samples (wood / PVC), by accounting for different steel ball sizes and overall impact energies. The latter values were calculated according to Equation (1), by taking advantage of slow motion records from the high-speed camera:

$$E = \frac{1}{2} m\, v^2 \tag{1}$$

The maximum impact velocity of each test is presented in Table 1, as a function of ball size and level of impact energy, when damage of glass panel occurred.

Tab. 1.1. Impact resistance of windows under different ball sizes and impact velocity

Ball mass [kg]	Energy [J]	Impact velocity [m/s]	Impact horizontal distance [m]	Window frame
2.644	*7.72*	*2.42*	*1.30*	*wood*
2.644	*3.36*	*1.60*	*0.90*	*wood*
2.644	*8,90*	*2.59*	*1.40*	*wood*
4.571	*19.75*	*2.94*	*0.15*	*PVC*

CONCLUSIONS

The paper presented a series of ball drop impact experiments, carried out to estimate the dynamic resistance of glass windows. Traditional samples with wood frame were taken into account, and compare with PVC framed systems. The fundamental vibration frequency and modal shape of the examined windows were first explored, based on modal analysis. Later on, ball drop impact tests were carried out. The study is part of an ongoing project that will include analytical and numerical analyses of the examined systems.

REFERENCES

[1] Bedon, C., Zhang, X., Santos, F., Honfi, D., Kozłowski, M., Arrigoni, M., Figuli, D., Lange, D. (2018) Performance of structural glass facades under extreme loads – design methods, existing research, current issues and trends. Construction and Building Materials. Vol. 163, pp. 921-937

[2] Wang, X., Yang, J., Xu, H. (2018) Experimental investigation on the Impact Resistance of Laminated Glass with Various Glass Make-ups. Challenging Glass 6 – Conference on Architectural and structural Applications of Glass

[3] Xue, L., Coble, C.R., Lee, H., Yu, D., Chaparala, S. And Park, S. (2013) Dynamic analysis of the thin glass under ball drop impact with new metrics. Proceedings of the ASME 2013 International Technical Conference and Exhibition on Packing and Integration of Electronic and Photonic Microsystems InterPACK2013

[4] Bedon, C., Kalamar, R., Eliasova, M. (2017). Low velocity impact performance investigation on square hollow glass columns via full-scale experiments and Finite Element analyses. *Composite Structures*, 182, 311-325

[5] Figuli, L., Zvaková, Z., Bedon, C. (2017) Design and analysis of blast loaded windows. *Procedia Engineering*. Vol. 192, pp. 177-182

[6] Figuli, L. (2019) Analysis, design and protection of blast loaded windows. Critical infrastructure protection: best practices and innovative methods of protection. Amsterdam: IOS Press, ISBN 978-1-61499-963-8. - pp. 27-43

A New Approach for Probability Distribution Estimation of Seismic Response in Structures with Nonlinear Shear Wall Behavior

Heekun Ju[1], Seung-Seop Jin[2], Hyung-Jo Jung[3]

[1] *Civil and Environmental Engineering, Korea Advanced Institute of Science and Technology, Republic of Korea.*
E-mail: heekun.ju@kaist.ac.kr

[2] *Sustainable Infrastructure Research Center, Korea Institute of Civil Engineering and Building Technology, Republic of Korea.*
E-mail: seungsab@kict.re.kr

[3] *Civil and Environmental Engineering, Korea Advanced Institute of Science and Technology, Republic of Korea.*
E-mail: hjung@kaist.ac.kr

ABSTRACT

A fragility curve needed for the seismic risk assessment of nuclear power plant (NPP) structures is obtained using response and capacity of the structure in a probabilistic manner. The structural response is traditionally assumed to have log-normal distribution. However, the log-normal assumption could be inappropriate for the structure with highly nonlinear behavior. In this research, structural response of a NPP structure mainly affected by shear wall exhibiting nonlinear hysteretic behavior is studied. Structural parameters associated with backbone curve of hysteresis curve is shown to have a considerable effect on the spectral acceleration response in the structure. Assuming the variation in the structural parameter value, probability distribution of the response is studied. Sampling-based simulation is conducted with parameter variation to verify the adequacy of log-normal assumption of the structural responses with strong nonlinear behavior. Log-normal distribution is fitted and tested with the responses from the simulation. A new approach for the probability distribution estimation is applied to the structural response which is not log-normally distributed. It is shown that the new approach is appropriate for expressing non-traditional probability distribution of response of nonlinear structures.

KEYWORDS: *Lognormal assumption, nonlinear response, probability distribution*

INTRODUCTION

For the seismic risk assessment for NPP structures, a fragility curve should be calculated to estimate the frequency of failure represented as a function of seismic intensity. The fragility curve is obtained using the response and capacity of the

structure in a probabilistic manner. NPP structures have a very thick shear wall as its essential structural element to resist the seismic loads. Shear walls under strong seismic excitation have hysteretic behavior which can affect the response largely (strong nonlinear behavior). Although the structural response is traditionally assumed to be log-normally distributed, the log-normal assumption could be inappropriate for the structure with strong nonlinear behavior.

In this research, we study on the nonlinear behavior of the structure with a shear wall and the parameters which have a considerable effect on the structure is determined. To verify the adequacy of using the log-normal distribution under the strong nonlinear responses of the structure with the parameter variability, sampling-based simulation is conducted to obtain the nonlinear responses of the structure with the parameter variability. Traditional probability distribution estimation uses log-normal distribution to fit the nonlinear responses. The traditional assumption was shown to be not always valid based on the Kolmogorov-Smirnov (K-S) test results. Probability distribution with atypical shape is estimated using a new approach.

STRUCTURAL MODEL AND PARAMETER VARIATION

Analytical model of a NPP structure is constructed using open source program OpenSees. A lumped-mass model is applied as the structural model because it is more suitable for numerous number of analysis when a sample-based probabilistic approach is used. Nonlinear behavior of shear wall can be defined by hysteretic model consisting of backbone curve and a hysteretic rule. A backbone curve defines the response under monotonic loading, and a hysteretic rule decides how the element behaves under cyclic loading.

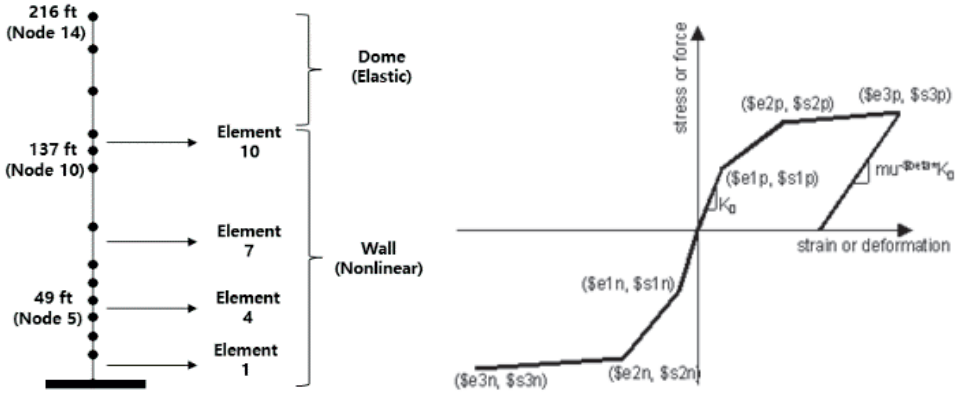

Figure 1: NPP structure model (left); backbone curve of hysteretic model [1] (right)

Hysteretic Material which is supported on OpenSees program can represent the hysteretic behavior of shear wall using several parameters associated with backbone

curve and the cyclic response including strength deterioration, pinching effect and others. Figure 2 shows floor response spectrum obtained from the results of the nonlinear structural model. Amplitude of structural response increase linearly when the structural model is linear, but the result in figure 2 shows frequency shift of the peaks and the amplification of amplitudes not proportional to the seismic intensities. It is observed that the nonlinearity increases as seismic intensity increases.

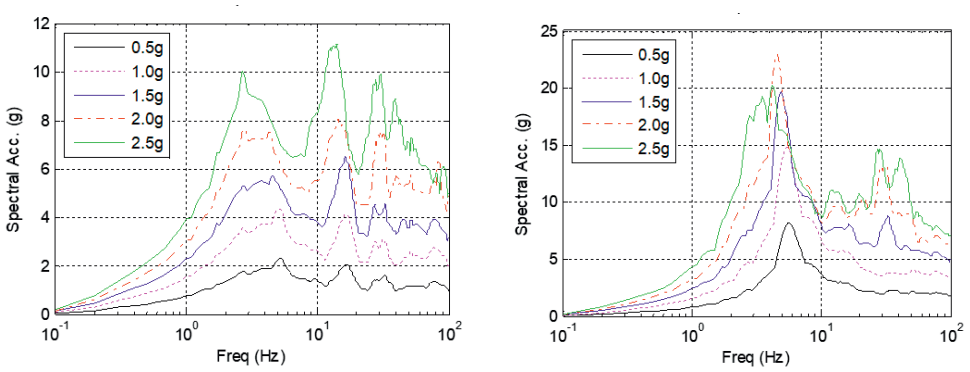

Figure 2: Floor response spectrum of a nonlinear structural model: at node 5 (left) and 14 (right)

Parameters associated with backbone curve, elastic modulus and damping coefficient are considered to represent structural uncertainties. Latin hypercube sampling method is used to construct the cases to probabilistically represent the parameter variation. Sufficient number of cases are sampled to reliably develop the probability distribution of the results.

PROBABILITY DISTRIBUTION ESTIMATION

The K-S test is performed to compare the estimated log-normal distribution with actual empirical distribution. Spectral acceleration results are fitted to log-normal distribution and the equality of the fitted distribution and the actual distribution is identified using the K-S test. As a result of the K-S test, the log-normal distribution is not always valid under strong nonlinear behavior and our result reveals that the log-normal distribution assumption is not appropriate under the strong nonlinear behavior. The left side of the figure 3 shows the example case of the actual distribution and the fitted log-normal distribution together. The K-S test says that the two distribution is not equal; other distribution model should be tested. However, the actual distribution does not follow typical probability distributions. To address this issue, a new method to appropriately express the probability distribution to relieve any constraints for a distributional assumption of the nonlinear response is adapted. Gaussian mixture model (GMM) can represent probability density function parametrically with a weighted sum of Gaussian

densities [2]. Parameters in GMM can be estimated using Expectation-Maximization (EM) algorithm. Right side of figure 3 represents the probability distribution fitted using GMM and the actual distribution. Comparing the traditional method with the GMM, it is verified that the new method is much better to express the probability distribution of seismic response in a structure with nonlinear shear wall behavior.

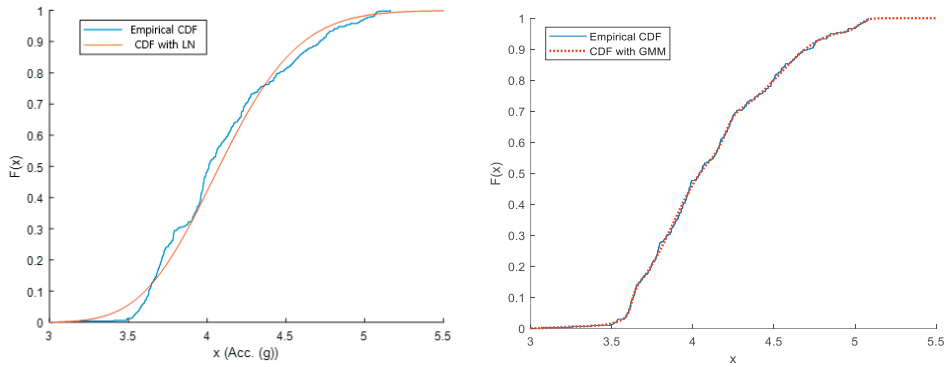

Figure 3: Lognormal distribution fitting (left); probability distribution fitting with GMM (right)

CONCLUSIONS

NPP structures under strong seismic motion can exhibit highly nonlinear response due to the hysteretic behavior of shear walls. Floor response spectrum of nonlinear structural model reveals frequency shift, broadening and amplitude changes of the peaks. The traditional log-normal assumption of the structural response can be invalid when the structure behaves highly nonlinearly. Instead of typical probability distribution model, GMM was shown to be a very flexible method for estimating probability distribution of highly nonlinear structural response.

ACKNOWLEDGEMENT

This work was supported by the Korea Institute of Energy Technology Evaluation and Planning (KETEP) and the Ministry of Trade, Industry & Energy (MOTIE) of the Republic of Korea (No. 201810102410).

REFERENCES

[1] Scott M, Filippou F. (2013) Hysteretic Material. OpenSees.

[2] Reynolds D. (2009) Gaussian Mixture Models. In: Li S.Z., Jain A. (eds) Encyclopedia of Biometrics. Springer, Boston, MA

Proposal for the definition of the attention level classes of bridges

G. Buratti[1], A. Cosentino[1], F. Morelli[1], W. Salvatore[1]

[1] *Department of Civil and Industrial Engineering, University of Pisa, Italy.*
E-mail: francesco.morelli@ing.unipi.it

ABSTRACT

The management of existing bridges and viaducts is a very current and complex issue. Especially after the recent collapses of some bridges in Italian territory, the necessity to develop a simple management and maintenance system of these structures has become apparent, in order to avoid structural failures and to improve their structural safety. Applying the currently existing codified methods for the structural assessment to all bridges on the Italian territory is unthinkable, because of the vastness and the variety of infrastructural assets, that include very different typologies of structures. It would take a lot of time and high economic investments, therefore, the standardized methods are usually applied in limited cases. In order to define an intervention priority, a simple methodology to evaluate the structural risk associated to all bridges is necessary. To this end, in this paper, a classification of the bridges, based on the "level of attention" associated to each one, is proposed. The definition of attention level classes is based on the results of visual inspections of the structures, that allow to evaluate the state of conservation of the bridges and to know their main characteristics. Combining the state of conservation with the other factors influencing risk it is possible to make a reliable estimate of the structural risk associated with each bridge and to evaluate the necessity and the urgency of an intervention. This paper presents the main characteristics of the methodology and its application to a sample of Italian bridges.

KEYWORDS: *bridge, road network, structural risk, quick survey, bridge management*

INTRODUCTION

Bridge infrastructures have a crucial role within the road networks. The recent failures of bridges in Italian road networks have highlighted how severe the social and economic consequences of the failure or simply of the closure of a bridge are. These events led public administrations to focus the attention to the infrastructural heritage under their jurisdiction. They are called to deal with several not trivial problems peculiar of the Italian infrastructural heritage. First of all, the infrastructural heritage is vast and various, in terms of structural typologies, construction period, static scheme, materials, etc., and managed by different administrative bodies. Therefore, it is not

easy having the complete knowledge of all structures in the territory, considering the limited available temporal and economic resources. Moreover, the construction of most of the existing bridges dates back to the 2^ post-war period, because of the necessity to replace destroyed bridges during the war as soon as possible. Therefore, most of them are built more than 50 years ago and without paying more attention to the quality of construction materials and details. Many others were built in even less recent periods and date back to 1800 and to beginning of 1900. This led that the majority of bridges were designed in respect of traffic loads lower than the loads to which the structures are currently subjected or codified by the current technical standards. Finally, there was an almost complete absence of monitoring and maintenance over the years, especially for bridges within minor roads. This caused the progressive deterioration of the conservation state of many structures, that suffer from the effects of time without an adequate control and maintenance. These considerations underline the necessity to improve the knowledge of the infrastructures and to define methods of structural risk assessment that can harmonize both the necessity to have a wide and complete survey of the current structural risk associated with all bridges in the Italian territory and the limited temporal and economic resources to invest in it. It is inconceivable to apply sophisticated and accurate methods of evaluations, such as the one foreseen by the national code, to all structures in the territory, but it is necessary to proceed for following levels of analysis, in order to apply simple and quick methods of evaluation to a great number of bridges and more time-consuming and costly ones to a limited number of selected structures. The main scope of this paper is to provide a new multi-level approach that allows to define an order of priority, classifying structures on the basis of simple methods of evaluation, and identify those that require more in depth analysis. It represents a decision support to management bodies of the infrastructures, to decide how and where allocate their economic and temporal resources, in all phases of a management system.

MULTI-LEVEL APPROACH OF ASSESSMENT AND ANALYSIS

A five levels (from Level 0 to Level 4) approach is proposed. They are represented in Figure 1. As the level rises, the accuracy of the assessments, the completeness of analysis and the time required to conclude them increase. The five levels provided are strictly connected each other. The results obtained by the application of each level are used as input data for the subsequent levels. The analysis foreseen in the *Level 0* are applied to all bridges in the territory, aiming at establishing a priority order for the inspections to be executed in the *Level 1*. The analysis foreseen in the *Level 1* give as result a classification of the structures in 5 classes of **level of attention**, that is defined through an algorithm that combines classes of hazard, classes of vulnerability and

classes of exposition. For each class of level of attention, possible measures to be taken are proposed and defined, according to the scheme in Figure 1.

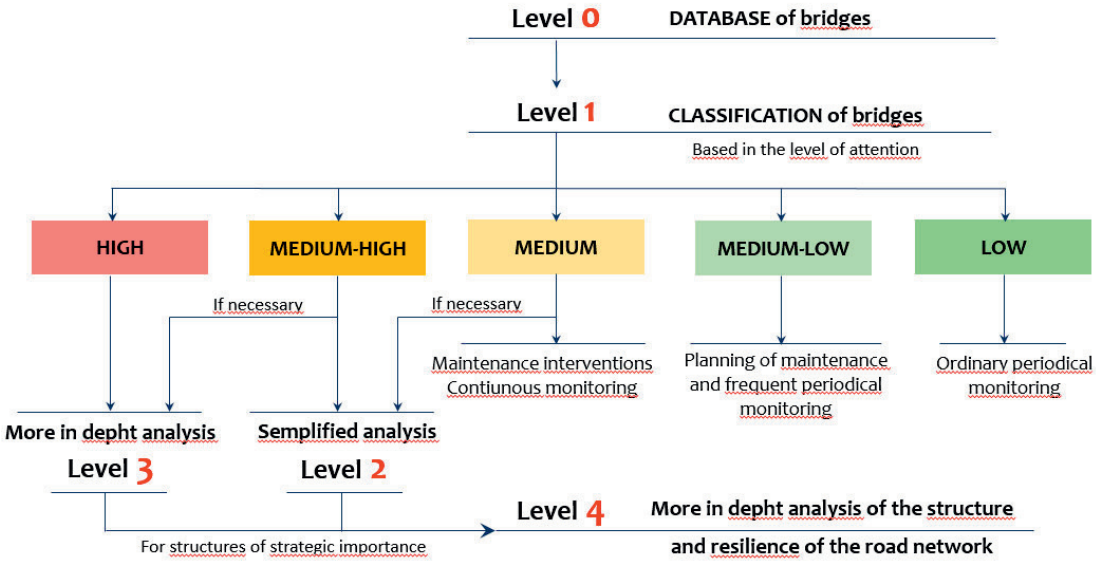

Figure 1: Scheme that summarizes the multi-level approach.

THE ATTENTION LEVEL CLASSES OF BRIDGES

The main focus of the multi-level approach is the **classification of bridges** based on the level of attention associated with each one. The level of attention is defined by the combination of classes of hazard, vulnerability and exposition, with a framework that brings to mind the typical one for the definition of seismic risk. Each factor is determined, in turn, by the combination of two parameters. **Hazard** depends on the state of deterioration and the period of construction of the bridge. The state of deterioration is evaluated through visual inspections that allow to identify the current degradation phenomena and their severity. The period of construction suggests the rapidity of the degradation developing, supposing that it was nil at construction time.
Vulnerability depends on the vulnerability associated with the static scheme and the length of the bridges on the basis of the redundancy of static scheme, susceptibility to fragile collapses and sensitivity of the construction materials to deterioration. The vulnerability of the static scheme is combined with the period of construction, in order to consider the standards in force and the design traffic loads. **Exposition** depends on the Average Daily Traffic (ADT) and the heavy one. These data, usually, are known to the management bodies, so they can be acquired simply. The classes individuated by the level of traffic are combined with the indication of the presence or the absence of sustainable alternative routes, in order to take into account the resilience of the road network. The three factors are obtained by the combination of the various parameters such as shown in Figure 2.

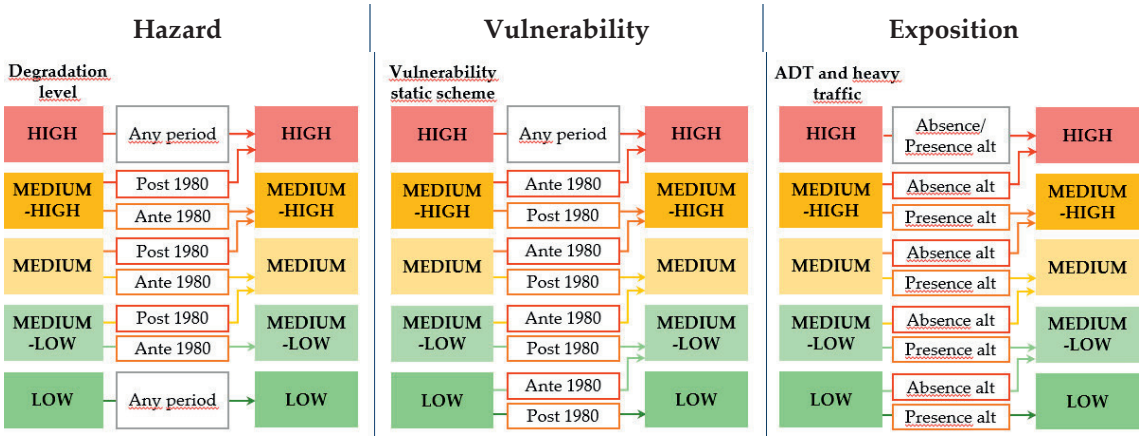

Figure 2: Scheme of combination for the determination of classes of the three considered factors.

The three factors do not have the same importance in the determination of the level of attention. If the hazard class is high, indeed, the level of attention of the bridge is high, regardless the other classes. This method of classification was calibrated and validated through its application on bridges under the jurisdiction of the Province of Pisa. Visual inspections and surveys of deterioration phenomena were carried out on more than 100 bridges. These inspections, as well as allowed to compile a database with all information about the structures (*Level 0*), allowed to determine all factors useful to determine the level of attention class of each bridge (*Level 1*). A classification of these 100 bridges was obtained and the more critical structures were individuated. The application of the method demonstrated that it well reflects the judgement of the inspectors about the possible level of risk associated with analyzed bridges. Moreover, it is based on simple, quick and economically sustainable methods of evaluation, that foresee only visual inspections, to carry out without particular or sophisticated instruments, and that need a little input data that can be acquired simply.

CONCLUSIONS

Differently from other methods of classification existing in scientific literature, [1] and [2], the proposed method of classification gives indication about the level of attention that a bridge requires simply and using a little input data that can be acquired without huge economic investments. Through the multi-level approach, the management bodies have a tool of knowledge of its infrastructures and indications about how to act in all phases of management activity, as well as a tool to identify the needs of more in depth analysis and interventions and their urgency.

REFERENCES

[1] Cias and 4EMME, Manuale "Valutazione dello stato dei ponti", 2011.

[2] CEB - FIP, Strategies for Testing and Assessment of Concrete Structures - Guidance Report, 1998.

Calibration of a structural health monitoring system for multiple-isolated structures using the dynamic response

P. Di Mascio[1], F. Potenza[2], V. Gattulli[3]

[1] *University "Nicolò Cusano", Doctoral School in Industrial and Civil Engineering.*
E-mail: paolo.dimascio@unicusano.it

[2] *Department of Civil, Construction-Architectural and Environmental Engineering, University of L'Aquila, Italy,*
E-mail: francesco.potenza@univaq.it

[3] *Department of Civil and Geotechnical Engineering, Sapienza University of Rome, Italy.*
E-mail: vincenzo.gattulli@uniroma1.it

ABSTRACT

The paper analyses the dynamic response of multiple base-isolated structures with the aim of accurately calibrating and selecting the sensor sensitivities for their structural monitoring. A first approach is devoted to the development of an analytical simple model composed by linear-superstructures posed on a common nonlinear base isolation system. The dynamic response of such model subjected to stochastic dynamic excitation will be evaluated through an iterative linearization procedure based on the determination of the covariance matrix. The results give an indication of the acceleration level induced on the isolated structures induced by environmental noise. Instead, the prediction of the seismic response will be assessed through a numerical algorithm dedicated to the nonlinear dynamic analysis of multiple building base isolated structures (3DBASIS-M). The fusion of all results will be useful to better identify the features of the accelerometer sensors on the basis of defined objective. The methodology will be applied to a preliminary design of a permanent seismic monitoring system for the real case of the Department of Human Science Building belonging to the University of L'Aquila.

KEYWORDS: *stochastic dynamic load, monitoring system design, sensor sensitivities, nonlinear dynamics*

INTRODUCTION

Base isolation has become a popular solution to reduce seismically induced acceleration and relative displacement in buildings. This paper shows a preliminary proposal for the designing of a seismic monitoring system for multiple-base isolated structure through the prediction of both nonlinear stochastic response and seismic response.

DYNAMIC OF A SIMPLE ANALYTICAL MODEL FOR MULTIPLE-ISOLATED STRUCTRUES

The dynamic of multiple-isolated structures is evaluated through a simple analytical model composed by n simple oscillators posed on nonlinear base isolation system (Figure 1). In the Figure 1, M_i, K_i and C_i represent the mass, stiffness and damping of the i-th oscillator while M_b, K_d and C_d are the global stiffness and damping of the base isolation system. U_i, U_b and U_g are the absolute displacements of the oscillators, isolated base and ground, respectively. Introduced the following dimensionaless variables:

$$u_i = \frac{U_i}{L},\ u_i = \frac{U_b}{L},\ u_i = \frac{U_g}{L},\ d_i = \frac{U_i - U_b}{L},\ d_b = \frac{U_b - U_g}{L},\ \rho_i = \frac{M_i}{M_b},$$

$$\omega_i^2 = \frac{K_i}{M_i},\ \omega_b^2 = \frac{K_b}{M_b},\ \beta_i = \frac{\omega_i}{\omega_b},\ \xi_i = \frac{C_i}{2\omega_i M_i},\ \xi_b = \frac{C_b}{2\omega_b M_b}, \tau = \omega_b t \tag{1}$$

the nonlinear equations look as:

$$\mathbf{M}\ddot{\mathbf{d}} + \mathbf{C}\dot{\mathbf{d}} + \mathbf{K}_\mathrm{L}\mathbf{d} + (1-\alpha)\mathbf{h}z = -\mathbf{r}\ddot{u}_g$$
$$z = -\gamma\left|\dot{d}_b\right|z|z|^{n-1} - \beta\dot{d}_b|z|^n + A\dot{d}_b \tag{2}$$

where the hysteretic component of the restoring force, (1-α)**h**z, is here represented by an adjunct variable z whose evolution is described through a Bouc-Wen model. The variable α is the post-to-preyielding stiffness ratio while **h** and **r** are the allocation vector of the hysteretic force and the external forces. The vector **d** contains the relative displacements (d_i, d_b) while $\mathbf{K}_\mathrm{L}$ is the linear stiffness matrix. In the Bouc-Wen model the parameters γ and β control the shape of the hysteresis loop, A the restoring force amplitude and n the smooth transition from elastic to plastic response (for large value of n the model tends to an elasto-plastic behaviour).

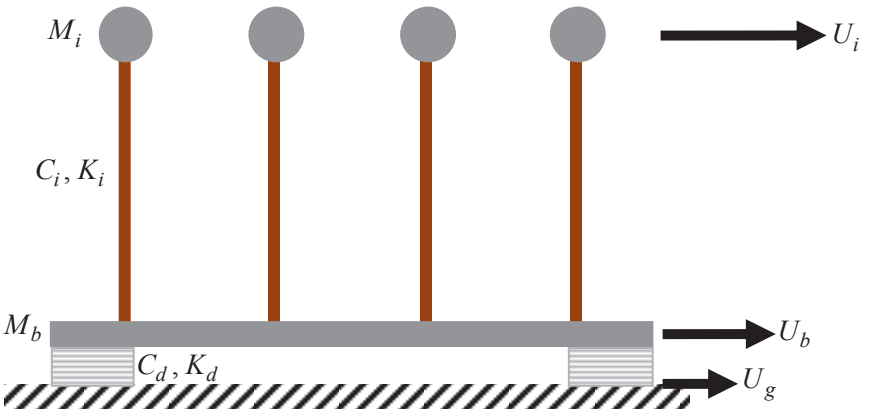

Figure 1: Sketch of an analytical model representative of multiple-isolated

The nonlinear stochastic response can be calculated through the covariance matrix **Γ** coming from the solution of the following Lyapunov equation and after having carried out an equivalent system linearization [1], [2].

$$\mathbf{0} = \mathbf{A}_s\boldsymbol{\Gamma} + \boldsymbol{\Gamma}\mathbf{A}_s + 2\pi\mathbf{B}_s\mathbf{S}\mathbf{B}_s \tag{3}$$

where **S** is the power of white noise while $\mathbf{A}_s$ and $\mathbf{B}_s$ are the space-state matrices that assume the following form:

$$\mathbf{A}_S = \begin{bmatrix} \mathbf{0}_{3x3} & \mathbf{I}_{3x3} \\ -\mathbf{M}^{-1}\mathbf{K} & -\mathbf{M}^{-1}\mathbf{C} \end{bmatrix}, \boldsymbol{B}_s = [\mathbf{0}_{1x3}^{\mathrm{T}} \quad -\mathbf{r}^{\mathrm{T}}]^{\mathrm{T}} \tag{4}$$

As well described in [1], since the coefficients defined in the linearization process depend by the standard deviations to solve the Lyapunov Equation (Eq. (3)) an iterative solution is required.

In the Figure 2 are reported some examples of dynamic response of the analytical model under both white noise and seismic input. In the first case (Figure 2a-c), the response has been evaluated by equivalent linearization and represented through the standard deviations varying the power of white noise (**S**). In the second case (Figure 2d-f), has been calculated the seismic response under Kobe earthquake by direct integration. It is evident that the whole scenario of different levels of dynamic amplification can give useful information about an optimal calibration of the type of sensors to be used. Of course, a more detail will be assessed through a numerical algorithm dedicated to the nonlinear dynamic analysis of multiple building base isolated structures (3DBASIS-M [3]).

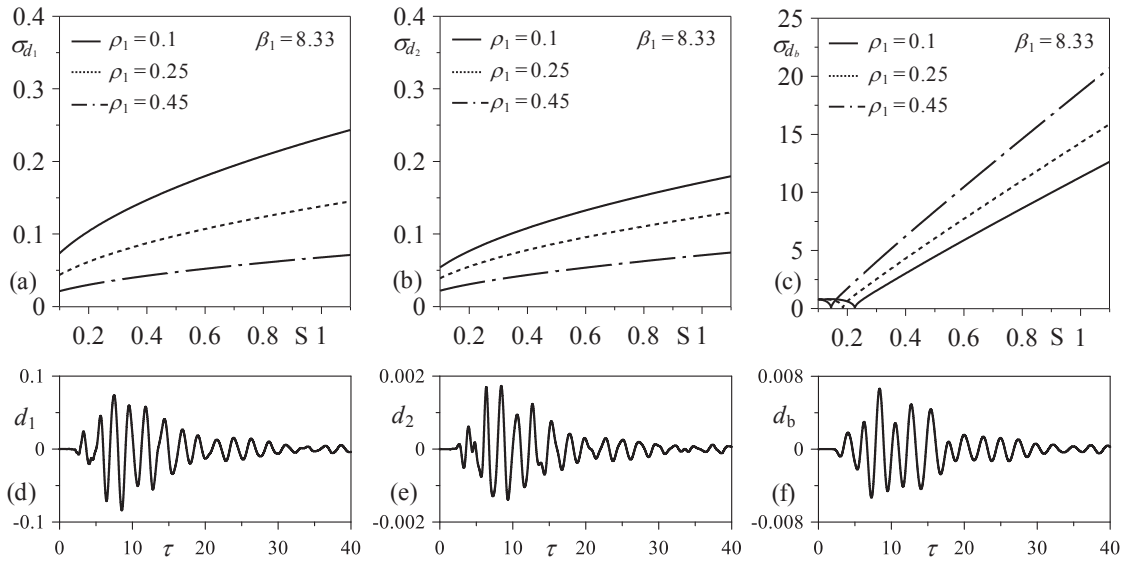

Figure 2: Nonlinear stochastic response evaluated by equivalent linearization (β_2 = 6.25, ρ_2 = 0.3, a-c). Example of seismic response: Kobe earthquake, β_1 = 2.50, ρ_1 = 0.1, β_2 = 6.25, ρ_2 = 0.3 (e-g).

CASE STUDY

The information coming from both the simple analytical model and numerical approach (3DBASIS-M) will be used to calibrate a structural health monitoring system for the buildings of the Dept. of Human Science at the University of L'Aquila. As shown in Figure 3, they are by 4 building placed on a single isolated plate.

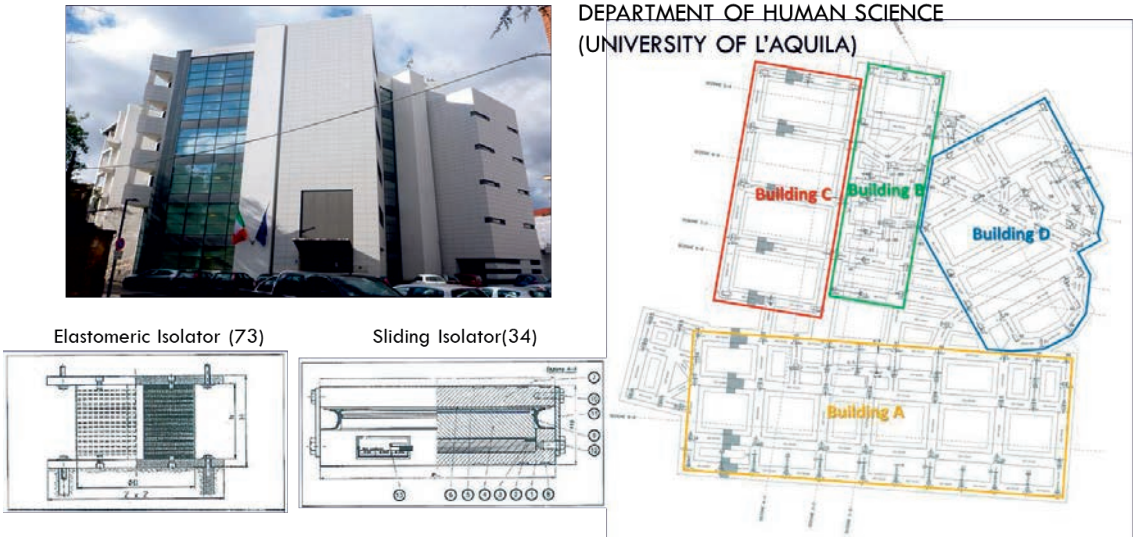

Figure 3: Example of multiple-isolated structures: Dept. of Human Science (L'Aquila, Italy).

CONCLUSIONS

The paper regarded the development of a simple analytical model able to predict the dynamic response of multiple base-isolated structures. The evaluation of both nonlinear stochastic response and seismic response could be useful for optimizing the sensor sensitivities for seismic monitoring. A further development of the work will be to propose a relationship between the acceleration amplitude and the sensors sensitivities. A case study will be analyzed to verify the potentiality of the method.

ACKNOWLEDGMENTS

This work is part of a project that has received funding from the Re-search Fund for Coal and Steel under grant agreement No 800687.

REFERENCES

[1] Wen Y.K. (1980) Equivalent Linearization for Hysteretic System Under Random Excitation. *Journal of Applied Mechanics*. **47**:150-154.

[2] Xu J., Spencer B.F., Lu X. (2017) Performance-based optimization of nonlinear structures subject to stochastic dynamic loading. Engineering Structures **134**:334-345.

[3] Tsopelas P.C., Nagarajaiah S., Constantinou M.C., Reinhorn A.M. (1994) Nonlinear dynamics of multiple building base isolated structures. Computer & Structures. **50**:99-110.

Dynamic identification on an ancient steel bridge of six spans

S. Ivorra[1], M. Buitrago[2], Elisa Bertolesi[3], B. Torres[4], D. Bru[5]

[1] *Department of Civil, University of Alicante, Spain.*
E-mail: sivorra@ua.es

[2] *ICITECH, Technical University of València, Spain.*
E-mail: mabuimo1@upv.es

[3] *ICITECH, Technical University of València, Spain.*
E-mail: ***elber4@upv.es***

[4] *Department of Civil, University of Alicante, Spain.*
E-mail: Benjamin.torres@ua.es

[5] *Department of Civil, University of Alicante, Spain.*
E-mail: David.bru@ua.es

ABSTRACT

This paper addresses the experimental campaign developed to obtain the main dynamic characteristics of an ancient steel bridge built in 1918 with a total length of 169 m. This five span bridge are built with riveted Pratt trusses, these trusses present different boundary conditions on its supports. The five piles are built with the same configuration and material, presenting a central pile with 22.6 m height. The static and dynamic tests presented in the document shows the real behavior obtained in some load tests developed using real trains at different velocities after the development of some important retrofitting works developed to maintain the use of the bridge with the actual regulations. Several seismic accelerometers were placed on the bridge in selected positions and many elements of the trusses were monitored with fiber optic sensor to monitor the bevaviour of the bridge in static and dynamic conditions. The document shows the main vertical frequencies and damping ratios obtained after a dynamic analysis, as well the critical elements of this bridge. The actual tests shows a good behaviour of the structures and are agree with the numerical analysis developed to project the retrofit of this.

KEYWORDS: *Fiber optic sensor, accelerometer, steel bridge, static load test, dynamic load test.*

INTRODUCTION

The aim of structural health monitoring is to develop systems that provide information on significant damage to or relative changes in a structure. In many geotechnical and civil engineering applications, its use is fundamental in order to monitor the safety level in real time and optimize maintenance work [1].

Obtaining these objectives requires the use of sensors installed in the structure to provide information on important parameters regarding its state. Mechanical strain and accelerations are one of the parameters that provide most information on the state of the structure [2].

In this case, Quisi Bridge is an ancient steel bridge built in 1918. Over the last few years, repairs and reinforcement of the structure have been carried out to adapt the structure to the demands imposed by the current bridge regulations, that is, for the load value of the 4100 Series Train with a total load of 92.8 ton. Reinforcements consist of the welding of sheets in bars and joints, both the structure of the board and the pile. After these reinforcement operations, static and dynamic load tests have been carried out to verify that the real behavior of the structure corresponds to that theoretical in the repair and reinforcement project.

This paper present the dynamic and static load test developed to obtain the real behavior of the bridge. Monitoring systems used were (1) fiber optic sensors to obtain strain in and temperature [3, 4], (2) accelerometers to obtain modal frequencies and eigenvalues, (3) displacement transducers to obtain main relative displacement between structure and abutments and (4) digital leveling topography to obtain vertical displacements. The actual tests shows a good behaviour of the structures and are agree with the numerical analysis developed to project the retrofit of this.

CHARACTERISTICS OF THE STEEL BRIDGE.

The structure is approximately 170 m long, formed by six spans, with lengths 21.48 + 21.12 + 42.00 + 42.00 + 21.12 + 21.48 m. The two centrals present a continuous hyperestatic structural configuration, while the four lateral ones have an isostatic configuration. Hyperestatic structural configuration are composed by two parallel Pratt trusses with a total width of 4 m. Isostatic spans are composed by two parallel Pratt trusses with a total width of 2.8 m.

TRAIN USED IN THE TESTS.

To carry out the test, a 2500 Series diesel train that covers the Benidorm/Denia route was used. The total weight of an empty 2500 Series train is 558.4 kN (fully loaded is

662.4 kN) divided among four twin-axle bogeys with a total length of 34.79 m. In this case, a double configuration was used (Figure 2).

Figure 2: 2500 Serie Train vertical load, double configuration.

RESULTS.

Figure 3 show the strains recorded in the upper beam of the trusses during the dynamic load test. The results are shown for two load tests one at 50 km/h and another at 20 km/h. In view of the results, a small amplification of the strain is observed as a consequence of the increase in speed. If we consider the strain in the static load test, the impact factors oscillate between 1.02 and 1.21.

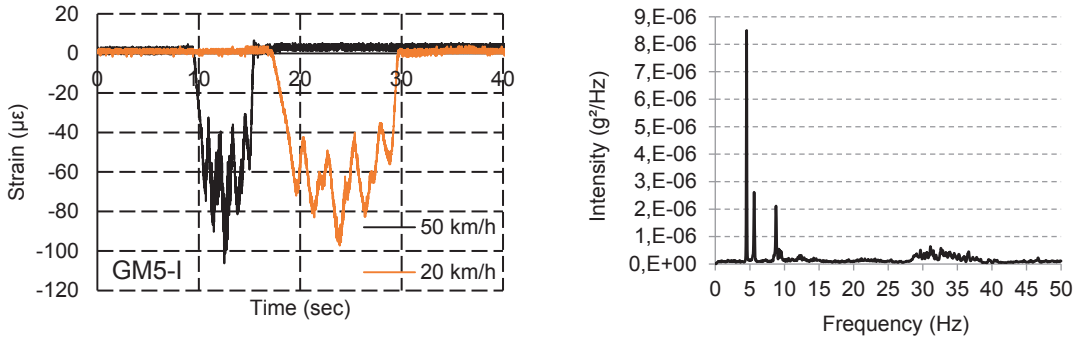

(a) (b)

Figure 3: (a) Strain in upper beam of the trusses, during dynamic load test. (b)- FFT for accelerometer placed in the center of hyperestatic span.

Figure 4 show the Fast Fourier Transform (FFT) and allow us to clearly identify the fundamental frequency of the hyperstatic bridge of 4.54 Hz. For the case of the isostatic span, the fundamental frequency of vibration of the first mode is 8.74 Hz. Figure 5 shows the comparatives of the first vibration mode, obtained experimentally and by means of theoretical simulation. The results show a high degree of fit. Table 1 shows the comparison between real and theoretical vibrational frequencies.

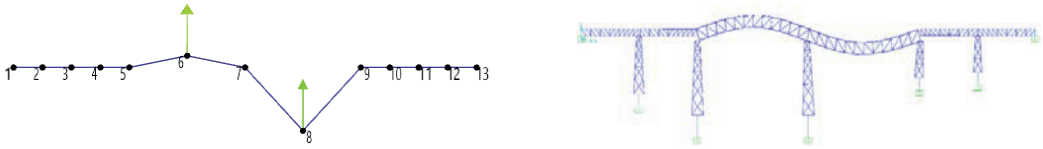

4.54 Hz 4.6 Hz

Figure 5: Real and theoretical vibrational mode

Tab. 1 Vibrational Frequencies (Hz) for different vibrational modes.

	Mode1	**Mode2**	**Mode3**	**Mode4**	**Mode5**	**Mode 6**
Experimental	4.54	6.785	8.74	8.79	8.74	8.74
Theoretical	4.6	6.33	8.54	8.78	8.98	9.13
Experimental/Proyecto	1.32%	6.71%	2.29%	0.11%	2.75%	4.46%

The damping factor has been analyzed through the logarithmic decrement of the accelerations recorded on the free vibration signal, which is defined as:

$$\delta = \frac{1}{n} \ln\left(\frac{A_o}{A_n}\right)$$

Where n is the number of cycles of the interval measured at the fundamental frequency, Ao the amplitude of the initial dynamic response, An the amplitude of the dynamic response at the end of the interval. The values obtained for the average damping factor of this bridge are 2.87 and 2.6 %

CONCLUSIONS

The actual tests shows a good behaviour of the structure and are agree with the numerical analysis developed to project the retrofit.

REFERENCES

[1] B. Torres Górriz, Paula Rinaudo, Pedro A. Calderón (2017). Comparison between point and long-gage FBG-based strain sensors during a railway bridge load test. Strain 2017; e12230. https://doi.org/10.1111/str.12230

[2] P. A. Calderón, B. Glisic, Influence of mechanical and geometrical properties of embedded long-gauge strain sensors on the accuracy of strain measurement. Meas. Sci. Technol. 2012, 23, 15.

[3] B. Torres, I. Payá-Zaforteza, P. A. Calderón, J. M. Adam, Analysis of the strain transfer in a new FBG sensor for structural health monitoring Eng. Struct. 2011, 33, 9.

[4] A Bueno, B Torres, D Barrera, P Calderón, S Sales. Monitoring of a steel incrementally launched bridge construction with strain and temperature FBGs sensors. Optical Sensing and Detection 7726, 772620

Computer-Aided Seismic Reliability Analysis of Critical Infrastructure: Smart Water Network

S.S. Yoon[1], Y.J. Lee[2], H.J. Jung[1*]

[1] *Department of Civil and Environmental Engineering, KAIST, Republic of Korea.*
E-mail: yss3366@kaist.ac.kr, hjung@kaist.ac.kr

[2] *School of Urban and Environmental Engineering, UNIST, Republic of Korea.*
E-mail: ylee@unist.ac.kr

ABSTRACT

In this study, a probabilistic seismic reliability model was proposed to evaluate the performance of an urban water transmission network. The proposed reliability model consists of an input seismic generation module including probabilistic seismic hazard analysis and a hydraulic analysis module using EPANET. The hydraulic analysis module involves the deterioration of the pipeline, the numerical modeling of the water network facilities, and the interdependency between water and electric power network. For numerical simulations, a MATLAB code has also been developed to enable the EPANET analysis with pressure driven analysis and numerical modeling of network systems. In order to verify the proposed seismic reliability model, a real water network was adopted and the location and magnitude of the earthquake were determined by the probabilistic seismic hazard analysis. In addition, two performance indices (system serviceability index, nodal serviceability index) were introduced for the network performance evaluation. As a result of the numerical analysis, a water network was found to be significantly influenced by not only the magnitude of the earthquake but also the deterioration of pipeline and interdependency of an electric power network.

KEYWORDS: *Smart water network, flow-based network analysis, seismic reliability model, probabilistic seismic hazard analysis*

INTRODUCTION

In recent times, frequent earthquakes have caused human casualties and property damage, resulting in increased social disruption. The critical lifeline infrastructure throughout the city can be directly or indirectly damaged, and it causes significant difficulties in daily life. The Northridge earthquake (1994) in California, USA and the Kobe earthquake (1995) in Japan led to immense damage to waterworks facilities. The Northridge earthquake (M 6.7) resulted in approximately 74 breaks to the main pipeline of diameter over 600 mm and 1013 breaks in the main pipeline below the diameter of 600 mm. In Kobe earthquake (M 6.9), there were 23 breaks to the main water line, limiting

the water supply to approximately 15 million people. In addition, the Kaikoura earthquake (M 7.8) in New Zealand (2016) had a significant economic impact on other lifelines (indirect losses) as well as the water lifeline itself (direct losses) [1].

GROUND MOTION PREDICTION EQUATION

For water supply facilities such as a water treatment plant, water storage tank, and water pumping plant, PGA is known to be suitable for predicting the failure probability, whereas PGV is known as the intensity measure for predicting the failure probability of buried pipelines. In this study, PGV and PGA were predicted using the GMPE proposed by Wang and Takada [2] and Kawashima et al. [3], respectively. Each proposed GMPE is as follows:

$$log(PGV_j) = 0.725M_i + 0.00318H - 0.519 - 1.318\,log(R_{ij} + 0.334e^{0.653M_i}) \quad (1)$$

$$PGA_j = 403.8 \bullet 10^{0.265M_i} \bullet (R_{ij} + 30)^{-1.218} \quad (2)$$

where H is the length of the focal depth (km), and PGA (cm/s^2) and PGV (cm/s) represent the ground motion intensity [1].

SEISMIC VULNERABILITY ANALYSIS OF WATER FACILITIES

The US Federal Emergency Management Agency (FEMA) and American Lifelines Alliance (ALA) presented the failure probability of water network facilities. According to the report, the bulk of historical earthquake records show the failure probability of buried pipes based on the repair rate (number of breaks per unit length). The repair rate is calculated based on the regression curve, which represents the number of pipe breaks due to ground motion [1, 4].

$$RR_i\ (breaks/km) = \kappa(PGV_i)^{\tau} \quad (3)$$

where $\boldsymbol{PGV_i}$ is ground motion of midpoint of the *i*-th pipeline, and κ and τ are the scaling and exponent parameters, respectively. Detail information of failure probability of other network facilities are described in other papers [1, 4].

HYDRAULIC SIMULATION AND PERFORAMCNE INDEX

To evaluate the required demand performance of the damaged water network, the entire network is simulated using the EPANET program by employing pressure-driven analysis (PDA). For numerical modelling of buried pipelines, damage states are classified into three types: leakage, breakage, and intact case. The broad approach proposed by Hwang et al. [5] is adopted to evaluate the leakage and breakage conditions of damaged pipelines. In the EPANET analysis, an emitter is used to calculate the leakage and breakage discharge flows, and the emitter coefficient can be evaluated using the orifice flow rate equation [1].

In addition, the performance of the entire network system is evaluated based on hydraulic analysis. In this study, the system serviceability index (S_S) [6] and the nodal serviceability index (N_S) [7], which is known to be reliable factors of water supply systems, is utilized [1].

NUMERICAL EXAMPLE

An earthquake of magnitude 6.0–8.0 was generated using the epicenter of the selected input earthquake and the parametric study was performed by increasing the interdependency of the 154 kV substation and the pumping plant to 0, 0.5, and 1. Simultaneously, the elapsed time was increased from 0 to 30 years to evaluate the seismic performance of the water network owing to pipeline deterioration. Fig. 1 represents the entire water transmission networks and network facilities including substations [1].

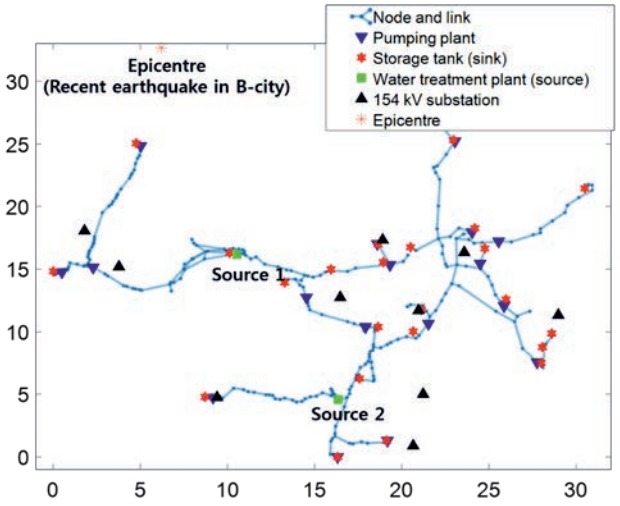

Figure 1: Construction of water transmission network of A-city, South Korea [1]

NUMERICAL RESULTS

Fig. 2 shows the fragility surface of the system serviceability and nodal serviceability of the network, depending on the magnitude of the earthquake, elapsed time, and interdependency ratio.

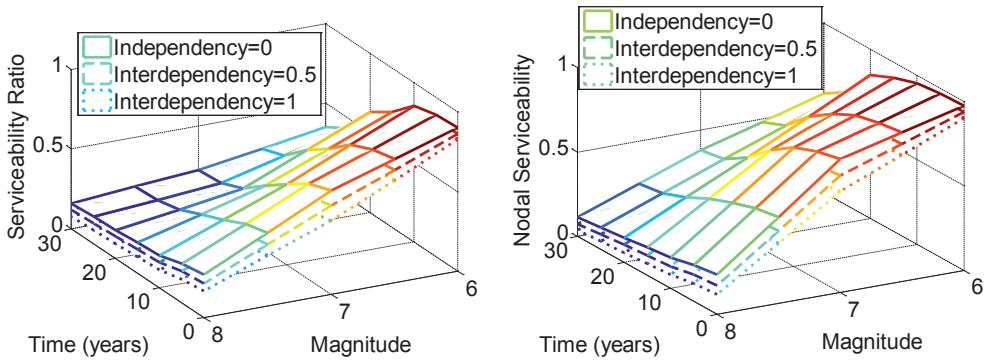

Figure 2: Seismic fragility surface of water transmission network [1]

The network performance decreases as the magnitude of the earthquake increases and as the elapsed time increases. When the elapsed time was more than 20 years, the effects of the ground motion intensity and pipeline deterioration increased. In addition, it can be observed that the influence of the substation on the network performance becomes greater as the interdependency of the substation increases [1].

CONCLUSIONS

In this paper, we propose a comprehensive approach to evaluate the flow-based seismic risk analysis of water transmission networks. The proposed method consists of three phases: earthquake generation model, update of orifice flow, and performance evaluation of water networks. To perform a hydraulic analysis, MATLAB-based computer code was developed and an actual water transmission network of South Korea was constructed. The results from the proposed approach quantitatively show that the water network is significantly affected by not only the magnitude of the earthquake but the interdependency and pipeline deterioration.

ACKNOWLEDGMENTS

This research was funded by Construction Technology Research Program funded by Ministry of Land, Infrastructure and Transport (MOLIT) of Korean government (grant number 19SCIP-C116873-04).

REFERENCES

[1] Yoon, S. S., Lee, Y. J., Jung, H. J. (2019) A comprehensive approach to flow-based seismic risk analysis of water transmission network. *Structural Engineering and Mechanics* (under review).

[2] Wang, M., Takada, T. (2005). Macro-spatial correlation model of seismic ground motions. *Earthquake spectra* **21(4)**: 1137-1156.

[3] Kawashima, K., Aizawa, K., Takahashi, K. (1984). Attenuation of peak ground motion and absolute acceleration response spectra. Paper presented at the Proceedings, Eighth World Conference on Earthquake Engineering.

[4] Yoon, S. S., Lee, Y. J., Jung, H. J. (2018) A Comprehensive Framework for Seismic Risk Assessment of Urban Water Transmission Networks. *International Journal of Disaster Risk Reduction* **31***:* 983-994.

[5] Hwang, H. H., Lin, H., Shinozuka, M. (1998). Seismic performance assessment of water delivery systems. *Journal of Infrastructure Systems* **4(3)**: 118-125.

[6] Wang, Y., Au, S.-K., Fu, Q. (2010). Seismic risk assessment and mitigation of water supply systems. *Earthquake spectra* **26(1)**: 257-274.

[7] Cullinane, M. J., Lansey, K. E., Mays, L. W. (1992). Optimization-availability-based design of water-distribution networks. *Journal of Hydraulic Engineering* **118(3)**: 420-441

Damage Detection

Guided Waves Approach for Monitoring Weld Zone in an I-shape Steel Beam

J.Q. Tu[1], C.B. Yun[1], X. Xu[1,*], Z.F. Tang[2], J.J. Wu[2]

[1] *College of Civil Engineering and Architecture, Zhejiang University, PR China.*
E-mail: tujiaqi@zju.edu.cn, ycb@zju.edu.cn, xianxu@zju.edu.cn

[2] *Institute of Advanced Digital Technologies and Instrumentation, Zhejiang University, PR China.*
E-mail: tangzhifeng@zju.edu.cn, 11425023@zju.edu.cn

ABSTRACT

Steel beams with I-shaped cross-sections have been widely used as major load-carrying structural members. The weld zone in an I-beam is vulnerable to fatigue type damage during the long service life, which might result in a catastrophic failure. In this study, a guided waves based damage detection method is presented for monitoring the weld zone in an I-shape steel beam. Pulse-echo method is employed using piezoelectric sensors. At first, semi-analytical finite element (SAFE) analysis was carried out for selecting proper wave modes with high sensitivity to the weld zone in the cross section. Then, 3D finite element analysis was performed for verification. Cross-correlation coefficients of the wave signals between the damaged and intact cases were calculated to detect the existence of damage. Time-of-flight (ToF) information was utilized for damage localization. Principal component analysis (PCA) was performed to improve the robustness of damage detection under temperature variation.

KEYWORDS: *Guided waves, I-beam, weld zone, damage detection, SAFE, ToF, PCA*

INTRODUCTION

For an I-shape beam, fillet weld is one of the most common ways to connect the web plate and flange plate. To realize quick scanning over long length of structural members, ultrasonic waves based SHM system is a promising approach [1]. Enough wave energy shall be focused to the weld zone to enhance the detection precision. However, the area of the weld zone in the I-shape beam is usually less than 2% of the whole cross section. Furthermore, some parts of the structural cross section are usually connected to other structural members. Therefore, appropriate sensor type, sensor locations, and exciting frequency range shall be considered carefully.

DISPERSIVE CHARACTERISTICS OF GUIDED WAVES

The dimension and physical parameters of the I-shape beam tested in this paper are shown in Table. 1. The total length of the beam is 1 meter. Dispersion curve for phase velocity was obtained by SAFE method as shown in Fig. 1 (a). Wave modes were searched for higher energy concentration in the weld zone. Considering the performance

of the experimental instrument, the searching frequency range was set from 30 to 70 kHz. Fig. 1 (b) shows the 13th wave mode at 40 kHz. The energy ratio of the bottom weld zone to the whole cross section is 2.22% for this mode, which is relatively high compared to the other wave modes. For example, the energy ratio is only 0.15% for the 6th wave mode as shown in Fig. 1 (c). Hence the 13th wave mode at 40 kHz was chosen as the exciting wave mode for damage detection in the weld zone.

3D wave propagation analysis was carried out using ABAQUS for selecting sensor locations in the I-shaped cross-section. At first, 11 locations were considered for both actuating and sensing as shown in Fig. 2 (a). Numerical results indicate that Locations 5 and 6 are the best to excite the 13th wave mode, which shows relatively high energy distribution in the weld zone. Fig. 2 (c) shows 2D-FFT curve for a set of simulated time-history signals along the welding line, which shows good agreement with the SAFE results.

Table. 1. Geometrical dimensions and physical parameters of I-shape beam

Young Modulus	Poisson's Ratio	Density	Thickness	Flange Width	Web Height	Weld Size
*206*Gpa	*0.28*	*7850kg*/m^3	*6mm*	*120mm*	*100mm*	*5mm*

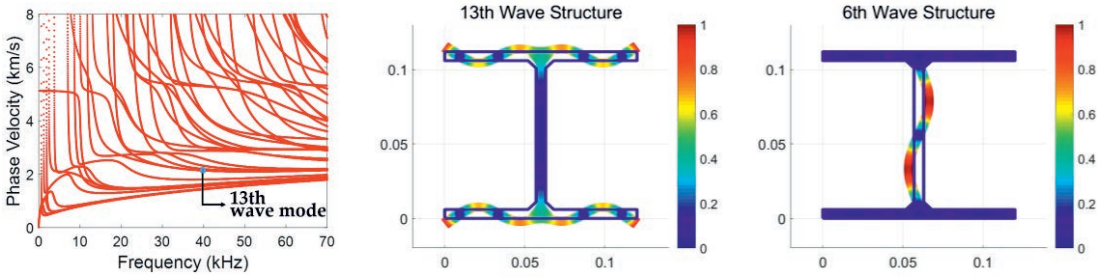

a) b) c)

Figure 1: Dispersion curve for an I-shaped beam: a) phase velocity; b) the 13th wave mode; c) the 6th wave mode

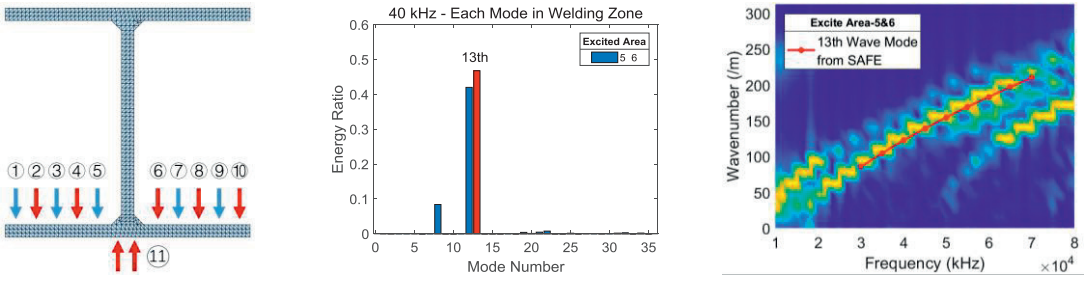

a) b) c)

Figure 2: Excitation scheme: a) potential sensor locations and excitation directions; b) energy percentage of each wave mode in the weld zone at 40kHz with sensors at Locations 5 and 6; c) 2D-FFT curve by 3D simulation

EXPERIMENTS FOR DAMAGE DETECTION

Experiments were conducted on a steel beam with same properties as in the simulation study. A pair of piezo-electric transducers were installed at Location 5 and 6. Tests were conducted at three conditions: intact specimen, specimen with an additional mass (1cm*5mm quadrate cross section) at 0.7m and specimen with a cut (5mm*5mm triangular cross section, 1cm long) on the weld zone in the middle as shown in Fig. 3. Sinusoidal wave with Hanning-window at 40 kHz was used as the excitation signal at 2 sensors as shown in Fig. 3. Fig. 4 shows the signal received at the intact state and its Hilbert envelope along with the one obtained at the cut damage state. The acoustic distance was calculated for wave packet using the ToF and the group velocity [1]. Damage detection was carried out using residual signals between the damaged and intact signals as shown in Fig. 5. To improve the damage identification, cross-correlation analysis was performed between the intact and damaged signals. Each time history was divided into 20 segments, and the cross-correlation coefficient was calculated at each time segment. Results of the damage existence and localization are shown in Fig. 6.

To investigate the temperature effect on the wave signal, the test beam was placed in a temperature chamber to obtain signals at 15 - 40 °C.

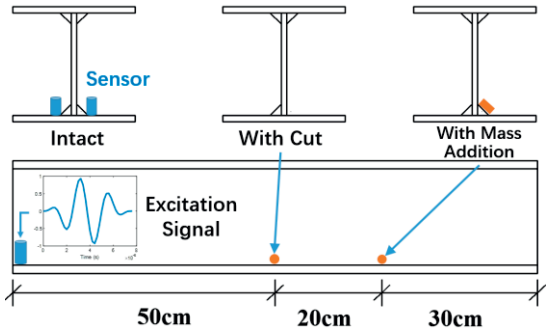

Figure 3: Experiment layout

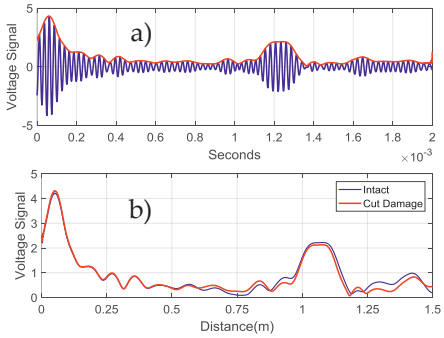

Figure 4: Signal with Hilbert Envelope

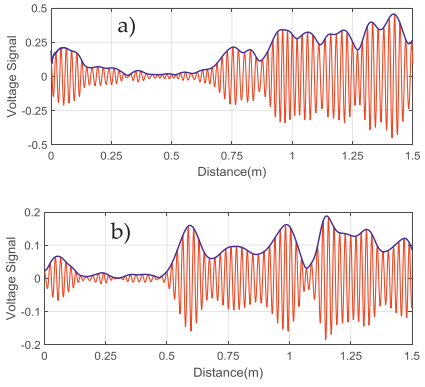

Figure 5: Residual signals: a) between intact and mass-added; b) between intact and cut damage

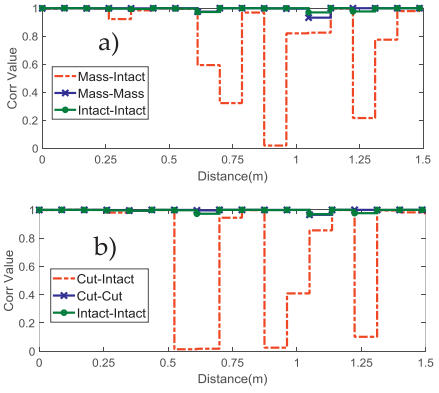

Figure 6: Cross-correlation value at each time segment: a) between intact and mass-added; b) between intact and cut damage

Signals at the intact state under various temperature are shown in Fig. 7. Fig. 4 and Fig. 7 indicate that the cross-correlation analysis under large temperature variation may cause false alarm in damage detection. Thus, PCA [2] was carried out to detect abnormity under various ambient temperature. 105 measurements from intact condition were used as the base signals for the PCA. Large number of measurements were obtained as test signals: 200 for intact condition, 230 for cut damage and 100 for mass-added condition. Q-index was evaluated for each test signal using the first 4 PCs determined from the base signals. The damage existence was determined by observing the step change in Q-index as in Fig. 9 (a). To estimate damage location, the cumulative contribution rate of Q-index ($Q_t/Q_T, t \in [0,T]$) was calculated at each time instance in comparison with the whole propagation history. For the intact state, Q_t/Q_T-index grows smoothly. However, when abnormity exists at a certain time instance, a jump has been observed in Q_t/Q_T-index as in Fig. 9 (b).

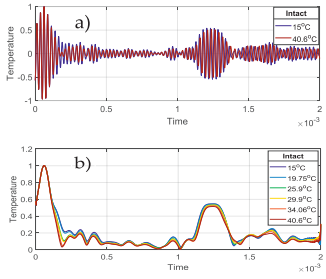

Figure 7: Signals under different ambient temperature

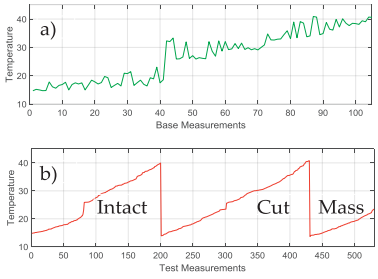

Figure 8: Ambient temperature at each measurement

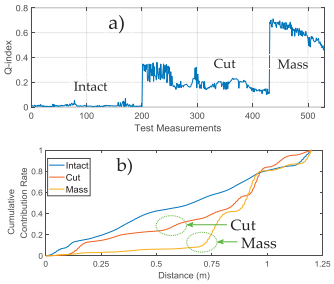

Figure 9: a) Q-index; b) Q_t/Q_T-index

CONCLUSIONS

Guided wave based damage detection is presented for the weld zone of an I-shape steel beam. SAFE analysis and 3D simulation on wave propagation were performed for selecting sensor locations and input frequency. Laboratory experiments were conducted on a beam under different damage states. At first, damage detection was carried out based on the residual signals between the damaged and intact cases using the ToF information. PCA was also employed to detect damage under various ambient temperature. It has been found that small cut and additional mass inflicted in the weld zone were successfully detected and localized.

REFERENCES

[1] Wu, J. J., Tang, Z. F., Lv, F. C., Yang, K. J., Yun, C.B., Duan, Y. F. (2018) Ultrasonic guided wave-based switch rail monitoring using independent component analysis. Meas. Sci. Technol. 29:115102.

[2] Mujica, L., Rodellar, J., Fernandez, A., Guemes, A. (2011) Q-statistic and T²-statistic PCA-based measures for damage assessment in structures. Structural Health Monitoring 10(5):539-553.

Guided Wave Method for Tension Monitoring and Damage Detection in Cables

X. D. Sui[1], Y. F. Duan[1]*, C. B. Yun[1], Z. F. Tang[2], P. F. Zhang[3]

[1] *College of Civil Engineering and Architecture, Zhejiang University, China.*
E-mail: 11712067@zju.edu.cn, ceyfduan@zju.edu.cn, ycb@zju.edu.cn

[2] *Institute of Advanced Digital Technologies and Instrumentation, Zhejiang University, China.*
E-mail: tangzhifeng@zju.edu.cn

[3] *Institute of Advanced Manufacturing Engineering, Zhejiang University, China.*
E-mail: zhangpengfei@zju.edu.cn

ABSTRACT

Health monitoring of cables in civil engineering structures is a great challenge, because their integrity is directly related to the safety of the whole structure. This study presents a guided wave method to estimate the existing cable tension and detect the cable damages such as wire breakage and corrosion. Pitch-catch and pulse-echo methods are applied using a magneto-strictive transducer. Three pairs of permanent magnets are used to create an uniform magnetic field on the cable cross section. Three groups of coils with different configurations are used for transmitter and receiver to provide dynamic magnetic field. Present study was carried out for a strand with 7 wires. Firstly, the optimal excitation frequency was determined based on the wave dispersion properties obtained from the semi-analytical finite element analysis on the cable. Then, experimental study was performed for the damage location and severity determination with multiple cases of wire breakages and corrosion using the time of flight information and amplitude of the reflected wave packets from the damages. Finally, the tension force was obtained using the change of group wave velocity for the first-arrival wave packet.

KEYWORDS: *Guided waves, magneto-strictive transducer, wire breakage, corrosion, tension estimation*

MAGNETO-SRTICTIVE TRANSDUCER DESIGN

Ferromagnetic materials show two magneto-strictive phenomena, which can be used to generate and measure the guided waves. At first, simulation analyses are made on the permeability using a commercial software Maxwell to determine the optimal properties of the permanent magnet for the static magnetic field provided. Fig. 1(a) shows the magnet unit consisting of three NdFeB N35 permanent magnets with the size 15×6×6mm and three saddle blocks connecting the magnet loop.

As for the coils for providing dynamic magnetic field, three groups of coils are arranged in parallel for the receiver, while in series for the transmitter as in Fig. 1(b).

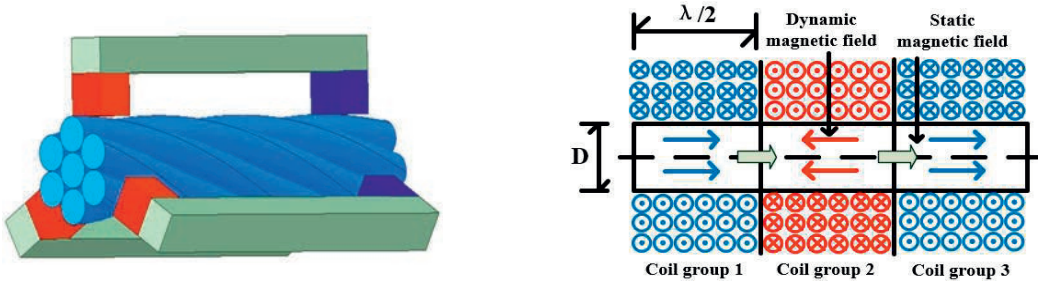

(a) (b)

Figure 1: (a) Permanent magnet for static magnetic field; (b) Coils for dynamic magnetic field

DISPERSION PROPERTY BY SEMI-ANALYTICAL FINITE ELEMENT METHOD

The semi-analytical finite element (SAFE) analysis method is employed to calculate the dispersion curves for the 7-wire strand. By this method, 3D wave propagation can be analyzed by a 2D model assuming the waves propagate along the longitudinal direction with a harmonic exponential solution $e^{i(kz-\omega t)}$.

The 7-wire strand consists of 6 helix wires and 1 straight core wire with the outer diameter OD=15.2mm, elastic modulus E=210×10^3 MPa, Poisson's ratio ν=0.29, and density ρ=7850 kg/m^3. Fig. 2(a) shows the group velocity dispersion curves which can be used to select the exciting frequency. Accordingly, 80kHz was chosen as the exciting frequency in this experiment. Fig. 2(b) shows the longitudinal mode L(0,1) with the wave velocity 4800m/s.

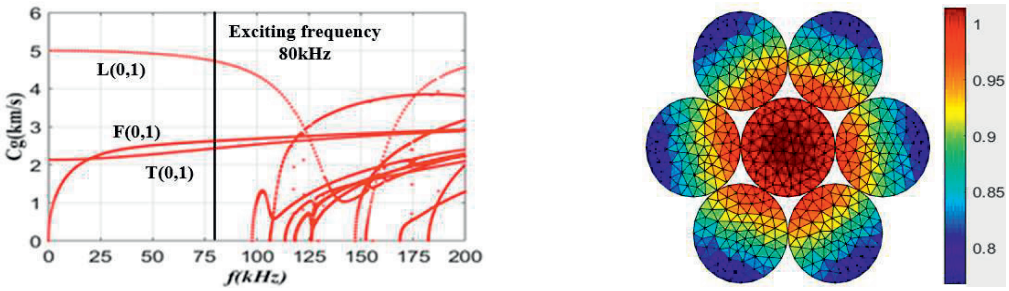

(a) (b)

Figure 2: (a) Dispersion curves for group velocity; (b) Mode shape of L(0,1)

WIRE BREAKAGE DETECTION

Experiments were carried out for detection of artificial wire breakages in the 7-wire strand. Fig. 3(a) depicts the layout of the transducers and the positions of damages, whereas Fig. 3(b) shows signals received at the transducer. Wave Packets 1-2 are for the excitation signals and Wave Packets 3-8 are for the reflected signals from 3 defects, while Wave Packets 9-10 are for those reflected from the free end.

The wave velocity obtained from the experiment is 5000m/s, which agrees the results of the SAFE analysis curve with an error of 4%. The acoustical distances were calculated for the wave packets, which match well with the real damages locations with errors less than 2%. Meanwhile, the amplitudes of the wave packets reflected from the defects increase gradually with the severity. Currently, study is being carried out for better qualification of the damage severity using advanced signal processing method.

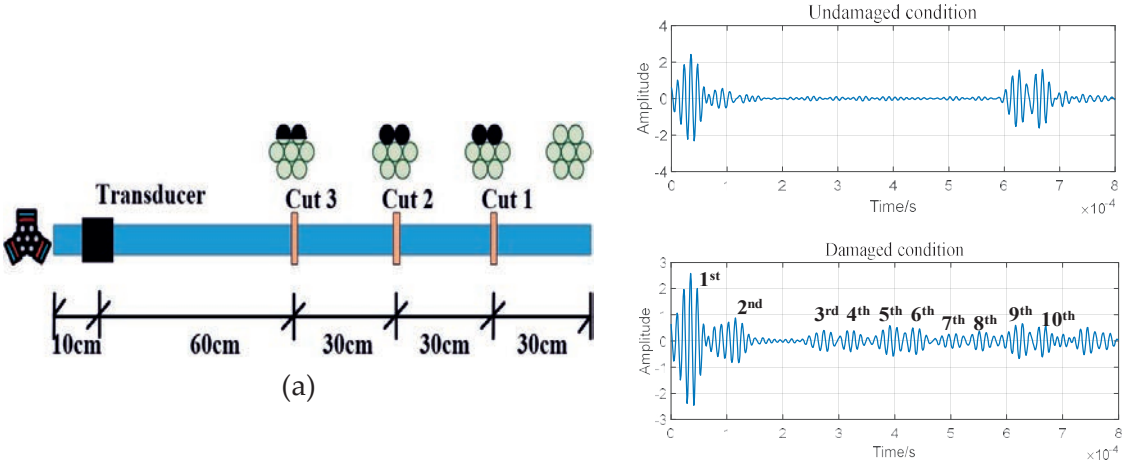

(a) (b)

Figure 3: (a) Layout of the experiment; (b) Received signals from the transducer

CORROSION DETECTION

The corrosion of the 7-wire strand is simulated by reducing the wire cross section locally with the length of 5cm as in Fig. 4(a). Fig 4(b) gives the received signals, which clearly show Wave Packet 3 reflected from the corroded region. In the experiments, the outer diameter of the 7-wire strand reduces gradually from 15.2mm to 11mm. The amplitude of Wave Packet 3 increases slowly till the outer diameter reduces to 13.0mm, but the amplitude increases more significantly after this corrosion state.

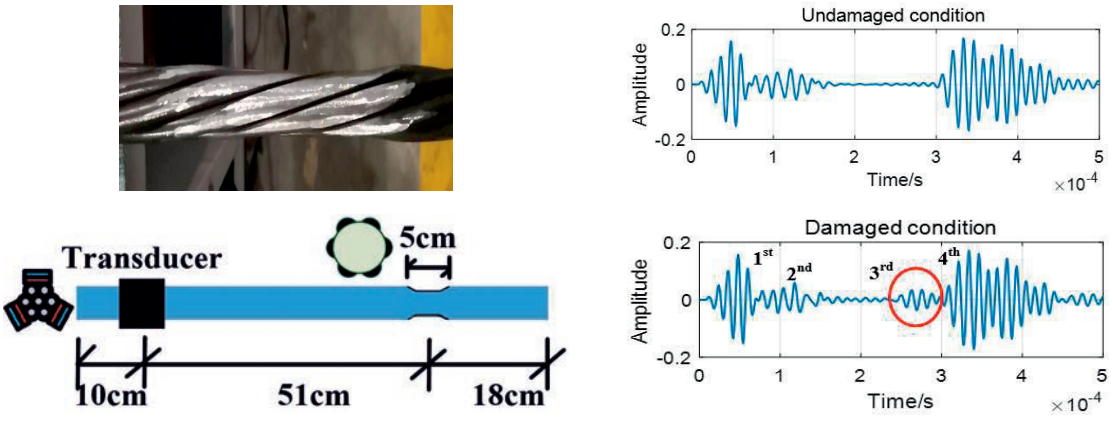

(a) (b)

Figure 4: (a) Layout of the experiment; (b) Received signals

TENSILE FORCE ESTIMATION

The effect of cable tension on the propagation properties of the guided wave is investigated. For a homogeneous and isotropic infinite waveguide subjected to an external load, the wave velocities of the longitudinal waves can be written as [1]:

$$V_L = \sqrt{\frac{\lambda+2\mu}{\rho}}\left\{1+\frac{\sigma}{2(\lambda+2\mu)(3\lambda+2\mu)}\times\frac{\lambda+\mu}{\mu}(4\lambda+10\mu+4m)+\lambda+2l\right\} \quad (1)$$

where ρ is the density, σ is the tensile stress, λ and μ are Lame's elastic constants, and *m,n* and *l* are Murnaghan's third order elastic constants.

Pitch-catch method is applied for the force estimation in the 7-wire strand as in Fig. 5(a). Fig. 5(b) shows the change of the group velocity of the first-arrival wave packet with the increasing external force from 50-130kN. Compared with the wave velocity at 50kN, it reduces 1.8% when the external load increase to 130kN, which can be used to measure the absolute tensile force in the cable.

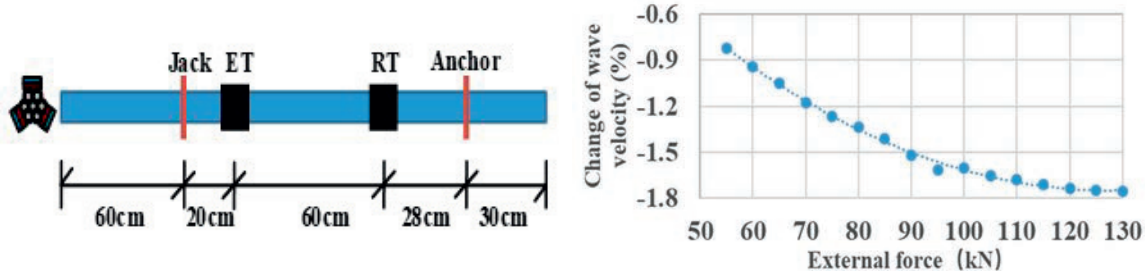

(a) (b)

Figure 5: (a) Layout of the experiment; (b) Changes of the first-arrival wave velocity

CONCLUSION

In this study, a guided wave method is presented for damage detection and tensile force estimation in a 7-wire strand using magneto-strictive transducers. Artificial wire breakage and corrosion are inflicted at various locations and with different severities. Damage locations have been successfully estimated using time of flight information, while the damage severities can be determined from the amplitude change of the wave packets reflected from the damages. The change of the wave velocity of mode L(0,1) can be used as an indicator to measure the change of tensile force, which was proven to be effective from the experiment results.

REFERENCES

[1] Chaki S, Bourse G. (2009) "Guided ultrasonic waves for non-destructive monitoring of the stress levels in prestressed steel strands". Ultrasonics, 49(2):162-171.

Damage detection of non-linear reinforced concrete structure by means of single sensing node

S. Quqa[1], L. Landi[2], P.P. Diotallevi[3]

[1] *Department of Civil, Chemical, Environmental, and Materials Engineering, University of Bologna, Italy. E-mail: said.quqa2@unibo.it*

[2] *Department of Civil, Chemical, Environmental, and Materials Engineering, University of Bologna, Italy. E-mail: l.landi@unibo.it*

[3] *Department of Civil, Chemical, Environmental, and Materials Engineering, University of Bologna, Italy. E-mail: pierpaolo.diotallevi@unibo.it*

ABSTRACT

This paper presents an application of an output-only structural identification algorithm specifically designed for low-cost monitoring systems on a structure with strongly non-linear behavior. The identification procedure is conducted simulating the presence of a single smart sensor node on the specimen, in order to identify the natural frequencies and amplitudes of collected accelerations in real time. The estimated parameters are used to develop a non-linear frequency-amplitude model representing the structural response, subsequently employed for damage detection.

KEYWORDS: *Damage detection, non-linearity, non-stationarity, operational modal analysis*

INTRODUCTION

In the field of structural health monitoring, modal parameters (i.e., natural frequencies, modal shapes, and damping) are among the most used for damage identification, because of their direct physical interpretation [1]. Variations in modal parameters, indeed, generally denote a change in the structural dynamic behavior and are often associated with ongoing damage.

Although modal analysis is based on linear models, civil structures generally exhibit some degree of non-linearity [2]. This fact is usually neglected, assuming that the signals on which modal identification is performed are collected under low-intensity excitation and stationary environmental conditions. However, depending on the construction technology, some structures may reveal their non-linear behavior even under ambient vibration, which is always present during operating conditions. Furthermore, ambient excitation is generally non-stationary and its intensity may vary over time. The direct comparison of modal parameters obtained during different

identification sessions may therefore be misleading for the identification of damage, since the differences of the estimated parameters could also be due to variations of the exciting input or to environmental effects [2].

In this paper a damage-sensitive feature is proposed, computed through the parameters obtained during the recursive fitting of instantaneous frequency-amplitude data, obtainable my means of a single sensing node.

DETAILS OF THE PROCEDURE PROPOSED

First, the modal identification algorithm presented in [3] is applied to extract the filtered components from acceleration data collected on the structure. The algorithm consists of a first initialization phase that involves the construction of a wavelet filter bank used to decompose the acquired signal into separate modal responses, and a real-time processing phase that lies in the estimation of instantaneous frequencies and amplitudes using the Teager energy operator. At least two channels of acceleration (i.e. collected by different sensors or in different directions) must be used to decompose the structural response. As new values of frequency and amplitude are available, they become part of a sliding window in which the data is sorted by frequency. In particular, each new frequency-amplitude couple of values substitutes the nearer value in terms of amplitude. This procedure is adopted instead of using a traditional time-based forgetting factor in order to minimize the issues related with the non-stationarity of the excitation intensity, which would result in an abrupt change of the identified parameters.

A median filter is then applied to limit the fluctuations of amplitude values, which are employed as input data for an identification procedure based on non-linear least squares. The model employed to perform the identification procedure has been chosen with the form of the skew-normal distribution [4], multiplied by the factor $m/2$, where m is the mean value of the amplitudes in the window analyzed. In particular, the equation used in this study for data fitting is:

$$y(x) = \frac{m}{\omega\sqrt{2\pi}} e^{-\frac{(x-\xi)^2}{2\omega^2}} \int_{-\infty}^{\frac{\alpha}{\omega}(x-\xi)} \frac{1}{\sqrt{2\pi}} e^{-\frac{t^2}{2}} dt \quad (1)$$

The identification can therefore be performed repeatedly, obtaining the recursive update of the model described in relation (1), the parameters of which (i.e., $\boldsymbol{\omega}$, $\boldsymbol{\xi}$, and $\boldsymbol{\alpha}$) can be employed to compute the instantaneous mean ($\boldsymbol{\mu}$), variance ($\boldsymbol{\sigma^2}$) and skewness ($\boldsymbol{\gamma}$) of the skew-normal distribution, as explained in [4]. The damage-sensitive feature proposed in this paper takes into account these three parameters and can be interpreted as an approximation of the mode of the distribution:

$$m_0 = \mu - \frac{\sigma\gamma}{2} \quad (2)$$

APPLICATION

The case study analyzed in this paper is a full-scale 7-story slice of a reinforced concrete building, tested on the shake table of the Network for Earthquake Engineering Simulation of the University of California-San Diego (UCSD-NEES) with ambient vibration and low-intensity white noise excitation tests, performed after inducing progressive damage scenarios. More detailed information about the specimen and the test setup can be found in [5]. Two channels of acceleration data collected at the top level of the structure has been used in this study with a sampling frequency of 100 Hz. The instantaneous frequency and amplitude of the first vibration mode are extracted by means of the identification algorithm [3], post-processed through a median filter with a window of 600 samples and reported in Figure 1. Here, the line color depends on the signal amplitude, as reported in the color bar at the right side of the figure.

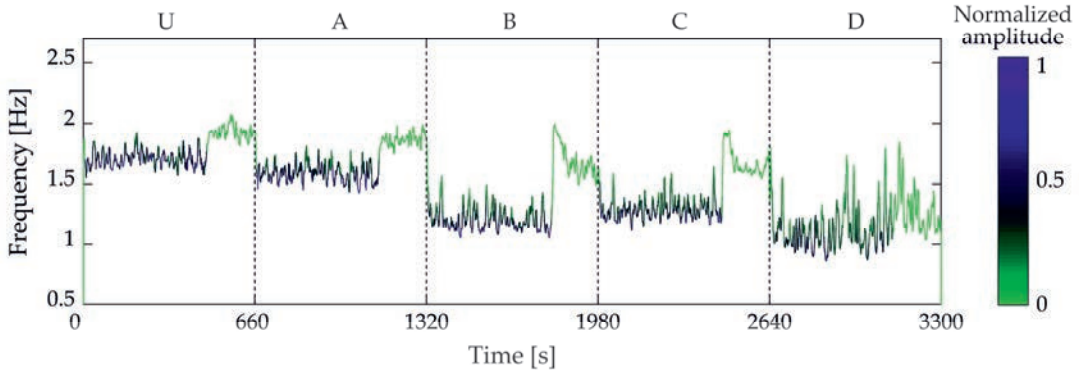

Figure 1: Instantaneous frequency of the first vibration mode, represented as a function of time and instantaneous amplitude.

The dashed vertical lines represent the limits between five different conditions: the interval from 0 to 660 seconds describes the structural behavior in undamaged condition (U), while during the following intervals, data coming from progressively induced damage scenarios (A, B, C, and D) are used. Moreover, in the first part of each interval the acceleration recordings collected under 0.05g RMS white noise excitation are used, while, in the remaining part, the instantaneous parameters are evaluated under low-amplitude ambient vibration. From Figure 1 it is possible to notice how the instantaneous frequency is strongly dependent on amplitude variations, presenting abrupt alterations when moving from high to modest amplitude values. In particular, changes due to amplitude variations are higher than those due to the entry into a different damage scenario. This fact makes instantaneous frequency unusable as the only parameter for damage identification purposes. In Figure 2 the recursive identification procedure is illustrated: 2000 samples (20 sec.) of frequency-amplitude data at a time (a) are fitted to the model proposed (b), the parameters of which are used to compute the damage-sensitive feature presented in equation (2).

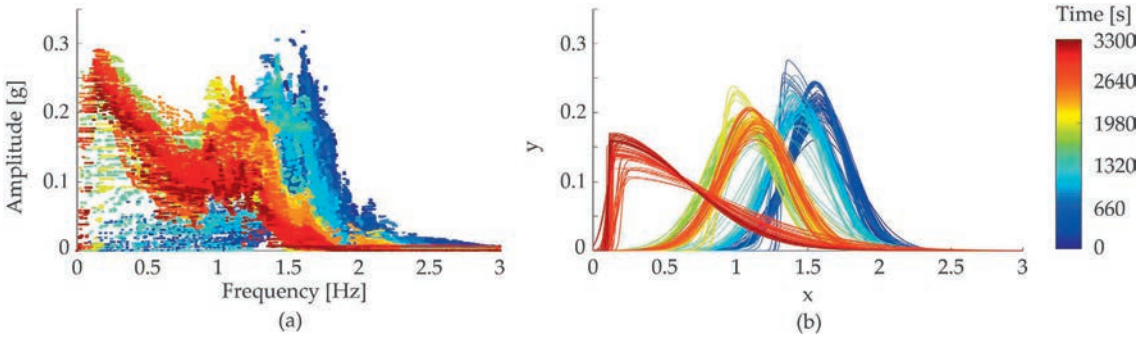

Figure 2: Recursive fitting procedure of registered data (a) into model (b), represented over time.

In Figure 3, the percentage variation of the damage-sensitive feature with respect to the mean value computed over a baseline of 30 samples is reported over time as a damage index. It is possible to observe that the feature proposed follows the progressive damage, not depending on the amplitude level. On the other hand, when a new scenario occurs, the parameters tend to new values more slowly than the instantaneous frequency, depending on the length of the window used for model fitting.

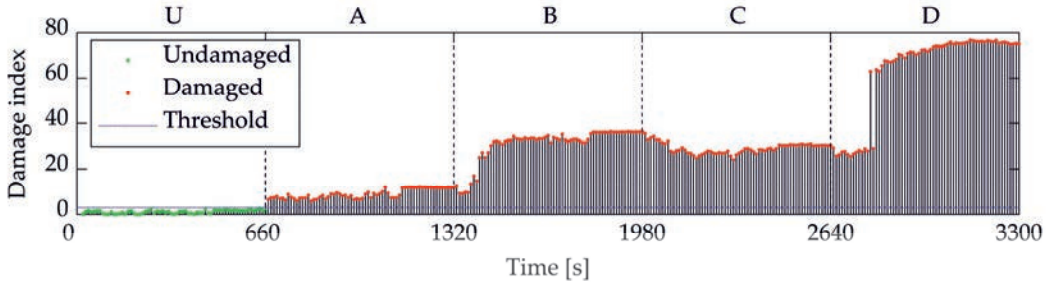

Figure 3: Variation over time of the damage-sensitive feature proposed in this study.

CONCLUSIONS

Using the instantaneous frequency-amplitude data obtained from a single sensing node, a damage-sensitive feature which does not depend on frequency variations due to the non-linearity of the structure examined is proposed. The analysis of the variation of this feature with respect to a baseline condition allows a robust detection of damage.

REFERENCES

[1] Brincker R., Ventura C. E. (2015) Introduction to operational modal analysis. Wiley, New York.

[2] Worden K., Tomlinson G. R. (2001) Nonlinearity in structural dynamics: detection, identification and modeling. Institute of Physics Publishing Ltd, Bristol.

[3] Quqa S., Landi L., Diotallevi P. P. (2019) Real-time damage detection through single low-cost smart sensor, Paper No. C19614. COMPDYN 2019, Crete, GR, June 24-26, 2019.

[4] Azzalini A. (2013) The skew-normal and related families. Cambridge University Press.

[5] Moaveni B., He X., Conte J. P., Restrepo J. I. (2010) Damage identification study of a seven-story full-scale building slice tested on the UCSD-NEES shake table, Structural Safety **32**:347-356.

A statistically based method for the selection of sensors networks in dynamic damage detection of beams

E. Lofrano[1], A. Paolone[1], M. Pingaro[1], P. Trovalusci[1]

[1] *Dep. of Struct. and Geotechnical Engineering, Sapienza University of Rome, Italy.*

E-mail:{egidio.lofrano,achille.paolone,marco.pingaro,patrizia.trovalusci}@uniroma1.it

ABSTRACT

In this work uncertain vibrations of beam-like structures are considered. Attention is paid to sensors placement and a statistically based method for the selection of sensors networks is proposed. The objective is to characterize the SHM process in terms of identifiability and maximum accuracy that a given network of sensors can provide, regardless of the damage detection techniques to be developed downstream.

KEYWORDS: *uncertain beams, damage detection, sensors network, perturbation approach*

INTRODUCTION

Uncertainties are unquestionably involved in the structural behavior of all real-life structures. In this work attention is paid to optimal sensors placement for dynamic damage detection. In the technical literature there are many works dedicated to the optimal placement of sensors: in [1] improved genetic algorithms are used; [2] considers optimal placement for multi-setup modal analysis; in [3] several methods are compared for a suspended bridge; invertibility conditions of linear system can be found in [4]. However, all these works focus on experimental modal analysis, whereas the optimal sensors placement on damaged structures received less attention [5]. Within this framework, the approach here proposed is pivoted on the closed-form solution of the 1-D continuum dynamic problem provided by a perturbation approach [6], where the smallness parameter acts as damage parameter and is assumed Gaussian distributed. Then, the damage probability is evaluated and compared with the probability of detecting the damage with a given sensors network.The discrepancy among the two values is therefore a measure of the network capabilities in the damage detection and can be profitably implemented for selection purposes.

PROPOSED METHOD

We assume: $\rho(x,\varepsilon)=\rho$, $B(x,\varepsilon)=B_0+\varepsilon B_1(x)$, $|\varepsilon|\ll 1$ and $\varepsilon\sim\mathcal{N}(\mu_\varepsilon,\sigma_\varepsilon)$, where ρ is the linear mass density, x is the abscissa along the beam and B is the flexural stiffness, that is

assumed as a sum of an initial flexural stiffness B_0 and a perturbation term. Specifically, in our applications we pose a negative function $B_1(x)$ (which represents the damaged area), so that the random parameter ε can be considered as a random damage, where $\varepsilon = 0$ for an healthy beam, whereas $\varepsilon > 0$ indicates a damage state (and the higher the parameter, the greater the damage). The governing equation in the modal space:

$$\frac{\varepsilon B_1''(x)\phi_i''(x,\varepsilon) + 2\varepsilon B_1'(x)\phi_i'''(x,\varepsilon) + (B_0 + \varepsilon B_1(x))\,\phi_i''''(x,\varepsilon)}{\rho\phi_i(x,\varepsilon)} = -\frac{\ddot{q}_i(t,\varepsilon)}{q_i(t,\varepsilon)} = \omega_i^2(\varepsilon) \quad (1)$$

being $(\bullet)' = \partial(\bullet)/\partial x$, $(\dot{\bullet}) = \partial(\bullet)/\partial t$) and where $\phi_i(x,\varepsilon)$ are the mode shapes (eigenvectors) and $\omega_i(\varepsilon)$ the relevant (circular) frequencies (related to the eigenvalues λ_i: $\omega_i(\varepsilon) = \lambda_i^2(\varepsilon)\sqrt{B_0/\rho}$). Since ε is a small parameter, Eq. (1) can be solved through a perturbation approach. Moreover, the dynamic system under investigation is non-defective, therefore the eigensolution admits a perturbation series of integer powers of the small parameter:

$$\lambda_i(\varepsilon) = \lambda_{0i} + \varepsilon\lambda_{1i} + \varepsilon^2\lambda_{2i} + \ldots \quad \phi_i(x,\varepsilon) = \phi_{0i}(x) + \varepsilon\phi_{1i}(x) + \varepsilon^2\phi_{2i}(x) + \ldots \quad (2)$$

The damage occurrence is $P_d = P(\varepsilon > 0) = \int_0^\infty f(\varepsilon)\,d\varepsilon$, where $f(\varepsilon)$ is the probability density function of ε. In our case, since the random parameter ε has been assumed gaussian distributed, the probability of damage P_d depends only on the ratio among the standard deviation σ_ε and the mean value μ_ε, that is, P_d is a function of the coefficient of variation $CV_\varepsilon = \sigma_\varepsilon/\mu_\varepsilon$. The probability to detect the damage by dynamic analysis is related to the reduction of the eigenvalues:

$$P_{ddi} = P(\lambda_i(\varepsilon) < \lambda_{0i}) = P(\lambda_i(\varepsilon) - \lambda_{0i} < 0) \quad i = 1, \ldots, n_\lambda \quad (3)$$

being n_λ the number of the first (measured) eigenvalues (related to sampling frequency of the sensors). Using Eq. $(2)_1$, the differences $\lambda_i(\varepsilon) - \lambda_{0i}$ can be written as $\varepsilon\lambda_{1i} + (\varepsilon/\sigma_\varepsilon)^2\,\sigma_\varepsilon^2\lambda_{2i}$, where ε is gaussian distributed, $\varepsilon \sim \mathcal{N}(\mu_\varepsilon, \sigma_\varepsilon)$, whereas the term $(\varepsilon/\sigma_\varepsilon)^2$ has a noncentral chi-squared distribution $\mathcal{X}^2(k_\chi, \lambda_\chi)$, with a unitary degree of freedom k_χ and noncentrality parameter λ_χ equals to $(\mu_\varepsilon/\sigma_\varepsilon)^2$. Therefore, the probability density function of the term $\lambda_i(\varepsilon) - \lambda_{0i}$ is a mixture of two known distributions. For the sake of brevity, the relevant probability P_{ddi} is here explicitly evaluated only in the case when the two derivatives λ_{1i} and λ_{2i} are both negative (which is the most usual case):

$$\begin{cases} P_{ddi} = \gamma_{1i} w_{1i} \frac{1}{2}\left(1 + \mathrm{Erf}\left[\frac{1}{\sqrt{2}CV_\varepsilon}\right] + \mathrm{Erfc}\left[\frac{\lambda_{1i}+\lambda_{2i}\mu_\varepsilon}{\sqrt{2}CV_\varepsilon\lambda_{2i}\mu_\varepsilon}\right]\right) + \gamma_{2i} w_{2i} \quad i = 1, \ldots, n_\lambda \\ w_{1i} = \dfrac{|\lambda_{1i}|}{|\lambda_{1i}| + \sigma_\varepsilon^2|\lambda_2|} \quad w_{2i} = \dfrac{\sigma_\varepsilon^2|\lambda_{2i}|}{|\lambda_{1i}| + \sigma_\varepsilon^2|\lambda_{2i}|} \end{cases} \quad (4)$$

being Erf the error function and Erfc the complementary error function, and where $\gamma_{1i} = 1 - |\tilde{A}_{1i} - A_{1i}|/A_{1i}$ and $\gamma_{2i} = 1 - |\tilde{A}_{2i} - A_{2i}|/A_{2i}$ are penalty indexes affecting the first and the second order term, respectively. A_{1i} and A_{2i} are the analytical absolute values of the

areas under the graph of $|\phi_{1i}(x)|$ and $|\phi_{2i}(x)|$, respectively, whereas $\tilde{A}_{1i}$ and $\tilde{A}_{2i}$ are the discretized counterparts:

$$\begin{cases} A_{1i} = \int_0^L |\phi_{1i}(x)|\, dx & \tilde{A}_{1i} = \sum_{s=1}^{n_s} |\phi_{1i}(x_s)| \, \dfrac{x_{s+1} - x_{s-1}}{2} \\ A_{2i} = \int_0^L |\phi_{2i}(x)|\, dx & \tilde{A}_{2i} = \sum_{s=1}^{n_s} |\phi_{2i}(x_s)| \, \dfrac{x_{s+1} - x_{s-1}}{2} \end{cases} \quad \text{with: } x_0 = 0,\ x_{n_s+1} = L \tag{5}$$

Then, for a given beam and a given network, we measure the capability in damage detection via the average difference $\Delta P = \sum_{i=1}^{n_\lambda} \frac{1}{n_\lambda}(P_d - P_{ddi})$ depending on: the number n_λ of measured eigenvalues, the positions x_s of sensors along the beam axis, the number n_s of sensors, $\Delta P = \Delta P(n_\lambda, n_s, x_s)$. For a given number n_λ of measured eigenvalues, the optimal sensors placement can be defined as the one requiring less sensors, introducing the optimization problem $\min n_s : \Delta P \leq \tilde{\Delta} P$, where $\tilde{\Delta} P$ is a chosen threshold value for the difference among the two probability.

CASE STUDY

A simply supported (hinged-hinged) beam is considered. Undamaged scenario is: bending stiffness $B_0 = 162 \cdot 10^6\ \mathrm{Nm}^2$, linear mass density $\rho = 450\ \mathrm{kg/m}$, length $L = 6\ \mathrm{m}$, where values are consistent with a concrete beam of Young's modulus $E = 30 \cdot 10^9$ Pa, volume mass density $\rho_V = 2500\ \mathrm{kg/m}^3$ and rectangular cross-section of base 0.30 m and height 0.60 m. Damage is introduced using for $B_1(x)$:

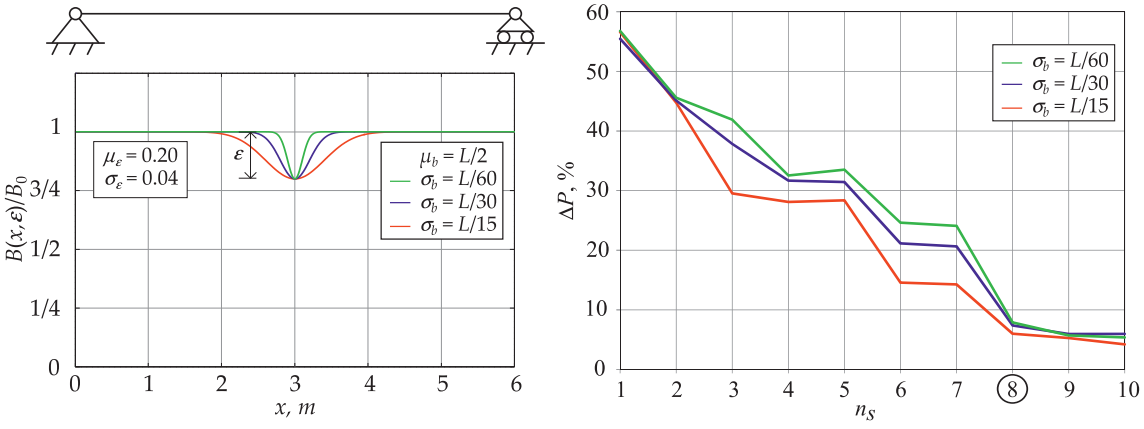

Figure 1: Case study (left) and selection of the optimal sensors placement (right).

$$B_1(x) = -B_0\, e^{-\frac{(x-\mu_b)^2}{2\sigma_b^2}} \Rightarrow B(x,\varepsilon) = B_0 \left(1 - \varepsilon\, e^{-\frac{(x-\mu_b)^2}{2\sigma_b^2}}\right) \tag{6}$$

where μ_b characterizes the position of the damage and σ_b the relevant spatial amplitude. Here the damage is assumed centered at the midspan ($\mu_b = L/2$) and scattered around it ($\sigma_b = \{L/15, L/30, L/60\}$), see Fig. 1. For the gaussian random parameter ε, a mean

value $\mu_\varepsilon = 0.20$ and a standard deviation $\sigma_\varepsilon = 0.04$ are used. Four measured eigenvalues ($n_\lambda = 4$) are assumed for the sensors, and the network in considered with equally spaced sensors: under these hypotheses, the optimization problem is only the number n_s of sensors. Figure 1 shows the values of the average difference ΔP when n_s is increased from 1 to 10. When the number of sensors increases, there is a sharp reduction of the percentage difference; moreover, as the physics of the problem suggests, the reduction is wider with increasing damaged area (i.e. σ_b). Lastly, if a threshold value $\tilde{\Delta} P$ of 10% is adopted, the optimal sensors placement requires eight sensors (value circled in Fig. 1), regardless the amplitude of the damaged area.

CONCLUSIONS

The main goal of this paper is the identification of the damages in transversely vibrating uncertain 1-D continua. A perturbation technique has been used to obtain the asymptotic eigensolution up to the second order, where the smallness parameter acts as Gaussian distributed damage parameter. The proposed method has been successfully implemented to compare several sensors scenarios of a simply supported beam undergoing a non-localized damage centered at the midspan.

References

[1] H.Y. Guo, L. Zhang, L.L. Zhang, J.X. Zhou, Optimal placement of sensors for structural health monitoring using improved genetic algorithms. *Smart Mater Struct*, **13**(3), 528–534, 2004.

[2] J. Zhang, K. Maes, G. De Roeck, E. Reynders, C. Papadimitriou, G. Lombaert, Optimal sensor placement for multi-setup modal analysis of structures. *J Sound Vib*, **401**, 214–232, 2017.

[3] M. Meo, G. Zumpano, On the optimal sensor placement techniques for a bridge structure. *Eng Struct*, **27**(10), 1488–1497, 2005.

[4] K. Maes, E. Lourens, K. Van Nimmen, E. Reynders, G. De Roeck, G. Lombaert, Design of sensor networks for instantaneous inversion of modally reduced order models in structural dynamics. *Mech Syst Signal Pr*, **52-53**, 628–644, 2015.

[5] H. He, H. Xu, X. Wang, X. Zhang, S. Fan, Optimal Sensor Placement for Spatial Structure Based on Importance Coefficient and Randomness. *Shock Vib*, **2018**, 1–14, 2018.

[6] E. Lofrano, A. Paolone, M. Vasta, Identification of Uncertain Vibrating Beams through a Perturbation Approach. *ASCE-ASME J. Risk Uncertain. Eng. Syst. A*, **2**(2), 1–11, 2016.

Automated Structural Damage Detection for a Simple Beam Structure using Deep Convolutional LSTM

Jongbin Won[1], Jong-Woong Park[2]

[1] *School of Civil and Environmental Engineering, Chung-Ang university, South Korea*
E-mail: jbwon90@gmail.com
[2] *School of Civil and Environmental Engineering, Chung-Ang university, South Korea*
E-mail: jongwoong@cau.ac.kr

ABSTRACT

The most challenging issues lies in the structural damage detection the extraction of features or indices that is resulted from the structural damage. Existing machine learning-based methods have used limited dynamic characteristics such as natural frequencies and mode shapes for damage identification. This study presents damage detection approach to automatically identify damage locations from a set of acceleration and strain responses using deep convolutional LSTM. The proposed method input finite length of the time-series responses and outputs damage location. The proposed method has been numerically validated on a simple beam structures to investigate the accuracy and robustness for damage identification.

KEYWORDS: *Automated structural damage detection, Deep-Learning damage detection, Deep Convolutional LSTM, Damaged state responses*

1. Introduction

In recent years, the aging of large structures has become an unavoidable problem, which has raised importance of structure health monitoring (SHM). Therefore, many studies are being conducted to ensure structural integrity and to detect structural damage. SHM applications begin with measuring dynamic response of structures using multiple sensors. However, because the limited information can be obtained from time-domain data directly, various feature extraction methods are used to convert low-level sensor signals to damage-sensitive features.

One way for feature extraction is computing dynamic signatures of the structure or designing their derivative to obtain a higher sensitivity of damage. Natural frequency and mode shapes are well used due to the convenience in measurement [1, 2]. However, due to difficulty of extracting dynamic features from measurements , accurate FE model is required to damage identification in reversely from the measurements.

Recently, deep learning techniques have been utilized in structural damage detection field for automated feature detection and damage identification [3]. Although partial successes were obtained, the performances of neural networks are greatly influenced by input shape. For example, CNN-based Deep network can be used for time-series measurement for damage identification, but the input size is limited to few seconds of measurements due to computational constraints.

To address these limitations, this paper employs Natural Excitation Technique (NExT) to fix input size of time-series data and Multivariate Attention LSTM-FCNs (MALSTM-FCN) [4] for detecting structural damage from time-series measurement directly.

2. Methodology

This paper presents an approach to detect structural damage directly from time-series measurements. MALSTM-FCNs is designed to process low-level sensor data, to learn features, and to achieve damage detection simultaneously.

The overview of the proposed method (see Figure 1) is organized as follows: (1) numerical simulation is conducted to obtain structural responses data; (2) a MALSTM-FCN presented in Figure 2 is trained on the data set; (3) the classification performance of designed deep networks with single damage in the beam are evaluated and compared.

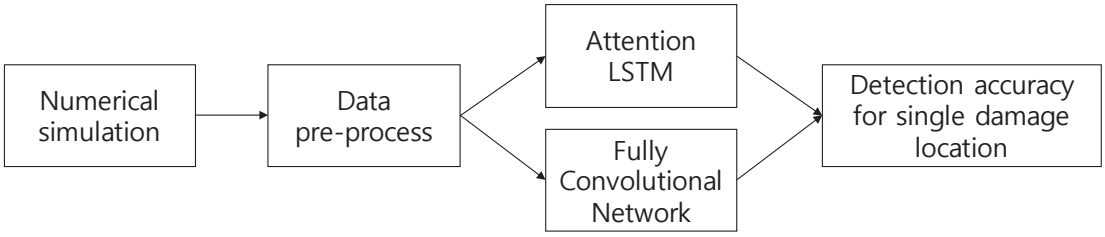

Figure 1: The overview of the methodology

2.1 Multivariate Attention LSTM-FCN

MALSTM-FCN was proposed to conduct damage classification using time-series input data. MALSTM-FCN comprises of a fully convolutional block and a LSTM block, as depicted in Figure 1. The fully convolutional block contains three temporal convolutional blocks, used as a feature extractor. Each convolutional block contains a convolutional layer, with filter size of 128 or 256, and is succeeded by a batch normalization, with a momentum of 0.99 and epsilon of 0.001. The batch normalization layer is succeeded by the ReLU activation. In addition, the first two convolutional blocks conclude with a squeeze and excite block. The LSTM block comprise of Attention LSTM layer, which is followed by a dropout.

Tab.1. The detailed configuration of the MALSTM-FCN

Layer	Type	BN	Activation
ALSTM	*ALSTM*	*F*	*None*
	Dropout	*F*	*None*
FCN	*Conv1D*	*T*	*ReLU*
	Conv1D	*T*	*ReLU*
	Conv1D	*T*	*ReLU*
	Pooling	*F*	*None*

Tab. 2. Configurations of training process

Name	Value	Description
Batch size	*128*	*The size of data batch*
Steps per epoch	*50*	*The number of steps in a single training epoch*
Learning rate	*1e-5*	*Learning rate of Adam optimizer*
$\boldsymbol{\beta_1}$	*0.9*	*A parameter of Adam, weight of the momentum term*
$\boldsymbol{\beta_2}$	*0.999*	*A parameter of Adam, controlling the decay of learning rate*

3. Numerical Validation

A simply supported beam with a length of 50 m was considered in this study for numerical validation. The beam has a rectangular cross-section with 4 m width and 2 m height, and the beam is divided into 10 equal Euler–Bernoulli beam elements. A random force was applied at node No. 2 as an excitation for 20 seconds. Acceleration and strain responses are measured with 100 Hz under signal RMS noise of 1mg and 0.1 micro-strain.

Tab. 1. The detailed configuration of the MALSTM-FCN

Total Length	50 m
Depth	*4 m*
Width	*2 m*
Young's modulus	*210 GPa*
Mass density	*7850* kg/m^3

Damage is simulated by decreasing flexural rigidity of the beam and three levels of damage are considered with damage levels of 20%, 30% and 40% . Single damage is occurred randomly on an element of the beam. For training, three types of data are prepared: 1) acceleration from all 9 nodes, 2) 9 acceleration measurements applied with NExT and 3) 3 acceleration and strain measurements from node No. 2, 5, 8 with NExT applied. A total of three simulation cases shown in Tab 4. are considered to evaluate the

performance of proposed method.

Tab. 4. Training data set cases

Case	Data shape	Description
1	*(9, 2000)*	*9 acceleration data, 2000 time stamps*
2	*(9, 1024)*	*9 acceleration data, 1024 time stamps by auto-correlation*
3	*(6, 1024)*	*3 acceleration, 3 strain data, 1024 time stamps by auto-correlation*

4. Conclusion

The purpose of this work is extracting features of the structure condition from responses data directly by the learning algorithm. The classification accuracy using categorical cross-entropy presents that how the network well predicts the location of single damage.

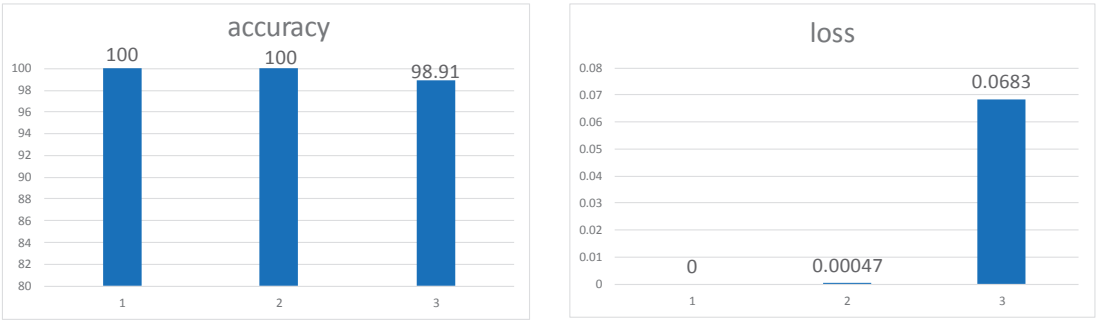

Figure 2: The classification accuracy of categorical cross-entropy

The result shows that auto-correlation technique can reduce the time stamps which are equal to the data input shape of network that allow the use of fixed data size as an input for time-series damage identification. Moreover, sensor fusion of acceleration and strain have shown the possibility of damage detection with reduced number of sensors.

REFERENCES

[1] Cawley, P. and R.D.J.T.J.o.S.A.f.E.D. Adams, *The location of defects in structures from measurements of natural frequencies*. 1979. **14**(2): p. 49-57.

[2] Farrar, C., G.J.J.o.s. James III, and vibration, *System identification from ambient vibration measurements on a bridge*. 1997. **205**(1): p. 1-18.

[3] Adeli, H. and X. Jiang, *Intelligent infrastructure: neural networks, wavelets, and chaos theory for intelligent transportation systems and smart structures*. 2008: CRC press.

[4] Karim, F., et al., *Multivariate lstm-fcns for time series classification*. 2018.

Dynamics and damage in the Quisi steel truss bridge

M. Crognale[1], V. Gattulli[1], S. Ivorra[2], F. Potenza[3]

[1] *Department of Civil and Geotechnical Engineering, Sapienza University of Rome, Italy.*

E-mail: marianna.crognale@uniroma1.it

vincenzo.gattulli@uniroma1.it

[2] *DIC, University of Alicante, Spain.*

E-mail: sivorra@ua.es

[3] *DICEA, University of L'Aquila, Italy.*

E-mail: francesco.potenza@univaq.it

ABSTRACT

Quisi Bridge located in Benissa (Alicante) is an historic steel truss structure, which is investigated with different techniques to assess fatigue damages. A method based on vibration measurements, is illustrated to determine defect-induced reduction of stiffness, (combination of damage intensity and extension). Natural frequency change for a structural damage in a truss member is quantified through a classical FEM procedure in which a damaged truss element is defined and implemented. This model is used to produce pseudo-experimental response of a damaged truss which is dynamically excited by white noise. Stochastic Subspace Identification (SSI) has permitted to identify the main modal parameters related to both damaged and undamaged truss system. A damage index depending on Stiffness Reduction Factor (SRF) permits to determine the damage description based on measured quantities.

KEYWORDS: *Damage Identification, Steel Structures, Stochastic Subspace Identification.*

INTRODUCTION

Steel truss railway bridges are subject to potential damage, mainly due to fatigue phenomena and corrosion. Recently, vibration-based damage identification is proposed in conjunction with other techniques [1]. Classically, the use of vibration relies on the comparison between identified undamaged and damaged modal properties of simple structural elements. The knowledge of mechanical models which describe the damage effect on structural dynamics, is also used [2] [3]. The cited approach is followed in the case of steel truss structure such as the Quisi Bridge, in order to determine a damage identification methodology for a simple 2D truss model (Fig.1).

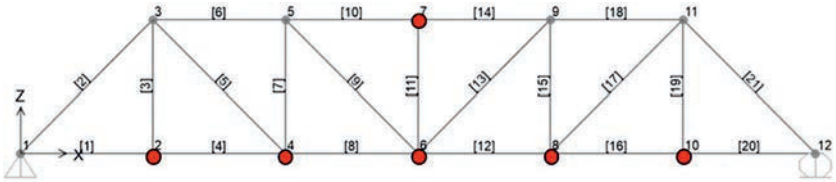

Figure 1: 2D truss simple model and sensor layout.

Damage is described as a cross-section area reduction of a truss member, through the introduction of the following damaged truss stiffness matrix:

$$\mathbf{K_d^e} = \frac{EA}{L} \cdot \frac{(1-\zeta)(1+\delta\zeta-\zeta)}{[(1-\zeta)(1-\delta)+\delta]^2} \begin{bmatrix} 1 & 0 & -1 & 0 \\ 0 & 0 & 0 & 0 \\ -1 & 0 & 1 & 0 \\ 0 & 0 & 0 & 0 \end{bmatrix} = \frac{EA}{L}(SRF)\mathbf{K^e} \quad (1)$$

where the damage intensity ζ and extent δ have been represented in non-dimensional form as:

$$\zeta = \frac{EA - EA_d}{EA},\ \delta = \frac{L_d}{L},\ 0 \le \zeta \le 1, 0 \le \delta \le 1 \quad (2)$$

SRF is the Stiffness Reduction Factor which is a combination of these two parameters affecting the stiffness and consequently the frequencies. Several damage scenarios were considered: the damage parameters ($\delta = 0.3, \zeta = 0.5$) were applied consecutively to truss element number 2, 5 and 6 in Fig. 1.

The dependence of the frequencies on the SRF is described by numerical evaluation FEM. The procedure uses pseudo-experimental response, generated from the numerical model under white noise. As sketched in Fig. 1, vertical accelerations of the bridge were evaluated in six nodes of the model (2, 4, 6, 7, 8 and 10). Based on these measurements a dynamic identification of the modal parameters was made by SSI in time domain (Fig. 3 shows the stabilization diagram). Fig. 2 shows pseudo-experimental response before and after damage.

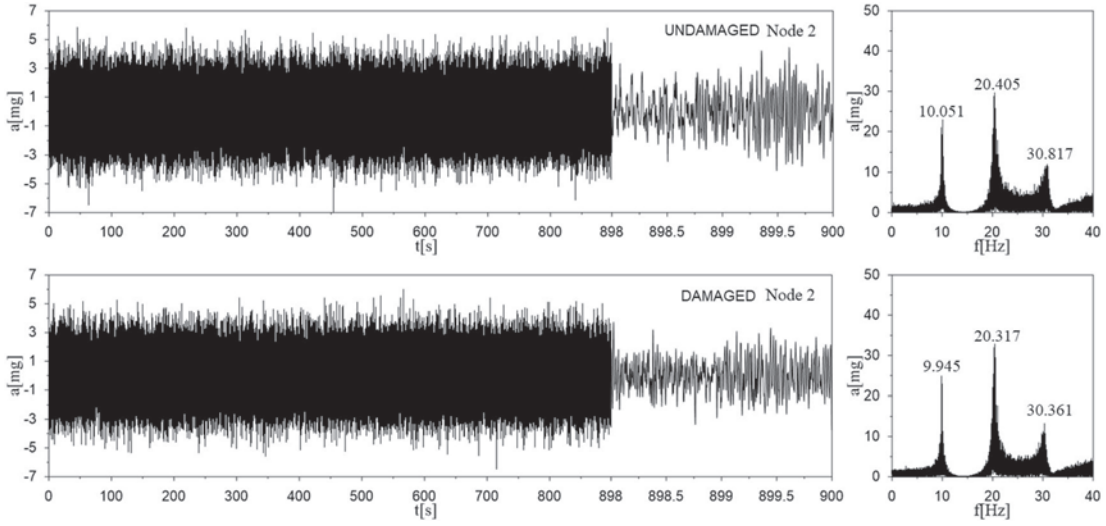

Figure 2: Time histories and FFT under white noise for node 2 - damaged truss member 6.

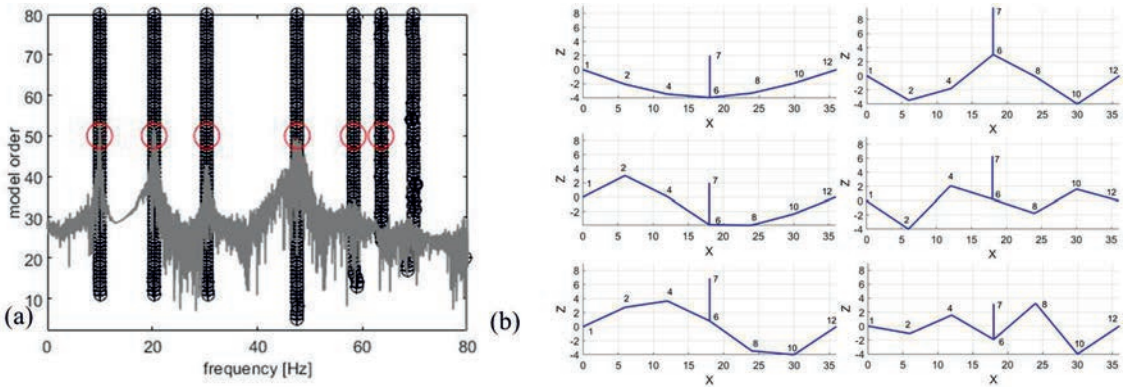

Figure 3: (a) Stabilization diagram obtained by the SSI-covariance driven procedure. (b) First six mode shapes identified from pseudo-experimental data.

MODAL AND DAMAGE IDENTIFICATION

The inverse problem of damage identification is addressed using a procedure based on comparison between the numerical and the experimentally measured dynamical response of the truss. Only an optimum number of modes are needed to be considered to univocally determine the curve SRF(δ,ζ) in the damage parameter plane (δ,ζ). The number of modes that are necessary to achieve a unique solution in the optimization problem depends on the position of the damaged element in the truss. The objective function $\mathcal{L}(\zeta,\delta)$ based on frequency measurements is defined as follows:

$$\mathcal{L}(\zeta,\delta)=\sum_{i=1}^{k}\left|\frac{\omega_{d,i}^{EX}-\omega_{d,i}^{NM}(\zeta,\delta)}{\omega_{u,i}^{EX}}\right|^{2} \tag{3}$$

where $\omega_{d,i}^{EX}$ and $\omega_{d,i}^{NM}(\zeta,\delta)$ are the i-th experimental and numerical frequencies of the damaged element respectively, while $\omega_{u,i}^{EX}$ represents the corresponding frequency in the undamaged state. Thus, an optimal estimate of the damage is given by the parameter combination T$=(\bar{\zeta},\bar{\delta})$ corresponding to the SRF$(\bar{\zeta},\bar{\delta})$ that in the parameters space minimizes the objective function $\mathcal{L}(\zeta,\delta):\Pi\rightarrow\mathbb{R}^{+}$ measuring the error between the experimental and the analytical frequencies. Fig. 4 shows results of the performance of index $\mathcal{L}$ in the detection of curve SRF (δ,ζ) varying the number of modes k.

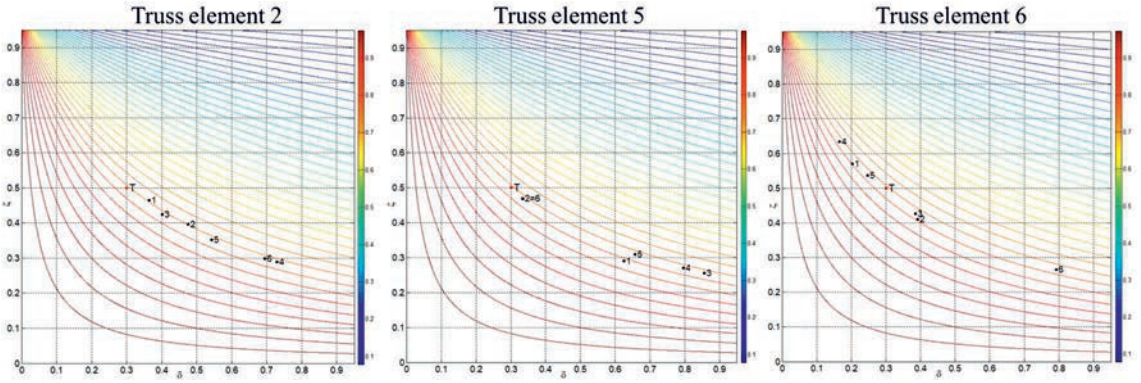

Figure 4: Effects of number of modes in the detection of SRF$(\boldsymbol{\delta},\boldsymbol{\zeta})$ curve.

QUISI BRIDGE CASE STUDY

The Quisi Bridge is located in Benissa (Alicante) was built in 1914 and it is part of the 9th FGV Railway Line. The structure consists in a top-bearing Pratt type truss. It is 170 m long with six spans of different length (Fig. 5). A 3D FE model of the main span permits to evaluate frequencies variation due to damage affecting an element with SRF = 0.76923. The frequency variation for the first four modes in percentage are $(f_{iu}-f_{id})/f_{iu}$ = [0.15, 0.02, 0.14, 0.09]. In the real case the damage affecting one single element influences the natural frequencies with quite small variation.

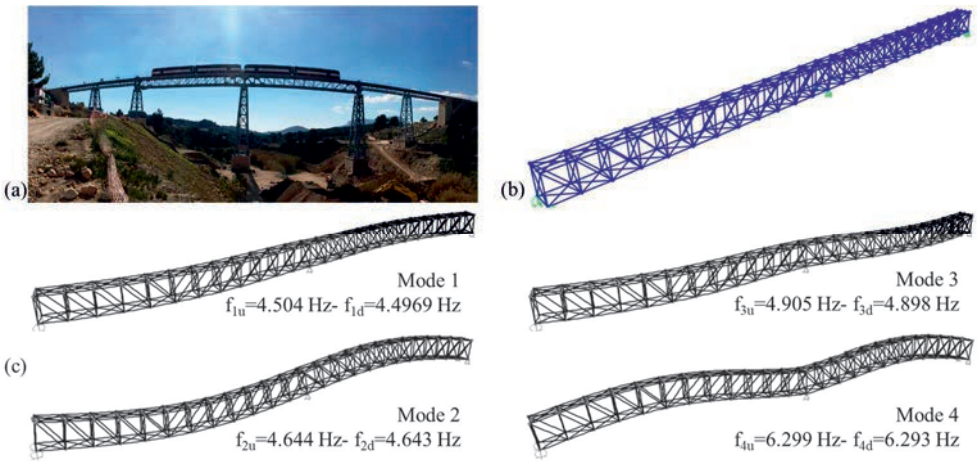

Figure 5: (a) Quisi Bridge; (b) FE model of Quisi Bridge main spans; (c) First modes of vibration.

CONCLUSIONS

A procedure to identify the overall stiffness reduction factor produced by damage in truss element has been proposed. The results obtained through pseudo-dynamic testing and FEM analysis for a simple truss evidences the obtainable resolutions in damage indicator with the increase of a number of modes. For the main span of the Quisi Bridge the frequency variation produced by damage appears to be quite low evidencing the needs of introducing also other sources of data to assess the damage identification.

ACKNOWLEDGMENTS

This paper is a part of a project that has received funding from the Research Fund for Coal and Steel under grant agreement No 800687.

REFERENCES

[1] Potenza F, Castelli G, Gattulli V, Ottaviano E. Integrated process of image and acceleration measurements for damage detection, EURODYN 2017.

[2] Vestroni F, Cerri MN. Detection of damage in beams subjected to diffuse cracking, *Journal of Sound and Vibration*, 2000.

[3] Lepidi M, Gattulli V. Static and dynamic response of elastic suspended cables with thermal effects, *Internation Journal of Solid and Structures*, 2012.

Vibration-based Damage Identification in the UHPFRC Strengthened Buna bridge

H. Martín-Sanz[1], Konstantinos Tatsis [1], D. Damjanovic [2], I. Stipanovic [3], A.Sanja [3], U. Bohnic [3], E. Brühwiler [4], and E. Chatzi[1]

[1] *Department of Civil, Environmental and Geomatic Engineering (IBK), ETH Zürich, Zürich, Switzerland.*

[2] *Faculty of Civil Engineering, University of Zagreb, Zagreb, Croatia*

[3] *Department of Materials and Laboratory of Concrete, Institut ZAG, Ljubljana, Slovenia*

[45] *Structural Maintenance and Safety Laboratory (MCS), EPFL, Laussane, Switzerland.*

ABSTRACT

The Buna Bridge, a steel Croatian riveted bridge from 1893, was decommissioned in 2010. As part of a research investigation, the structure was rehabilitated by means of a novel strengthening solution, comprising a layer of Ultra High Performance Fiber Reinforced Cementituos-composite (UHPFRC) atop the main girders. An extensive experimental campaign was carried out in the laboratory, including static and dynamic tests, and comprised three phases, namely prior to and after rehabilitation, and after artificial damages of increasing severity were introduced on the steel structure by progressively cutting into a zone of the main beam flanges.

The results obtained from the dynamic experiment measurements are analyzed in this paper, in order to explore the capability for damage identification. To this end, vibration-based criteria are employed in order to identify and localize the artificially introduced damage, relying on mode shape curvatures and modal flexibility. The efficacy of each approach is assessed in terms of accuracy in identifying the damage patterns of increasing severity with limited sensing information.

KEYWORDS: *UHPFRC, rehabilitation, damage detection, modal analysis.*

INTRODUCTION

A major current civil engineering challenge is linked to the management of our aging infrastructure. Adequate strategies for tackling this challenge may only be perceived when acting across the full spectrum of Structural Health Monitoring (SHM), i.e., when ensuring detection, localization, and quantification of damage, eventually prompting remedial action, such as rehabilitation. In this case study, we demonstrate implementation of a vibration-based experimental testing technique for SHM, and we then proceed to validate efficacy of UHPFRC strengthening for steel bridges, an implementation which is so far less exploited [1]. The proposed strengthening approach offers reductions in repair times, CO^2 emissions and rehabilitation costs.

The Buna bridge, part of the Croatian railway network, was constructed in 1893 and decommissioned in 2010. Its handling weight, only 90 KN, permitted its transportation to laboratory facilities, where it was tested prior to and after rehabilitation, by means of static and dynamic tests. The reader is referred to the work of Martín-Sanz et al. [2] for further information on the conducted tests and the implemented strengthening approach, comprising a layer of UHPFRC atop the girders. This project serves as a demonstrator of applicability of this solution by means of testing and numerical simulations. Whereas the first part of the test observed the differences between the unstrengthened structure and the UHPFRC-strengthened solution, the second phase of the study is focused on SHM verification. We seek to detect and localize damage through the tracking of the variability in modal shapes curvature, as this evolves through testing. Shifts in modal frequencies, may suffice for reporting initiation of damage in a structure, when properly normalized against environmental variability [3]. However, the task of localization, when relying purely on measurement data, requires the further consideration of spatial quantities, such as mode shapes or their derivatives, i.e., modal curvatures, which are also less sensitive to temperature influences [4]. In this work, artificial damage is induced in the case-study structure, and located thereafter by means of the aforementioned vibration-based damage criteria.

CASE-STUDY

The Buna bridge case-study presents a span close to 8.9 m and it was composed of two main I girders of 0.9 m depth. **Figure 1** (left) represents the bridge before rehabilitation, with the right sub-figure illustrating a typical cross section of the strengthened structure. This project investigates the UHPFRC potential for rehabilitation of steel structures by means of an extensive monitoring campaign, comprising static and dynamic tests at three different stages: firstly, for the original structure (as-is), secondly, for the UHPFRC-strengthened system, and finally, for the rehabilitated structure after introduction of artificial damage. The last two stages are compared in this work for the purpose of damage detection and localization on the basis of variability in mode shape curvatures.

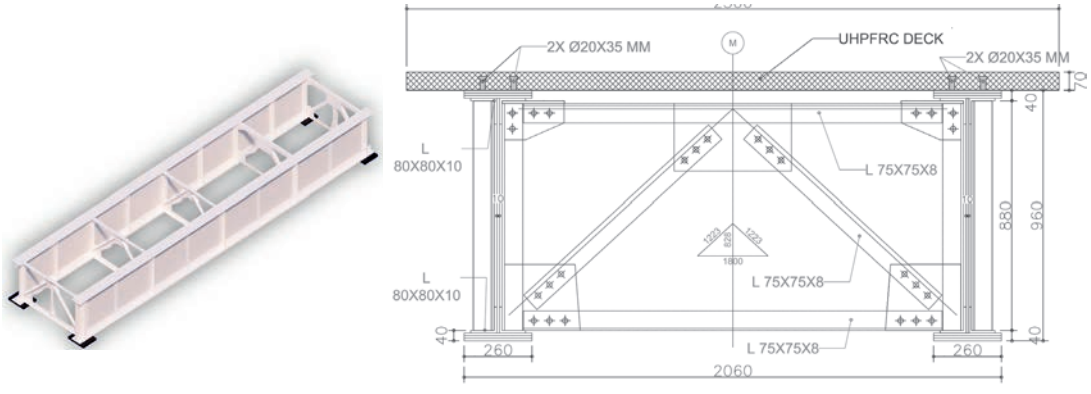

Figure 1 On the left, structure prior to rehabilitation. On the right, typical cross section of the bridge including the strengthening with a UHPFRC slab.

To this end, a roving test was conducted employing 15 accelerometers and a shaker, implemented at the same positions, for both the health and damaged stage of the UPHFRC system. The distribution of sensors is presented in **Figure 2**. In order to cover the whole structure, 119 points were measured on the girders and 61 on the slab. The modal analysis was performed with the Poly-reference least squares complex frequency domain estimator (pLSCF) from the MACEC Matlab toolkit using all these points.

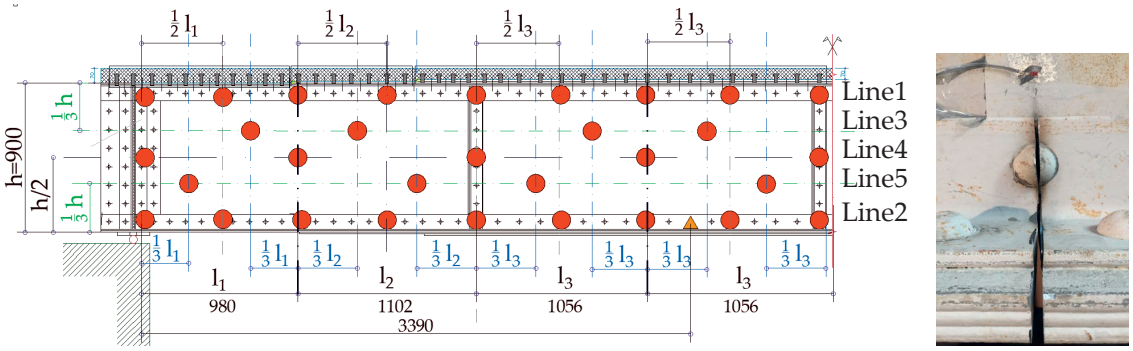

Figure 2. On the left, representation of the accelerometers (red) on one girder and the induced damage (orange). Dimensions in mm. On the right, detail of the artificial damage.

The damage was induced by means of a cutting torch, at the bottom flange of on the girders, as indicated in **Figure 2** (right).

DAMAGE DETECTION

Once the mode shapes are computed, a damage indicator for the purpose of localization may be obtained through use of the mode shape curvature, which is calculated as follows:

$$C_j(k) = \frac{\Phi_j(k-1) - 2\Phi_j(k) + \Phi_j(k+1)}{\Delta x^2} \quad [1]$$

where C_j represents the mode shape curvature in the direction of the sensing points, Φ_j designates the corresponding mode shape and Δx denotes the distance between 2 consecutive measurement points. A damage indicator may be obtained by computing the normalized absolute difference between the mode shape curvature at the current state and the one at a reference, i.e., healthy state. In order to exploit information from all identified modes, the change of curvature associated with each mode can be summed to a single indicator, or alternatively kept in a vector. For the case study described herein, 3 mode shapes from one girder have been analyzed, prior to and after damage, and aggregated into a single indicator. **Figure 3** illustrates the damage indicator obtained at lines 1 and 2 (refer to **Figure 2**), in the vertical direction, employing the mode shape curvatures as well as the same indicator for mode shapes. Furthermore, the table in the right provides the frequencies and Modal Assurance Criterion (MAC) values. As

expected, the indicator for mode shape curvatures presents greater accuracy, providing a higher damage value around the cutting, even for the sensors placed on the top flange (more distant to the damage location).

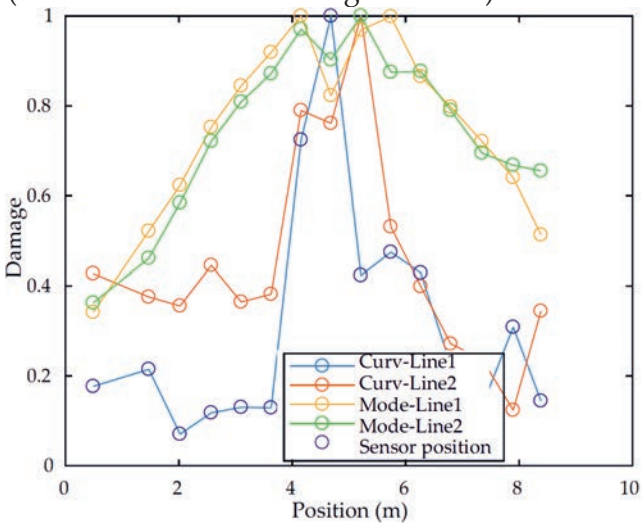

Freq (Hz) Before	Freq (Hz) After	MAC
24.04	*22.90*	*0.98*
65.23	*65.39*	*0.65*
86.47	*87.78*	*0.81*

Figure 3. Damage indicator for the three mode shapes indicated in the right table (curvatures and mode shapes).

CONCLUSIONS

In this work, application of UHPFRC strengthening on a steel bridge is demonstrated, with subsequent demonstration of an SHM solution for possible damage detection. The SHM solution is demonstrated in laboratory conditions, but could also be implemented as a permanent low cost sensing solution on a field operating system. In this respect, we demonstrate an approach for treating existing infrastructure by means of monitoring and efficient repair.

REFERENCES

[1] Martín-Sanz, H., Chatzi, E. and Brühwiler, E., 2016. The use of ultra high performance fibre reinforced cement—based composites in rehabilitation projects: A review. In Proceedings of the 9th International Conference on Fracture Mechanics of Concrete and Concrete Structures FraMCoS-9, Berkeley, CA, USA (Vol. 29).

[2] Martín-Sanz, H., Tatsis, K., Damjanovic, D., Stipanovic, I., Duvnjak, I., Bohnin, U., Brühwiler, E. and Chatzi, E.N., 2019. Getting More Out of Existing Structures: Steel Bridge Strengthening via UHPFRC. *Frontiers in Built Environment*, 5, p.26.

[3] Martín-Sanz, H., Tatsis, K., Dertimanis, V., Avendaño-Valencia, L. D., Brühwiler, E. and Chatzi, E. S. Monitoring of the UHPFRC strengthened Chillon viaduct under environmental and operational variability conditions. *Structure and Infrastructure Engineering, in press*.

[4] Tatsis, K., Ntertimanis, V.K. and Chatzi, E., 2018. On damage localization in wind turbine blades: a critical comparison and assessment of modal-based criteria. *7th World Conference on Structural Control and Monitoring (7WCSCM).*

Structural Control

Passive Control Strategy for Wind-induced Parametric Instabilities in Suspension Bridges

A. Arena[1], W. Lacarbonara[1]

[1] *Department of Structural and Geotechnical Engineering, Sapienza University of Rome, Italy.*

E-mail:{andrea.arena,walter.lacarbonara}@uniroma1.it

ABSTRACT

A nonlinear reduced-order model of suspension bridges (SB) is presented to study the dynamical response and to investigate aerodynamic stability control strategies coping with vortex-induced vibrations (VIV) leading to principal parametric resonances scenarios. A passive control system consisting of a vibration absorber is incorporated in the model by coupling the dynamics of the bridge with those of an eccentric mass viscoelastically connected to the deck. A direct asymptotic approach is used to investigate the dynamic instabilities induced by the parametric-type forces in the case of a 2:1 ratio between the frequency of the aerodynamic loads and the fundamental torsional frequency of the bridge. It is shown how an optimized passive control system can increase the range of wind speeds for which the bridge does not undergo large-amplitude parametric oscillations signaling the loss of stability of the fundamental equilibrium configuration.

KEYWORDS: *suspension bridges, parametric resonances, passive vibration control*

INTRODUCTION

Suspension bridges (SB) are structures characterized by a relatively low flexural-torsional stiffness which implies remarkably low natural frequencies in the fundamental torsional and vertical bending modes. Moreover, their mechanical behavior is mainly governed by the suspension cables which are structural elements whose geometric nonlinearities play a fundamental role in their static and dynamic response of SB. When subject to severe wind excitations, suspension bridges may be affected by dynamic instability phenomena, such as flutter, arising from the self-excited nature of the aerodynamic loads [1, 2] or parametric instabilities due to vortex-induced vibrations (VIV) [3, 4, 5] in which the aerodynamic loads generated by the airflow separation across the bridge deck section act as a multiplicative forcing term that can induce flexural-torsional parametric instabilities in the bridge at wind speeds lower than those that can induce flutter. In the present work, a nonlinear reduced-order model of SB is coupled with the time-varying

aerodynamic loads to obtain the equations of motion for the study of principal parametric resonances. The equations of motion are reduced by the Faedo-Galerkin approach adopting the bridge deck eigenfunctions as trial functions. Nonlinear aerodynamic effects due to flow separation are accounted for by using a quasi-steady aerodynamic theory. The method of multiple scales [6] is adopted to investigate the dynamic instabilities induced by the parametric-type forces in the case of a 2:1 ratio between the frequency of the VIV and the fundamental SB torsional frequency. A passive control system is then studied and optimized so as to increase the range of wind speeds for which the bridge stability with respect to parametric resonance is ensured.

MODEL FORMULATION

The here proposed structural model of suspension bridges is parameterized by one single space coordinate along the bridge span-wise direction and the equations governing the dynamic aeroelastic response are obtained via a total Lagrangian formulation. The cables equilibrium is described by the dimensionless catenary $y_c(x)$ while the kinematic variables are defined as the vertical (in-plane) displacement $v(x,t)$ and the torsional rotation $\phi(x,t)$. All parameters of the mechanical system are cast in nondimensional form. In particular, let $\eta_c = \int_0^1 \sec\theta_c^3 dx$, δ_c and δ represent the nondimensional catenary characteristic length, with $\theta_c = \arctan y_c'$, cables horizontal distance and deck width, respectively; let κ_c, κ_t and β_c be the nondimensional cables stiffness, deck torsional stiffness and horizontal component of the cables prestress tension, respectively, and, finally, let μ_c, $J\mu_d$, c_f and c_t represent the nondimensional mass, mass moment, and damping flexural and torsional coefficients, respectively. Then, the second-order (in time) aeroelastic governing equations can be cast in nondimensional form as

$$
\begin{aligned}
&\left(1+2\mu_c\sec\theta_c\right)\ddot{v} + c_f\dot{v} + v'''' - 2\,\beta_c\,v'' \\
&\qquad - \frac{\kappa_c}{\eta_c}\left(y_c''+v''\right)\int_0^1\left[2y_c'v' + \cos^2\theta_c\left(v'^2+\delta_c^2\phi'^2\right)\right]dx \\
&\qquad - \frac{2\delta_c^2\kappa_c}{\eta_c}\,\phi''\int_0^1\left(y_c'\phi' + \cos^2\theta_c\,v'\,\phi'\right)dx = L\,, \\
&\left(J\mu_d + 2\delta_c^2\,\mu_c\sec\theta_c\right)\ddot{\phi} + c_t\dot{\phi} - \left(\kappa_t + 2\delta_c^2\beta_c\right)\phi'' \\
&\qquad - \frac{\delta_c^2\kappa_c}{\eta_c}\,\phi''\int_0^1\left[2y_c'v' + \cos^2\theta_c\left(v'^2+\delta_c^2\phi'^2\right)\right]dx \\
&\qquad - \frac{2\delta_c^2\kappa_c}{\eta_c}\left(y_c''+v''\right)\int_0^1\left(y_c'\phi' + \cos^2\theta_c\,v'\,\phi'\right)dx = M
\end{aligned}
\tag{1}
$$

where the dot and the prime indicate differentiation with respect to the nondimensional time t and space x, respectively, while L and M are the nondimensional aerodynamic lift and moment per reference length, respectively. In the context of a quasi-steady aerodynamic formulation, the dimensionless aerodynamic loads are directly expressed as func-

tions of the static coefficients in terms of the effective dynamic angle of attack $\alpha_{\mathrm{E}} = \phi - \left(\dot{v} + \frac{\delta}{4}\dot{\phi}\right)/\bar{U}$, where $\bar{U}$ is the nondimensional wind speed, as $L = p\,\delta\,C_{\mathrm{L}}\,(\alpha_{\mathrm{E}})\sin\Omega t,\ M = p\,\delta^2\,C_{\mathrm{M}}\,(\alpha_{\mathrm{E}})\sin\Omega t$, being p the nondimensional aerodynamic pressure. Further details of the aerodynamic formulation and the expressions of the static coefficients C_{L} and C_{M} can be found in [7]. Structural and geometrical parameters of the Runyang Suspension Bridge [2] are considering to analyze the case-study here investigated.

ASYMPTOTIC ANALYSIS

The method of multiple scales[6] is here employed to perform the perturbation analysis of the equations of motion governing the dynamics of the suspension bridge. The perturbation analysis will be carried out studying the effects of cubic nonlinearities thus including the terms of the perturbation problems up to order ϵ^3. Thus the parametric forcing term and the damping term are rescaled to appear at third order. Moreover, to make use of complex algebra, let $\sin\Omega t = \frac{1}{2}i(e^{-i\Omega T_0} - e^{i\Omega T_0})$ where $T_0 = t$ is the nondimensional fast time scale and $T_2 = \epsilon^2 t$ is the nondimensional slow time scale in terms of which the nondimensional time derivative is $d/dt = \partial_0 + \epsilon^2\partial_2$. The system exhibits secular terms due to the parametric resonance caused by the 2:1 frequency ratio of the vortex-induced wind excitation with the lowest bridge mode expressed as $\Omega = 2\omega + \epsilon\sigma$. Hence, substituting the external resonance condition into the solvability equation, the following modulation equations for the complex amplitudes A and A^* are obtained:

$$\begin{aligned} &i\omega(\partial_2 A + \alpha A) - (i\omega\beta_1\bar{U} + \beta_2\bar{U}^2)e^{i\sigma T_2}A^* + \gamma A^2 A^* = 0 \\ &i\omega(\partial_2 A^* + \alpha A^*) - (i\omega\beta_1\bar{U} - \beta_2\bar{U}^2)e^{-i\sigma T_2}A - \gamma A^{*2} A = 0 \end{aligned} \tag{2}$$

By introducing the polar form of the complex-valued modal amplitudes (i.e., $A = \frac{1}{2}a(T_2)e^{\varphi}(T_2)$)

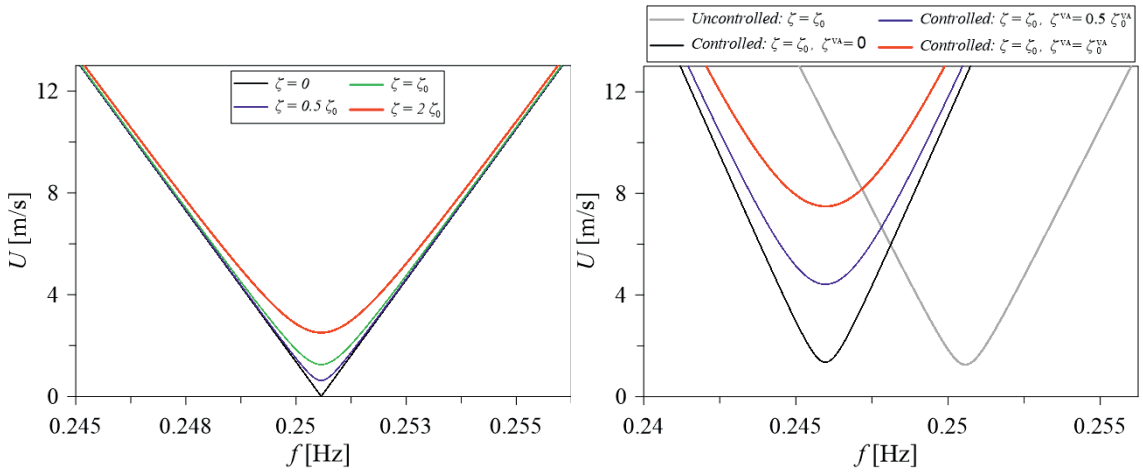

Figure 1: (left) Stability regions showing the sensitivity to structural damping ζ (right) stability regions for the parametric response controlled via VA.

and the relative phase $\Gamma = \sigma T_2 - 2\varphi$ it is possible to obtain the normal form of the modulation equations that governs the dynamics of the real modal amplitude $a(T_2)$. In Fig. 1 (left) (where f is the dimensional frequency of the VIV and U is the dimensional wind speed) are shown the instability regions obtained for the uncontrolled system and their sensitivity with respect to structural damping. Fig. 1 (right) shows the response for the controlled case where the presence of the vibration absorber (VA) lowers the system frequency because of its added mass and increases the critical wind speed (i.e., the speed which leads to the onset of the parametric resonance) by increasing its damping.

CONCLUSIONS

A parametric nonlinear model of SB, including geometric nonlinearities and nonlinear aerodynamics, was proposed to study wind-induced parametric instability and to provide the control of such instability through a passive VA. Investigations via perturbation approach and optimization of the VA mechanical characteristics were carried out to show the effectiveness of the VA system in controlling instability arising from wind-induced parametric aerodynamic loads.

References

[1] Simiu E., Scanlan R.H. (1996) Wind effects on structures-fundamentals and applications to design. Wiley-Interscience.

[2] Arena A., Lacarbonara W. (2012) Nonlinear parametric modeling of suspension bridges under aeroelastic forces: torsional divergence and flutter. Nonlinear Dyn, 70(4), 2487510.

[3] Sarpkaya T. (1979) Vortex Induced Oscillations. J Appl Mech, 46, 241- 258.

[4] Larsen A. (2008) Aerodynamic stability and vortex shedding excitation of suspension bridges. AWAS conf., 115-128.

[5] Arena A., Lacarbonara W., Rega G. (2016) Vortex-induced dynamic instabilities in suspension bridges due to parametric and autoparametric resonance. IMSE conf., Padova, Italy

[6] Nayfeh A. H., Mook, D.T. (1995) Nonlinear oscillations, Wiley Classics Library Edition Published.

[7] Arena A., Lacarbonara W., Marzocca P. (2016) Post-critical behavior of suspension bridges under nonlinear aerodynamic loading. J Comput Nonlin Dyn, 11, 1-11.

Investigation on Nonlinear Parametric Vibration control of Stay Cable with Super-Long Span

M. Liu[1], R.Q. Long[1], L.F. zheng[1]

[1] *School of Civil Engineering, Harbin Institute of Technology, 92 West Dazhi Street, Harbin, Heilongjiang, 150090, China*

E-mail: liumin@hit.edu.cn

ABSTRACT

In this paper, the vibration equation of the inclined cable under axial cosine excitation in the lower end is derived. The multi-scale method is applied to the theoretical analysis for the equation, and the solutions to the steady-state periodic motion of the cable in the 1:2, 1:1 and 2:1 resonance are obtained. Based on the analysis, it could be concluded that a small excitation amplitude can arouse the large vibration for main parameter resonance. The occurrence of the main parameter resonance requires a minimum initial excitation amplitude, and the minimum value increases with the increase of cable's damping ratio.

KEYWORDS: *Stay cable, parametrical vibration, Multi-scale method, Vibration Control, damping, excitation amplitude*

INTRODUCTION

As the span of a cable-stayed bridge increases, the stay cable becomes longer and longer, and large amplitude parametrical vibration has become one of the prominent vibration hazards of the cable. Secular vibration will cause the fatigue fracture of the cable, and destroy the anticorrosion system, in severe cases, the cable will fail, seriously affecting the safety and durability of the bridge (Wu et al., 2003).

The problem of cables' parametric vibration had been paid great attention by many scholars. Lots of theoretical and experimental researches on the mechanism and control of the parametric vibration were carried out, and many valuable results had been obtained (Macdonald 2016; Ouni et al. 2012). However, the characteristic of the parametric resonance in a stay cable are not well explained theoretically. The mechanism of parametric vibration and its control for a super-long stay cable needs to be further studied to provide a theoretical basis for numerical analysis and experimental research.

In this paper, on the basis of the cable's sag curve solution including the chordwise force of gravity, the vibration equation of the inclined cable under axial cosine excitation in the lower end is derived. The multi-scale method is applied to the theoretical analysis

for the equation, and the solutions to the steady-state periodic motion of the cable in the 1:2, 1:1 and 2:1 resonance are obtained. Based on the analysis, it could be concluded that a small excitation amplitude can arouse the large vibration for main parameter resonance. The occurrence of the main parameter resonance requires a minimum initial excitation amplitude, and the minimum value increases with the increase of cable's damping ratio.

EQUATIONS OF IN-PLANE PARAMETRICAL VIBRATION OF STAY CABLE

The coordinate system is defined in Figure.1. When the cable vibrates, the displacement from the axial equilibrium position is u(x,t), and from the transverse v(x,t). The inclined angle of the chord from the horizontal is α.

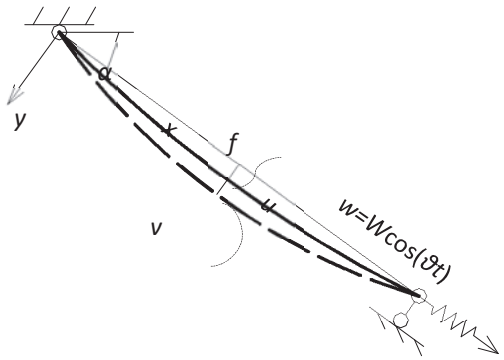

Figure 1: Stayed-cable in-plane vibration model caused by axial excitation

The mass per unit length, chord length, cross-sectional area, elastic modulus, damping, initial tension, micro-segment initial length and dynamic length of the cable are *m*, *L*, *A*, *E*, *c*, H_0 ,*ds* and *dp*, respectively. The axial excitation of the cable is expressed as $d = D\cos(\theta t)$, and the gravity sag curve equation of the stay cable is given by

$$f(x) = \frac{mg\cos\alpha}{2H_0}x(L-x)\left[1-\frac{\lambda}{3}\left(1-2\frac{x}{L}\right)\right] \tag{1}$$

Where $\lambda = mgL\sin\alpha / H_0$. According to Tagata's experiment, the first vibration mode of the cable is obtained as

$$\ddot{Y} + 2\omega\xi\dot{Y} + [\omega^2 + \beta_1\cos(\theta t)]Y + \beta_2 Y^2 + \beta_3 Y^3 + \beta_4\cos(\theta t) = 0 \tag{2}$$

Where ξ is the damping ratio of the cable, ω is the first modal frequency of the cable considering the sag and geometric nonlinearity, determined by $\omega^2 = \frac{\pi^2 H_0}{mL^2}\left(1+\frac{8\chi^2}{\pi^4}\right)$, in which $\chi^2 = \frac{64R^2EAL}{H_0 L_e}$.

It can be seen from the Eq.(2) that the square and cubic nonlinear terms, and the time-varying parameter excitation and the external excitation terms are included, showing very strong nonlinearity.

THEORETICAL ANALYSIS BASED ON MULTI-SCALED METHOD

Using the multi-scale method, Eq.(2) could be rewritten as

$$\ddot{Y} + \omega^2 Y = \eta\left[-2\omega\zeta\dot{Y} - \beta_{10}\cos(\theta t)Y - \beta_{20}Y^2 - \beta_{30}Y^3\right] - \beta_4\cos(\theta t) \quad (3)$$

As well as the occurrence of the primary resonance when $\theta \approx \omega$, the super-harmonic resonance occurs when $\theta \approx \omega/3$ or $\theta \approx \omega/2$, and the sub-harmonic resonance occurs when $\theta \approx 2\omega$ or $\theta \approx 3\omega$**.** In this paper, the main parametric resonance at $\theta \approx 2\omega$ is emphatically analyzed. In order to facilitate the subsequent analysis, here a typical super long stay-cable, the longest cable S36 from the Hutong Yangtze River Bridge under construction was introduced.

Table 1. Parameters values for a typical super long stay-cable

Basic parameters	*Initial tension, H_0*	*12183 kN*
	Mass per unit length, m	*145.0 kg/m*
	Length, L	*594.35m*
	Inclination angle, α	*26.48°*
	Cross-sectional area, A	*173.57 cm²*
	Yong's modulus, E	*205 GPa*
	Fundamental frequency, ω/2π	*0.244 Hz*
Non-dimensional parameters	*Ratio of sag to span, R*	*0.0078*
	Ratio of cable weight chord component to initial tension, λ	*0.0309*
	Irvine parameter, χ^2	*1.1263*

The main parametric resonance will occur at $\theta \approx 2\omega$. The minimum excitation amplitude required for the main parametric resonance is

$$D_{\min} = \frac{4\omega^4\xi\left(\gamma^2-1\right)}{2\beta_2\tilde{\beta}_4 + \tilde{\beta}_1\omega^2\left(\gamma^2-1\right)} \quad (4)$$

Where $\gamma = \theta/\omega$, $\tilde{\beta}_1 = \frac{\pi^2 EA}{mL_e L^2}$, $\tilde{\beta}_4 = \frac{32EAR}{\pi mLL_e}$. For a specific damping ratio ξ, the existence region of real solution a0 determined by Eq.(4) can be illustrated in the coordinate plane defined by parameters γ and D. Considering the different damping ratios, the existence domain of the primary parameter resonance of the cable is shown in Fig.3. It can be seen that the minimum excitation amplitude required to excite the primary parameter resonance increases with the increase of damping ratio. The upper limit of the excitation amplitude at different frequency ratios in the domain is less affected by the cable's damping ratio.

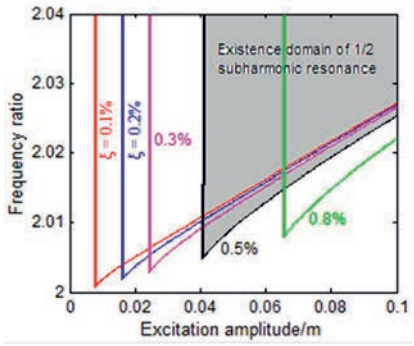

Figure 3: Existence domains of the main parameter resonance of cable with different damping ratios

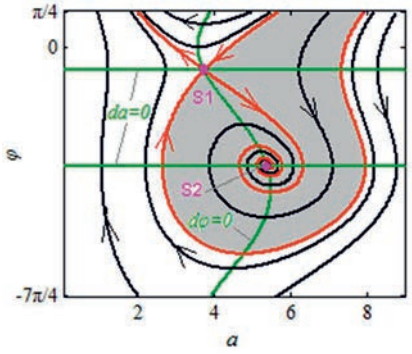

Figure 4：Phase trajectories of cable when the main parametric resonance occurs

According to Lyapunov's first approximate stability criterion, because of $\xi > 0$, the sufficient condition for the steady-state solutions a_0 and φ_0 to be asymptotically stable is simplified to $r > 0$, that is, $a_0^2 > p$. Therefore, comparison with Eq.(4), in the two branches of the frequency response curves, the larger one is stable, and the smaller one is unstable. respectively. Besides, the phase trajectories in the phase plane by numerical integration could be obtained shown in Fig.4. It is found that S1 is a saddle point, S2 is the stable focus, that is, the smaller amplitude corresponding to S1 is unstable, and the larger corresponding to S2 is stable, which is consistent with the above theoretical analysis. The shaded region is the attraction basin of S2, where the main parameter resonance may occur.

CONCLUSIONS

In this paper, the parametric vibration and its control were analyzed, the results come to the conclusions as following:

1. A small excitation amplitude can arouse the large vibration for main parameter resonance, which should be paid attention to control.
2. The occurrence of the main parameter resonance requires a minimum initial excitation amplitude, and the minimum value increases with the increase of cable's damping ratio. With the extension of time, the cable's vibrations are ultimately stable forced vibrations.

REFERENCES

[1] Macdonald J.H.G. (2016) Multi-modal Vibration Amplitudes ofTaut Inclined Cables Due to Direct and/or Parametric Excitation. Journal of Sound and Vibration, 363: 473-494.

[2] Ouni M.H.E., Kahla N.B., Preumont A. (2012) Numerical and Experimental Dynamic Analysis and Control of a Cable Stayed Bridge under Parametric Excitation. Engineering Structures, 45(15): 244-256.

[3] Wu, Q., Takahashi, K., Okabayashi, T., Nakamura, S.(2003) Response characteristics of local vibrations in stay cables on an existing cable-stayed bridge. Journal of sound and vibration, 261(3): 403-420.

Optimal Design Of Linear and Nonlinear Seismic Isolation Systems for Fuel Storage Tanks based on Metamaterial Concepts

F. Basone[1], M. Wenzel[2], O.S. Bursi[2], R. Andreotti[2]

[1] *Department of Civil and Geotechnical Engineering, University of Enna Kore, Italy.*
E-mail: francesco.basone@unikore.it

[2] *Department of Civil, Environmental and Mechanical Engineering, University of Trento, Italy.*
E-mail: roberto.andreotti@gmail.com

ABSTRACT

This paper introduces a novel seismic isolation system based on metamaterial concepts for the reduction of ground motion-induced vibrations in fuel storage tanks. Based on this concept, we propose the so called Metafoundation for large fuel storage tanks, which is able to shield fuel storage tanks from earthquakes. Such type of foundation might include linear or non-linear resonators, that might act differently on the coupled tank-foundation system. An optimization procedure is formulated in the frequency domain, accounting for ground motion as a stochastic stationary process.

KEYWORDS: Metafoundations, multiple tuned mass damper (MTMD), optimization procedure stochastic linearization technique, dynamic reduction.

INTRODUCTION

In order to reduce tank vibrations, we have explored an innovative type of foundation based on metamaterials concepts. As a result, we conceived the so called Metafoundation for large fuel storage tanks, which allows for the attenuation of seismic excitations. The Metafoundation require a different approach for an optimum design with respect to traditional foundations, even if the behavior is linear. Moreover the Metafoundation might be endowed with non-linear hysteretic springs, that can have further benefits on the overall system performance. The present work shows an optimization procedure of the Metafoundation in the frequency domain. The implemented optimization procedure allows us to examine the impact of massive resonator with varying frequencies or hysteretic spring-dampers. For this purpose, we develop and optimize two finite locally resonant Metafoundation systems: i) a foundation endowed with resonators and linear viscous dampers tuned to multiple frequencies; and ii) a foundation equipped with nonlinear hysteretic dampers e.g wire ropes. Both are optimized considering the stochastic nature of ground motion, modelled with a modified Kanai-Tajimi filter in the stationary frequency domain. Finally, the performance of each type of Metafoundation is demonstrated through the response of the coupled system to different seismic records.

DESCRIPTION AND MODELLING OF THE FOUNDATION-TANK COUPLED SYSTEM

The hydrodynamic response of a tank-liquid system is mainly characterized by the impulsive and convective mode of vibration. Since there are significant differences in their natural periods, they can be considered uncoupled. Malhotra established a procedure for the estimation of the own mass and period of the two modes. Steel columns with hollow steel sections and concrete slabs that define the unit cells compose the foundation. In each unit cell, there is a concrete mass that is linked to the steel-concrete composite structure. Herein after, we carry

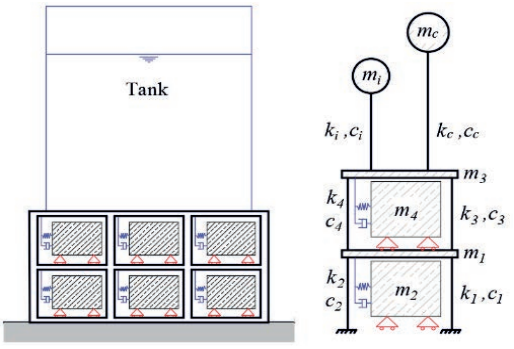

Figure 1. Tank-foundation coupled systems

on an optimization procedure that takes the feedback of a superstructure and the relevant earthquake frequency content into account.

The Metafoundation modelling is carried out condensing all the degrees of freedom as shown in Figure 2. Therefore, being interested in the motion along, let us say the *X* direction, each layer consists of only two DoFs: one for the resonators and one for the cells, respectively. Considering a system with one layer and a system with 2 layers, mass, damping and stiffness matrix result in 4x4 or 6x6 matrices respectively. Steel columns are designed to remain elastic for PGAs corresponding to a return period of 2475 years.

OPTIMIZATION PROCEDURE OF THE METAFOUNDATION

Herein we propose two optimization procedures that evaluate the optimal parameters of the resonators, namely k_2 and ζ_2. Mass m_2 is not considered as a parameter to optimize since we want the resonators to exert the largest mass compatible with the unit cell dimensions.

In order to apply the optimization procedures described in the previous section, three different types of soils—soft, medium, and rock soil—modeled with the KTCP filter are considered. Furthermore, we evaluated the PSD of the ground motions representative for the construction site, with which we evaluated the parameters of the KTCP filter (S_0, ω_g, ζ_g, ω_1, and ζ_1).

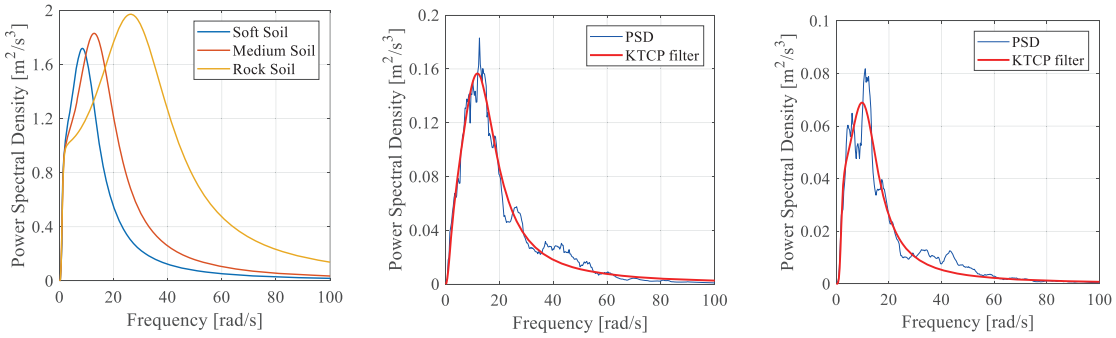

Figure 2. PSD functions of filtered white noises, in order: KTCP filter for three types of soil, average PSD and KTCP fit for OBE events, and average PSD and KTCP fit for SSE events

For obtaining the response of the system we consider the equation of motion of the coupled tank foundation system and of the resonator:

$$M\ddot{u}(t) + C\dot{u}(t) + Ku(t) - Y(t) = -M\tau\ddot{u}_g \tag{1}$$

$$m_{jl}\ddot{y}_{jl}(t) + m_{jl}2\zeta_{rl}\omega_{rl}\dot{y}_{jl}(t) + m_{jl}\omega_{rl}y_{jl}(t) = -m_{jl}\left[\ddot{u}_g(t) + \ddot{u}_j(t)\right] \tag{2}$$

where $\mathbf{Y}(t)$ is the force of the resonator on the system. Through modal transformation, EOMs can be transferred to generalized coordinates and, introducing the concept of transfer function $U(\omega) = H(\omega)F(\omega)$, the transfer functions of the interstorey drift Dj ($i\omega$), relative velocity Vj ($i\omega$), and absolute acceleration Aj ($i\omega$) can be evaluated. The Wiener-Khintchine transformations allows for calculating variance of drift, velocity and absolute acceleration as

$$\sigma_{D_j}^2 = \int_0^{+\infty} \left|D_j(\omega)\right|^2 S_{\ddot{u}_g}(\omega)\, d\omega \qquad \sigma_{V_j}^2 = \int_0^{+\infty} \left|V_j(\omega)\right|^2 S_{\ddot{u}_g}(\omega)\, d\omega \qquad \sigma_{A_j}^2 = \int_0^{+\infty} \left|A_j(\omega)\right|^2 S_{\ddot{u}_g}(\omega)\, d\omega \tag{3}$$

More precisely, to evaluate the effectiveness of the Metafoundation and the optimal stiffness and damping ratio of the system, two parameters, the performance index (PI) and the energy dissipation index (EDI), are defined based on the reduction of the absolute acceleration of the impulsive mass m_i and the energy dissipated by the resonators, obtained from the variance of velocity:

$$PI(\zeta_2, \omega_2) = \frac{\sigma_{A_j}^2}{\sigma_{A_j}^2} \qquad EDI(\zeta_2, \omega_2) = \sum_{r=1}^{N} E[\Delta E_{d_r}(\zeta_2, \omega_2)] \Big/ \sum_{j=1}^{N} E[\Delta E_{input}(\zeta_2, \omega_2)] \tag{4}$$

The optimization problem is then stated as

$$\zeta_{2,opt},\omega_{2,opt} = \min\left[\mathrm{PI}(\zeta_2,\omega_2)\right] \qquad \zeta_{2,opt},\omega_{2,opt} = \max\left[\mathrm{EDI}(\zeta_2,\omega_2)\right] \tag{5}$$

Figure 3 shows the PI and EDI optimization surfaces of single layer foundation. From both optimization procedures, it is clear that the performance of the system is directly depending on the slenderness of the foundation. This result was confirmed from time history analyses.

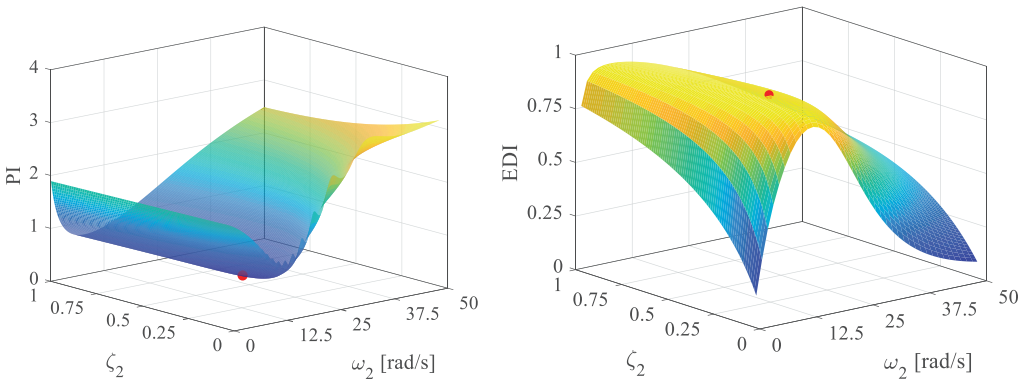

Figure 3. Optimization surfaces of single layer foundation with SSE records.

CONDENSED, REDUCED AND FULL MASS SYSTEM OPTIMIZATION

As indicated in figure 4, in this section we investigate how considering one, two, or three different resonators might add benefits to the overall performance of the system.

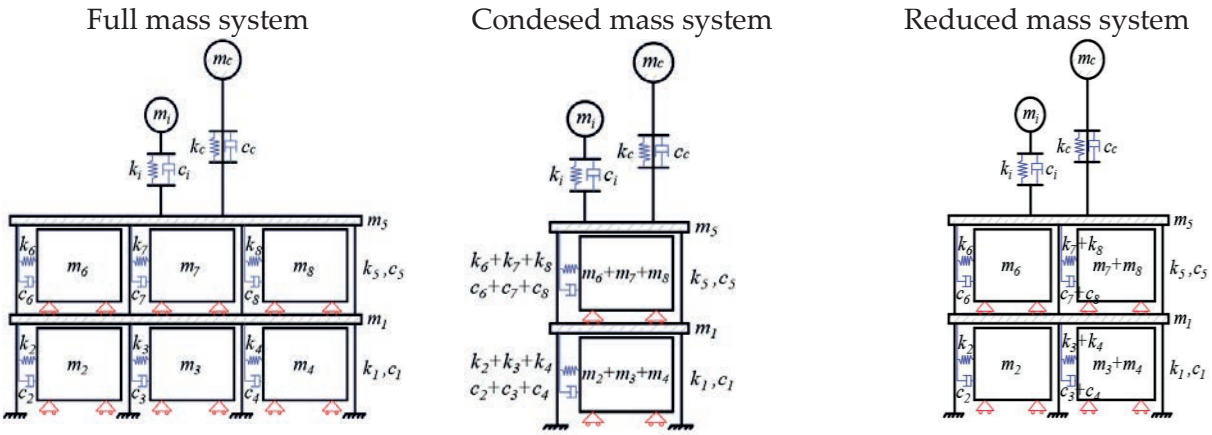

Figure 4. Modeling of the Metafoundation.

In order to evaluate the dynamic properties of reduced system, we employ the System Equivalent Reduction Expansion Procedure, i.e. SEREP (O'Callahan et al. 1989), which is based on the following transformation:

$$\mathbf{T} = \boldsymbol{\Phi}_n \boldsymbol{\Phi}_a^g \qquad \boldsymbol{\Phi}_a^g = \left(\boldsymbol{\Phi}_a^T \boldsymbol{\Phi}_a\right)^{-1} \boldsymbol{\Phi}_a^T \tag{6}$$

With the transformation matrix $\mathbf{T}$ the system matrices can be reduced to $\tilde{\mathbf{M}} = \mathbf{T}^T\mathbf{M}\,\mathbf{T}$, $\tilde{\mathbf{K}} = \mathbf{T}^T\mathbf{K}\,\mathbf{T}$ and $\tilde{\mathbf{C}} = \mathbf{T}^T\mathbf{C}\,\mathbf{T}$, while the forcing term becomes $\tilde{\mathbf{F}} = -\mathbf{T}^T\mathbf{M}\boldsymbol{\tau}\,\ddot{u}_g$. The optimization procedure previously exposed was used herein. The design variables $\zeta_{k,n}$ and $f_{k,n}$, that define damping ratio and frequency of the *n*-th resonator in the *k*-th layer, are collected in the parameter vector

$$\mathbf{X} = \left[\zeta_{1,1},\ldots,\zeta_{k,n},\ldots,f_{1,1},\ldots,f_{k,n}\right]^{\mathrm{T}} \tag{7}$$

The optimization problem can thus be stated,

$$\min_{k,n}\ \mathrm{PI}_{dr}(\mathbf{X}) \text{ and } \min_{k,n}\ \mathrm{PI}_{acc}(\mathbf{X}) \tag{8}$$

When analyzing the results of the optimization procedure and comparing the different systems to each other, the PI value slightly decreases from CMS to RMS, while no significant advantage is obtained with the FMS. However, these reductions are very small due to the fact that we constraint the maximum mass possible, compatibly to unit cell dimensions.

METAFOUNDATION ENDOWED WITH NON-LINEAR WIRE ROPES

In Bouc-Wen model, the restoring force of the elasto-plastic hardening reads

$$R(t) = \alpha\, k\, u(t) + (1-\alpha) k\, u_y\, z(t) \tag{9}$$

whereas the dimensionless hysteretic component z is given by the solution of the non-linear differential equation

$$\dot{z}(t) = u_y^{-1}\left[A\dot{u}(t) - \gamma\left|\dot{u}(t)\right|\left|z(t)\right|^{n-1} z(t) - \beta\dot{u}(t)\left|z(t)\right|^{n} \right] \tag{10}$$

Herein we propose an optimization procedure in the frequency domain of the Metafoundation equipped with non-linear components. In order to obtain a solution for the non-linear problem, we start with the EOMs of the non-linear system,

$$\mathbf{M}\,\ddot{\mathbf{u}}(t) + \mathbf{C}\,\dot{\mathbf{u}}(t) + \mathbf{K}^{\mathrm{L}}\,\mathbf{u}(t) + \mathrm{u_y}\,\mathbf{K}^{\mathrm{NL}}\mathbf{z}(t) = \mathbf{F}(t) \tag{11}$$

A stochastic linearization technique (SLT) is employed to replace the non-linear terms contained in the product $\mathrm{u_y}\,\mathbf{K}^{\mathrm{NL}}\mathbf{z}(t)$ with equivalent linear terms. The non-linear differential equation becomes,

$$\dot{z} + c_{eq}\dot{u} + k_{eq} z = 0 \tag{12}$$

where c_{eq} and k_{eq} are linearization coefficients that are "equivalent" in a statistical sense. By following the procedure introduced by Maldonado et al (1987) and Bartels and Steward (1972) we obtain the linearized equation of motion and transmission matrix

$$-\omega^2 u_0 e^{i\omega t} m + i\omega u_0 e^{i\omega t} c + \alpha u_0 e^{i\omega t} k - \frac{i\omega}{i\omega + k_{eq}} c_{eq}(1-\alpha) k u_y u_0 e^{i\omega t} = F_0 e^{i\omega t} \tag{13}$$

$$\mathbf{H}(\omega) = \left[-\omega^2\mathbf{M} + i\omega\mathbf{C} + \mathbf{K}^{\mathrm{L}} - c_{eq}^{n,k}\,\frac{i\omega}{i\omega + k_{eq}^{n,k}}\, u_y \mathbf{K}^{\mathrm{NL}} \right]^{-1} \tag{14}$$

The optimization procedure in the non-linear case consists to collect the design variables $k_{k,n}$, $A_{k,n}$, $\beta_{k,n}$ and $\gamma_{k,n}$ in the parameter vector $\mathbf{X}^{\mathrm{NL}}$ as in (). Optimizations of one and two-layered CMS are carried out. About the parameters β and γ that describe dissipation characteristics of wire ropes, the results obtained from the optimization procedure show that an increase of β, i.e. a decrease of γ, does not entails a significant reduction of the PI_{dr}.

REFERENCES

[1] Bartels R, Stewart GW (1972) Solution of the matrix equation AX + XB = C. Comm A.C.M., 15(9): 820–826

[2] Basone F, Wenzel M, Bursi OS, Fossetti M (2018) Finite locally resonant Metafoundations for the seismic protection of fuel storage tanks. Earthquake Engng Struct Dyn, pp. 1-21

[3] Bonelli A, Bursi OS (2004) Generalized-α methods for seismic structural testing. Earthquake Engng Struct Dyn, 33, pp. 1067-1102

[4] La Salandra V, Wenzel M, Bursi OS, Carta G, Movchan AB (2017) Conception of a 3D metamaterial-based foundation for static and seismic protection of fuel storage tanks. Front Mater

[5] Maldonado O, Singh MP, Casciati F, Faravelli L (1987) Stochastic response of single degree of freedom hysteretic oscillators. Technical Report of Research Supported by The National Science Foundation Under Grant Number CEE-8412830

[6] Malhotra PK, Wenk T, Wieland M (2000) Simple procedure for seismic analysis of liquid-storage tanks. J Int Assoc Bridge Struct Eng 10(3): 197-201

[7] O'Callahan J, Avitabile P, Riemer R (1989) System Equivalent Reduction Expansion Process (SEREP). Proceedings of the 7th International Modal Analysis Conference, Las Vegas, Jan. 1989, pp. 29-37

Construction-Induced Vibration Impact Assessment and Mitigation for Hospital Redevelopment Project in Hong Kong

Zimo Zhu[1], Shiguang Wang[2], Songye Zhu[3]

[1] *Department of Civil and Environmental Engineering, The Hong Kong Polytechnic University, Hong Kong, China.*
E-mail: z-zimo.zhu@connect.polyu.hk

[2] *Department of Civil and Environmental Engineering, The Hong Kong Polytechnic University, Hong Kong, China.*
E-mail: shiguang.wang@connect.polyu.hk

[3] *Department of Civil and Environmental Engineering, The Hong Kong Polytechnic University, Hong Kong, China.*
E-mail: songye.zhu@polyu.edu.hk

ABSTRACT

Redevelopment of old building in urban area is a good solution to increase land utilization efficiency in metropolitans like Hong Kong. This construction activity will generate vibrations and may influence the hospital buildings nearby. Hospitals are usually expected to maintain normal operations during the construction. This paper demonstrates the construction-induced vibration impact assessment and mitigation measures for hospital redevelopment project in Hong Kong. The empirical formula to estimate the vibration generated by construction has been proposed and refined by field test. The calculated ground vibration level is inputted in the 3D finite element model built in ANSYS. The indoor floor vibrations at different locations are simulated by the model. The vibration criteria for medical equipment are determined by questionnaire sent to manufacturers. Several vibration mitigation measures have been proposed for the sensitive equipment.

KEYWORDS: *Construction-induced vibration, vibration mitigation, finite element modelling*

INTRODUCTION

Hong Kong is a densely populated city and is confronted with the problem of serious shortage of land supply. Redevelopment in urban area has therefore become a promising solution. The construction activities will inevitably induce ground-borne vibration, which may cause problems to the nearby buildings and people. However, the hospitals are usually expected to maintain normal operation during redevelopment

construction. The medical equipment and patients in hospital are relatively sensitive to vibration. Thus, the vibration impact assessment and mitigation before the hospital redevelopment is assumed necessary and important.

Various studies have been focused on the assessment of construction-induced vibrations. Different construction methods, such as vibratory pile drivers [1], impact pile drivers [2] and others, will induce different vibrations. Therefore, different empirical formulae are proposed. Vibration criteria for buildings and human comfort have been defined in various guidelines such as Guideline proposed by The California Department of Transportation [3] and specification published by ASHRAE [4]. The commonly accepted vibration criteria (VC) and vibration mitigation measures for sensitive medical equipment is rather limited at this stage.

In this paper, empirical formula is proposed and refined through field trial pile test. Method to determine VC of medical equipment is presented. Several possible mitigation measures are proposed as well.

CONSTRUCTION – INDUCED VIBRATION IMPACT ASSESSMENT

The impact of construction-induced vibration on nearby buildings depends on construction methods, source distance, soil properties and other many factors. To predict and quantify the vibration strength has drawn research interests in the past decades. Head and Jardine [5] proposed a simple empirical formula to predict vibrations generated by dynamic piling processes:

$$PPV = C\left(\frac{\sqrt{W}}{D}\right)^n \quad (1)$$

where C is a parameter determined by field measurement, usually within the range from 0.5 to 1.5; D describes the distance from the vibration source to the location of interest; n depends on soil conditions and W is the energy per cycle.

For construction activities without detailed information about energy W, equation (2) proposed by The California Department of Transportation could be adopted [3]:

$$PPV = \bar{C}\left(\frac{1}{D}\right)^n \quad (2)$$

where $\bar{C}$ and n can be determined according to field test. Before the commencement of this redevelopment project, trial pile test has been carried out. The parameters in empirical equation have been determined according to the test results.

Given that predicted vibration was determined through empirical formula, dynamic simulation could be carried out. A 3D finite element model of the concerned hospital building was built in ANSYS. The concerned structure is a 28-storey building. Beams and columns were modeled by element Beam188 with rectangular cross sections in

ANSYS, and core walls and floor slabs were modeled by Shell63 element. Element Combine14 was used to model the raft foundation below the superstructure. The simulated piling location is consistent with the future construction location. And the inputted excitation loads on foundation are calculated by the above empirical formula accordingly. Vibration attenuation from foundation to top and floor vibration distributions could be assessed through the model.

To assess vibration impact on sensitive medical equipment, the VC of the concerned equipment shall be confirmed. The vibration limits considering building functionality are 800, 400 and 200 μm/s for workshop, office and residential areas respectively as defined in specification published by ASHRAE [4]. Questionnaires are designed and distributed to manufacturer for medical equipment without detailed vibration tolerance information. Based on the suitable operation environment (workshop, office or residential areas), the VC for medical equipment can therefore be determined.

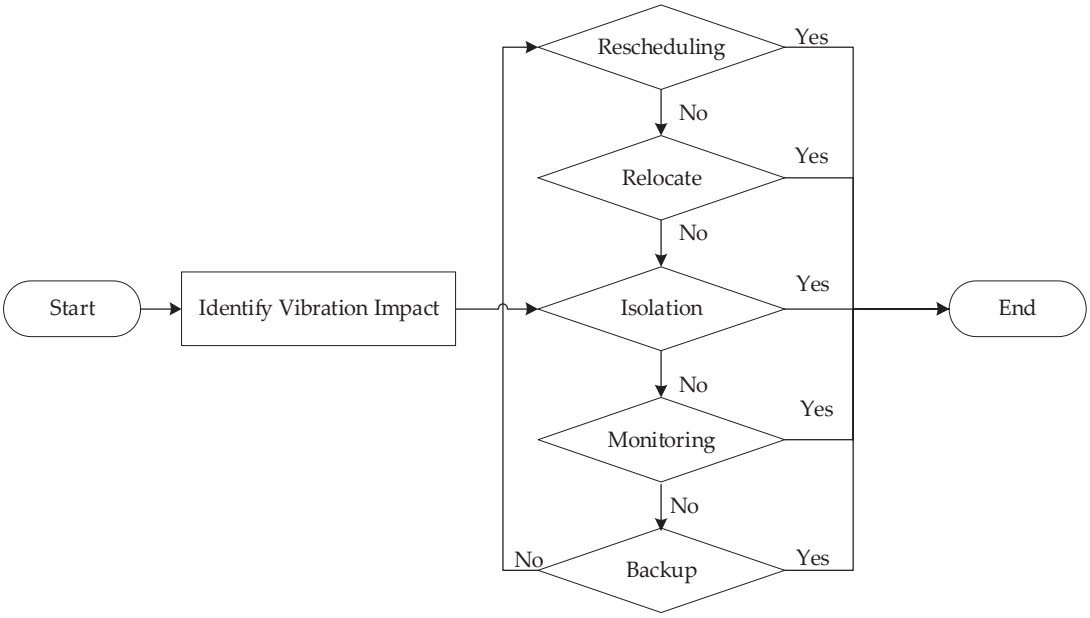

Figure 1: Vibration mitigation measures

VIBRATION MITIGATION MEASURES

By comparing the predicted floor vibration during construction and vibration criteria of concerned equipment, the vibration impact can therefore be assessed. The vibration mitigation measures are shown in **Figure 1**. Rescheduling the equipment operation time out of the construction period is firstly preferred. If not possible, the hospital may

consider relocate the equipment to places with lower predicted vibration level. Providing isolation devices for medical equipment that cannot be rescheduled or relocated is an alternative vibration mitigation measure. For bulky items, real-time vibration monitoring system is designed. The accelerometers are placed near the concerned medical equipment, the real-time vibration level is calculated and showed on concerned monitoring point.

CONCLUSIONS

In this paper, the construction-induced vibration assessment and mitigation for hospital redevelopment has been demonstrated. The empirical formula to estimate the vibration generated by construction has been proposed and refined by field trial pile test result. The calculated vibration level is inputted in the 3D finite element model built in ANSYS. Several vibration mitigation measures have been proposed for the sensitive equipment.

Construction-induced vibrations highly depend on the construction methods and site conditions. By considering these uncertainties, caution shall be exercised when using the prediction results. And analysis of the real-time vibration monitoring results will be beneficial to future refinement of the formula and dynamic model.

REFERENCES

[1] Athanasopoulos, G. A., & Pelekis, P. C. (2000). Ground vibrations from sheetpile driving in urban environment: measurements, analysis and effects on buildings and occupants. Soil dynamics and earthquake engineering, 19(5), 371-387.

[2] Masoumi, H. R., Degrande, G., & Lombaert, G. (2007). Prediction of free field vibrations due to pile driving using a dynamic soil–structure interaction formulation. Soil Dynamics and Earthquake Engineering, 27(2), 126-143.

[3] California Department of Transportation (2010). The Transportation and Construction Induced Vibration Guidance Manual, California, USA.

[4] ASHRAE (American Society of Heating, Refrigerating and Air-conditioning Engineers), (2011). ASHRAE Handbook 2011, Ventilating and Air-conditioning Engineers, Inc., Atlanta, USA.

[5] Head, J. M., & Jardine, F. M. (1992). Ground-borne vibrations arising from piling (No. 142).

Swing motion control of suspended structure by innovative Active Rotary Inertia Driver system

Zhang Chunwei[1], Wang Hao[2]

[1] *School of Civil Engineering, Qingdao University of Technology, Qingdao.*
E-mail: zhangchunwei@qut.edu.cn

[2] *School of Civil Engineering, Qingdao University of Technology, Qingdao.*
E-mail: wanghao@qut.edu.cn

ABSTRACT

The traditional TMD and AMD are ineffective for swing motion control of suspended structural system. The Tuned Rotary Inertia Damper (TRID) has limited robustness and application aspect due to its nature of being a passive tuning control system. In this paper, through the integration of active control philosophy with the rotary tuning inertia control concept, a new control system named Active Rotary Inertia Driver (ARID) is proposed. Firstly, the analytical model corresponding to the in-plane swing motion mode of the suspended structure subjected to point source excitations with the ARID control system is established based on the Lagrangian principle. Then, the equations are linearized for the purpose of engaging the LQR control algorithm. The effectiveness analysis is carried out using Simulink. Lastly, a shaking-table experiment system is developed to validate the effectiveness of the ARID control system. The dynamic characteristics of the ARID system in terms of tuning capabilities and transfer functions are investigated through a series of shaking table tests and simulations. There is a very good agreement between the test results and simulation results. The performance of the ARID control system for swing motion control of the suspended structure has also been validated. The results of the paper establish a good theoretical foundation for future researches concerning the ARID control method.

KEYWORDS: *suspended structures, swing motion control, active control, Active Rotary Inertia Driver, shaking table experiment*

INTRODUCTION

Vibration control techniques have been widely applied in civil engineering, mechanical engineering, aerospace engineering and other fields. The applications of vibration control devices are very common Ref. [1]. The pendular vibration of the suspended structure is a typical form of motion. It mainly includes three basic modes according to

the relationship between the lifting point and the moving direction of the structure: the swing vibration mode, the sway vibration mode, and the swing and sway coupling vibration mode. Based on many practical applications and studies, it can be observed that traditional vibration control devices such as Tuned Mass Damper (TMD), Active Mass Damper (AMD) are reliable and efficient for vibration control of civil engineering structures. While they are almost ineffective in swing vibration control of suspended structures Ref. [2]. According to the suspended structures swing vibration control, we have proposed a kind of device called Tuned Rotary Inertia Damper (TRID) system Ref. [3,4]. In this system, mass with rotary inertia is attached to the suspended structure. The torsional spring element embedded with damping mechanism is installed between the inertia mass and the structure. The effectiveness of the TRID system for swing vibration control was verified by theoretical analysis and experiment. However, the TRID system has some defects such as the swing angle is too small to start the TRID system normally, and the TRID miniaturization device has time lag effect.

In this paper, a kind of active control system for swing motion control named Active Rotary Inertia Driver is proposed based on the TRID system. Instead of rectilinear motion in traditional devices and working relying on the torsional spring element, rotary inertia of the ARID system is driven by a rotating actuator. Regarding this system, no frequency modulation and initial incentive are needed to make the system work Ref. [5]. The outline of the article is as follows. Firstly, the mathematical model of the proposed system is derived based on Lagrangian principles. Secondly, the LQR controller is designed based on the model and the effectiveness of the system is analyzed. Finally, a series of shaking table experiments are conducted to investigate the effectiveness of the ARID system.

MATHEMATICAL MODEL

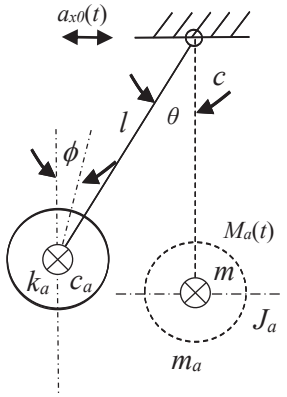

Figure 1: Simplified analysis model of suspended structure with ARID system

Simplified analysis model of suspended structure with the ARID system is developed in order to investigate the dynamic characteristics of the ARID system, which is shown in

Figure 1.The model consists of two degrees of freedom used as generalized coordinators, which are the swing angle θ and the rotary inertia relative rotation angle with respect to the ground base ϕ. The suspended structure has the swing length l. The suspended particle mass and the damping coefficient are m and c respectively. The ARID system rotary inertia mass is m_a, the system rotary inertia is J_a, rotational stiffness coefficient is k_a, and the damping coefficient is c_a. The acceleration at the suspended structure suspension point is $a_{x0}(t)$, and output torque of the ARID system is $M_a(t)$.The Lagrangian equations are adopted to derive the model of the entire system. The system motion equations can be expressed as

$$(m+m_a)l^2\ddot{\theta}+c\dot{\theta}+(m+m_a)gl\sin\theta = -(m+m_a)l\cos\theta a_{x0}(t)+c_t(\dot{\emptyset}-\dot{\theta})+k_t(\emptyset-\theta)-M_a(t) \quad (1)$$

$$J_a\ddot{\emptyset}+c_t(\dot{\emptyset}-\dot{\theta})+k_t(\emptyset-\theta)=M_a(t) \quad (2)$$

SHAKING TABLE EXPERIMENT OF THE ARID SYSTEM

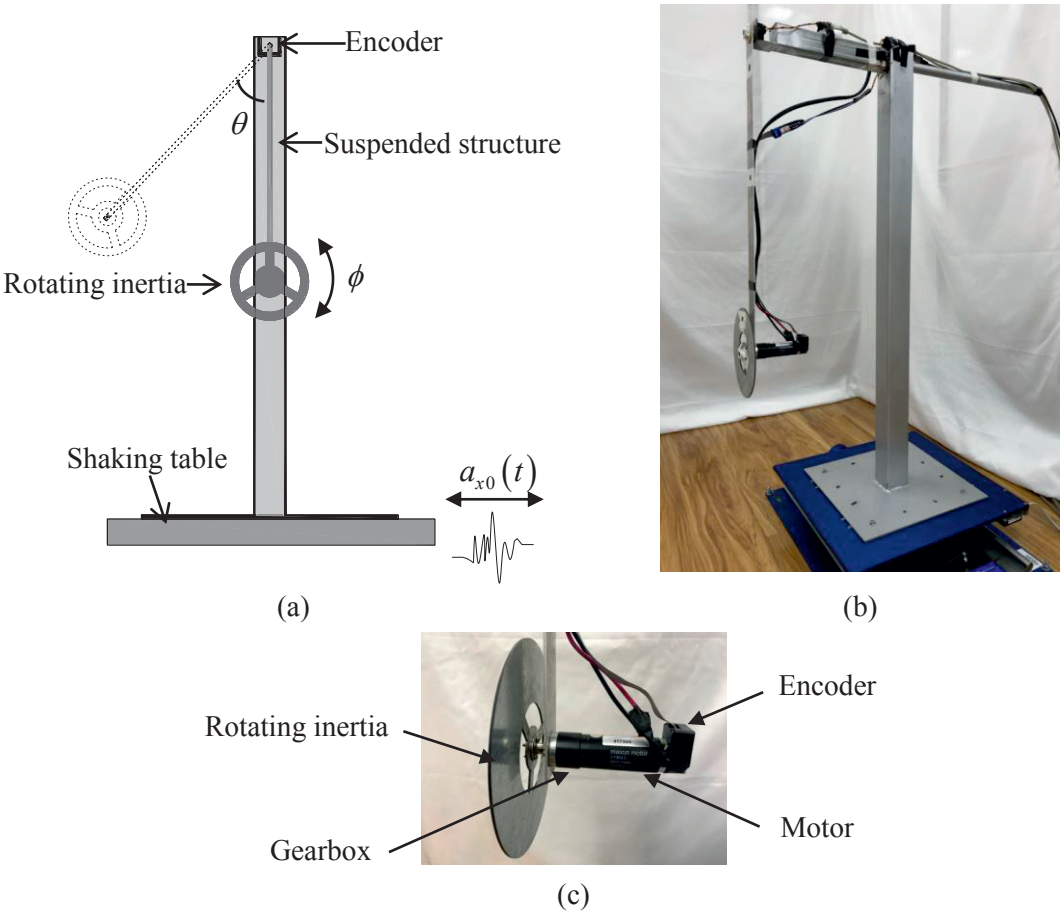

Figure 2: Small scale experiment platform :(a) schematic description of test setup;(b) picture of test setup;(c) picture of the ARID system.

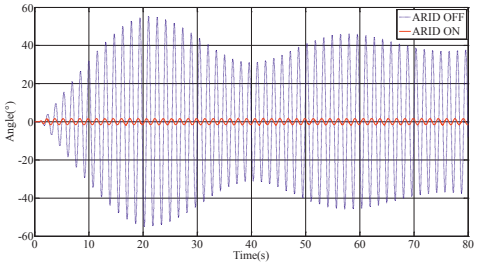

Figure 3**:** Time history of swing angle

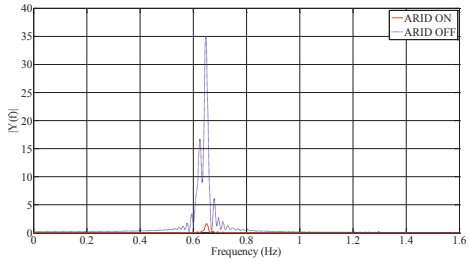

Figure 4**:** Amplitude frequency curve

Tab. 1.2. Control results of suspended structures with resonance harmonic excitation

Case	Peak angle/°	Peak decay rate	RMS decay rate
ARID OFF	*55.28*	*96.66%*	*97.21%*
ARID ON	*1.85*		

In the ARID ON case, the angle is controlled within 5 degrees and the angle frequency is relatively stable. The ARID system can significantly inhibit the angle spectrum of the structure.Fom the results of the experiment, it can be concluded that the ARID system has good effectiveness in swing motion control.

CONCLUSIONS

The Active Rotary Inertia Driver system (ARID) for swing vibration control is proposed in this paper. The analysis model of the suspended structure with ARID system is established. And the LQR controller is designed for the ARID system. The numerical analysis and the experiments have been carried out. The numerical and experimental results validate the effectiveness for swing motion control of the proposed ARID system.

REFERENCES

[1] Ou Jinping. (2003) Structural Vibration Control: Active, Semi-active and Smart Control. Beijing: Science Press.

[2] Zhang C, Li L, Ou J. (2010) Swinging motion control of suspended structures: Principles and applications. *Structural Control and Health Monitoring*, 2010, 17(5): 549-562.

[3] Zhang Chunwei, Xu Huaibing, Li Luyu, Ou Jinping. (2010) Structural pendulum vibration control methods based on tuned-rotary-inertia-damper (I): Parametric impact analysis and bench-scale model tests. *Control Theory & Applications*, 2010, 09:1159-1165.

[4] Xu Huaibing, Zhang Chunwei, Li Luyu, Ou Jinping. (2010) Structural pendulum vibration control methods based on tuned-rotary-inertia-damper (Ⅱ) Full scale model experiments and miniaturization study. *Control Theory & Applications*, 2010, 10:1315-1321.

[5] Soong T T, Author, Reviewer B F S.(1992) Active Structural Control: Theory & Practice . *Journal of Engineering Mechanics*, 1992, 118(6):1282-1285.

A Novel inerto-viscous damper for seismic vibration control

M. Abdeddaim[1], A.A. Kasar[2], N. Djedoui[3] and A. Ounis[3]

[1] *Faculty of science and technology, Mohamed Khider University of Biskra, Algeria.*
E-mail: m.abdeddaim@univ-biskra.dz

[2] *Head, Civil engineering, Sagar Institute of Science and Technology, Bhopal.*
E-mail: arnav.kasar@gmail.com

[3] *LARGHYDE laboratory, Department of Civil engineering and hydraulics, Mohamed Khider University of Biskra, Algeria*
E-mail: n.djedoui@univ-biskra.dz and a.ounis@univ-biskra.dz

ABSTRACT

The destructive nature of earthquakes resulted in many engineering challenges, focusing mostly on the control of seismic induced vibrations. Among the key solutions toward seismic protection of structures, the vibration control device made their way to be one of the most studied research topics. Lately, a new rotational inertia based device has been introduced, known as "inerter" this device is capable of developing a fictive mass related to the relative acceleration between it nodes. This work presents a novel inerto-viscous damper, which combines the "inerter" device with classical viscous damper. A multi-degree of freedom system subjected to earthquake record is used to demonstrate the potency of the inerto-viscous dampers. Through a time history analysis, results obtained shows a significant reduction in the structure response equipped with a novel inerto-viscous damper, compared to other structures with normal viscous damper and no damper. The study also examines an optimal ratio between the inerter fictive mass and the viscous device damping based on the results obtained.

KEYWORDS: *inerter, viscous damper, inerto-viscous damper, vibration control*

INTRODUCTION

Throughout the history of buildings technology, the seismic protection of the structure represented one of the biggest challenges for the engineering community. Recently, a new mass amplification device known as "inerter" was introduced for civil engineering use [1]. Mainly studied as a device capable of reproducing a large fictive mass, it is coupled with tuned mass dampers resulting in lightweight TMDs knows as TMD-Inerter [2-4]. In this work, a hybrid control device is obtained by attaching an inerter with a viscous damper in parallel. The effectiveness of the proposed hybrid

device is investigated for seismic response control, for this purpose a benchmark scaled structure is equipped with an inerto-viscous damper and submitted to earthquake record. State space representation is used. The following dynamical parameters were investigated, top floor displacement, inter-story drift and damper force.

MATHEMATICAL FORMULATION OF THE INERTER

The inerter is a combination of a rack and a set of pinions rotating about a shaft, a simple inerter scheme is depicted (i.e., Figure 1), The two extremities of the inerter, represented by *a* and *b* in Fig. 1, are connected to the pinion (of radius ρ) through racks and are responsible for reversing the direction of reactions (represented by *F(t)*) at both ends. A flywheel having a radius *R* and mass *m* is mounted on the other end of the shaft, to reduce the impact through its higher inertia.

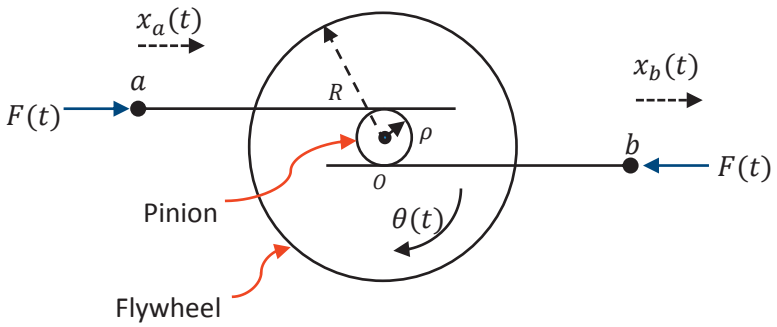

Figure 1: A simplified mechanical model of an inerter [5]

The mechanical linear equation of the inerter, which represents the force produced by this device, is given in Eq. 1

$$F(t) = \frac{1}{2} m \frac{R^2}{\rho^2} [\ddot{x}_a(t) - \ddot{x}_b(t)] \quad (1)$$

The term $\frac{1}{2} m \frac{R^2}{\rho^2}$ is denoted as the inertence b of the device, and is expressed in unit of mass (kg). The device inertence can be augmented by serially increasing the number of pinions. Hence, the general force equation of the inerter can be written as:

$$F(t) = b[\ddot{x}_a(t) - \ddot{x}_b(t)] \quad (2)$$

MATHEMATICAL FORMULATION OF THE INERTO-VISOUCS DEVICE

The hybrid device proposed in this work is a result of the assembly of an inerter with a viscous damper in parallel, as it can be seen (i.e., Figure 2). This, will ensure a highly rotational inertial force combined to a viscous damping, resulting from the inerter and the viscous damper, respectively.

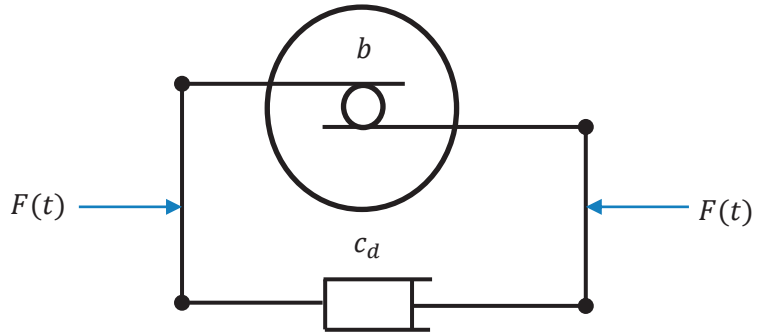

Figure 2: Mechanical model of an inerto-viscous damper

The force produced by the hybrid device depicted above (i.e. Figure 2) can be expressed by the equation (3), due to the parallel assembly adopted for herein. The general expression of the force is the sum of the two forces resulting from the inerter and the viscous damper.

$$F(t) = b[\ddot{x}_a(t) - \ddot{x}_b(t)] + c_d[\dot{x}_a(t) - \dot{x}_b(t)] \quad (3)$$

The term c_d denotes the damping parameter of the viscous damper.

NUMERICAL STUDY AND RESYLTS

In order to Study the effect of the proposed device, a reduced model three story benchmark structure is equipped with the inerto-viscous damper [6]. The structure is submitted to a scaled record of the El Centro earthquake using MATLAB. The dynamical parameters investigated are maximum top floor displacement (D_{max}), maximum inter-story drift (Δ_{max}) and maximum damper force (F_{max}). The results obtained are compared to a structure without a damper, a structure with an inerter damper only and a viscous damper only. The obtained results are expressed in table 1.

Tab. 1. Results for uncontrolled and controlled cases.

Dynamical parameter	Uncontrolled	Controlled		
		Inerter damper	Viscous damper	Inerto-viscous damper
D_{max} [cm]	*0.9712*	*0.7048*	*0.3847*	*0.2934*
$\Delta_{max,1}$ [cm]	*0.5469*	*0.4312*	*0.1909*	*0.1703*
$\Delta_{max,2}$ [cm]	*0.3167*	*0.1780*	*0.1331*	*0.0899*
$\Delta_{max,3}$ [cm]	*0.3167*	*0.0996*	*0.0749*	*0.0581*
F_{max} [N]	/	*727.53*	*323.88*	*657.85*

Note: $\Delta_{max,1}$, $\Delta_{max,2}$ and $\Delta_{max,3}$ denotes Δ_{max} for the first, second and third floor; respectively.

As it can be seen from table 1, an important response reduction is obtained when using the inerto-viscous damper; this response reduction is more significant compared to

other control cases. The maximum percentages reductions are 69.7% and 81.6% for top floor displacement and top floor inter-story drift, respectively. It is also noticed from table 1 that, despite the large force produced by the inerter, the reduction was not important compared to the hybrid damper.

CONCLUSIONS

A hybrid damper used for seismic response control is studied. The damper is a result of a parallel assembly of an inerter and a viscous damper. The performance of the device is investigated on a three story benchmark structure model submitted to earthquake record. Dynamic responses obtained are compared with those using simple passive devices (i.e. inerter and viscous damper). The following conclusion can be drawn:

- The combination of an inerter and a viscous damper in parallel results in a very efficient control device, defined as inerto-viscous damper in this study.
- Compared to other passive control devices the inerto-viscous damper is more effective.
- The effectiveness of the proposed hybrid device is investigated through two dynamic parameters namely maximum top floor displacement and maximum inter-story drift.
- The proposed device achieves better performance with less force input compared to other passive devices.

REFERENCES

[1] Smith, M.C. (2002) Synthesis of mechanical networks: The inerter. *IEEE Transactions on automatic control* **47**(10): p. 1648:1662.

[2] Marian, L. and A. Giaralis (2014) Optimal design of a novel tuned mass-damper–inerter (TMDI) passive vibration control configuration for stochastically support-excited structural systems. *Probabilistic Engineering Mechanics*,. **38**: p. 156-164.

[3] Marian, L. and A. Giaralis (2017) The tuned mass-damper-inerter for harmonic vibrations suppression, attached mass reduction, and energy harvesting. *Smart Structures and Systems*,. **19**(6): p. 665-678.

[4] Giaralis, A. and A.A. Taflanidi (2018) Optimal tuned mass-damper-inerter (TMDI) design for seismically excited MDOF structures with model uncertainties based on reliability criteria. *Structural Control and Health Monitoring*, **25**(2): p. e2082.

[5] Abdeddaim, M., A.A. Kasar, and N. Djedoui (2018) Seismic vibration control using a novel inerto-elastic damper. in MATEC Web of Conferences. EDP Sciences.

[6] Battaini, M., F. Casciati, and L. Faravelli (1998) Fuzzy control of structural vibration. An active mass system driven by a fuzzy controller. *Earthquake Engineering and Structural Dynamics*, **27**(11): p. 1267-1276.

Topology Optimization Design of Seismically Excited Structures with Dampers

F. Gomez[1], B.F. Spencer Jr.[2]

[1] *Department of Civil and Environmental Engineering, University of Illinois at Urbana-Champaign, USA. E-mail: gmzsnch2@illinois.edu*

[2] *Department of Civil and Environmental Engineering, University of Illinois at Urbana-Champaign, USA. E-mail: bfs@illinois.edu*

ABSTRACT

Supplemental damping devices present an attractive mean to mitigate the response of dynamically excited structures. Typically, dampers are designed only after the main structure is completed, and they are added with the goal to increase structural damping and effectively reduce the dynamic response. Topology optimization offers the possibility of obtaining material layout distribution to meet the loading demands; however, most approaches only accommodate static deterministic loads, but dynamic responses are required to design damping systems and the most severe loads that civil structures withstand are stochastic and dynamic. This study proposes a method to obtain simultaneously optimal topology and distribution of damping devices for stochastically excited structures. The ground excitation is modeled as a stationary zero-mean filtered white noise, the excitation model is combined with the structural model to form an augmented representation, and the stationary covariances of the structural responses of interest are obtained by solving a Lyapunov equation. The objective function is defined in terms of the stochastic response. The proposed optimization scheme is illustrated for a building with viscous dampers subjected to stochastic ground motion excitation. The results presented herein demonstrate the efficacy of the proposed approach for efficient simultaneous optimization of topology and damping distribution of stochastically excited structures.

KEYWORDS: *Topology optimization, Stochastic dynamics, Supplemental Damping, Finite element, Lyapunov equation.*

INTRODUCTION

Topology optimization provides a general approach to obtain optimal material layout in a prescribed domain according to some cost function with appropriately specified design constraints [1]. It has been successfully applied to continuous domains subjected

to deterministic static or dynamic loadings [1]. However, such deterministic approaches cannot accommodate stochastic dynamic loads which civil structures frequently undergo, such as winds, earthquakes, traffic, etc. [2], and therefore, produce suboptimal designs. Recently, Gomez and Spencer [3] developed a general topology optimization framework for structures subjected to stationary stochastic excitation; the performance function was formulated in terms of the response covariances, which are obtained through solution of a large-scale Lyapunov equation.

Significant research has been focused on the optimal distribution of supplemental damping devices to reduce seismic response [4]. However, simultaneous optimization of topology and damping distribution has only been studied recently by Gomez and Spencer [5] due to the complexity of the problem given by the stochastic dynamic nature and the non-proportional damping. This study extends the topology optimization framework for stochastically excited structures [3,5] to perform simultaneous optimization of topology and discrete viscous damping distribution. An illustrative example is provided for the optimization of a mid-rise building subjected to a stochastic ground motion.

PROBLEM FORMULATION

This section summarizes the formulation of the optimization problem. Further details in the formulation and numerical solution can be found in previous studies [3,5].

Design variables in continuous-domain topology optimization are chosen as the relative density in each element. For element n, the relative density variable is denoted by z_n. Additional design variables c_k are chosen to represent supplemental damping at the k^{th} floor and are normalized such that their sum is at most 1. The optimization formulation is thus given by

$$\begin{aligned} &\min_{\mathbf{z},\mathbf{c}} \ \max_{i=1,\ldots,N_{\mathrm{f}}} \sigma_{\theta_i}^2(\mathbf{z},\mathbf{c}) \\ &\text{s.t.} \quad V(\mathbf{z}) - V_{\max} \le 0 \quad \text{and} \quad \mathbf{c}^{\mathrm{T}}\mathbf{1} - 1 \le 0 \\ &\qquad z_i \in [\varepsilon, 1] \quad \text{for} \quad i = 1,\ldots,N_{\mathrm{el}} \\ &\qquad c_i \in [c_{\min}, 1/N_{\mathrm{d}}] \quad \text{for} \quad i = 1,\ldots,N_{\mathrm{f}} \end{aligned} \tag{1}$$

where θ_i is the interstory drift of the i^{th} floor, V is the volume, $V_{\max}$ is the volume limit, ε is the lower bound on the density variables, N_{el} is the number of elements, N_{f} is the number of floors, $c_{\min}$ is the lower bound on the damping variables, and N_{d} is the minimum number of dampers specified.

The material properties for intermediate relative densities are obtained using an interpolation rule; in this work SIMP interpolation is used for stiffness and mass [2] given by; and the additional damping force in each floor is given by

$$
\begin{aligned}
E(z) &= \left[\varepsilon_0 + (1-\varepsilon_0) z^p\right] E_0 \\
\rho(z) &= \begin{cases} z^q \rho_0 & \text{if } z \geq 0.1 \\ a_0 z^{p+3} \rho_0 & \text{if } z < 0.1 \end{cases} \\
f_i^d &= c_i c_{\text{sum}} \left(\dot{u}_i - \dot{u}_{i-1}\right)
\end{aligned}
\tag{2}
$$

Numerical details to obtain efficiently the response and their sensitivities and to update the design variables are given in a previous study [3]. A linear hat filter was applied to the performance function sensitivities to avoid numerical instabilities [1].

ILLUSTRATIVE EXAMPLE

In this section, the proposed framework is illustrated by minimizing the variance of the maximum interstory drift of a 9-story building subjected to a seismic ground motion in the horizontal direction [6].

The design domain is a 45 m x 36 m rectangle, which is discretized using 180 x 144 Q4 elements. The solid linear elastic material has the following properties: Young's modulus E_0 = 210 GPa, Poisson's ratio ν = 0.3, density ρ = 7500 kg/m^3. The domain has a uniform thickness of 0.05 m; the continuum domain is assumed to be in plane stress; and the maximum allowable volume is 20% of the solid domain. The domain is bounded by columns varying linearly from W14x500 to W14x257 and the same material properties; the columns are discretized so that their nodes coincide with the Q4 elements. Additional floor lumped masses of 85 000 kg are included at each column axis and floor. A rigid diaphragm is applied in each floor. The radius of the filter is equal to 0.40 m. Rayleigh damping is used with 0.1% damping ratios for the first 2 modes to account for intrinsic damping in the structure. Two different sums of damping coefficients are considered.

Figure 1 and 2 show the results for topology optimization and damping variable distribution for c_{sum} equal to 10^6 and 10^7 N-s/m, respectively.

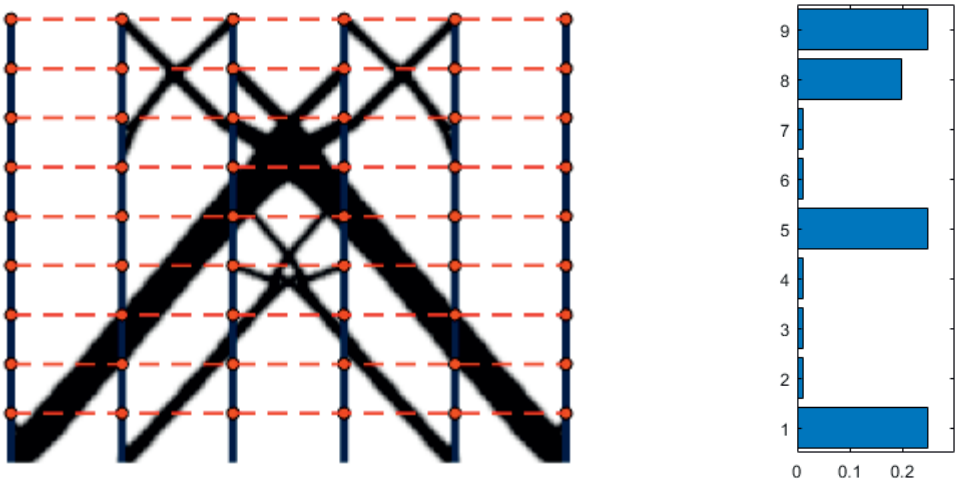

Figure 1: Optimal topologies (left) and damping distribution (left) for c_{sum}=10^6 N-s/m.

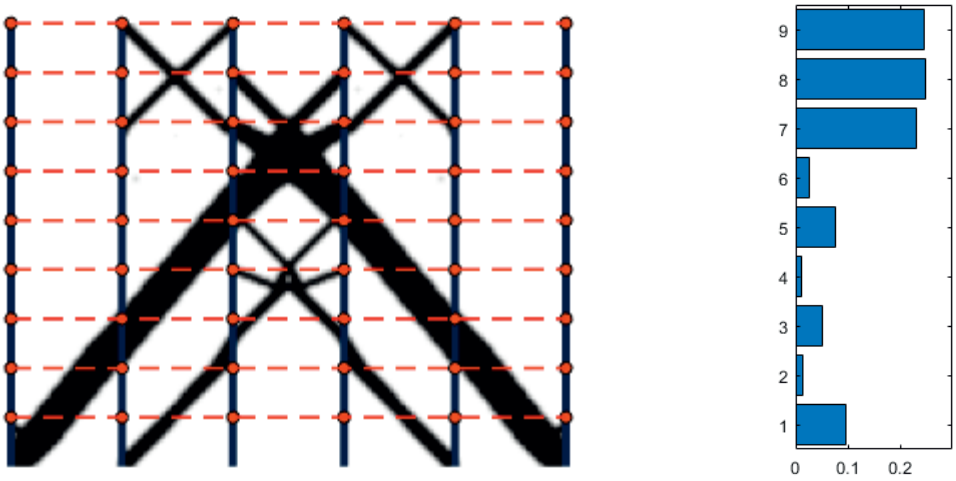

Figure 2: Optimal topologies (left) and damping distribution (left) for $c_{sum}=10^7$ N-s/m.

CONCLUSIONS

This paper proposed a methodology for simultaneous optimization of topology and supplemental damping of buildings subjected to stochastic ground motions. The input was considered as a filtered white noise, and the performance was given in terms of the maximum covariance of the response. The design variables were chosen as the relative densities in each element and the relative damping coefficient in each floor. The proposed method was illustrated by conducting topology optimization of the lateral system of a 9-story building under stochastic earthquake loading. The results demonstrate the efficacy of the proposed approach for simultaneous topology and damping distribution optimization of stochastically excited buildings.

REFERENCES

[1] Bendsøe, M.P., Sigmund, O. (2003) Topology optimization: theory, methods, and applications. Springer.

[2] Soong, T.T., Grigoriu, M. (1993) Random vibration of mechanical and structural systems. PTR Prentice Hall.

[3] Gomez, F., Spencer, B.F. Jr. (2019) Topology optimization framework for structures subjected to stationary stochastic dynamic loads. *Structural and Multidisciplinary Optimization*, **59:** 813.

[4] Zhang, R.H., Soong, T.T. (1992) Seismic design of viscoelastic dampers for structural applications. *Journal of Structural Engineering*, **118**(5): 1375-1392.

[5] Gomez, F., Spencer, B.F. Jr. (2018). Topology optimization for stochastically-excited structures with supplemental dampers. 7th World Conference of Structural Control and Monitoring, Qingdao, China.

[6] Ohtori, Y., Christenson, R.E., Spencer, B.F. Jr., Dyke, S.J. (2004) Benchmark control problems for seismically excited nonlinear buildings. *Journal of Engineering Mechanics*, **130**(4): 366-385.

Numerical Investigation of a New Hybrid Electromagnetic Damper for Reducing Cable Vibration

S. Kye[1], H.S. Kim[2], H.J. Jung[3]

[1,2] *Department of Civil and Environmental Engineering, Korea Advanced Institute of Science and Technology, Republic of Korea.*
E-mail: skkye@kaist.ac.kr, rlagudtn0934@kaist.ac.kr

[3] *Department of Civil and Environmental Engineering, Korea Advanced Institute of Science and Technology, Republic of Korea.*
E-mail: hjung@kaist.ac.kr

ABSTRACT

Cable vibration is directly related to the serviceability and safety of the cable-supported bridges. The proposed hybrid electrodynamic cable damper has advantages of being able to control vibration like a conventional coil typed electromagnetic damper while maintaining a damping force approximate to that of a conventional eddy current typed electromagnetic damper. Electromagnetic finite element analysis was performed to investigate the damping performance and feasibility of energy harvesting function. As a result, the proposed hybrid electrodynamic cable damper showed improved performance compared to the electromagnetic damper in terms of maximum damping force, damping coefficient, and damping density. And the power amount produced by the damper showed the feasibility to construct a cable vibration monitoring system.

KEYWORDS: *Hybrid electrodynamic damper, Electromagnetic analysis, Cable vibration, Finite element analysis*

INTRODUCTION

Recently, due to the wide potential of electrodynamic cable dampers, various researches have been carried out for field application [1]. In this study, a new type of electrodynamic damper with improved structure is proposed. The conventional eddy-current typed electromagnetic damper has a high damping force but has a limitation that it functions only as a passive type of control. The coil typed electromagnetic damper has high controllability but low damping force and damping density. The proposed hybrid electrodynamic damper is designed to overcome the disadvantages of conventional eddy-current typed and coil typed electromagnetic damper. A permanent magnet was added inside the driving part to add a magnetic circuit. The conductors on the outside of the driving part were reinforced and the teeth connected to the back iron were arranged. The magnetic, electrical, and physical

behavior characteristics of the hybrid electrodynamic damper with the new structure type were investigated through electromagnetic transient analysis.

ELECTROMAGNETIC ANALYSIS

The proposed hybrid electrodynamic cable damper is divided into a driving part to be fastened to the cable and a fixed external part. The damper model and the external circuit are shown in Figure 1. Inside, neodymium (NdFeB-N45M) permanent magnets were placed. The permanent magnets were restrained by different magnetization directions in the axial direction based on the iron poles at the boundaries between the upper and lower portions and the magnets.

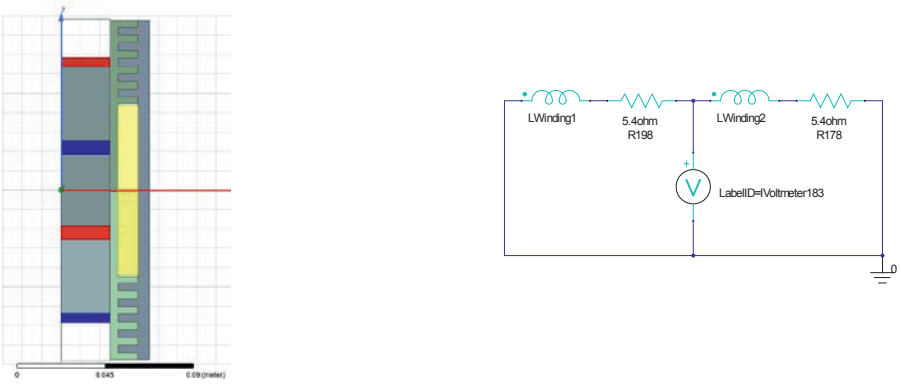

(a) Analysis model (b) External circuit

Figure 1: Analysis model and external circuit of hybrid electrodynamic cable damper.

The internal driving part has an air gap from the outside. Two solenoid coils were placed on the inner side and oxygen-free copper on the outer side. Each was separated through a slot. The coil reduces damping force due to series resistance and inductance but is essential for control. At the outer upper and lower parts, oxygen-free copper and teeth connected to back iron were arranged. Teeth strengthen the absolute damping force compared to a coil typed electromagnetic damper. In the external circuit, the inductor is connected in series with the measured resistance value in each winding.

Pure iron was applied to the iron poles and the thickness was adjusted in consideration of magnetic saturation. The intensity of the magnetic field at both ends of the air gap according to the iron pole thickness is shown in Figure 2. When the magnetic field intensity outside the air gap was distributed in the range of 1.5 ~ 2.0 T, the maximum potential was observed at the upper and lower parts of 5 mm and 7 mm, respectively.

The transient analysis was performed for the electromagnetic analysis, and the mesh was given considering the electrostatic conditions. Figure 3 shows the field plots of the damper. The upper and lower magnetic circuits pass through teeth and windings, and the center magnetic circuit is formed inside the windings. It can be seen that the magnetic field is concentrated on the outer surfaces of the four iron poles.

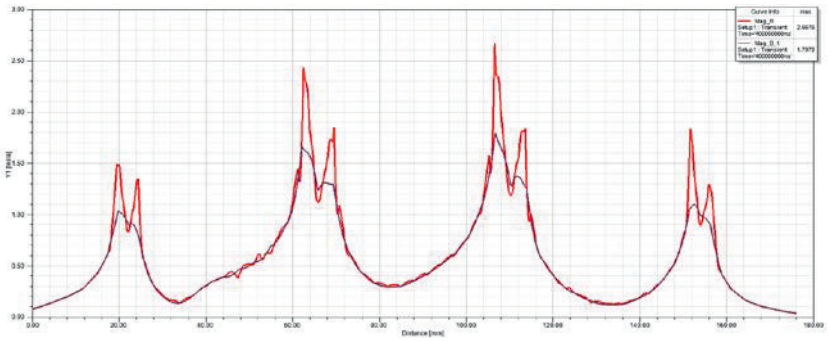

Figure 2: Magnetic field strength by iron pole thickness.

The permanent magnet drive was excited with a sinusoidal wave of 12 mm, 5 Hz. As a result, the maximum damping force was 980 N. In the permanent magnet movement, the induced electromotive force is generated in the coil in the direction to resist the change of the magnetic flux by the Faraday's electromagnetic induction law. The maximum induction current was 12.5 A, and the maximum power was 7.9 W.

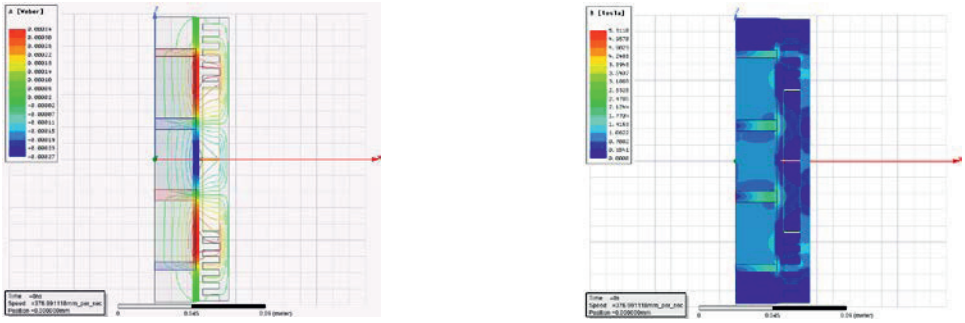

(a) Magnetic flux line (b) Magnetic field strength distribution

Figure 3: Field plots of the hybrid electrodynamic damper.

In order to investigate the dynamic characteristics of the hybrid electrodynamic damper, the damping force hysteresis according to the displacement and velocity was examined. The results are shown in Figure 4.

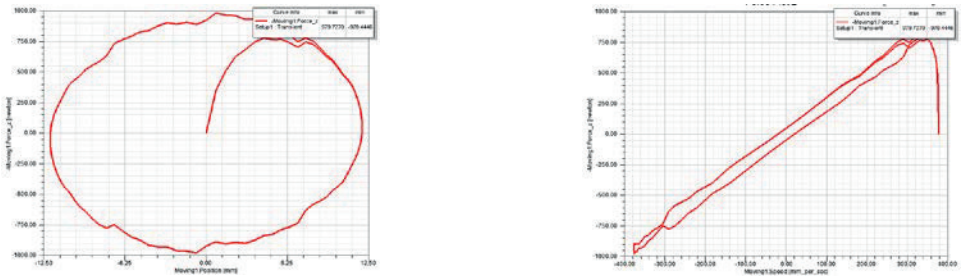

(a) (b)

Figure 4: Hysteresis curve of damping force according to displacement and velocity

The maximum damping force appeared at a point with a phase difference of 0.01 second from the maximum velocity point. In addition, it is confirmed that a relatively constant damping coefficient appears around the range of ± 0.3 m/s.

As a result of the comparative analysis, the maximum damping force, damping coefficient, and damping density are increased compared with the conventional coil typed electromagnetic damper under the same excitation condition. The comparison results are shown in Table 1. The conventional coil typed electromagnetic damper used for the comparison is based on the results of previous studies [2].

Table 1: Damping performance comparison of hybrid electrodynamic damper

	CEMD[1]	**HEDD[2]**	**Comparison**
Max. damping force (N)	*484*	*980*	*×2.025*
Damping coefficient (kN·s/m)	*1.278*	*2.602*	*×2.036*
Damping density (kN·s/m⁴)	*327.010*	*1,325.345*	*×4.053*

1: Coil typed electromagnetic damper, 2: Hybrid electrodynamic damper

CONCLUSIONS

To investigate the electromagnetic and physical characteristics and feasibility of energy harvesting function of the proposed hybrid electrodynamic damper, electromagnetic finite element analysis was performed. As a result, the maximum damping force of the hybrid electrodynamic damper was 980 N, the damping density was 1,325.345 kN·s/m^4, and the amount of electric power was 7.9 W. The analytical results show that the proposed hybrid electrodynamic cable damper has better damping performance than the conventional coil typed electromagnetic damper. And demonstrated the feasibility of constructing a cable vibration monitoring system through the power generated by the damper. However, since the simulation results are performed under ideal conditions, it is expected that the performance will be reduced when the damper prototype is manufactured. Therefore, it is expected that the improved performance will be achieved through the improvement of the damper structure through the optimization in the future.

ACKNOWLEDGMENT

This research was funded by Construction Technology Research Program funded by the Ministry of Land, Infrastructure, and Transport (MOLIT) of the Korean government, grant number 19SCIP-C116873-04.

REFERENCES

[1] H.Y. Jung, I.H. Kim, and H.J. Jung (2017) Feasibility Study of the Electromagnetic Damper for Cable Structures Using Real-Time Hybrid Simulation, Sensors, Vol. 17, No. 11.

[2] S. Kye, H.J. Jung, H.Y. Jung (2019) Experimental Investigation on a Cable Structure Equipped with an Electrodynamic Damper and Its Monitoring Strategy through Energy Harvesting, Sensors, Vol. 19, No. 11.

Experimental Investigation on Inertial Mass Damper for Cable Vibration Mitigation

S.H. Dong[1], Y.F. Duan*[1], C.B. Yun[1], H.M. Zhang[1]

[1] *College of Civil Engineering and Architecture, Zhejiang University, China*
E-mail: dshhxd@hotmail.com, ceyfduan@zju.edu.cn, ycb@zju.edu.cn,melanie_zhm@163.com

ABSTRACT
The negative stiffness of an active or semi-active damper system has been proven to be very effective to reduce the dynamic response. Therefore, dissipation devices possessing the property of negative stiffness, such as inertial mass dampers (IMD), draw much attention recently. In this study, an IMD was designed and manufactured, which consists of an inerter providing negative stiffness and a viscous shear damper. Then its vibration mitigation performance was investigated for a long cable. At first a numerical simulation study was carried out on the damping performance considering the effects of the inertial mass and viscous damping coefficient. Optimal values for the inertial mass and viscous damping were determined. Then an experimental study was performed on a scaled cable (19m long) for a stay-cable (577m long) of Sutong Bridge, in Jiangsu, China. The experimental results show that the vibration reduction performance of the proposed IMD is much better than that of a conventional viscous damper.

KEYWORDS: *inertial mass damper, negative stiffness, cable vibration control, experimental investigation*

INTRODUCTION
Cables are widely used in cable-supported bridges and long-span structures due to their economy, beauty, and light weight. However cables are prone to severe vibration because of their low inherent damping and high flexibility. Those vibrations can be detrimental to the serviceability and safety of the structures. Many studies show that negative stiffness devices, such as inertial mass dampers, are very effective to reduce those undesirable vibrations. In this paper, cable vibration control with an IMD is presented. A prototype of an IMD is designed and manufactured, and numerical and experimental studies are conducted to investigate the control performance.

PROTOTYPE OF INERTIAL MASS DAMPER
A prototype of an IMD, which consists of a ballscrew with a flywheel and a viscous shear damper, is designed and manufactured. The schematic is showed in Fig. 1. The IMD may be installed as fixed on the bridge deck and connected to a cable as in Fig. 2-a. The cable vibration leads to a vertical reciprocating motion of the ballscrew and the shear plates. The vertical motion is transformed to a rotation motion of the flywheel by the ballnut, which induces large inertial mass causing negative stiffness effect to the IMD-cable system. Property of the inertial mass can be adjusted by the size of flywheel, whereas the force from the shear damper depends on the viscosity of damping fluid and the sizes of plates.

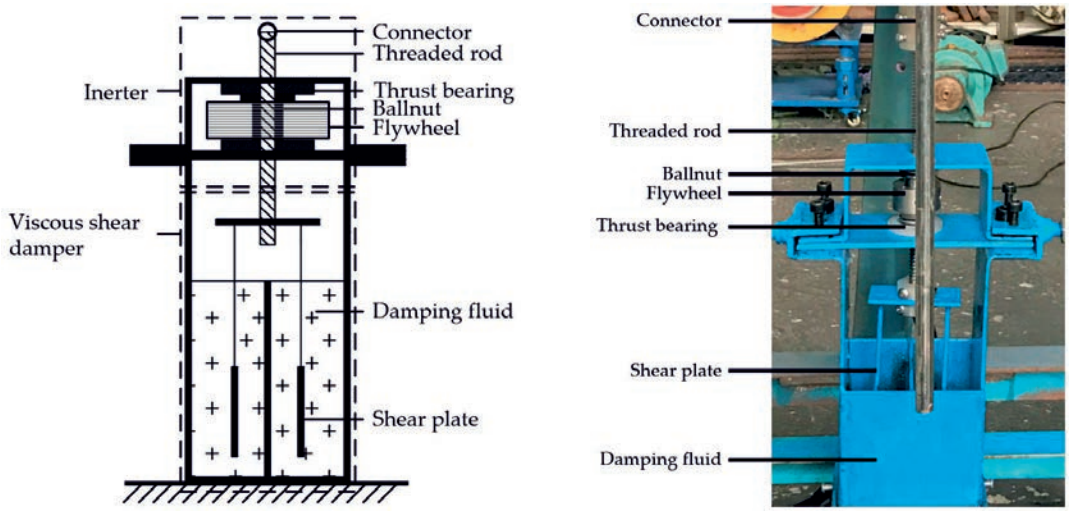

a. Configuration sketch of IMD b. Prototype of IMD

Figure 1: The schematic of inertial mass damper

NUMERICAL SIMULATION OF IMD-CABLE SYSTEM

The equation of motion of a sagged cable with an IMD can be expressed in Eq. (1). The damper's force on the right side of Eq. (1) can be obtained as a superposition of a inertial force and a viscous damping force from the IMD:

$$\ddot{v}(x,t)+c\dot{v}(x,t)-\frac{v''(x,t)}{\pi^2}+\frac{\lambda^2}{\pi^2}\left[\int_0^1 \ddot{v}(x,t)\right]=(m_e\ddot{v}(x,t)+c_d\dot{v}(x,t))\delta(x-x_d) \quad (1)$$

where $v(x,t)$, $\dot{v}(x,t)$ and $\ddot{v}(x,t)$ are the displacement, velocity and acceleration of the cable, respectively. c is the inherent cable damping. λ is the sag-extensibility parameter defined by Irvine and Caughey[1]. x_d denotes the damper location. m_e and c_d are the dimensionless inertial mass and equivalent viscous damping of the IMD[2] as:

$$m_e=\frac{\overline{m}_e L\omega_0^2}{\pi^2 T},\quad c_d=\frac{\overline{c}_d L\omega_0}{\pi^2 T} \quad (2)$$

where $\overline{m}_e$ and $\overline{c}_d$ are defined in Eq. (3)[2]. ω_0 is the first natural frequency of the cable. L and T denote the cable length and tension.

$$\overline{m}_e=\beta^2 J=\left(\frac{2\pi}{L_d}\right)^2\frac{m\left(r^2+R^2\right)}{2}=2\left(\frac{\pi}{L_d}\right)^2\left(r^2+R^2\right)m,\quad \overline{c}_d=2\eta A/t \quad (3)$$

in which, β, J and L_d are the transmission ratio, the moment of inertia of the flywheel, and the pitch of the ballscrew. m, r and R are the mass, inside radius, and outside radius of the flywhee. η is the viscosity of the damping fluid. A and t are the area and the thickness of the shear plates. The complex eigenvalues are obtained by using a standard Galerkin method[3]. A parametric study is conducted for the IMD for a 19m long cable with $\lambda^2=7.95$ shown in Fig. 2-a. The IMD location (x_d) is taken as 2% of the cable length. The modal damping ratio of the first mode is shown various dimensionless IMD parameters in Fig. 2-b. The highest modal damping ratio of the first mode is obtained as 5.01%, which is significantly higher than 1% commonly provided by a conventional cable damper at the 2% location.

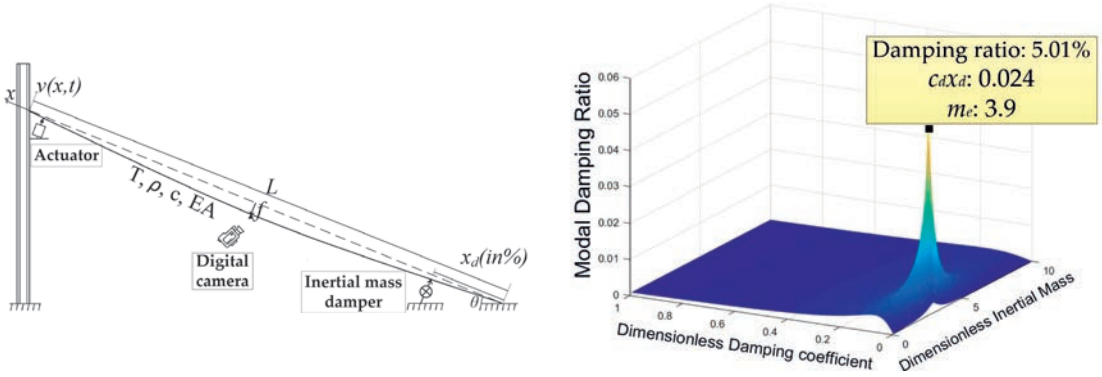

a. IMD-cable system b. Theoretical damping ratio for IMD design

Figure 2: IMD-cable system and modal damping ratio

EXPERIMENT

Experiments were carried out on a scaled cable structure with parameters shown in Tab. 1. A sinusoidal excitation at the first natural frequency (1.402 Hz) of the cable was applied perpendicularly to the cable. The excitation was removed after the vibration reached the steady state. Various IMD designs were considered, corresponding to 4 kinds of damping fluid with different viscosity (c_d) and 6 kinds of flywheels with different mass (m_e). The displacement responses were measured at the cable midpoint using a non-contact measurement with a digital camera. The modal damping ratio was evaluated from the decaying part of the response using a Hilbert-transform. The displacement responses of Group 2 (c_dx_d=0.024) are shown in Fig. 3.

Tab. 1 Cable parameters

Length (m)	Inclination (°)	E-module (×10^{6}N)	Mass per length (kg/m)	Tension (kN)	First natural frequency(Hz)	Sag (λ^2)
19.2	15	0.911	0.76	1.286	1.402	7.95

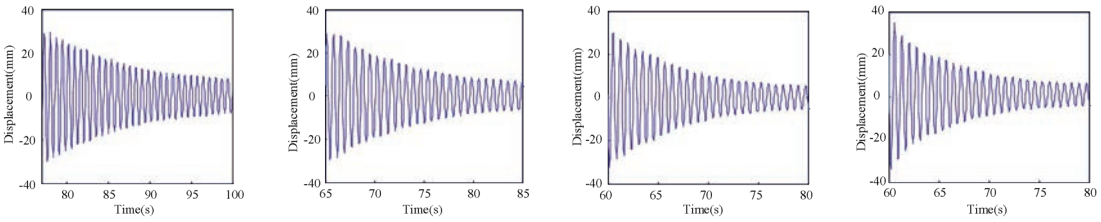

a. without flywheel b. with flywheel-1 (m_e=3.25) c. with flywheel-2 (m_e=3.49) d. with flywheel-3 (m_e=3.73)

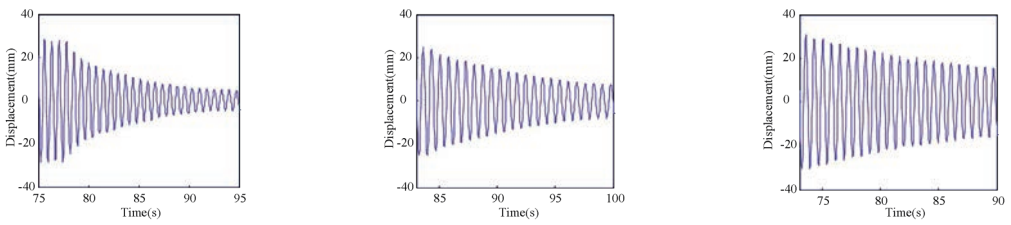

e. with flywheel-4 (m_e=3.9) f. with flywheel-5 (m_e=4.84) g. with flywheel-6 (m_e=6.43)

Figure 3: Displacement measurements for Group 2 (c_dx_d=0.024)

The comparisons of the modal damping ratios between the experiment and theoretical results are shown in Fig. 4. Good agreement can be observed between two results, except for Group 2. Case **e** of Group 2 is the optimal design case, whose first modal damping ratio is 5.01% as mentioned before. But the experiment result only reaches 2.08%. This may be due to the following reasons: 1. The numerical simulation shows that the modal damping ratio is very sensitive to inertial mass. The error in the machining error for the flywheel may cause big amplification in the modal damping ratio. 2. The friction in the ballnut and ballscrew is not included in the theoretical values, whereas the friction in the current IMD is fairly large. 3. The displacement of the IMD at the current experiment is very small. However, those problems may be resolved in the case of a real scale cable. But even so, the modal damping ratio of Case **e** is still 5 times higher than the conventional viscous damper under the same condition in Case **a** as in Fig. 3.

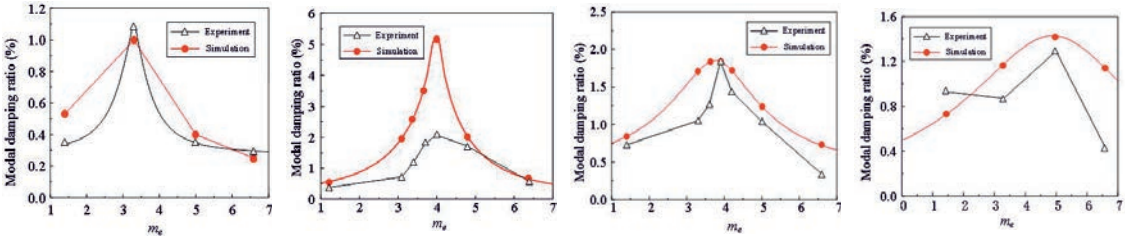

Group 1: ($c_d x_d$=0.008) Group 2: ($c_d x_d$=0.024) Group 3: ($c_d x_d$=0.04) Group 4: ($c_d x_d$=0.056)

Figure 4: Comparison of modal damping ratios

CONCLUSIONS

In this study, a prototype of an IMD is designed and manufactured. The numerical simulation of the IMD-cable system is carried out. The optimal parameters of the IMD are obtained considering the first mode. Experiment study shows the success of the vibration reduction of IMD. The performance of IMD is much better than the conventional viscous damper, in terms of modal damping ratio, though some experiment results show significant differences from the theoretical expectation.

REFERENCES

[1] Irvine, K., Caughey, H. M. (1974). The linear theory of free vibrations of a suspended cable. *Proceedings of the Royal Society of London. Series A, Mathematical and Physical Sciences*, **341**(1626), 299-315.

[2] Lu, L. , Duan, Y. F. , Spencer, B. F. , Lu, X. , Zhou, Y. (2017). Inertial mass damper for mitigating cable vibration. *Structural Control and Health Monitoring, e1986.*

[3] Johnson, E. A. , Spencer, B. F. , Fujino, Y. (1999) Semiactive damping of stay cables: a preliminary study, #362. *Proceedings of SPIE - The International Society for Optical Engineering, 1.*

Mechatronics and Automated Inspection

Vision-based bridge component recognition and position estimation toward rapid automated inspection

Y. Narazaki[1], V. Hoskere[2], B.F. Spencer jr.[3]

[1] *Department of Civil and Environmental Engineering, University of Illinois at Urbana-Champaign, USA. E-mail: narazak2@illinois.edu*

[2] *Department of Civil and Environmental Engineering, University of Illinois at Urbana-Champaign, USA. E-mail: hoskere2@illinois.edu*

[3] *Department of Civil and Environmental Engineering, University of Illinois at Urbana-Champaign, USA. E-mail: bfs@illinois.edu*

ABSTRACT

This research investigates implementation of human inspector's visual perception during bridge inspection to achieve autonomous navigation of UAVs for efficient data collection after damaging events (e.g. earthquakes). Using video data, implementation of two types of perception is investigated: the recognition of structural component types and their positions. The recognition of structural component types is implemented using fully convolutional networks (FCNs) combined with recurrent neural networks (RNNs), which provides consistent recognition results both in time and space. The estimation of position is implemented using CNN-SLAM algorithm, which estimates camera trajectories and depth maps from the image sequences. To facilitate the investigation of recognition and position estimation algorithms, synthetic environments were developed and used effectively. The perception of bridge components implemented in this study will be a building block for the autonomous navigating agents for rapid bridge inspections.

KEYWORDS: *Bridge inspection, computer vision, machine learning, Recurrent Neural Network (RNN), Simultaneous Localization and Mapping (SLAM)*

INTRODUCTION

Bridge is one of the important transportation infrastructure which needs to be maintained appropriately both in normal and emergency times. On the other hand, bridges spread over broad areas, which makes the visual inspection by human inspectors time-consuming and labor-intensive. The demands for the efficiency of bridge inspections are particularly difficult to meet after damaging events, such as earthquakes and typhoons, because limited number of inspectors need to evaluate bridges in the

entire affected area within a limited amount of time. To facilitate rapid inspection under the scarcity of time and resources, automation of one of the most time-consuming and labor-intensive part of the bridge inspection is desired, namely, accessing and navigating through the bridges to collect visual information of the structural components of interest. Implementation of human inspector's perception during the bridge inspection is a key step toward autonomous navigation and data collection for rapid bridge inspection. This research investigates the recognition of structural component types and their positions using video data. The recognition of structural component types is implemented using fully convolutional networks (FCNs) combined with recurrent neural networks (RNNs), which provides consistent recognition results both in time and space. The estimation of position is implemented using CNN-SLAM algorithm, which estimates camera trajectories and depth maps from the image sequences. The perception of bridge components implemented in this study will be a building block for the autonomous navigating agents for rapid bridge inspections.

METHODS

The recognition of bridge component types are implemented by combining single image-based semantic segmentation algorithm (Fully Convolutional Networks, or FCN) with the recurrent neural network units [1], [2]. The single image-based bridge component recognition using FCN takes a primary role of identifying types of bridge components in complex scenes using network configurations investigated in [3]–[5]. While the single image-based FCN can identify bridge components when the image contains global context, the approach faces increasing difficulty when the video zooms up to parts of the structural components and starts lacking the high-level scene contexts. To address the challenge, Recurrent Neural Network (RNN) units were inserted on top of the FCN to

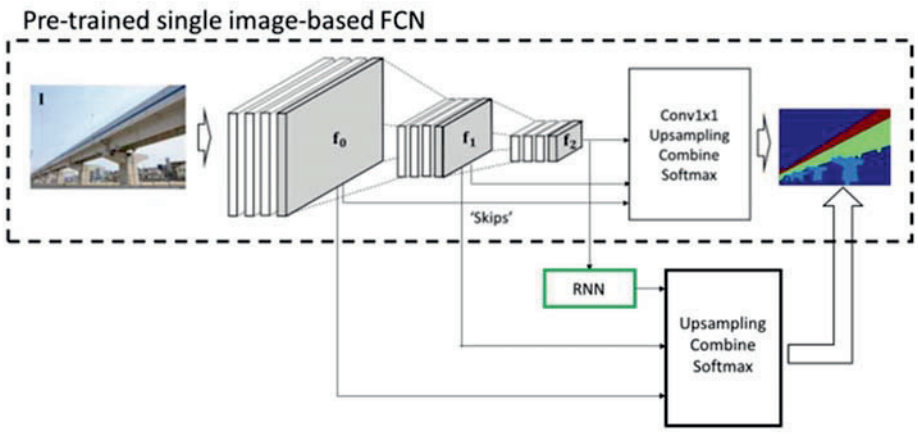

Figure 1: Network configuration for the recognition of bridge component types[1].

store information from previous frames as hidden states [1]. In particular, this research

uses ConvLSTM[6], which is one of the powerful RNN architecture to model long-term patterns appearing in sequences of 2D data. By combining the output of the ConvLSTM units and lower-level features from the FCN, the resulting semantic segmentation was consistent both in time and space.

After recognizing bridge component types, 3D locations of the target structural components need to be identified to achieve desired autonomous UAV navigation for rapid bridge inspection. Localization of objects using incoming video stream is categorized into a problem of Simultaneous Localization and Mapping (SLAM) [7], [8]. This research investigates the use of CNN-SLAM algorithm [9], which combines CNN-based dense prediction and direct SLAM approach to get dense and accurate depth estimation using video stream. In particular, this research used deep FCN with 58 convolutional layers to predict depth map.

Collection of data used to evaluate algorithms discussed in this research is not straightforward. For the recognition of bridge component types using RNN, annotated video data is needed to train and test the image-processing algorithms. However, labelling each frame of video data is labor intensive and almost impractical. For position estimation, we need datasets with ground truth values to validate the performance of the algorithms. To address this challenge, this research investigated the use of synthetic data using Unity3D game engine [10]. For the tasks of bridge component recognition, a synthetic environment of concrete girder bridge with surrounding environment was created, and a UAV was flied randomly around the bridge to collect video data mimicking actual bridge inspection process. For the CNN-based depth prediction as part of the CNN-SLAM algorithm, large-scale city model and a UAV navigating randomly are used to train the network for broad range of views in urban environments.

CONCLUSIONS

This research investigated the computer implementation of human inspector's perception during inspection process to achieve autonomous UAV navigation for efficient rapid bridge inspection. The research discussed two tasks performed by human inspectors to understand the surrounding environment: recognition of bridge component types and estimation of 3D locations of the identified components. Using synthetic video data of concrete girder bridge and large-scale urban city section, RNN units for the recognition of bridge component types and FCN for depth prediction for the CNN-SLAM algorithms were trained and integrated into the entire framework. The bridge component recognition and localization investigated in this research will be a critical component of the desired autonomous system for the rapid bridge inspection.

REFERENCES

[1] Narazaki, Y., Hoskere, V., Hoang, T. A., and Spencer, B. F. (2018) Automated Bridge Component Recognition using Video Data, The 7th World Conference on Structural Control and Monitoring (7WCSCM), Qingdao, China, July 22-25, 2018.

[2] Spencer, B. F., Hoskere, V., and Narazaki, Y. (2019) Advances in Computer Vision-Based Civil Infrastructure Inspection and Monitoring, Engineering, vol. 5, no. 2, pp. 199–222.

[3] Narazaki, Y., Hoskere, V., Hoang, T. A., Fujino, Y., Sakurai, A., and Spencer, B. F. Vision-based Automated Bridge Component Recognition with High-level Scene Consistency, Submitt. to Comput. Civ. Infrastruct. Eng., *under review*.

[4] Narazaki, Y., Hoskere, V. Hoang, T. A., and Spencer, B. F. (2017) Vision-based automated bridge component recognition integrated with high-level scene understanding, The 13th International Workshop on Advanced Smart Materials and Smart Structures Technology (ANCRiSST), Tokyo, Japan, July 22-23, 2017.

[5] Narazaki, Y., Hoskere, V., Hoang, T. A., and Spencer, B. F. (2017) Automated Vision-based Bridge Component Extraction Using Multiscale Convolutional Neural Networks, The 3rd Huixian International Forum on Earthquake Engineering for Young Researchers, Urbana-Champaign, USA, Aug 11-12, 2017.

[6] Shi, X., Chen, Z., Wang, H., and Yeung, D.-Y. (2015) Convolutional LSTM Network: A Machine Learning Approach for Precipitation Nowcasting, Adv. neural Inf. Process. Syst., pp. 802–810.

[7] Engel, J., Schöps, T., and Cremers, D. (2014) LSD-SLAM: Large-Scale Direct Monocular SLAM, Springer, Cham, pp. 834–849.

[8] Mur-Artal, R., Montiel, J. M. M., and Tardos, J. D. (2015) ORB-SLAM: A Versatile and Accurate Monocular SLAM System, *IEEE Trans. Robot.*, vol. 31, no. 5, pp. 1147–1163.

[9] Tateno, K., Tombari, F., Laina, I., and Navab, N. (2017) CNN-SLAM: Real-Time Dense Monocular SLAM With Learned Depth Prediction, in CVPR, 2017, pp. 6243–6252.

[10] Unity website: https://unity.com/

A Study of FLC Application for Robot Manipulator Suspended from Crane Hoist Model

C. Peng[1], Y. Jiang[2], J. Zhang[3]

[1] *School of Construction Management Technology, Purdue University, USA.*
E-mail: peng211@purdue.edu

[2] *School of Construction Management Technology, Purdue University, USA.*
E-mail: jiang2@purdue.edu

[3] *School of Construction Management Technology, Purdue University, USA.*
E-mail: zhan3062@purdue.edu

ABSTRACT

Cranes are commonly used to lift and move heavy objects in construction projects. Complex mobile robotic systems have recently expanded to be configured for a wide variety of new ground-based applications in construction projects. However, it is difficult to reach workspace at elevations for these heavy robots. To address that, the author focuses on controller design using cranes carrying ground-based robotic system, which enables the heavy robots to reach the entire workspace with the help of the crane. The main challenge is the end point position control of operating robot manipulators when hoisted by a crane in a dynamic environment with uncertain vibrations and movements. Due to the complexity of this problem, the model used in the simulation is simplified and the position control scheme decouples the control of crane pendulum and robot manipulator. First, numerical modeling and data generation performed for kinetic and dynamic analysis of the system simplified as a 2DOF robot connected with a double pendulum system in free vibration. Second, ANFIS fuzzy logic controllers are trained and controller system structure applied to enable the manipulator model following the prescribed trajectory. Subsequently, a Multi-body model was built for motion visualization and simulation shown successfully damping the vibration was conducted using MATLAB and Simulink. Finally, results and limitations of this study are discussed.

KEYWORDS: *Fuzzy Logic Controller, ANFIS, double pendulum, robot manipulator, simulation test*

INTRODUCTION

The control of crane systems in construction is a well-established research field.[3] Most works focused on anti-sway with trolley motion. In the meantime, ground-based mobile robot system expanded applications in construction filed. Also previous works on oscillatory base robot manipulator have been discussed [1] based on lumped mass with one translate motion only. Therefore, developing efficient controlling system to

extend the capability of heavy robots operating in higher workspace with the help of widely equipped cranes is essential. This paper proposed using cranes carrying a platform with ground-based robotic systems mounted to it and focused on position control of the manipulator operating under vibration between the crane hoist and the robot. This application use ANFIS based fuzzy logic position control scheme decouples the control of crane pendulum and robot manipulator and create simulation model with planiar motion constraints testing the results.

MODEL FORMULATION

Mathematical model of the double pendulum crane system and simplified 2DOF planiar robot manipulator system connected at the robot base is obtained from independently known dynamics of the two subsystems. Figure 1 below shows the schematic view of physical model of the two systems separately, where active payload on the left and the oscillatory base x_b on the right are jointly considered as the robot base in our combined model. The dynamic EOM can then be represented as [1]

$$\begin{bmatrix} M_r(q) & M_{br}^T(x) \\ M_{br}(x) & M_b + M_{b/r}(\mathrm{x}) \end{bmatrix} \begin{Bmatrix} \ddot{q} \\ \ddot{x_b} \end{Bmatrix} + \begin{bmatrix} C_r(q,\dot{q}) & C_{br}(\mathrm{x},\dot{x}) \\ C_b\dot{x_b} & C_{br}(\mathrm{x},\dot{x}) \end{bmatrix} + \begin{bmatrix} 0 & 0 \\ 0 & K_b \end{bmatrix} \begin{Bmatrix} q \\ x_b \end{Bmatrix} = \begin{bmatrix} \tau_r \\ \tau_b \end{bmatrix} \quad (1)$$

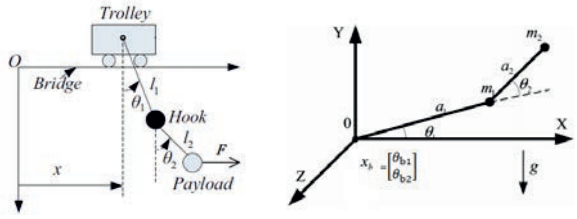

Figure 1: schematic view of the subsystems physical model.

MODELING INVERSE KINEMATICS

In a two-joint robotic arm system, in order to control the arm to perform tasks it is designated to do, a typical problem is the inverse kinematic equation given the desired motion of the free end of the second link. It is possible to mathematically deduce the angles at the joints given the desired location of the end point. Fuzzy logic controller used here taking advantage of solution of the kinetic equation of motion of a fixed base 2DOF manipulator and obtain the training dataset using the numerical output of desired motion as the input. This approach can train ANFIS fuzzy logic controllers without requiring initial training data from experiment or simulation. In the generation of the training data, boundaries are set as maximum angles. Two ANFIS controllers are trained for q_1 and q_2 separately and then validation error test proves the controllers give low errors within desirable operating range $[-\pi,\pi]$, where the trained ANFIS networks are then used as a part of a larger control system with compensation from oscillatory of the robot base.

TRAINING ANFIS MODEL

The adaptive network-based fuzzy inference system (ANFIS) has been used to optimize the fuzzy IF-THEN rules and membership functions to derive a more efficient fuzzy control.[2] The structure of the ANFIS is comprised of five layers (Fig2). Neuro-Fuzzy Designer in MATLAB is used to design and train the controllers. The algorithm uses the Takagi-Sugeno-Kang (TSK) inference system which assign arbitrarily parameters and performed fuzzy reasoning for the training data to tune the parameter sets.[1] Two controller *yd2q1* and *yd2q2* are trained to control q_1 and q_2 from desired motion coordinates. Two parameter {a,b,c} sets of the bell-shaped membership functions chose for each input are the training results to calculate the membership values.

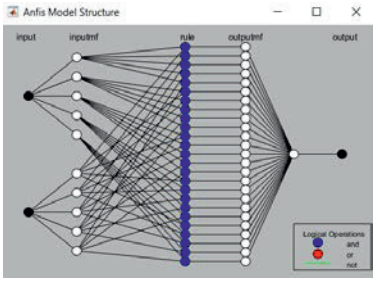

Figure 2: Adaptive network-based fuzzy inference system (ANFIS) model design structure.

SIMULATION STUDY

A 3D Simscape Multibody model was built for motion visualization. This model contains simplified 3D manipulator arms and pendulum. Four joints needed to be controlled can only rotate in the X-Z axis plane. Details of the Simscope model of two subsystems shown in Figure 3.

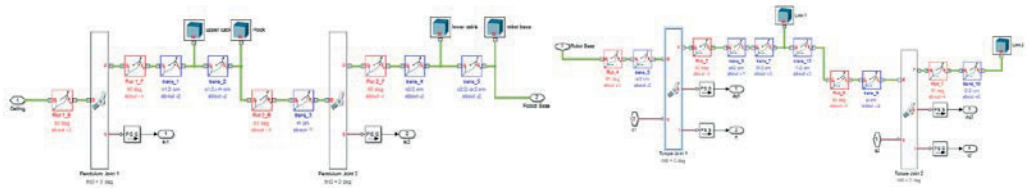

Figure 3: Simscope model of Double-pendulum system (left) and 2DOF manipulator (right)

The models created are then used as well as the two ANFIS controllers trained before as parts of a larger control system in Simulink (Fig4).

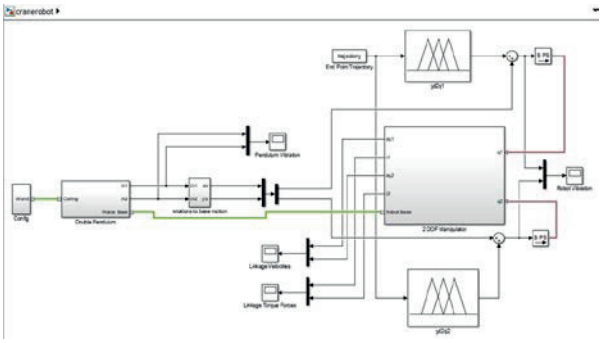

Figure 4: Final Simulink (Simscope) model of the controller system.

Simulation runs for a short circular path of the end point of manipulator and the motion and force damping results of robot arms vibration angles q, their velocity $\dot{q}$, pendulum vibration angles θ, and the torque force of robot joint actuators τ shown in Figure 5.

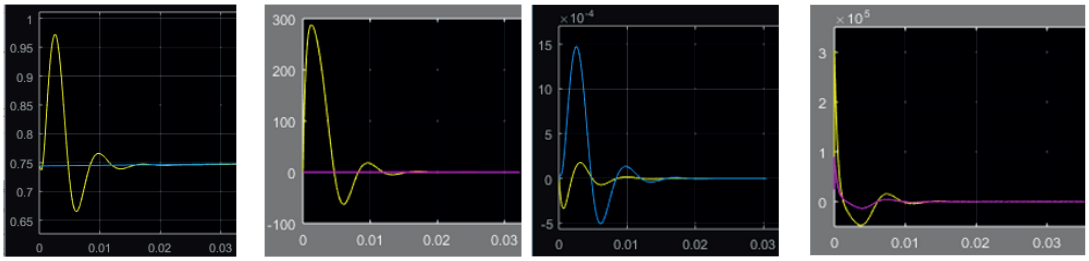

(a) (b) (c) (d)

Figure 5: Simulation test scope result of (a) Robot arms vibrations q, (b) Robot arm rotate velocities $\dot{q}$, (c) Pendulum vibrations θ, and (d) Torque force of robot joint actuators τ.

CONCLUSIONS

A FLC application of training and testing of ANFIS fuzzy logic controllers using MATLAB and Simulink with a simulation study has been proposed. The strategy trained FLC using obtained training dataset from numeric data generation and then applied them to enable quick damping end point motion of the simplified 4DOF planiar manipulator system caused from dynamics of a robot system suspended from crane hoist although the model are simplified under 2D rotations. More future works can be followed : 1. Update and retrain the controller model for dynamic system with more Degree of freedoms; 2. Use the industrial fetch robot or design simple experiment manipulators, set up tracking sensors as experiment apparatus for position and force tracking control simulation. 3. Compare tracking results and test the efficiency of the controller with other strategies such as PID based on some experiment data.

REFERENCES

[1] Lin, J, and Lin, C. (2015). Hybrid fuzzy position/force control by adaptive network-based fuzzy inference system for robot manipulator mounted on oscillatory base. Journal of Vibration and Control, 21(10), 1930-1945.

[2] Lin, and Huang. (2007). A hierarchical fuzzy approach to supervisory control of robot Manipulators with Oscillatory Bases. Mechatronics 17.10 (2007): 589-600.

[3] Ramli, M, Abdullahi, J, and Lazim. (2017) Control Strategies for Crane Systems: A Comprehensive Review. Mechanical Systems and Signal Processing 95.C: 1-23.

[4] Zhang, M, Rong, T, and Li. (2016). Adaptive tracking control for double-pendulum overhead cranes subject to tracking error limitation, parametric uncertainties and external disturbances. Mechanical Systems and Signal Processing, 76-77, 15-32.

[5] Harber, J. A., and Singhose, W. (2016). (n.d.). A Dual Hoist Robot Crane for Large Area Sensing.

Damage Detection of Vision-based Bridge Inspection System using Unmanned Aerial Vehicle

J.H. Lee[1], S. Yoon[1], J.W. Park[2], H.J. Jung[3]

[1, 3] *Dept. of Civil and Environmental Engineering, Korea Advanced Institute of Science and Technology, Republic of Korea.*

E-mail: archi_tensai@kaist.ac.kr(J.H.Lee), yss3366@kaist.ac.kr(S.Yoon), hjung@kaist.ac.kr(H.J.Jung)

[2] *Dept. of Urban Design and Studies, Chung-Ang University, Republic of Korea.*

E-mail: jongwoong@cau.ac.kr

ABSTRACT

In this paper, bridge inspection techniques based on an unmanned aerial vehicle (UAV) were analyzed from the point of view of actual field application and methods possible solutions for addressing the problems were discussed. In particular, a new no-reference quality measure was proposed to solve the quality issue, and an experiment was conducted to detect cracks on the surface of actual bridges. In addition, in order to solve the damage localization problem, a matching method based on the features between the high-resolution image and the image including the damage was applied. As a result, it was able to successfully detect the cracks with an error within 0.14 mm.

KEYWORDS: *UAV, Bridge Inspection, Computer Vision, Damage Detection.*

INTRODUCTION

As the aging of bridges became a social issue, many researchers became interested in the maintenance technology to check and diagnose the objective condition of structures. However, as the number of inspection areas and target structures increased, existing maintenance methods that rely on visual inspection through workers were inefficient in terms of time and cost, and it revealed the limitation that the results depend on the worker's subjectivity. On the other hand, an inspection technology using an unmanned aerial vehicle (UAV) equipped with high-performance video equipment had the advantage of being able to detect and inspect damage occurring in various parts of bridges, and it was possible to access easily the areas where inspection worker were difficult to access so it emerged as an alternative to the existing method. However, there was a false-alarm issue that it was difficult to detect various damages such as micro cracks when applying a computer vision based novel technology to a bridge inspection method using UAV. In order to solve the false-alarm issue, research was conducted to apply the deep-learning technology using learning images of various shapes and sizes (Cha, 2018). The application of the deep-learning technology solved false-alarm issues and resolved localization issues of cracks to enable multiple high-resolution image processing based on the fast computing speed.

In this paper, bridge inspection techniques based on UAV were analyzed from the point of view of actual field application and possible solutions for addressing the problems were discussed. In particular, we developed a measure related to image quality and applied the Mask-RCNN algorithm and the computer vision technology to confirm the size of the crack, and the position of the crack was determined by using the high resolution matching image.

PROPOSED METHODOLOGY

As shown in figure 1, the bridge inspection scenario using UAV was composed of image acquisition, image quality evaluation, and quantification based on deep-learning and image processing technique (IPT), and damage localization using high-resolution image.

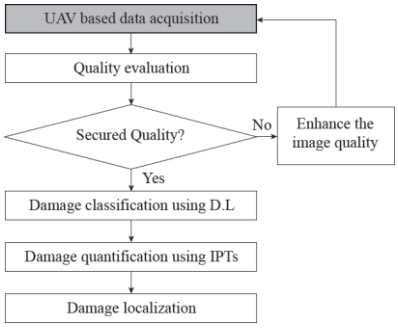

Figure 1. Mission flow for bridge inspection using UAV systems

In the quality evaluation step, a new quality measure was proposed to evaluate the degree of motion blur that could occur in the images taken by the UAV. Since the variance of the gray intensity was lowered when blur occurred, the sum of the variance of gray intensity (SGV) in the horizontal direction was set as a reference as shown in Eq.1.

$$\boldsymbol{SGV_k} = \sum_{i=1}^{M}\sum_{j=1}^{N}\frac{\sqrt{\left(G_k(i,j)-G_k(i,j+1)\right)^2+\left(G_k(i,j)-G_k(i+1,j)\right)^2}}{\sqrt{M^2+N^2}} \quad (1)$$

Where, SGV_k represents the quality measure of the kth image, M presents the number of horizontal pixels in the image, N represents the number of vertical pixels in the image, G_k means the gray-intensity function of the kth image.

The deep-learning and image processing techniques were applied in this study, which was excellent for classifying and detecting various types of damage (Kim and Cho, 2019). In addition, PTgui pro Software was used to match the feature points of multiple single images. Based on 103 4K images, the result was 28436 x 13003 pixels.

EXPERIMENTAL VALIDATION

In order to verify the proposed bridge inspection technology, an experiment was conducted to detect and quantify the damage using the data taken from the bridge. The

target bridge was a concrete box girder bridges with various damages, and target area was selected as one-side of a pier. The UAV used in the experiment was designed for bridge inspection, and equipped with various sensors such as gimbal, IMU, Camcorder. The resolution of the aerial imagery was 4K (3840 x 2160) and the pixel resolution was 0.28 mm/pix.

Figure 2. Target bridge and inspection UAV

After the quality evaluation process for a total of 103 frames covering the entire area, we confirmed whether the deep learning algorithm can be applied to the frame. In the case of the 11th frame as seen figure 3, since the quality score was distributed around the average value, the next step could be applied.

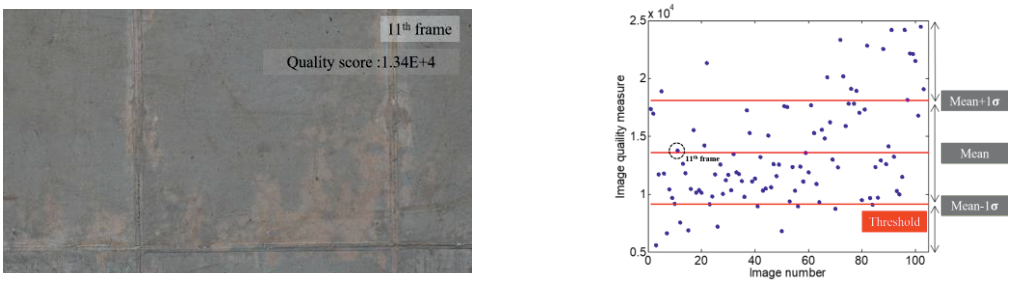

(a) Quality score of 11th frame (b) Scoring the entire frame

Figure 3. The result of applying quality measurement to UAV imagery

After that, damage detection step using deep-learning was performed on frames satisfying a certain level of quality threshold, and the result was shown in figure 4.

Figure 4. Some results of classification and identification after applying Mask-RCNN

The cracks were classified by applying the Mask-RCNN to 103 frames covering the entire inspection area. Six cracks were detected in the 11th frame. The size of the cracks

was quantified using image processing and compared with the actual values measured using an actual crack detector. As shown in Table 1, when the size of the cracks on the bridge surface was quantified using UAV, it was generally estimated to be larger than the actual crack size. As seen from all the cases, the error was estimated to be within 0.14 mm, and this error can be regarded as an error depending on the measurement position of the crack. In addition, since the position of the frame containing the cracks was confirmed in the entire stitched image.

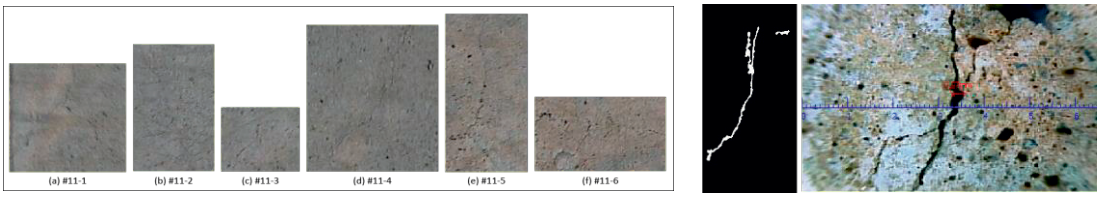

Figure 5. Cracks and quantification results included in 11th frame

Tab. 1. Comparison of quantified cracks with actual measured values

(mm)	**Crack 1**	**Crack 2**	**Crack3**	**Crack4**	**Crack5**	**Crack6**
Estimated	*0.28*	*0.28*	*0.56*	*0.84*	*0.28*	*0.56*
Measured	*0.20*	*0.22*	*0.42*	*0.76*	*0.27*	*0.50*
Error	*+0.08*	*+0.06*	*+0.14*	*+0.08*	*+0.01*	*+0.06*

CONCLUSIONS

In this study, we proposed a general inspection scenario to solve the problem from the viewpoint of actual field application, which was not covered in the previous study of inspecting the bridge using the UAV. In order to secure the quality of images captured through UAV, a new quality measurement was proposed. Also deep learning and IPT were used to quantify the size of the cracks and to solve the damage localization issue using stitched images. As a result of applying it to the actual site, it was able to successfully detect cracks on the surface, and the error was within 0.14 mm.

ACKNOWLEDGEMENT

This research was funded by Construction Technology Research Program funded by Ministry of Land, Infrastructure and Transport (MOLIT) of Korean government, grant number 19SCIP-C116873-04.

REFERENCES

[1] Cha, Y. J., Choi, W., Suh, G., Mahmoudkhani, S., & Büyüköztürk, O. (2018). Autonomous structural visual inspection using region-based deep learning for detecting multiple damage types. Computer-Aided Civil and Infrastructure Engineering, 33(9), 731-747.

[2] Kim, B., & Cho, S. (2019). Image-based concrete crack assessment using mask and region-based convolutional neural network. Structural Control and Health Monitoring, e2381.

Design and simulation of a wall-climbing drone for bridge inspection

M. Romano[1], E. Ottaviano[1], A. Gonzalez-Rodriguez[2], F.J. Castillo-Garcia[2], D.A.B. Rodriguez-Rosa[2]

[1] *Department of Civil and Mechanical Engineering, University of Cassino and Southern Lazio, Italy.*
E-mail: ***ottaviano@unicas.it***

[2] *School of Industrial Engineering of Toledo, University of Castilla-La Mancha, Spain.*
E-mail: ***fernando.castillo@uclm.es***

ABSTRACT

Large research activity is devoted to the inspection of large structures difficult to access using mobile robots, mainly UAVs, hybrid mobile robots, and climbing robots. The latter type requires the installation of additional infrastructure or the use magnetic-based technology or vacuum adhesion. UAVs represent for outdoor inspection the most efficient solution, offering an excellent platform to carry devices and sensors. Beside these great advantages there are some limitations, one is related to the security distance that must be kept during the flight operation, which does not allow to the system to get close or attached to the surface to explore. In addition, for the inspection of civil structures exposed to harsh environmental conditions such as strong winds, this approach is exposed to risk of collision and damage of the robot. In order to overcome those limitation related to vertical surfaces, large infrastructures and outdoor inspection, wall climbing drones have been developed in the very recent years. According to this new design concept, the robot has two operation modes, it can fly like drones but it can stick and climb a vertical surface, like a wall-climbing robot. The motivation for developing this kind of robot is to create hybrid solutions unaffected by the environmental conditions, as well as the wall conditions like surface material or shape. Wall-climbing systems are based on wall-sticking mechanism, tilt-rotor-based drones, or multi oriented rotors. In this paper, we propose and discuss the design and simulation of a wall-climbing drone based on a multirotor with legs equipped by passive wheels.

KEYWORDS: *Robotics, Mechatronics, Bridge Inspection; Wall-Climbing Drone*

INTRODUCTION

The integrity of large structures like bridges, buildings, large aircrafts, solar panels and wind turbines, is closely related with security. Nowadays, due to the aging of large structures and potential concerns about their potential collapse, a great interest in

structural health monitoring has highlighted all over the world. In particular, steel structures and steel bridges, constituting a major part in civil infrastructure; require adequate maintenance and health monitoring. All over the world, many thousands of steel bridges are either deficient or functionally obsolete, which likely presents a growing threat to people's safety. Traditionally, rope certified bridge inspectors analyze steel bridges manually. Often, it is dangerous for the inspectors to climb up or hang on cables to inspect large bridges with high structures. In addition, reports from visual inspection may vary among inspectors; therefore, the structural health condition may not be assessed precisely. Many efforts have been devoted in the recent years to the inspection of large structures difficult to access taking advantage of automatic or robotic solutions like mobile robots [1], UAVs [2], and wall-climbing robots [3]. Referring to bridge inspection, lately robotic solutions deal with the latter two types, UAVs and wall-climbing systems equipped with non-destructive evaluation systems such as a camera and a 3D structure sensor [4]. In the very recent years, hybrid solutions named as wall-climbing drones have been developed. These new systems can fly like drones but can also stick and climb a vertical surface, as wall-climbing robots. In particular, those systems use a perching technique that does not require the installation of additional infrastructure. Developed solutions are SCAMP (Stanford Climbing and Aerial Maneuvering Platform) proposed in [5]; VOLIRO, which is a solution with 6 multi oriented rotors, which are capable of orienting by 360 deg independently [6]. EJBOT is a double rotor tracked robot, in which the rotors are used to keep the contact with the vertical wall [7]. In this paper, we propose the design and simulation of a wall-climbing drone, and a first design prototype is under construction based on the obtained results of the simulations.

MECHANICAL DESIGN OF THE WALL-CLIMBING DRONE

The proposed robot should possess the following characteristics: two operation modes namely fly and motion over a vertical surface by keeping the contact at a given distance; ability to carry suitable sensors; low-cost and easy in use. The motivation is to create a wall-climbing robot that is unaffected by the environmental conditions, as well as the wall condition. It is intended to be used either for indoor and outdoor applications. Wall-climbing systems that can be used are wall-sticking mechanism, tilt-rotor-based drones, or multi oriented rotors. We have chosen to develop a drone with four fixed rotors (quadrotor) for flying mode and modify the initial design adding two rotors with fixed axes mounted orthogonally with respect to the first four. Additionally, two mechanical limbs with wheels at the end tips are used. The additional two rotors give suitable propulsion to adhere to the vertical wall, the wheels at the leg tips allow to climb with low friction. The proposed solution is shown in Figure 1.

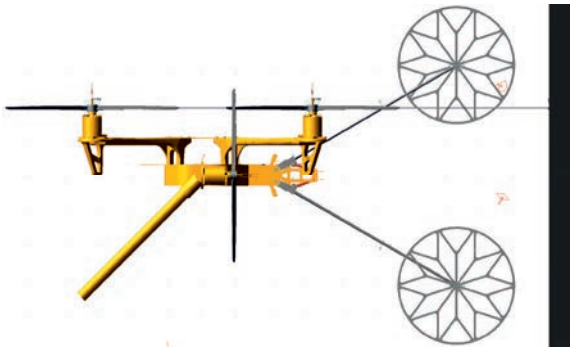

Figure 1: Mechanical design solution for the proposed wall-climbing drone.

Two legs equipped with lightweight wheels are used to keep the contact with the wall. Stability is ensured with suitable springs that allows damping and mitigate the contact with the surface to inspect. The spring design is shown in Figure 2. Main characteristics of the designed spring are K=1000N/m; C = 100 Ns/m; L = 32.34mm; L_0 (F=0) = 30mm. The legs' maximum span ranges from 60 to 140 deg.

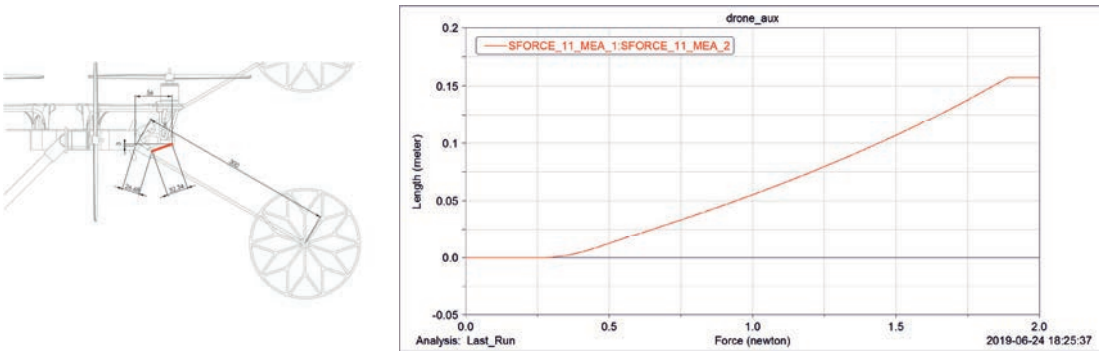

a) b)

Figure 2: Spring: a) mechanical design; b) stiffness of the system.

SIMULATION RESULTS

A simulation of the operation of the designed wall-climbing drone has been carried out to size the actuation and spring to allow the robot sticking and climbing a vertical surface. A motion sequence of the simulation is shown in Figure 3, in which the approach and contact with a vertical wall is considered. For the proposed simulation, only the horizontal propulsion is taken into account, with a motion law of the motors displayed in Figure 4a. The contact with the wall starts, and then the horizontal propulsion force is increasing to get the drone closer to the wall. Distance from the wall is displayed in Figure 4b. It is worth to note that the force of the propellers does not start from zero, there is an initial force required to approach the wall. Then this force grows so that the drone gets closer to the wall.

Figure 2: Motion sequence of the simulation for the wall-climbing drone in Figure 1.

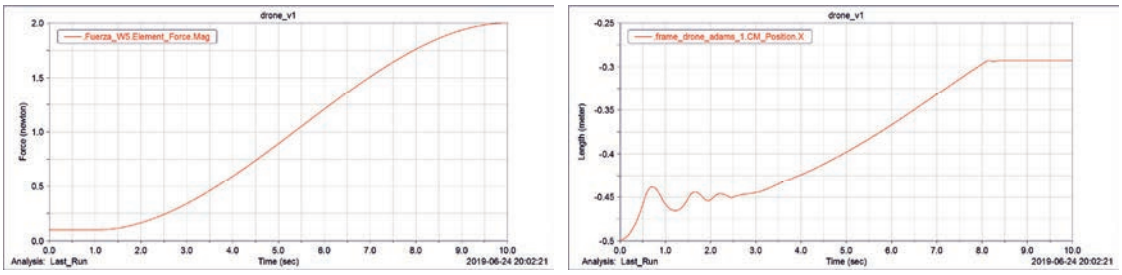

a) b)

Figure 3: Simulation for the contact: a) horizontal propulsion; b) distance from the wall.

CONCLUSIONS

In this paper, we have presented the design and first simulation results of a wall-climbing drone for bridge inspections. Based on the results of these simulations, a prototype is under construction for experimental tests.

ACKNOWLEDGMENTS

This paper is a part of a project that has received funding from the Research Fund for Coal and Steel under grant agreement No 800687.

REFERENCES

[1] Ottaviano E., Rea P., Castelli G., (2014), THROO: a Tracked Hybrid Rover to Overpass Obstacles, *Advanced Robotics*, Vol. 28, Iss. 10, pp. 683-694, 2014, **doi=10.1080/01691864.2014.891949**.

[2] Wilkins W., Mitchell G (2017) Drone Surveying: 3-D Enabled Automation of Roofing and Building Envelope Structures, *32nd RCI International Convention and Show*, pp. 247-263.

[3] Nansai S. ,Mohan R. E. (2016) A Survey of Wall Climbing Robots: Recent Advances and Challenges, *Robotics* 2016, Vol. 5, pp.14; **doi:10.3390/robotics5030014**

[4] Gattulli V., Ottaviano E., Pelliccio A. (2018) Mechatronics in the Process of Cultural Heritage and Civil Infrastructure Management. In: Ottaviano E., Pelliccio A., Gattulli V. (eds) Mechatronics for Cultural Heritage and Civil Engineering, **https://doi.org/10.1007/978-3-319-68646-2_1**

[5] Web: http://thenexttech.startupitalia.eu/53150-20160329-scamp-drone-arrampica-superfici, 2019

[6] Web: http://www.smartdrones.fr/voliro-un-drone-acrobate-a-6-rotors-2/0017062, 2019

[7] Alkalla M. G., Fanni M. A., Abdelfatah M. M., (2018) A Novel Propeller–Type Climbing Robot for Vessels Inspection, *IEEE International Conference on Advanced Intelligent Mechatronics* (AIM).

Augmented Reality Interface with Strain Gauge Sensors for Railroad Bridge Inspections

M. Agüero[1], D. Maharjan[1], M. Rodriguez[1], F. Moreu[1]

[1] *Department of Civil, Construction, and Environmental Engineering, University of New Mexico, USA*
E-mail: magueroinjante@unm.edu
E-mail: dmaharjan@unm.edu
E-mail: mdpilar@unm.edu
E-mail: fmoreu@unm.edu

ABSTRACT

The application of sensors in structural health monitoring (SHM) is of utmost importance, as they record the behavior of structures and help engineers to make and prioritize informed decisions about necessary repairs or maintenance procedures. However, many sensors that are currently used require further processing of information obtained in the field later at the office or the decision-making headquarters. This approach to SHM delays decision making. Wireless sensors networks (WSN) are designed to analyze the data and present decisions remotely, however there is still a gap between remotely operated WSN and industry decisions. In general, industry relies on inspectors' decisions. If WSN could inform inspectors, industry decisions would be improved by data. The application of Augmented Reality (AR) tools, such as HoloLens, permits direct interaction with the real world for engineers and enables visualization and integration of SHM with inspectors at the field. For example, HoloLens make it possible to visualize information coming from the sensors in a graphic form in real time. This paper shows how to enable effective communication between the sensors and the HoloLens.

KEYWORDS: *Augmented Reality, Wireless Sensors, Strain Gauge Sensor, Real-time Monitoring*

INTRODUCTION

This paper presents a case study of the application of Augmented Reality (AR) tools to improve the availability of wireless sensors networks (WSN) data. SHM involves using an on-site, non-destructive sensing technology in order to determine whether a structure has experienced damage, and in case damage has occurred, to determine its location and severity. SHM technologies heavily rely on the application of sensors and the quality of data transferred by sensors. Sensors record the behavior of structures and help structural engineers to make and prioritize informed decisions about

necessary repairs, replacement of infrastructure or maintenance procedures. In the initial stages of the development of SHM technologies, contact sensors were used to detect damage on site. However, contact technologies require considerable human operation for sensor application, which makes them expensive to run. As an alternative, non-contact sensing approaches have been proposed, which rely on digital cameras and vision sensing algorithms. The non-contact technologies have shorter deployment time, require less frequent human operation on site, and they are more economical to operate. However, although many of them provide the necessary quantitative information, it is often difficult to collect the necessary data in the field, and it is frequently necessary to perform further processing of the data obtained in the field later in the office. Such an approach to data collection and analysis delays decision making. WSNs are designed to analyze the data so that the decisions could be performed remotely, but there is a gap between remotely operated WSNs and the way decisions are made in the industry. The industry relies on inspectors' decisions: if WSN provide direct information to inspectors, the industry decisions will be improved by the obtained data. The communication and the data transfer between WSN and databases can be significantly improved through the application of Augmented Reality (AR) tools. AR overlays the known attributes of an object in the corresponding position on the computer screen. In this way it allows integration of reality with a virtual representations provided by a computer in real time, so it permits engineers to directly interact with the real world and it enables visualization and integration of SHM with inspectors at the field. For example, HoloLens make it possible to visualize information coming from the sensors in a graphic form in real time, which enables effective communication from sensors to a database in real time in a reliable way. In this way inspectors can observe augmented data and compare it across time and space, which leads to the prioritization of infrastructure decisions based on accurate observations.

THEORETICAL STRAIN

This section outlines the application of a low-cost, battery-powered wireless intelligent sensors called Strain Gauge, which measures strain of different applications. For example, since strains are directly related to the structural condition of bridges, they can be applied to determine bridge serviceability. Furthermore, this section introduces the principles of estimating strain from strain gauge. As shown in Fig. 1, the strain is calculated at a specified point where the strain gauge is attached. This value is derived utilizing the strain-stress formula and deflection due to point load. As the equation is only valid for elastic behavior of ruler, some discrepancy with the experimental data is expected.

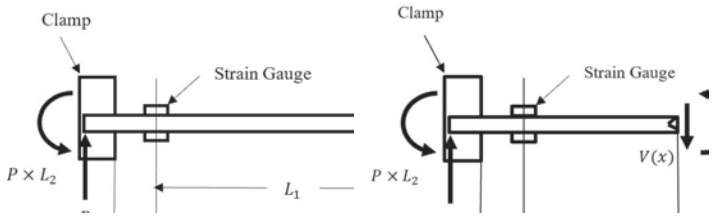

Figure 1: Theoretical strain definition.

Eq. (1) will define the theoretical strain, ε :

$$\varepsilon = \frac{Mc}{EI} \quad (1)$$

where, M represents the moment at L_1 given by $P \times L_1$, E is the Young's modulus of elasticity, I is the second moment of inertia and c is the maximum distance of compression from elastic neutral axis.

EXPERIMENT VALIDATION, RESULTS, AND EVALUATION

A cantilever ruler is utilized as the test specimen to conduct the experiment, see Fig. 2.

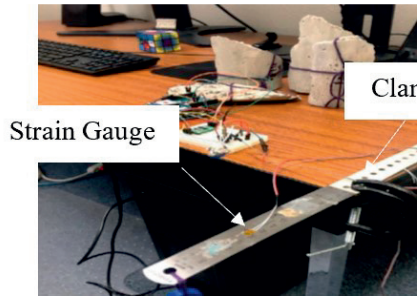

Figure 2: Experimental Set-Up for Loading.

The theoretical strain is calculated based on the formula obtained in Equation 1. This value is based on the load imposed (P), section property (I), material property (E) and the relative location of the sensor (L_1).

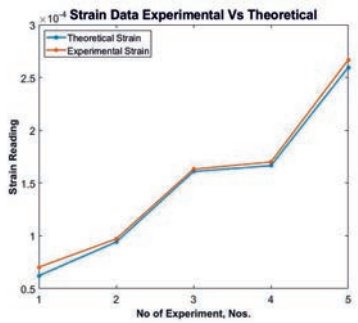

Figure 3: Strain Data Experimental Values Compared with Expected Values.

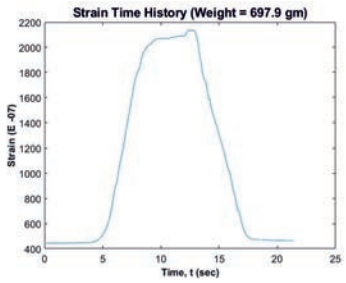

Figure 4: Strain visualized from experimental point loading.

We verified the workings of the strain gauge sensor by placing it on a cantilever ruler. The strain gauge sensor collected strain profile of the ruler motion.

AR AND DATABASE

The sensor sends data wirelessly to a database server, the database used is MySQL. The communication between the sensor and the server is done through a socket, in this case the socket used is Node.js. The source code was developed in Unity for use of the Microsoft HoloLens, see Fig. 5. The HoloLens application connects to the MySQL server and displays the sensor information in a graph; see Fig. 6.

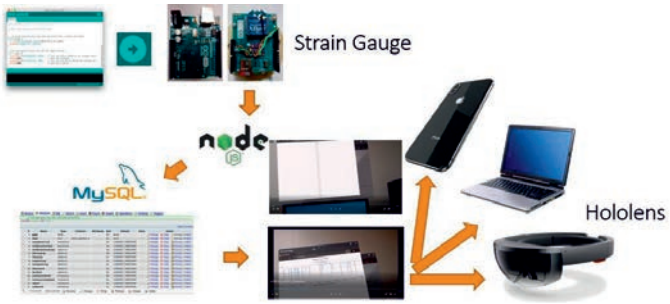

Figure 5: Strain Gauge to HoloLens Connection - Software Setup.

Figure 6 Real-time data visualization from low-cost sensors.

CONCLUSIONS

This paper has introduced a new Strain Gauge platform, which collects data with low-cost sensor to measure strain of different applications. In the experiment presented in the paper the platform allowed real-time visualization of data in HoloLens.

Enterprises and Drones: new systems for Drone Operations Management

C. Mozzetti[1], A. De Vitis[2], D. Spigarelli[3], G. N. Raganelli[4]

[1] *Aiviewgroup, Rome, Italy.*
E-mail: cmozzetti@aiviewgroup.com
[2] *Aiviewgroup, Rome, Italy.*
E-mail: adevitis@aiviewgroup.com
[3] *Aiviewgroup, Rome, Italy.*
E-mail: dspigarelli@aiviewgroup.com
[3] *Aiviewgroup, Rome, Italy.*
E-mail: graganelli@aiviewgroup.com

ABSTRACT

The development of drone activities into the Low Altitude Airspace (LAA) is a great opportunity for many companies. Work carried-out by drones (inspections, surveillance and control, mapping etc.) will be supported by other new activities and services that will pave the way for new business models and revenues. Enterprises are already building large fleets; managing the drones, the people and procedures using advanced platforms that utilize the collected data effectively. Working in compliance with airspace rules is fundamental for success. AI-Crew and AI-Inspection are two innovative platforms born to help Enterprises capitalize on drone airspace, maximizing their assets.

KEYWORDS: *Airspace, inspection, drone, management, operations*

INTRODUCTION

Enterprises have completed several experimenting activities on drone application for their own operation and maintenance processes. The past two years have given companies in telco, oil & gas, utilities, railways and highways, the opportunity to discover the potential and the business use-cases in which it is possible to reduce costs of activities such as inspections, monitoring, measuring and transportation. In the digital transformation process Enterprises are going through, drones are part of an IoT system that collect information. Therefore, there is a need to merge Staff and Fleet coordination with data from the company information systems, in order to protect brand responsibilities and for the valorization of data.

MODEL FORMULATION

After completing several experimenting activities on drone application for their own operation and maintenance processes, Enterprises now fully understand the advantages of using drones for their activities and incorporating this technology as a tool in their everyday operations. Many of these companies started purchasing commercial or custom drones from different providers, or in some cases to manufacture them internally; followed by the precise execution of operation's simulations, carried out by internal drone communities or relying on a variety of external expert consultants. Nowadays, many Enterprises own a relevant number of drones, creating what can be described as fleets. Since Enterprises are starting to own not only few, but hundreds of flying drones, the risk of uncoordinated and unauthorized actions and operations increases, as well as the risk of accidents. UAV Regulations imply that organizations must be certified with well-defined roles and responsibilities, and must have operation and maintenance procedures in place for pilots and fleets. The Accountable Manager of an Enterprise, often a top-level manager, must have full control over a fleet of hundreds of drones, the people who operates them, the internal authorization process for the mission etc. When a pilot in a company division carries out a mission, it has to be planned in compliance with national regulations, no-flight-zones, NOTAMs, and other relevant criteria. Thus, Enterprises need a platform with which they can manage their fleets, the organization and operations. Drones create a great amount of data: 4k optical sensors record gigabytes of information during each mission. This must be combined to the structural features, quality indicators and measurement of the inspected asset. Enterprises need platforms that can manage a workflow of data capture, classification, analysis and reporting. All of this completely integrated with an up-stream pre-existing Asset Management, and down-stream Predictive or Order Management. This is because the main information retrieved from an inspection is not only a series of photos or videos, but contains different parameters that indicate the conservation status of the asset, obtained by applying a specific defect catalogue and evaluation weights (intensity, extension and evolution) that are unique to the asset.

AI-Crew is a drone-management-platform that supports UAV Organizations for National Authorities' regulation compliance. It also manages the fleets, the documentation and personnel.

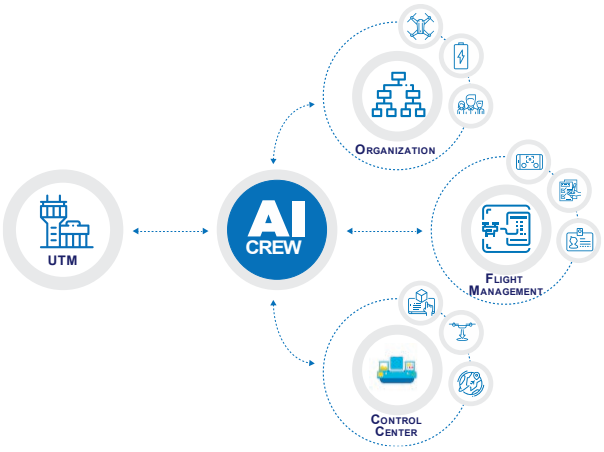

Figure 1: AI-Crew: bridging UTM operations and Enterprise needs

Through the Control Center module, AI-Crew allows an Enterprise to monitor an operation both from a synoptic point of view, as well as on a map with the possibility of communicating with pilots on the field. All data and videos can be seen real-time from the Control Center. Interactive airspace map allows to visualize real-time regulated areas and temporary flight restrictions, plan flights, interact with operators, and fly drones safely. Pilots, flight hours, authorizations, aircrafts and flight plans, all in one place. AI-Crew is a drone operation complete system that makes it easy to manage systems, people and missions. Every planned mission undergoes in-depth validation from the Enterprises control center and the integrated UTM system.

AI-Inspection platform was created to manage the workflow of UAV operations in inspections and monitoring, optimizing the cataloguing and predictive maintenance through defect analysis using algorithms in image processing, machine learning, and data consultation.

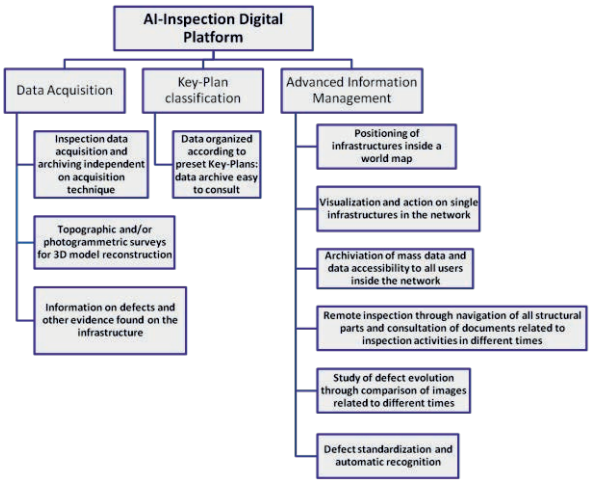

Figure 2: AI-Inspection, a complete workflow for UAV inspections

All the data acquired during an inspection collected by AI-Inspection, catalogued based on the key plan of the operation and its rules, and analyzed using machine learning & image recognition algorithms that automatically produce an inspection report. All this information can be temporally cross-checked and compared with the analytical and visual results obtained with previous inspections. AI-Inspection allows the management of different types of data for the purpose of inspections, documentation and maintenance by linking them to single structural elements.

CONCLUSIONS

The two presented platforms allow Enterprises to manage frequent and recurrent Drone activities in their complex organization, where it is fundamental to ensure efficiency and productivity while maintaining the compliance requirements with relevant regulations. As a drone service provider with yearly experience, Aiviewgroup understands the complexity behind organizing a drone operation and in this context has created these simple yet successful systems where every aspect of drone operation is taken care of across departments and in multiple jurisdictions. The combined adoption of these powerful tools allows the Enterprise to fully exploit the potential of Low Altitude Airspace.

REFERENCES

[1] Geovectoring: Reducing Traffic Complexity to Increase the Capacity of UAV airspace, Jacco Hoekstra, Joost Ellerbroek, Emmanuel Sunil, Jerom Maas

[2] DLR Blueprint Concept for Urban Airspace Integration

[3] European Drones Outlook Study - Unlocking the value for Europe

New Cable Climbing Robot for Automated Inspection of Cables of Suspension Bridge

S. Juarez-Perez[1], E. Ottaviano[2], D. Rodriguez-Rosa[1], A. Gonzalez-Rodriguez[1] and F.J. Castillo-Garcia[1].

[1] *School of Industrial Engineering, University of Castilla-La Mancha, Spain.*
E-mail: fernando.castillo@uclm.es

[2] *Department of Civil and Mechanical Engineering, University of Cassino and Southern Lazio, Italy.*
E-mail: ottaviano@unicas.it

ABSTRACT

This paper presents a new design of robot for climbing support cables of suspension bridges. A typical suspension bridges is a continuous girder suspended by suspension cables, which pass through the main towers aided by a special structure known as a saddle, and end on big anchorages that hold them. In this sense, the main forces in a suspension bridge are tensions in the cables and compression in the towers. The deck is usually a truss or a box girder and is connected to the suspension cables by vertical suspender cables or rods, called hangers, which are also in tension and are attached to the main suspension cables by means of support plates.

Although some cable climbing robot designs and prototypes can be found for inspecting suspension cables, these designs has been developed to climb up and inspect the main cables without considering the overpassing of hangers.

The proposal presented here is a 'open-robot' in its lower part which allows climbing suspension cables and inspecting them by cameras, overpassing the hangers.

KEYWORDS: *Robotics, Mechatronics, Bridge Inspection, Cable-climbing*

INTRODUCTION

Suspension bridges are key infrastructures in supporting our community. They carry pedestrian, heavy, rails or vehicle traffic over natural obstacles [1]. Usually, the desk of this kind of bridges is hung below suspension cables on vertical suspenders, called hangers. Main cables are suspended between towers and hangers support the weight of the deck and its traffic [2].

Periodic inspections tasks are therefore mandatory to ensure a proper maintenance of these structures. In particular, this paper proposes a novel design for inspecting main cables. Some works have presented robotic solutions for this purpose (e.g. [3-5]). The most of these works mainly tackle the problem of climbing cable ensuring the sufficient frictional force for maintaining the robot fixed to the cable, also allowing the movement

of the robot over the cable.

Nevertheless, hangers are attached to main cables by means of support plates as can be seen in Figure 1. In this sense, a robot to inspect main cables should be able to overpass these support plates while exerting enough frictional force to ensure its travelling over the main cable.

Figure 1: Main cable, hangers and support plates (Polvorines bridge, Toledo, Spain).

The design presented here has been development for Polvorines bridge, taking into account the main dimensions that restrict the design: main cable diameter and support plate dimensions.

NOVEL DESIGN

Figure 2 shows the proposed design.

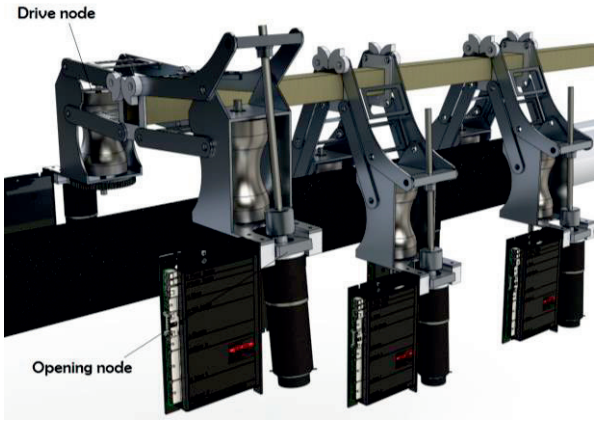

Figure 2: Cable climbing robot design

The robot has 3 similar nodes which are able to fix the robot to the cable by means of a direct contact. During the robot movements, two nodes are in contact to the cable to ensure the robot stability.

When overpassing obstacle, one node is open, the robot overpasses it and, consequently, the rest of nodes reproduces the same behavior. The sequence of movement for overpassing obstacle is described in Figure 3.

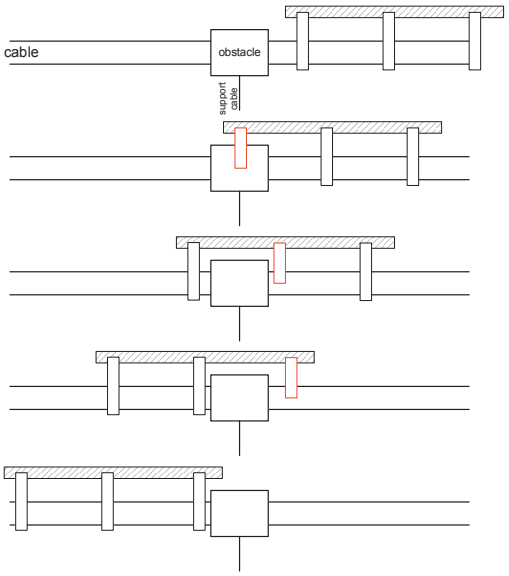

Figure 3: Overpassing obstacle sequence

In order to ensure a general-purpose design, the 3 nodes are similar and can be mounted on a support beam which can be scalable to other obstacle sizes.
With to objective to overpass the support cables (see Figure 3), the robot is completely opened in its lower part. This particular design makes that rotation δ (see Figure 4) could be possible and produces a robot instability. In order to avoid undesired rotation along the axis of the cable, the robot has been designed such as its center of mass is placed much lower that the cable axis.

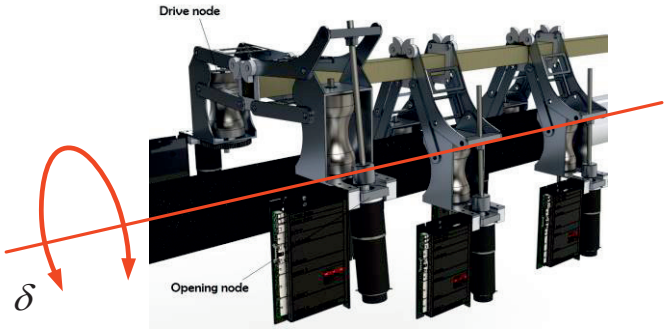

Figure 3: Rotation of cable climbing robot

This design is simpler than other ones and provides the ability to overpass not only obstacles in the cable path but also support cable which are often present in hanging bridges.
For inspection purpose, the robot will carry on a set of three industrial cameras E3ISPM with SONY IMX226 CMOS sensor (12MP) and USB3 interface. They are a reasonable compromise between image quality and price (320€). Lenses will also be

selected as a compromise between image quality and price. We find that a reasonable choice would be HM3528MP10 from ZLKC. These is a low distortion C-Mount 35mm 2/3"FA lenses rated at 10MP and priced around 100€ (see Figure 39.

a) b)

Figure 4: E3ISPM USB3 camera and ZLKC HM3528PM10 lens

The higher risk of this proposal is to establish the center of mass as lower as possible to ensure the robot stability when in presence of lateral disturbance, such as wind.

CONCLUSIONS

The proposed design here allows to climb main cables in suspension bridges with the ability of overpassing support plates which fix main cables to hangers. The design guarantees the friction force required for the movement and is formed by three nodes. The alternative opening moving of each node allows also to overpass the aforementioned obstacles. The design presented here is easily scalable to any size of main cable and obstacle.

REFERENCES

[1] Cho, K. H., Kim, H. M., Jin, Y. H., Liu, F., Moon, H., Koo, J. C., & Choi, H. R. (2013). Inspection robot for hanger cable of suspension bridge: Mechanism design and analysis. IEEE/ASME Transactions on mechatronics, 18(6), 1665-1674.

[2] Lin, W., & Yoda, T. (2017). Bridge Engineering: Classifications, Design Loading, and Analysis Methods. Butterworth-Heinemann.

[3] Xu, F., & Wang, X. (2008, July). Design and experiments on a new wheel-based cable climbing robot. In 2008 IEEE/ASME International Conference on Advanced Intelligent Mechatronics (pp. 418-423).

[4] Xu, F., Wang, X., & Wang, L. (2011). Cable inspection robot for cable-stayed bridges: Design, analysis, and application. Journal of Field Robotics, 28(3), 441-459.

[5] Cho, K. H., Jin, Y. H., Kim, H. M., Moon, H., Koo, J. C., & Choi, H. R. (2013, August). Caterpillar-based cable climbing robot for inspection of suspension bridge hanger rope. In 2013 IEEE International Conference on Automation Science and Engineering (CASE) (pp. 1059-1062).

Inspection and monitoring by enhanced mechatronic solutions in the Gran Sasso National Laboratories

C. Rinaldi[1], U. Di Sabatino[1], F. Potenza[1], V. Gattulli[2]

[1] *Dep of Civil, Construction-Architectural and Environmental Engineering, University of L'Aquila, Italy.*
E-mail: cecilia.rinaldi@graduate.univaq.it, umbertodisabatino@virgilio.it, francesco.potenza@.univaq.it

[2] *Department of Structural and Geotechnical Engineering, Sapienza University of Rome, Italy.*
E-mail: vincenzo.gattulli@uniroma1.it

ABSTRACT

Monitoring and automated inspection are needful to evaluate critical aspects related to the health of structures and infrastructures. The information coming from data processing could be used to program optimal maintenance interventions. Sometimes, the installation phase of special smart sensors constituting the monitoring network could be difficult due to the presence of inaccessible points. An example is represented by the underground galleries of the Gran Sasso National Laboratories, the most important underground research center dedicated to the study of fundamental constituents of matter. The stability of the rock of these galleries is provided above all by passive anchorages (rock bolts). They are the main structural elements to monitor to evaluate the actual conditions of the vault, but they are also the most difficult to monitor because they are stuck in the rock and, in some areas, they are situated under a cladding panel. It is evident how, in this special background, the inspection and monitoring of the vaults are challenging but also fundamental for both environmental and staff safety. In this work, methodologies based on the use of robotic systems will be presented to perform actions dedicated to the monitoring of the galleries.

KEYWORDS: *robotized inspection, mechatronic system, rock bolts, non-destructive testing*

INTRODUCTION

The Gran Sasso National Laboratories (Figure 1) are the largest and most important underground research center in the world within the Gran Sasso highway tunnel. The underground structures consist of three large galleries (called Hall A, B and C), situated under a rock layer about 1400 m thick. Within these sales are installed the apparatuses supporting the experiments in particle physics and nuclear astrophysics.

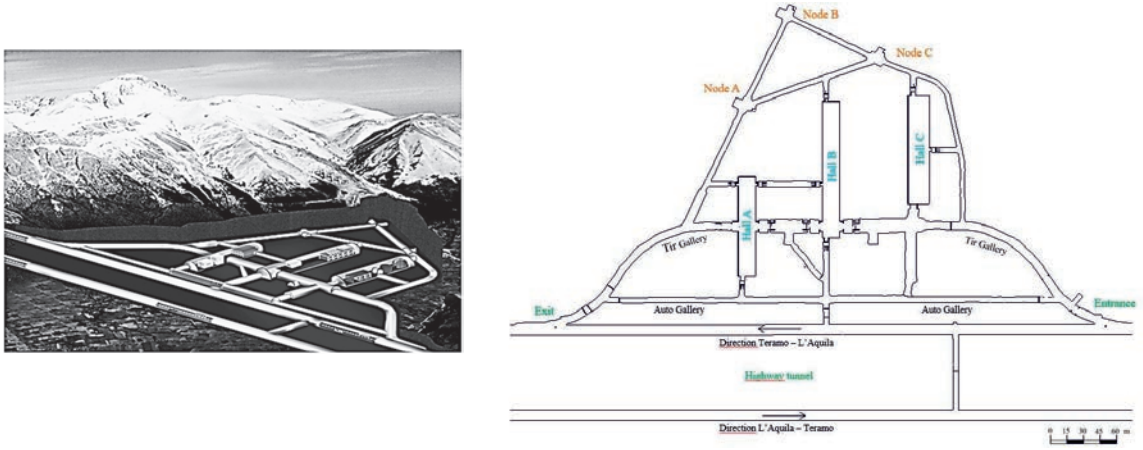

a) b)

Figure 1: Gran Sasso National Laboratories: a) 3D view; b) plan.

These underground structures were designed by Lunardi [1] and they were built in 1982. The tests carried out to estimate the resistance of the limestones showed their fragile behavior and the structural analysis pointed out the overcoming of load-bearing capacity of the same limestones during the excavations. For these reasons and because of the huge coverage, the designer decided to insert passive anchorages (Figure 2) to join the discontinuity points and to increase the shear strength of the rock. The technical characteristics of the anchorage used are: material martensitic stain-less steel (AISI 420), diameter 30.6 mm, length from 6 to 8 m, mesh of 2 meters for side. In the areas where the rock was more damaged, the length of anchorages is from 10 to 12 m and the mesh is denser.

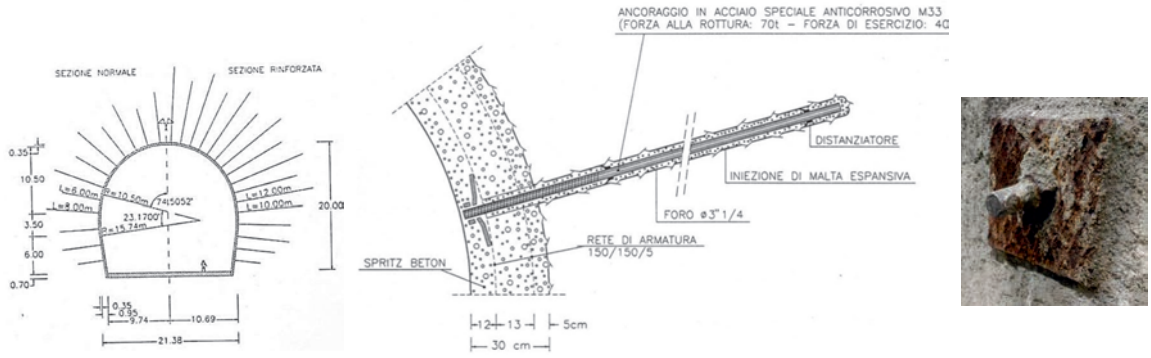

a) b) c)

Figure 2: Consolidation interventions in the galleries: a) gallery cross-section reinforced with rock bolts [1]; b) rock bolt details and spritz-beton coating [1]; c) actual condition of a rock bolt head (picture taken in an accessible point of galleries).

Thanks to these consolidation interventions, the coating facilities were designed with very thin thickness (spritz beton layer 35 cm thick, Figure 2b) and the use of the cement (source of harmful radiation for experiments) was minimized. To obtain optimal air

conditioning for the laboratory activities, the experimental halls were waterproofed and insulated using a PVC sheet and polyurethane panels (12cm thick) supported by an aluminum structure (Figure 3).

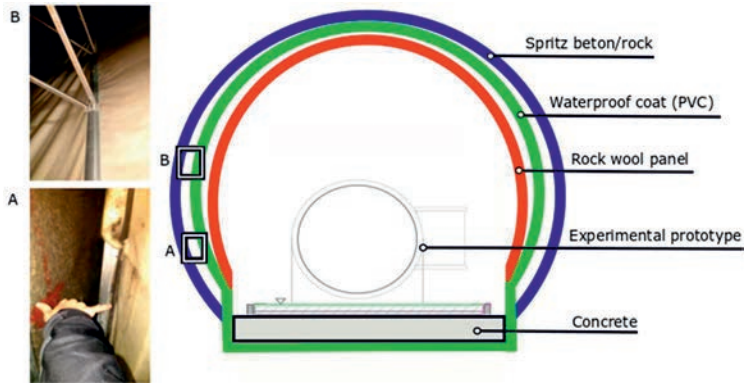

Figure 3: Gallery cross section with focus on the interspace between rock and PVC panels: picture A shows the order of magnitude of the interspace, picture B the aluminum structure.

MECHATRONIC SOLUTIONS FOR UNDERGROUND INSPECTIONS AND MONITORING

Tunnels and underground environments often are large-scale structures which may presents some inaccessible points. In these cases, the use of robotized tools is essential to perform a Structural Health Monitoring (SHM). Various approaches have been developed to replace standard manual procedures with safer and faster ones. Ultrasonic sensors have been widely used as non-destructive sensors [2], because they are cheap and reliable, but they can only detect the existence of objects without giving any further information about objects. Therefore, the combined use of ultrasonic and visual sensors has spread, thanks to the development of techniques able to automatically identify the crack and its depth using image processing [3], [4]. An autonomous robotic system for tunnel cracks and other visible defects assessment is reported in [5]. This system is composed of a mobile vehicle capable of extending an automated crane. A set of cameras (attached also to the crane) with computer vision algorithm are used for detecting the defects and an arm positioning algorithm is used for placing the ultrasonic sensors on detected cracks. As to the rock bolt monitoring, it can be performed with different smart sensors [6]**;** exciting with the guided ultrasonic waves is an appropriate way to monitor these elements because of their shape. The arrival time of the reflected waves returns the location of the defects. All these procedures are not applicable to this case of study. For example, a robotic system like the one described in [5] is not suitable to these galleries: it not possible to introduce a mobile vehicle because the galleries are occupied by experimental prototypes and instruments. Furthermore, the presence of the coating panels with their supporting

structures makes inspection actions more difficult. Climbing robots are getting attention for inspections of hard to reach environments like this one; robots inspired by climbing animals (such as frogs, geckos) have been designed, using bio-inspired adhesive technology to traverse a wide variety of surfaces [7]. A gecko inspired robot, like the one proposed in [8], equipped with a camera, may be the suitable candidate to be introduced in the interspace between the rock and the PVC panels to inspect the rock surface conditions.

CONCLUSIONS

In this work, issues related to the SHM of the galleries of the Gran Sasso National Laboratories have been presented, with focus on the inspection of the inaccessible points, such as the rock surface in the main galleries, coated by PVC panels. A climbing robot system has been proposed to perform inspection actions in the restricted interspace between the rock and the panels.

ACKNOWLEDGMENTS

This work is part of a project that has received funding from the Research Fund for Coal and Steel under grant agreement No 800687.

REFERENCES

[1] Lunardi P. (1990) La ricerca e la tecnologia nella realizzazione di grandi cavità sotterranee: il laboratorio di fisica nucleare del Gran Sasso. *International Conference "Se vogliamo il verde sopra utilizziamo lo spazio profondo"*, Milano.

[2] Yao F., Shao G., Tamaki A., Yamada H., Kato K. (1999) Development of 3D-ultrasonic-sensor and its application to the construction of large-scale environment model. *The 30th International Symposium on Robotics*, Tokyo, 305-310.

[3] Potenza F., Castelli G., Gattulli V., Ottaviano E. (2017) Integrated Process of Images and Acceleration Measurements for Damage Detection. *Procedia Eng.* **199**: 1894–1899.

[4] Mohan A., Poobal S. (2018) Crack detection using image processing: A critical review and analysis. *Alexandria Eng. J.* **57**:787-798.

[5] Merendez E., Victores J.G., Montero R., Martinez S., Balaguer C. (2018) Tunnel structural inspection and assessment using an autonomous robotic system. *AUTOMAT. CONSTR.* **87**:117-126.

[6] Song G., Li W., Wang B., Ho, S. (2017) A review of rock bolt monitoring using smart sensors. *Sensors* **17(**4): 776.

[7] Silva M.F., Machado A.T., Tar J.K. (2008) A Survey of Technologies for Climbing Robots Adhesion to Surfaces. *6th International Conference on Computational Cybernetics*, Slovakia.

[8] Unver O., Uneri A., Aydemir A., Sitti M. (2006) Geckobot: A Gecko Inspired Climbing Robot Using Elastomer Adhesives. *International Conference on Robotics and Automation. International Conference on Robotics and Automation*, Florida.

New Magnetic Climbing Robot for Automated Inspection of Steel Structures

D. Rodriguez-Rosa[1], G. Rubio-Gomez[1], E. Ottaviano[2], A. Gonzalez-Rodriguez[1] and F.J. Castillo-Garcia[1].

[1] *School of Industrial Engineering, University of Castilla-La Mancha, Spain.*
E-mail: fernando.castillo@uclm.es

[2] *Department of Civil and Mechanical Engineering, University of Cassino and Southern Lazio, Italy.*
E-mail: ottaviano@unicas.it

ABSTRACT

This paper presents a new design of a magnetic robot for climbing planar surfaces which main task is the inspection of steel bridges structures of huge dimensions. For this reason, robot has no umbilical cord together with a high autonomy.

The robot will work on different structures; therefore, it must be able to move through surfaces with different slopes. In flat surfaces, magnetic robots show a good performance, both with the robot supported on the floor or suspended by the horizontal plane. For these cases, the robot does not need a considerable tangential force, so gravity or magnetic force allows the robot movement. Problems appear when inspecting vertical surfaces, where wheels must develop a considerable tangential force in order to counter the gravity force. Friction coefficient of wheels with steel is usually low, so huge magnetic forces will be required to generate enough tangential force.

KEYWORDS: *Robotics, Mechatronics, Bridge Inspection, magnetic-climbing*

INTRODUCTION

Suspension bridges are key infrastructures in supporting our community. They carry pedestrian, heavy, rails or vehicle traffic over natural obstacles [1]. These structures require predictive maintenance in common parts as support beam or main towers. Some inspection tasks are based on visual inspection or required to place sensor system at particular point of interest.

At this point, the design of a robot with ability to move in flat steel surfaces is presented. The robot task is the inspection of steel bridges structures with huge dimensions. For this reason, the main goal is to obtain a robot with no umbilical cord together with a high autonomy [2]. The system must be able to transit though little obstacles like steps or welding cords, which will require the employment of magnetic wheels with a considerable size [3].

The robot will work on different structures; therefore, it must be able to move through surfaces with different slopes. In flat surfaces, magnetic robots show a good performance, both with the robot supported on the floor or suspended by the horizontal plane. For these cases, the robot does not need a considerable tangential force, so gravity or magnetic force allows the robot movement. Problems appear when inspecting vertical surfaces, where wheels must develop a considerable tangential force in order to counter the gravity force and allow the robot to work in steel walls. Friction coefficient of wheels with steel is usually low, so huge magnetic forces will be required to generate enough tangential force.

This problem becomes critical if the robot, as required, needs high autonomy due to the large workspace that bridge inspection requires. Large workspace yields to difficult in the employment of umbilical cords, on the other hand, batteries needed for high autonomy are large. Taking into account that the inspection areas are very large, a considerably high velocity for the robot will be desired. To accomplish all the exposed requirements for the robot, a high performance and speed locomotion system like wheel will be proposed, instead of other solutions like legs or caterpillar.

NOVEL DESIGN

The technical requirements of the prototype are:

- R1. Should be carry on a sensorization volume of 300 × 200 × 100mm for inspection purpose.
- R2. The payload should be up to 3kg.
- R3. Movement capability: should be able to execute complete manoeuvres in the wall including XY displacements and rotation, δ (see Figure 1: Movement capability.
- The rotation radius of δ should be as low as possible.
- R4. Obstacle overpassing: should be able to overpass a 6 mm of obstacle.
- R5. Linear manoeuvre speed about 0.2 m/s.

For developing the inspection tasks, we have chosen a 3-wheel configuration as shown in Figure 2.

The two forward wheels (red) are motorized and provide the movement capability since the rear one (green) is a passive wheel with two degree-of-freedom.

The robot rotation, δ, is reached by establishing different rotation speed to the forward wheels. In this sense, each forward wheel has a motor and they can exert different torques (T_1 and T_2 in Figure 2). This configuration provides a rotation point along the line that connect the axis of both forward wheels. Degree-of-freedom DOF1 of the rear wheel allows adapting this wheel to the aforementioned rotation point when the speed of motors changes.

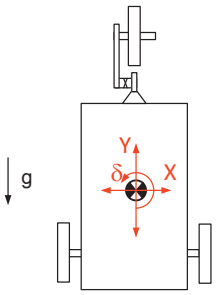

Figure 1: Movement capability.

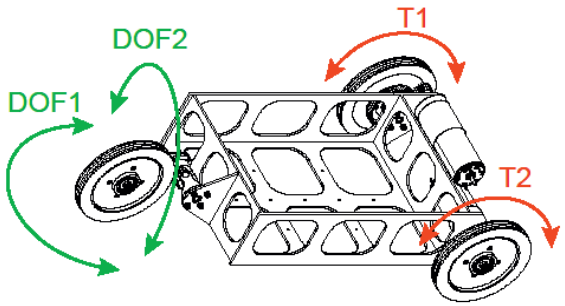

Figure 2: Movement capability.

In addition, a second degree-of-freedom (DOF2) has been added for ensuring that the rear wheel maintains perpendicular to the movement plane during manoeuvres and aid to the magnetic holding of the vehicle when, for example, a forward wheel overpasses any obstacle.

About magnetic attraction for ensuring contact between vehicle and wall, both forward wheels have been designed as in Figure 3.

Label 1 corresponds to cylindrical magnets which provide the magnetic attraction to attach the wheels to the wall. Label 2 shows two iron plates which conduce magnetic flux to the wall to move on. Label 3 is a flexible material with a high friction coefficient. Label 4 is a part which holds the magnets and the flexible material part. Finally, label 5 refers to the gear that connect to the motor for providing rotation movement to the wheel.

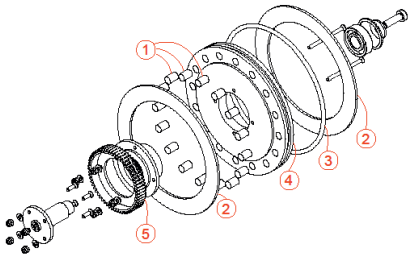

Figure 3: Magnetic wheels design.

Figure 3 shows the magnetic flux direction from magnet, to wall and back.

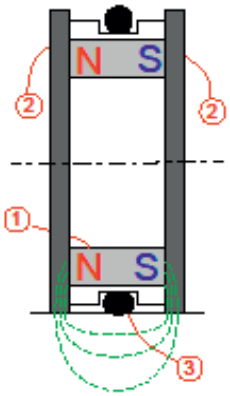

Figure 4: Magnetic flux between the wheels and the wall.

CONCLUSIONS

The proposed design here allows to climb flat surface provides 3 Degrees-of-Freedom for inspection tasks. Two forward motorized wheels which provide the movement capability since a passive rear one two degree-of-freedom allows to maximize the tangential force for avoiding loss of contact between the robot and the surface.

REFERENCES

[1] Cho, K. H., Kim, H. M., Jin, Y. H., Liu, F., Moon, H., Koo, J. C., & Choi, H. R. (2013). Inspection robot for hanger cable of suspension bridge: Mechanism design and analysis. IEEE/ASME Transactions on mechatronics, 18(6), 1665-1674.

[2] Shen, W., Gu, J., & Shen, Y. (2005, July). Proposed wall climbing robot with permanent magnetic tracks for inspecting oil tanks. In IEEE International Conference Mechatronics and Automation, 2005 (Vol. 4, pp. 2072-2077). IEEE.

[3] Yan, W., Shuliang, L., Dianguo, X., Yanzheng, Z., Hao, S., & Xueshan, G. (1999). Development and application of wall-climbing robots. In Proceedings 1999 IEEE International Conference on Robotics and Automation (Cat. No. 99CH36288C) (Vol. 2, pp. 1207-1212). IEEE.

Automatic vehicle passage detection using wireless accelerometers toward Bridge Weigh-In-Motion

T. Nagayama[1], S. Kato[1], H. Wang[1], D. Su[1], M. Nishio[2]

[1] *Department of Civil Engineering, the University of Tokyo, Japan.*
E-mail: nagayama@bridge.t.u-tokyo.ac.jp

[2] *Department of Engineering Mechanics and Energy, Tsukuba University, Japan.*
E-mail: nishio@kz.tsukuba.ac.jp

ABSTRACT

While the traffic loads need to be understood toward efficient management of bridges, the loads on each bridge are not well assessed. An easy-to-implement vehicle weight estimation technique toward Bridge Weigh-In-Motion (BWIM) using wireless accelerometers has been developed. An important step of the vehicle weight estimation is the detection of vehicle passage timing. This study proposes an application of Convolutional Neural Network (CNN) to the wireless accelerometer data to detect vehicle passages. The training data is created by analyzing video camera records of a few hours. After the training process, the passage of the vehicles can be detected only from the signals from wireless accelerometers placed at the girder ends. This automatic detection of vehicle passage is expected to allow the application of vehicle weight estimation algorithm to continuously measured bridge response data. The performance of the CNN-based vehicle detection is examined on a two-span continuous box-girder bridge. The detection success rate is confirmed high as compared to a simple method based on thresholds.

KEYWORDS: *Wireless accelerometers, Bridge Weight-In-Motion, Convolutional Neural Network*

INTRODUCTION

While Bridge Weigh-In-Motion (BWIM) has long been studied and practiced [1], the algorithms are in principle based on strain measurement. Installation of strain gauges and cabling are time consuming. The system cost including the installation is thus high preventing wide-spread use on many road bridges.

To improve the installation difficulty, the estimation of passing vehicle weight only using accelerometers installed on a bridge has recently been proposed [2]. Girder deflection numerically estimated from the measured vertical acceleration signals are

utilized and compared with the deflection estimated from the influence-lines. The weight estimation performance has been studied for single vehicle passages on a highway bridge.

Deflection estimation only using accelerometers has further been improved by employing inclination, which are estimated from longitudinal acceleration measurement [3][4]. The low frequency components of the longitudinal acceleration include the inclination; the inclinations measured along a bridge and the vertical accelerations are merged by a Kalman filter to estimate the deflection of the bridge. Because the Kalman filtering process does not include numerical integration, the deflection estimation does not suffer from integration error; the deflection estimation can be performed even for cases where multiple vehicles pass the bridge in series.

To apply this weight estimation using acceleration data, the timings of vehicle's entrance to and exit from the bridge need to be identified in advance. This study investigate the capability to estimate the vehicle entrance and exit only using accelerometers on the main girders near the joint.

VEHICLE PASSAGE RESPONSES AT GIRDER ENDS

The target bridge is a 2-span continuous steel box-girder bridge. The entrance and exit of vehicles on this bridge are investigated using acceleration responses recorded by 4 wireless accelerometers placed near the girder ends. The sensor arrangement is shown in Figure 1.

The sample bridge responses are shown in Figure 2. Small vehicle passage clearly shows the peaks corresponding to the entrance and exit. On the other hand, bus passage shows vibration components when the bus drive over the mid-support point. Only in terms of the response amplitude, the vehicle passage location cannot be identified. The sensor closest to the vehicle passage does not necessarily show the largest response. Therefore, the phase of the signal is also taken into account as shown in Figure 3.

The target bridge is a steel, two-span continuous, box-girder bridge on a general road (see Figure 1). The bridge has one lane for each direction. On the box girders on the both sides, 18 battery-operated wireless accelerometers were installed and the tri-axial accelerations were recorded at 100 Hz for 13 day continuously. The wireless sensor nodes are Sonas x01 [5], whose accelerometers are Epson M-A351 [6].

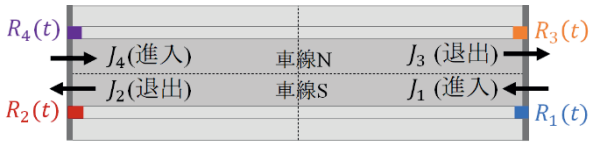

Figure 1: Target bridge and its drive lanes

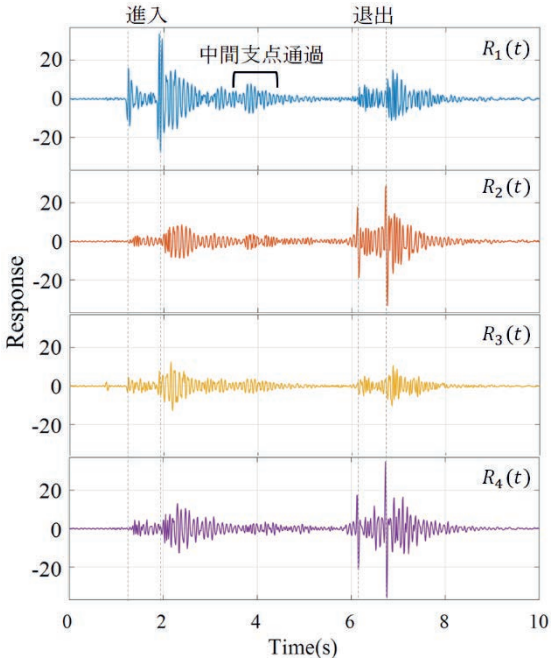

Figure 2: The bridge responses recorded during bus passages

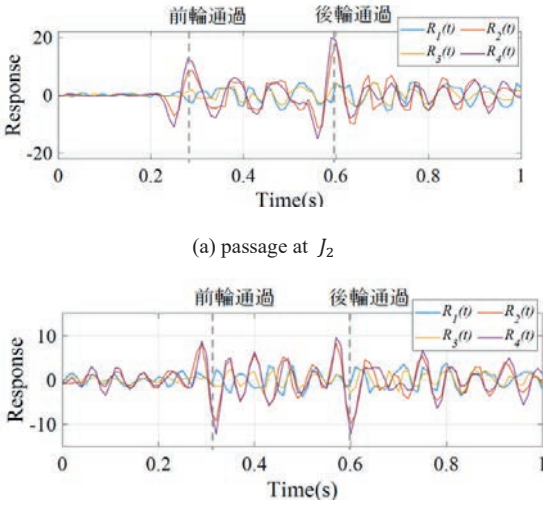

(a) passage at J_2

(b) passage at J_4

Figure 3: Vehicle passage responses (zoom-in)

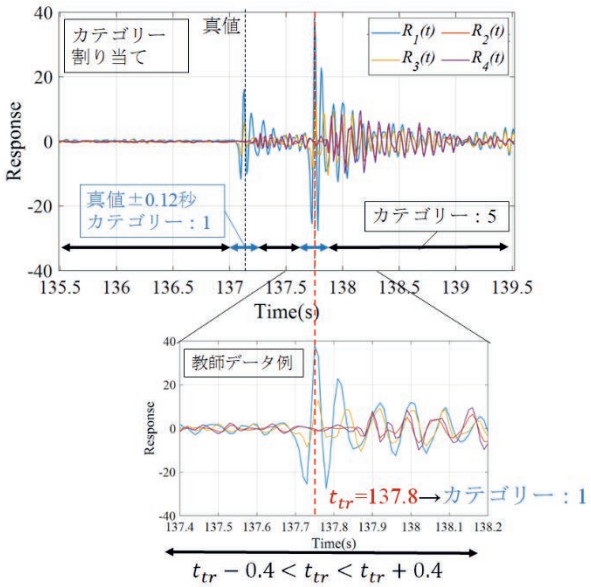

Figure 4: Training data

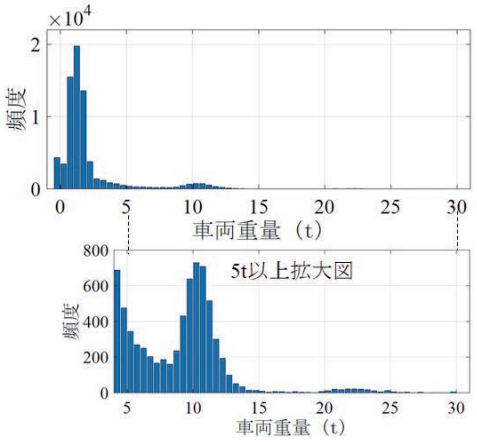

Figure 5: Estimated Vehicle weight

Tab. 1. Vehicle passage categories

Category	Vehicle passage	Location
1	yes	J_1
2		J_2
3		J_3
4		J_4
5	no	

Tab. 2. Classification accuracy

	Error acceptance(s)	Recall	Precision	Fvalue
CNN	0.5	75.4	80.6	77.9
	1.0	77.9	82.9	80.3
	1.5	80.6	84.9	82.7
Threshold (reference)	0.5	38.7	61.2	47.4
	1.0	41.4	65.0	50.6
	1.5	42.9	66.5	52.2

Using video camera records taken at the girder ends, the training data sets are prepared (see Figure 4). The data sets are categorized into 5 classes shown in Table 1. Then, Convolutional Neural Network is applied to classify the vehicle passage based on the acceleration measured at four sensors. Table 2 shows the categorization results and comparison with categorization based on threshold.

With the convolutional neural network, the vehicle classification accuracy was improved to about 80%. Figure 5 shows the vehicle weight estimation using the classification.

CONCLUSIONS

By applying Convolutional neural network to girder end acceleration data, the vehicle entrance to and exit from a bridge are detected. The detection accuracy is about 80 %. The detected vehicles are further analyzed to obtain the vehicle weight. The vehicle weight distribution is obtained only using the acceleration response measurement on a steel box-girder bridge.

ACKNOWLEDGMENT

This work was partially supported by Council for Science, Technology and Innovation, "Cross-ministerial Strategic Innovation Promotion Program (SIP), Infrastructure Maintenance, Renovation, and Management" (funding agency: JST), JSPS Kakenhi (Grant Number JP 17H03295), and Ministry of Internal affairs and communications SCOPE (Grant Number 181503008). The authors would like to express their sincere appreciation for the advice provided by Mr. Miyagishi and Mr. Oshima at City of Yokohama; Mr. Nakasendo and Mr. Furuta at Seiko Epson Corp.

REFERENCES

[1] F., Moses "Weigh-In-Motion system using instrumented bridges," Transportation Engineering Journal of ASCE, Vol. 105, No.TE3, pp.233-249, 1979.

[2] H. Sekiya "Field Verification over One Year of a Portable BridgeWeigh-in-Motion System for Steel Bridges," Journal of Bridge Engineering, Vol. 24, 2019

[3] T. Nagayama, C. Zhang "A numerical study on bridge deflection estimation using multi-channel acceleration measurement," Journal of Structural Engineering A, JSCE, Vol.63A, pp.209-215, 2017. https://doi.org/10.11532/structcivil.63A.209

[4] T. Nagayama, C. Zhang, D. Su, and S. Lee "Estimation of a continuous girder bridge's deflection using acceleration and inclination measurement," Proc. of 7th World Conference on Structural Control and Monitoring, Qingdao, China.2018.

[5] Sonas Inc. https://www.sonas.co.jp/sonasx/sonasx-spec

[6] Epson M-A351https://www.epson.jp/prod/sensing_system/pdf/m-a351_briefsheet_j_rev20180309.pdf